


For Reference

NOT TO BE TAKEN FROM THIS ROOM

Ex LIBRIS
UNIVERSITATIS
ALBERTAENSIS





Digitized by the Internet Archive
in 2019 with funding from
University of Alberta Libraries

<https://archive.org/details/Kasper1981>

THE UNIVERSITY OF ALBERTA

RELEASE FORM

NAME OF AUTHOR Bryon Lynn Kasper
TITLE OF THESIS An Interference-Rejecting Radiometer for
 Low Frequency Astronomy
DEGREE FOR WHICH THESIS WAS PRESENTED Doctor of Philosophy
YEAR THIS DEGREE GRANTED January 1981

Permission is hereby granted to THE UNIVERSITY OF ALBERTA LIBRARY to reproduce single copies of this thesis and to lend or sell such copies for private, scholarly or scientific research purposes only.

The author reserves other publication rights, and neither the thesis nor extensive extracts from it may be printed or otherwise reproduced without the author's written permission.

2

THE UNIVERSITY OF ALBERTA

An Interference-Rejecting Radiometer for Low Frequency
Astronomy

by



Bryon Lynn Kasper

A THESIS

SUBMITTED TO THE FACULTY OF GRADUATE STUDIES AND RESEARCH
IN PARTIAL FULFILMENT OF THE REQUIREMENTS FOR THE DEGREE
OF Doctor of Philosophy

Electrical Engineering

EDMONTON, ALBERTA

SPRING 1981

THE UNIVERSITY OF ALBERTA
FACULTY OF GRADUATE STUDIES AND RESEARCH

The undersigned certify that they have read, and recommend to the Faculty of Graduate Studies and Research, for acceptance, a thesis entitled An Interference-Rejecting Radiometer for Low Frequency Astronomy submitted by Bryon Lynn Kasper in partial fulfilment of the requirements for the degree of Doctor of Philosophy.

Dedicated to my wife Vicky
and to my Parents

For years of encouragement and understanding.

Abstract

A serious difficulty for low frequency radio astronomy either on the earth's surface or in any unshielded location near the earth is the presence of interfering terrestrial radio transmissions. Generally, however, interference will not exist simultaneously at all frequencies. Gaps in the spectrum which do not contain significant interference may be used to allow astronomical observations at times when adjacent interference would normally make observing impossible.

An experimental system is designed and built to investigate the possibility of on-line detection and rejection of narrowband terrestrial interference. Digital cross spectral analysis via the fast Fourier transform allows narrowband interference to be identified as peaks in the spectrum. A low-cost FFT processor designed and built for this purpose is described. The processor is capable of calculating a 256-point FFT in 2.458 msec for a real-time bandwidth of 52 kHz.

The expected distributions of cross and auto spectral components in the absence of interference are derived. Robust estimation which weights outlying points less heavily than those near the center of a distribution is employed to reject interference and estimate the centers of the cross spectra. The first deciles of the auto spectra are used as simple but accurate estimates of scale for the cross spectra. A robust procedure combining outlier rejection,

Huber M-estimation, and biweight M-estimation then determines the correlated broadband noise levels of the cross spectra while minimizing the effects of outliers.

Experimental testing of the system using an interferometer at 22.25 MHz during the winter of a solar maximum is described. Interference removal is found to be highly successful during periods with less than 30% and occasionally up to 50% of the bandwidth being occupied by interference. Low level interference during the night was encountered on 13 of 15 nights and was eliminated completely. Additional observing time of from 60 to 90 minutes was generally obtained in both the mornings and evenings. The distribution of interference amplitudes was found to be reasonably well represented by a power law.

Acknowledgements

The author expresses his sincere appreciation for the interest, advice, and support provided by his supervisors, Dr. D. Routledge and Dr. F.S. Chute, throughout this project.

The author is grateful to the staff of the Dominion Radio Astrophysical Observatory for their assistance during the field testing of the equipment. In particular, the author thanks Dr. P.E. Dewdney for help with the 22.25 MHz telescope and for many fruitful discussions on the nature of the interference problem, and Dr. R.S. Roger for instruction on the ionosphere.

Thanks is given for assistance and advice from the many people with whom the author has had the pleasure of associating at the University of Alberta, including Mr. P. Haswell, Mr. A. Huizinga, Mr. J. Radzion, Mr. D. Lind, Dr. J.F. Vaneldik, Dr. R. Gupta, Mr. D. Rudyk, Mr. J. Fearn, Mr. A. Vogan, Mr. J. Callaghan, Mr. B. Veidt, Mr. G. Bouchard, and Mr. L. Osler.

For the preparation of this manuscript, the author is deeply indebted to his wife, Vicky, for her unfailing efforts in a long and arduous task. For the majority of the drawings herein the author thanks the marvelous work of Mrs. L. Haswell.

The financial support provided by the following organizations is greatly appreciated: The National Research Council of Canada for two postgraduate scholarships; Alberta

Government Telephones for a Centennial Fellowship; and the Department of Electrical Engineering for part-time teaching assistantships. The research reported in this thesis was supported in part by the National Research Council of Canada.

Table of Contents

Chapter		Page
1	INTRODUCTION.....	1
	1.1 Decametric Astronomy.....	2
	1.1.1 Discrete Sources.....	3
	1.1.2 Extended Sources.....	5
	1.1.3 Existing Decametric Telescopes.....	6
	1.2 Limitations to Low Frequency Astronomy.....	7
	1.3 The Ionosphere.....	9
	1.4 Ionospheric Radio Propagation.....	11
	1.5 Ionospheric Effects on Radio Astronomy.....	14
	1.5.1 Absorption.....	14
	1.5.2 Refraction.....	14
	1.5.3 Scintillation.....	16
	1.6 Terrestrial Interference.....	18
	1.7 Previous Attempts to Deal with Interference.....	22
	1.8 Interference Detection via Spectral Analysis.....	24
	1.9 A Method of Rejecting Interference.....	26
2	THE FAST FOURIER TRANSFORM PROCESSOR.....	28
	2.1 Introduction.....	28
	2.2 FFT Basics.....	31
	2.2.1 Calculation of the Cross and Auto Spectra...31	
	2.2.2 Leakage and Windowing.....	34
	2.2.3 The Effects of Windowing.....	37
	2.2.4 FFT Quantization Errors.....	42
	2.2.4.1 Coefficient Quantization Errors....43	
	2.2.4.2 Arithmetic Roundoff Errors.....44	
	2.2.5 Arithmetic Overflow.....	45
	2.2.6 Overflow Correction.....	47
	2.3 Design of the FFT Processor.....	48
	2.3.1 The FFT Algorithm.....	50
	2.3.2 FFT Addressing.....	53
	2.3.3 Layout of the FFT Processor.....	56
	2.3.3.1 Analog-to-Digital Conversion.....58	
	2.3.3.2 Windowing.....	59
	2.3.3.3 Fast Fourier Transformation.....61	
	2.3.3.4 Power Spectrum Computation.....65	
	2.3.3.5 Accumulation.....	67
	2.3.3.6 The Microcomputer.....	71
	2.4 General Construction.....	74
	2.5 Laboratory Tests of the FFT Processor.....	75
	2.5.1 Comparison to Computer Simulations.....76	
	2.5.2 Windowing.....	76
	2.5.3 Phase Relationships of the Co and Quadrature Spectra.....	79
	2.5.4 Roundoff Noise.....	81
	2.5.5 Correlation Tests.....	88

3	RECEIVERS.....	92
3.1	Second Mixers and IF Amplifiers.....	92
3.2	RF Amplifier, First Mixer and First IF Amplifier..	98
3.3	Input Bandpass Filters.....	101
3.4	Synchronous Modulation.....	103
3.5	Local Oscillators.....	105
4	ROBUST ESTIMATION.....	107
4.1	Introduction.....	107
4.2	Definition of the Estimation Problem.....	107
4.2.1	Probability Density Function of Averaged Cross Spectra.....	108
4.2.2	Probability Density Function of Averaged Auto Spectra.....	113
4.2.3	Estimating the Variance of the Cross Spectra.....	114
4.2.4	Some Practical Considerations.....	117
4.3	A Survey of Robust Estimation.....	118
4.3.1	A Brief History.....	118
4.3.2	Tests for Outliers.....	120
4.3.3	Rejection of Outliers in Robust Estimation.	123
4.3.3.1	The α -Trimmed Mean.....	124
4.3.3.2	Skipped Estimates.....	125
4.3.4	Maximum Likelihood Estimation.....	127
4.3.5	Robust M-Estimators.....	131
4.3.6	Other Robust Estimators.....	134
4.4	The Performance of M-Estimators.....	134
4.4.1	The Influence Curve.....	134
4.4.2	Properties of M-Estimators.....	137
4.4.3	Comparison of Some Estimators.....	139
4.4.3.1	3σ Rejection Rule.....	139
4.4.3.2	Huber's M-Estimator.....	139
4.4.3.3	Hampel's Redescending M-Estimate...	140
4.4.3.4	Wave M-Estimate.....	141
4.4.3.5	Biweight M-Estimate.....	141
4.5	Adaptive Estimation.....	142
4.6	An Estimation Procedure.....	144
4.6.1	Estimation of Variance.....	145
4.6.2	Accuracy of the First Decile as an Estimator.....	147
4.6.3	Location Estimation.....	150
4.6.4	Evaluation of the Estimation Procedure.....	155
4.6.5	Possible Improvements.....	156
4.7	Summary.....	156
5	FIELD TRIALS.....	158
5.1	Introduction.....	158
5.2	Antennas.....	159
5.3	Cable Lengths and Losses.....	164
5.4	Bandwidth Decorrelation.....	166
5.5	System Operation.....	167
5.6	Data Analysis.....	172

6	OBSERVATION RESULTS.....	174
6.1	Plots of the Observations.....	175
6.1.1	Examples with No Interference Removed.....	175
6.1.2	Examples with Interference Removed.....	178
6.1.3	Examples of Spectra and their Histograms...	182
6.1.4	Morning Observations.....	187
6.1.5	Evening Observations.....	190
6.1.5.1	November 28.....	190
6.1.5.2	December 4.....	193
6.1.5.3	December 5.....	195
6.1.5.4	December 6.....	198
6.2	Scintillation.....	201
6.2.1	December 4.....	201
6.2.2	December 6.....	205
6.2.3	November 28.....	209
6.3	Estimation for the Auto Spectra.....	211
6.4	An Attempt at Daytime Observation.....	215
6.4.1	Frequency Changing.....	215
6.4.2	Daytime Results.....	216
6.5	A Probability Distribution for Interference.....	219
6.6	Comparison to the Log-Normal Distribution.....	230
6.7	General Comments on the Observations.....	232
7	CONCLUSIONS.....	234
7.1	System Performance.....	234
7.2	Recommendations for Further Research.....	237
	REFERENCES.....	240
	APPENDIX 1 - A Derivation of Equivalent Integration Time.....	248
	APPENDIX 2 - Products of Gaussian Variables.....	251
	APPENDIX 3 - Microcomputer Observing Program.....	256
	APPENDIX 4 - Robust Estimation Program.....	281
	APPENDIX 5 - FFT Processor Schematics.....	289

List of Tables

Table		Page
2.1	Spectral Correlation Coefficients for Kaiser-Bessel Window.....	40
2.2	Memory Addresses for an 8-Point Decimation-in-Time FFT.....	56
2.3	Powers of W for Coefficients in 8-Bit Decimation-in-Time FFT.....	56
2.4	Correlation Test Results.....	90
2.5	Auto Spectrum Levels and Cross Spectrum Variance ($K=10^5$).....	90
2.6	Variance of the Means of the Cross Spectra ($K=10^5$, No. of Components = 120).....	91
4.1	Variance-Covariance Matrix for the Complex Spectra of Two Partially Correlated Gaussian Signals.....	110
4.2	Numerical Properties of Some Robust M-Estimates...	140
4.3	Asymptotic Expected Value and Standard Deviation of Quantiles of the Normal Curve.....	149
5.1	Losses and Electrical Lengths of Receiver Cables at 5.0 MHz.....	166

List of Figures

Figure	Page
1.1	Diurnal Critical Frequency Variations.....15
2.1	Complex Butterfly Computation for Decimation-in-Time FFT.....52
2.2	Real Butterfly Computation for Decimation-in-Time FFT.....52
2.3	Butterfly Diagram for an 8-Point Decimation-in-Time FFT.....54
2.4	Block Diagram of the FFT Processor.....57
2.5	Windowing Stage.....60
2.6	Butterfly Processor.....63
2.7	Power Spectrum Computation.....66
2.8	Accumulation Stage.....68
2.9	The Microcomputer.....72
2.10	FFT Processor Spectrum of Sinusoid Using Rectangular Window.....77
2.11	FFT Processor Spectrum of Sinusoid Using Kaiser-Bessel Window.....78
2.12	Power of Cross Spectrum Sinusoidal Components vs Phase Angle.....80
2.13	Cross Spectra of Delayed Noise (Delay=100 μ sec)....82
2.14	Cross Spectra of Delayed Noise (Delay=200 μ sec)....83
2.15	Equivalent Noise Levels of Spectra vs Correlated Noise Input Level.....84
2.16	Roundoff Noise vs Sinusoidal Input Level.....86
3.1	Receivers.....93
3.2	Second Mixer and IF Amplifier.....94
3.3	RF Amplifier, First Mixer and IF Amplifier.....99
3.4	Input Bandpass Filter.....102

Figure		Page
3.5	Reversible Current Source for Synchronous Modulation.....	104
4.1	Influence Curves for Robust M-Estimates.....	136
4.2	Cumulative Area Under a Standard Normal Curve.....	148
5.1	A View of the DRAO 22.25 MHz Telescope.....	160
5.2	Basic Array Element for 22.25 MHz Telescope.....	161
5.3	Sub-Arrays of Polar Synthesis Telescope.....	163
5.4	Connections for Measurement of Cable Lengths and Losses.....	165
5.5	Equipment Layout in the Observatory Building.....	169
5.6	The FFT Processor.....	169
6.1	Fringes with Interference - November 29, 1979.....	176
6.2	Fringes with Interference - January 4, 1980.....	177
6.3	Fringes after Interference Removal - November 29, 1979.....	179
6.4	Fringes after Interference Removal - January 4, 1980.....	180
6.5	Spectra and Histograms - November 29, 1979.....	184
6.6	Spectra and Histograms - November 29, 1979.....	185
6.7	Spectra and Histograms - November 29, 1979.....	186
6.8	Fringes after Interference Removal - November 27-28, 1979.....	188
6.9	Fringes after Interference Removal - November 28, 1979.....	192
6.10	Fringes after Interference Removal - December 4, 1979.....	194
6.11	Fringes after Interference Removal - December 5, 1979.....	197
6.12	Fringes after Interference Removal - December 6, 1979.....	200
6.13	Fringe Phase and Amplitude - December 4, 1979.....	203

Figure	Page
6.14	Auto Spectra, their Geometric Mean, and Cross Spectrum Amplitude - December 4, 1979.....204
6.15	Fringe Phase and Amplitude - December 6, 1979.....206
6.16	Fringe Phase and Amplitude - December 6, 1979.....207
6.17	Auto Spectra, their Geometric Mean, and Cross Spectrum Amplitude - December 6, 1979.....208
6.18	Fringe Phase and Amplitude - November 29, 1979....210
6.19	Auto Spectrum Estimates - December 6, 1979.....212
6.20	Auto Spectrum Estimates - January 4, 1980.....214
6.21	Fringes after Interference Removal - January 6, 1980.....217
6.22	Histogram of Cross Spectrum Probability vs Amplitude - December 6-7, 1979.....223
6.23	Histogram of Cross Spectrum Probability vs Amplitude - December 4, 1979.....224
6.24	Histogram of Cross Spectrum Probability vs Amplitude - January 4, 1980 - 18:30 to 19:30.....225
6.25	Histogram of Cross Spectrum Probability vs Amplitude - January 4, 1980 - 20:00 to 21:00.....226
6.26	Histogram of Cross Spectrum Probability vs Amplitude - January 6, 1980.....227
6.27	Histogram of Cross Spectrum Probability vs Amplitude - December 5, 1979 - Frequency = 22.175 MHz.....228
6.28	Histogram of Cross Spectrum Probability vs Amplitude - December 5, 1979 - Frequency = 22.325 MHz.....229
6.29	Log-Normal Curves.....231
A5.1	Clipping Detector and Input Multiplexer.....291
A5.2	Window Multiplier and Coefficient Memory.....292
A5.3	Window Control and Clocking.....293
A5.4	Window Pseudorandom Sequence Generator.....294

Figure	Page
A5.5	Butterfly Processor.....296
A5.6	FFT Control and Clocking.....297
A5.7	Butterfly Pseudorandom Sequence Generator.....298
A5.8	Overflow Anticipation and Scaling Counter.....299
A5.9	Overflow Correction.....300
A5.10	Input Buffer and FFT Timing.....301
A5.11	FFT Address Generation.....302
A5.12	Output Buffer and Address Generation.....304
A5.13	Power Computation Board.....305
A5.14	Scaling Registers and Control.....307
A5.15	Accumulation and CCD Memory.....308
A5.16	Master Clock and DMA Control.....309
A5.17	DMA Buffers and Address Generation.....310
A5.18	Analog-to-Digital Conversion.....311

1. Introduction

Nearly all of man's knowledge of the universe beyond our own planet has been derived from the study of electromagnetic radiation emitted by the cosmos. Astronomy began at visible wavelengths and was confined there until 1932 when Jansky discovered extraterrestrial radio emissions and opened the door to an exciting new field of radio astronomy. Presently, astronomy is conducted from radio wavelengths up to gamma rays, with additional studies of cosmic rays, gravitational waves, and neutrino emissions.

Radio astronomy had its beginnings at decametre wavelengths, but quickly moved to higher frequencies as radio technology progressed. Because of a number of difficulties mainly associated with the ionosphere, low frequency astronomy has received comparatively little attention. In recent times, new regions of the spectrum have often yielded new and unexpected discoveries. A thorough exploration of the sky at decametric and longer wavelengths could therefore add considerably to our understanding of the universe.

The subject of this thesis is an experimental attempt to overcome one of the problems which plagues low frequency astronomy, namely interference from terrestrial radio transmissions. Digital spectral analysis is employed to produce spectra in which narrowband man-made signals stand out from broadband cosmic signals. By applying robust estimation techniques to the spectra, it is possible to

exclude the narrowband, interfering signals and accurately measure cosmic signals.

It is hoped that through the removal of terrestrial interference it will be possible to considerably enhance the accuracy of observations and to greatly extend the amount of time during which suitable observing conditions are present for low frequency astronomy.

This chapter will discuss decametric astronomy and the difficulties which it presents. The ionosphere and its effects on terrestrial and astronomical radio signals will be described. Previous attempts to deal with the problem of terrestrial interference will also be discussed.

1.1 Decametric Astronomy

The longest wavelengths where astronomy has been attempted to any degree are in the decametric region. There are a number of areas of astronomy for which decametric observations are important and can contribute significantly to the understanding of astrophysical phenomena. The following discussion is based upon Routledge [1], Dewdney [2] and Kraus [3].

Decametric astronomy may be divided into studies of discrete sources and extended sources. Discrete sources are point-like sources which are smaller in angular extent than the resolving power of a telescope, for example some distant galaxies. Intensities of discrete sources are expressed in terms of total observed flux density, $S(f)$, with the unit

being the Jansky (10^{-26} watt m^{-2} Hz^{-1}). Extended sources are larger in angular extent with an intensity which changes smoothly over the source, for example large interstellar clouds of ionized hydrogen (HII). Measurements are in terms of brightness, $B(f)$, in Jansky-steradian $^{-1}$, or equivalent black-body temperature, $T(f)$, in degrees Kelvin.

One of the most important features of radio sources is the spectrum (intensity vs frequency). No strong spectral lines have been found below 1000 MHz, thus at low frequencies radio emissions are not frequency selective. Instead, all frequencies are present producing a continuum of radiation with no discontinuities. Intensity is found to vary with frequency in a smooth fashion,

$$S(f) = (\text{const}) f^{-\alpha(f)}$$

or
$$T(f) = (\text{const}) f^{-\beta(f)}$$

$\alpha(f)$ and $\beta(f)$ are known as the flux density spectral index and temperature spectral index, respectively. They are generally positive, implying that intensity increases as frequency decreases.

1.1.1 Discrete Sources

Discrete sources may be classified as galactic or extragalactic. Galactic sources include supernova remnants and small HII regions.

Supernova remnants radiate due to the synchrotron mechanism. A supernova explosion produces an expanding cloud

of matter containing relativistic electrons (about 10^{12} eV) and magnetic fields. The electrons, which may continue to be generated by remnants of the explosion, interact with the magnetic field to produce synchrotron emission. If the electrons have an energy spectrum of the form

$$N(E) = (\text{const}) E^{-\nu}$$

where $N(E)$ = number of electrons as a function of energy

E = energy of electron

ν = energy spectrum index

then the synchrotron radiation will have a characteristic spectrum given by

$$S(f) \propto f^{-(\nu-1)/2}$$

Observations have shown that the above spectrum is typical of many non-thermal radio sources over a wide range of frequencies. However, at low frequencies the intensity would tend towards infinity, thus at some point a turn-over in the spectrum is necessary. Low frequency astronomy is necessary for investigations of the turn over of non-thermal radio sources, in order that the nature of such sources may be more clearly understood.

The study of synchrotron emissions produces information about the physical structure and the evolution of the sources. Calculations may be made of plasma densities, magnetic field strengths and relativistic particle densities. A number of mechanisms believed to cause

deviations from a straight power-law spectrum can also be examined. These include variations from a power law in the source of relativistic electrons, multiple sources of electrons with different energy spectra, thermal absorption by ionized gas either within the source or between the source and the earth, and synchrotron self-absorption within the source.

An interesting class of sources which has been discovered through decametric astronomy is steep spectrum sources possessing higher spectral indices than expected at low frequencies. Study of these objects, for example the source at the center of the Crab Nebula, may produce clues to the history of supernova remnants.

Extragalactic sources are generally galaxies or clusters of galaxies, some of which emit enormous amounts of energy. These extremely powerful radiation sources have attracted much attention because they defy many previously accepted notions about the universe. Optical counterparts of strong radio sources include giant elliptical galaxies, N-type galaxies, and quasi-stellar objects (quasars).

Extragalactic sources are non-thermal in nature and often emit because of the synchrotron mechanism. Low frequency studies of such objects may help to explain the origin of the enormous energies produced.

1.1.2 Extended Sources

With the comparatively low resolution of present

decametric telescopes, observable extended sources are confined to our own galaxy. The major type of extended source is interstellar plasma produced by low-intensity ultraviolet radiation from early-type stars and by low-energy cosmic rays. Although ionized hydrogen does emit thermal radiation at decametric wavelengths, it is most easily observable because of its absorption of non-thermal emissions from the galactic background. Free-free absorption causes HII regions to appear as localized areas of reduced brightness or reduced spectral index against the brightness of the galaxy. Low frequency telescopes provide one of the most sensitive methods of detecting interstellar HII.

Decametric mapping of the distribution of HII in the galaxy would be an important contribution to studies of galactic structure and galactic dynamics.

1.1.3 Existing Decametric Telescopes

High-quality low frequency radio telescopes are difficult and expensive to build. The frequencies and angular resolutions of 21 telescopes constructed since 1958 for use below 100 MHz are summarized in a CCIR Report [4]. Below 20 MHz the best resolution obtained has been a few degrees, and major studies have been limited to two source surveys ([5], [6]) and measurements of the galactic background ([7], [8]).

1.2 Limitations to Low Frequency Astronomy

There are three major factors which tend to discourage attempts at low frequency astronomy:

1. Very large antenna dimensions (several kilometers or more) are required for good resolution.
2. Low frequency signals are highly susceptible to distortion by the ionosphere. The ionosphere can cause refraction, scintillation and absorption of signals from cosmic sources.
3. No frequencies below 20 MHz have been set aside exclusively for radio astronomy¹. The radio spectrum in this region is used extensively for terrestrial communications. Long distance propagation via ionospheric reflections is possible, making it extremely difficult if not impossible to find sites for telescopes which are immune to terrestrial interference.

The resolution of an antenna in a plane is about equal to the half-power beam width in that plane [3]. In an idealized situation, the number of resolvable sources distributed uniformly over the sky is approximately given by

$$N_r = \frac{4\pi}{\Omega_A}$$

where Ω_A = antenna beam solid angle, rad². Beam solid angle is related to antenna effective aperture, A_e , and wavelength

¹A new band from 13360 to 13410 kHz was allocated to radio astronomy during the 1979 World Administrative Radio Conference in Geneva. This allocation is not exclusive but is to be shared with the Fixed service.

λ as follows:

$$\Omega_A = \lambda^2 / A_e$$

To maintain a given resolution the linear dimensions of an antenna must increase proportionally with wavelength. For example, to obtain a resolution of 5 arc minutes, as is possible at microwave frequencies with large dish antennas, would require an antenna 10 km in extent at 20 MHz. No antennas of that size presently exist. The largest ones built to date are about 3 km.

Fortunately, an antenna 10 km in extent or 100 km² in area need not be completely filled to produce the desired resolution. Early telescopes (for example Mills [9]) were built in the form of crosses, T's and circles to take advantage of this fact. Development of the principles of aperture synthesis by Ryle and Hewish [10] showed that an antenna may be decomposed into a number of elemental units, and that it is only the relative positions or spacings of the units which are fundamentally important. Measurements with a resolution equivalent to that of a very large filled antenna may be made by combining signals from smaller antennas with all the elemental spacings between them.

For sources which are not time-variable, the observations at different spacings need not be made simultaneously. Therefore an antenna of any chosen size may be synthesized by using just two small elementary units which can be moved to all of the required positions to

produce the spacings of the desired large antenna. Indeed, it is possible to let the rotation of the earth provide part of the movement of the two antennas relative to the sky. Such earth rotation aperture synthesis as described in Fomalont [11] is now commonly used for high resolution mapping of the sky.

The result of all this is that resolution at low frequencies is not fundamentally limited by the large antenna sizes required. Limitations due to the ionosphere are much more difficult to overcome.

1.3 The Ionosphere

The following discussion is derived mainly from Davies [12].

The earth's ionosphere is produced by high-energy radiation from the sun, mainly in the ultraviolet and soft X-ray regions. Electron density depends upon many factors, including the intensity and spectrum of incoming radiation (some of which may be screened by higher ionospheric layers), atmospheric density, and chemical composition at the altitude in question. Solar control results in a strong dependence on the time of day (or night), the season, latitude, and the level of solar activity at a given time. Also, the electrical nature of the ionosphere causes it to interact a great deal with the earth's magnetic field.

The ionosphere has attracted a tremendous amount of study since the 1940's, largely due to its importance in

radio communications. Although most of its properties have been characterized and its long-term behavior is reasonably well understood, day-to-day ionospheric activity is highly variable and somewhat unpredictable, much like the earth's weather.

The ionosphere is generally divided into a number of regions, the most important of which are termed the D, E and F regions. The D region extends in height from approximately 50 km to 90 km, the E region from 90 km to 130 km, the F region from 130 km to perhaps 500 km.

D-region ionization is largely a daytime phenomenon, as the relatively high atmospheric density allows rapid recombination after the ionizing radiation disappears. The D region is mainly responsible for the absorption of radio signals. AM radio transmissions, for example, are limited in daytime propagation distance by D-region absorption, whereas at night they can propagate much farther.

The E region is also normally significant only in daylight. It reflects radio signals below a maximum of about 10 MHz. The usual E-region ionization is not important for terrestrial propagation above this frequency. However, there is a version of the E region known as sporadic E which is sometimes very significant. Sporadic E, as the name suggests, is a transient, unpredictable and often localized phenomenon. When it is present, sporadic E can allow much longer distance radio communication at higher frequencies than would normally be expected.

During the day the F region splits into two layers. The lower one is termed the F_1 layer and the upper one, the F_2 layer. The F_1 layer, which disappears at night, reflects radio frequencies somewhat higher than those reflected by the E region. Like the E region, the electron content of the F_1 layer is higher in summer than in winter.

The part of the ionosphere which is the most important for HF radio communication, and also the most detrimental to radio astronomy, is the F_2 layer. This layer almost always contains the maximum electron density in the ionosphere. Recombination occurs very slowly, hence the F_2 layer is present at night and reaches a minimum electron density just before sunrise. The seasonal minimum is during the winter night, as it is for other layers. Surprisingly, however, the seasonal maximum occurs during the winter day rather than during the summer day. This peculiarity of the F_2 layer is termed the "winter anomaly".

1.4 Ionospheric Radio Propagation

The refractive index of an ionized medium depends upon the electron density. If the collision frequency between electrons and neutral molecules or ions is low (as in the rarified upper atmosphere of the E and F regions) then absorption of radio energy is negligible. If the magnetic field is assumed to be zero, then the refractive index is [13]

$$n = [1 - (f_p/f)^2]^{1/2} \quad (1.1)$$

where f_p is the plasma frequency given by

$$f_p = \left[\frac{Ne^2}{4\pi^2 \epsilon_0 m} \right]^{1/2} \quad (1.2)$$

with N = electron density

e = electronic charge

ϵ_0 = permittivity of free space

m = electron mass

If a magnetic field is present the situation becomes more complex. Two electromagnetic waves which are circularly polarized in opposite directions (termed "ordinary" and "extraordinary" waves) will propagate with two different indices of refraction. The refractive index for the extraordinary wave is the higher of the two.

The frequency at which the refractive index becomes zero is termed the critical frequency, f_c . At this frequency or below it a normally incident wave cannot propagate but is instead entirely reflected. Extraordinary waves exhibit a higher critical frequency, f_x , than do ordinary waves, f_o , due to the difference in refractive indices.

At frequencies above f_c an obliquely incident wave may still be completely reflected. The maximum frequency which will be completely reflected at a given angle of incidence ϕ_i is given by

$$f_{\max} = f_c \sec \phi_i \quad (1.3)$$

In propagation studies the term maximum usable frequency (MUF) is used for the maximum frequency which can be reflected between two points a given distance apart on the earth's surface. The angle of incidence for reflection at a given distance depends upon the height of the reflecting layer. If the curvature of the earth and ionosphere plus the normal height of the F_2 layer are considered, it may be shown [18] that the largest angle of incidence possible for reflection back to the earth's surface is usually about 74 degrees. The maximum usable frequency at this limiting angle is

$$MUF = f_c \sec 74^\circ = 3.6 f_c \quad (1.4)$$

From a propagation viewpoint, maximum usable frequency is quite important. D-region absorption increases with wavelength, so it is advantageous to operate on the highest frequency which will support reliable reflections. HF radio users, with the help of ionospheric propagation forecasts, often change operating frequencies to obtain maximum propagation distances.

Critical frequency and hence MUF vary regularly through the day as the sun's angle changes and through the seasons as the length of day and solar angle vary. In addition, a strong dependence exists on the 11-year sunspot cycle.

Figure 1.1, taken from Jordan and Balmain [19], illustrates diurnal critical frequency variations for the E, F_1 , and F_2 layers in winter and summer, and at sunspot minimum and maximum. The critical frequency of the F_2 layer, f_oF_2 , is higher during the day than at night, and higher in winter than in summer. At sunspot maximum f_oF_2 is approximately twice its value at sunspot minimum.

1.5 Ionospheric Effects on Radio Astronomy

The major effects which the ionosphere has on astronomical signals are absorption, refraction and scintillation.

1.5.1 Absorption

Virtually all absorption at decametric wavelengths occurs in the D region which is present only during the day. The degree of absorption is dependent on frequency and reaches a broad maximum near the gyro-magnetic frequency for an electron in the earth's magnetic field (1.2 to 1.4 MHz). A device called a riometer [20] may be used to measure absorption by monitoring the average signal strength from a broad area of the sky.

1.5.2 Refraction

For a plane, stratified ionosphere, incoming waves at a frequency f above the F-layer critical frequency f_c will propagate through the ionosphere provided that the source is

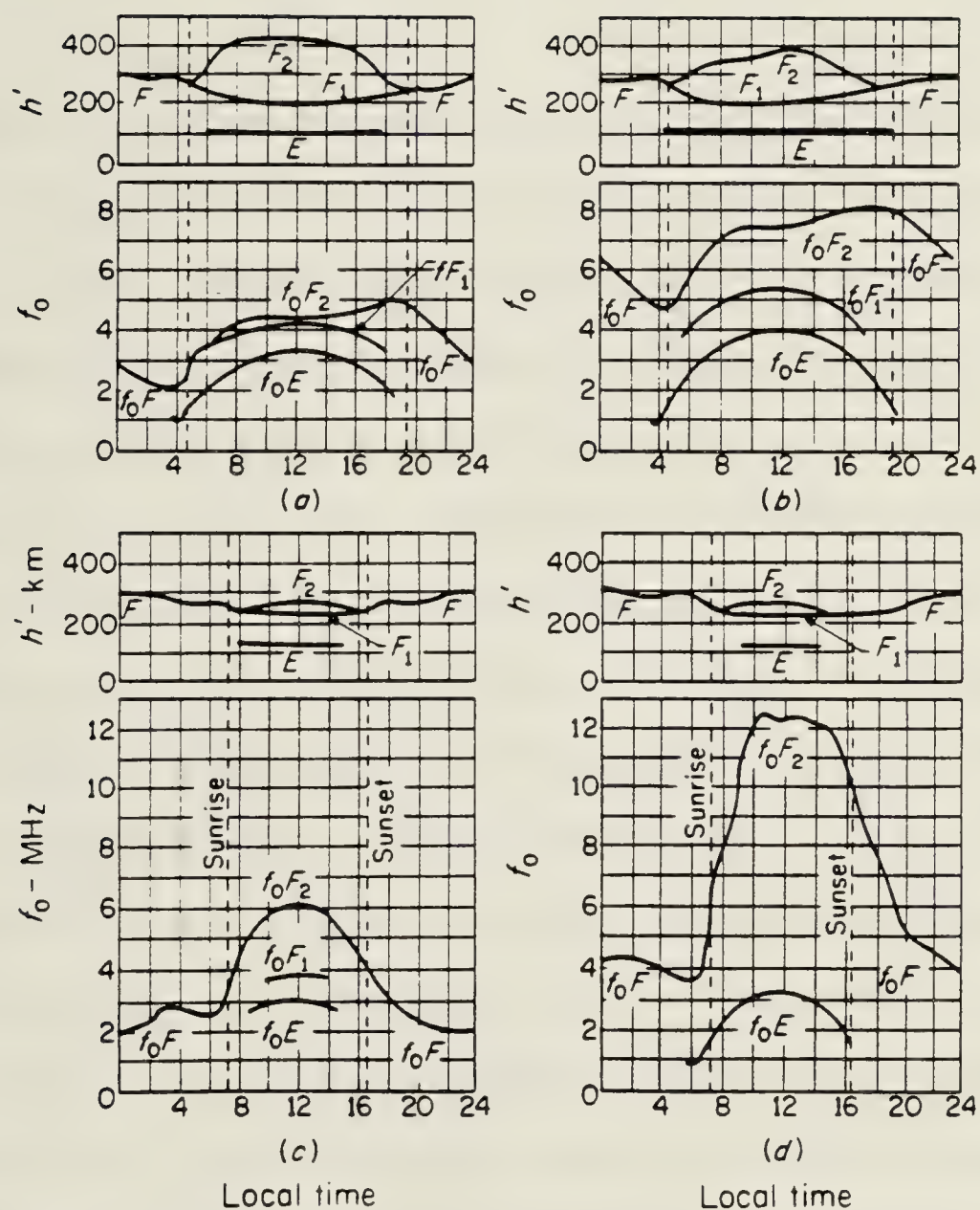


Figure 17-8. Diurnal variation of critical frequency and virtual height of the regular ionospheric layers: (a) summer at period of sunspot minimum; (b) summer at sunspot maximum; (c) winter at sunspot minimum; (d) winter at sunspot maximum.

Figure 1.1. Diurnal Critical Frequency Variations

within a cone centered on the zenith and defined by a limiting zenith angle [4]

$$\phi_c = \arccos (f_c/f)$$

For a spherical ionosphere the actual limiting angle will be slightly larger. Spherical stratification produces a slight refraction of signals passing through the ionosphere such that the apparent zenith angle is less than the true zenith angle by a small amount [21].

Uniform horizontal variations in ionospheric electron density, such as occur at sunrise and sunset, are another cause of refraction [22]. Such gradients may cause refraction of a few degrees if the observing frequency is less than twice the critical frequency.

Correction for refraction may be accomplished by monitoring the apparent positions of calibration sources, provided one is using an antenna which can provide a narrow beam to track the sources at any given time. However, as refraction is a time-varying phenomenon, it would be extremely difficult to correct for in the case of aperture synthesis which relies on time-invariant source positions.

1.5.3 Scintillation

A transient phenomenon which can seriously distort signals traversing the ionosphere is scintillation. If the ionosphere contains irregularities or inhomogeneities in electron content, then the index of refraction will vary for

rays having different paths. As a result, a plane wave impinging on the ionosphere will have horizontal phase variations when it emerges below the ionosphere. Such phase variations are converted to both phase and amplitude variations due to interference effects as the wave propagates towards the earth's surface. As a result, a radio source appears to "twinkle" just as a star does optically when seen through the turbulent atmosphere. A discussion of scintillation is contained in Briggs [23].

The irregularities which cause scintillation occur mainly in the F region and have been correlated with observations known as "spread-F" during ionospheric sounding [14]. Spread-F consists of multiple reflections of probing radio signals from points within the F region, and is consistent with the idea of irregularities in electron density in this region.

Fortunately, scintillation is present only on occasion. It is most frequently observed near the equinoxes of a solar maximum [15]. During solar minimum, scintillation occurs mainly at night, whereas during solar maximum it is equally likely by day or night. Geographically, scintillation is least likely at temperate latitudes. For astronomy, the severity of scintillation is dependent upon the scale of irregularities and upon antenna size. Irregularities are generally found to be from about 0.5 to 10 km in extent [4]. For antennas larger than 2 km, amplitude and phase variations will be produced across the aperture and may

distort the antenna beam. For smaller antennas (and larger beam widths) larger phase variations can be tolerated.

The effects of scintillation are most severe at low frequencies because the ionosphere's refractive index goes from 1.0 to 0.0 as frequency decreases and approaches the critical frequency. Fortunately, periods which are free of scintillation do occur, particularly during years of low solar activity. Such periods may last for weeks or even months. Maximum use must be made of these favorable conditions when they are present.

1.6 Terrestrial Interference

For radio telescopes operating at below 3 or 4 times f_c , interference from radio transmissions is a continuous problem. There are many paths which interfering signals can take, including single hops, multiple hops with intermediate reflections from the earth's surface (possibly at almost any angle), or multiple hops with intermediate reflections from the tops of patches of sporadic E ionization.

Often a signal will reach a receiving antenna simultaneously via a number of slightly different paths. The result is fading [24], as the signals will generally be different in phase. If all received components are approximately equal in amplitude but have random relative phase, the probability density of the resultant instantaneous amplitude A will have a Rayleigh distribution $f(A)$ given by

$$f(A) = \frac{2A}{A_m^2} \exp(-A^2/A_m^2) \quad (1.5)$$

where A_m^2 is the mean square value of A . A Rayleigh distribution is found to give a good approximation to the short-term distribution of wave amplitude at long distances when only sky waves (ionospheric reflections) are involved and no ground wave is received. In the case of a strong undisturbed component (such as a ground wave or specularly reflected sky wave) plus weak randomly scattered sky waves the resultant amplitude will have a Rice distribution given by

$$f(A) = \frac{A}{\Psi} \exp\left[-\frac{(A^2+B^2)}{2\Psi}\right] I_0\left[\frac{AB}{\Psi}\right] \quad (1.6)$$

where Ψ = total power in signal

A = amplitude of resultant

B = amplitude of undisturbed component

I_0 = modified Bessel function of the first kind of order zero

If the random components are very small relative to the undisturbed component, the Rice distribution converges to a normal distribution.

The above distributions are commonly observed for signals for which fading is present due to interference among multiple wavelets. The rate of such fading is generally quite rapid, occurring on a time scale of seconds to a few minutes.

Slower, long-term variations in signal strength occur due to changes in ionospheric conditions. Long-term variations in signal power p are experimentally found to fit a log-normal distribution [25] given by

$$f(p) = \frac{1}{p\sigma\sqrt{2\pi}} \exp \left[-\frac{[\log(p/m)]^2}{2\sigma^2} \right] \quad (1.7)$$

where m = median signal power, $m > 0$

σ = standard deviation of the natural logarithm of signal power

If signal strength is expressed logarithmically (in dB) then a normal distribution results.

$$f(p) = \frac{1}{\sigma\sqrt{2\pi}} \exp \left[-\frac{(p-m)^2}{2\sigma^2} \right] \quad (1.8)$$

where p = signal strength in dB

m = median signal strength in dB

σ = standard deviation of signal strength in dB

Measurements of hourly median signal strengths for a given time of day and a given season of the year have been found to fit the above distribution reasonably well [26].

Decametric interference is difficult to escape entirely. As mentioned before, propagation via ionospheric reflections is generally possible only if the transmitting frequency is not more than 3 or 4 times f_c . Most interference therefore subsides if the ionosphere's critical frequency drops, as radio users are forced to switch to lower frequencies to maintain reliable ionospheric skip. However, ground wave communication over shorter distances is

still possible, so not all higher frequency transmissions will cease. Also, if observations are carried out at night when electron densities are low there is a possibility that the critical frequency on the other side of the earth will be high enough to support propagation. Signals from the sunlit side may find ways to reach a telescope at night. A prime candidate to allow such an occurrence is sporadic E ionization [16]. At middle latitudes, sporadic E is more prevalent in summer than in winter and during the day rather than at night. However, it can possibly occur at any given time. One suspected source of sporadic E is meteor trails.

In any case, interference to low frequency astronomy can potentially occur at any time and any place on the surface of the earth.

Suggestions have been made that low frequency telescopes could be freed of ionospheric limitations by being built in space. An orbiting telescope, however, could be subject to as much or likely even more terrestrial interference than ground-based telescopes. One location which would perhaps be the most ideal is the far side of the moon [27]. However, such a telescope would appear to be a fair distance in the future.

Another interesting idea which has been proposed is the creation of a temporary window in the ionosphere through which decametric observations could be conducted [28]. Such a window might be created by injecting hydrogen into the night-time ionosphere to reduce electron densities.

Interference removal during observations through an artificial window would be highly desirable, as interference could be reflected from the remainder of the ionosphere surrounding the window. If one went to the trouble (and expense) of creating an artificial window, one would want to maximize the chances of successful observing.

1.7 Previous Attempts to Deal with Interference

Most low frequency astronomers in the past have simply waited for opportunities when ionospheric electron densities are low enough to prevent significant interference problems. Low frequency astronomy is most successful during a period of sunspot minimum. Winter nights are particularly attractive. However, even at such favorable times observing conditions are often unsuitable. For example, Dewdney [2] found that out of 70 nights of observing during a solar minimum only about 12 produced results of adequate quality for making synthesis maps. The remaining 83% of observations were unsatisfactory due to interference, scintillation and refraction.

A few limited attempts have been made in the past to eliminate interference received by low frequency telescopes.

In 1958, Shain [29] used a series of manually tuned filters in conjunction with a Mills cross telescope at 19.7 MHz. Four 4.5 kHz bandwidth filters could be adjusted to interference-free gaps in a 100 kHz wide section of the spectrum at 19.7 MHz. Adjustment was done by an

operator who monitored the filter outputs on a loudspeaker. Shain reports that there were generally a few gaps in the spectrum which would remain clear of interference, and the filter system was successful in reducing problems with terrestrial transmissions.

In Tasmania ([7], [30]) a swept filter technique has been used to avoid interference at frequencies of 4.7 and 10.02 MHz. A narrow filter of 2 to 3 kHz bandwidth was swept through a region of the spectrum 10 to 12 kHz wide at a rate of about 5 times per second. A minimum detection circuit then measured cosmic noise in clear channels between transmitting stations. Although this method does work, it limits the total observing bandwidth to a few kilohertz and is relatively insensitive to interference as the spectral resolution is poor. Effective integration times are also short.

Russian astronomers using the UTR-1 telescope at Grakovo [6] in 1966-68 have also reported on their methods of handling interference. Their receivers employed a variable bandwidth of from 3 to 14 kHz. The bandwidth was reduced at times when interference was being received. In addition, they mention "fast radiometer retuning" to avoid terrestrial signals, evidently implying the presence of a human operator who monitored received signals and kept the receivers away from interference.

Human interference detectors as at Grakovo and as mentioned by Shain are undoubtedly very sensitive to

interfering signals, particularly if auditory discrimination is employed. However, most humans would find 12 consecutive hours or so (in the middle of the night) of straining to hear radio signals somewhat tedious. A sensitive automatic system which could maximize the available interference-free bandwidth at any given time would probably be welcome.

With a view to characterizing the electromagnetic environment from 1.5 to 6.0 MHz, Wheeler [31] conducted a study which involved frequency-domain interference excising. The eventual objective of this work was the identification and rejection of narrowband interference from wideband (spread-spectrum) communications systems, which in principle is the same problem faced in radio astronomy. Wheeler recorded radio signals on magnetic tape and analyzed the power spectra digitally. Identifiable interfering signals were found to fit log-normal distributions, with distribution parameters depending upon the time of day and the season.

1.8 Interference Detection via Spectral Analysis

The proposed interference rejection system is based upon the correlation receiver, as this type of receiver is commonly used throughout radio astronomy for interferometry and aperture synthesis.

The simplest method of detecting interfering signals is through spectral analysis, as a priori knowledge of the frequencies and modulation of the signals is not required.

Terrestrial communications signals at decametric wavelengths are narrowband (except for military spread-spectrum systems) and may be distinguished from astronomical signals which are essentially Gaussian noise on that basis. Typical bandwidths of communications signals are 6 kHz for amplitude modulation (AM), 3 kHz for single-sideband (SSB), 1.2 kHz for frequency-shift-keyed telegraphy (FSK) and 100 Hz for continuous-wave telegraphy (CW). International agreements and government licensing restrict various classes of users to certain allocated frequency bands.

For a correlation receiver, spectral analysis is possible through calculation of the cross power spectrum. Such a spectrum consists of real and imaginary components at each frequency, with the real components (the in-phase or co spectrum) showing correlated signals which are in-phase (or in anti-phase) and the imaginary components (the quadrature spectrum) showing correlated components which differ in phase by 90 degrees (or 270 degrees).

In correlation analysis the process of averaging is used to improve signal-to-noise ratio if uncorrelated noise is present and signals are relatively stationary over the averaging interval. In astronomy, averaging or "integration" is usually essential as signals from sources are often very weak compared to uncorrelated noise received from other regions of the sky in the antenna beam at low frequencies or compared to receiver noise at high frequencies.

For the purpose of interference detection, the

sensitivity of a system employing cross spectral analysis will depend upon the resolution and the amount of averaging. For maximum sensitivity the resolution should be less than the bandwidth of the most distinguishing features of the spectra of interfering signals. AM and CW both involve the modulation of a continuous carrier. A steady carrier has zero bandwidth, implying that the sensitivity for detection of such signals will increase without limit as resolution is made finer. An FSK signal may or may not exhibit sharp peaks in its spectrum. A SSB signal generally will not contain any peaks. If peaks are not present then there is no advantage in having a resolution which is less than the signal's bandwidth.

Through averaging, the sensitivity will increase in proportion to the square root of the length of the averaging interval. The maximum averaging interval which may be used is limited by the duration of time over which the signal remains stationary (if the signal disappears or reverses its phase, continued averaging is counterproductive to its detection).

1.9 A Method of Rejecting Interference

The subject of the remainder of this thesis is an experimental system employing cross spectral analysis which was designed and built to investigate the possibility of detecting and removing terrestrial interference from signals received by a low frequency radio telescope. Spectral

analysis is accomplished in real time by a digital fast Fourier transform processor. Automatic computer analysis of the spectra is used to identify interference and to estimate the levels of broadband astronomical signals after interference has been excluded.

2. The Fast Fourier Transform Processor

2.1 Introduction

Spectral analysis in radio astronomy was initially accomplished with banks of analog filters dividing the spectrum into many separate channels. Analog filters, however, exhibit a number of problems. Precise filters require careful construction and are expensive. Temperature sensitivity and component aging cause the performance of analog circuits to change with time. These problems made astronomers look to stable digital circuits as an alternative.

Digital spectral analysis was pioneered by Weinreb [32] in 1963. Weinreb's technique involved the quantization of an analog signal into a one-bit digital signal. The digital signal was then correlated with delayed versions of itself to produce an autocorrelation function. A Fourier transform of the autocorrelation function produced the power spectrum. The advantage of Weinreb's method is that inexpensive and stable digital hardware replaces expensive and unstable analog hardware. The method can be easily adapted to cross spectral analysis and its performance can be improved by using more levels of quantization, as for example in the Dominion Radio Astrophysical Observatory's synthesis telescope [33].

Digital correlation spectrometers of this kind are well suited to high frequency radio astronomy where bandwidths of

many megahertz are necessary and can be obtained by employing a large number of correlators operating in parallel. In addition, spectral lines being observed are relatively weak in comparison to the total power being received, hence the dynamic range of the correlators need not be large and quantization can be relatively coarse. Coarse quantization allows the correlators to be simple and inexpensive, thereby making correlation spectrometers economically attractive.

In more recent years, the advent of the fast Fourier transform and improvements in digital technology have made spectral analysis by direct Fourier transformation a possibility. As is well known, the FFT reduces the number of arithmetic operations needed to calculate a discrete Fourier transform of N points from the order of N^2 to the order of $N \log_2 N$. For large N , savings in computation time are quite considerable.

By reducing the amount of computation required, the FFT has the potential for the construction of simpler spectrometers than the correlation spectrometers described above. A number of FFT Spectrometers such as one at the Dudley Observatory [34] are already in use for radio astronomy. However, though the *number* of arithmetic operations is less, the *complexity* of the operations is much greater. For example, the number of bits of accuracy must be larger to avoid the accumulation of roundoff errors. Also, the control circuitry needed is far more complex than for a

correlation spectrometer where all stages are essentially identical. Thus, the greater overhead in circuitry required for FFT spectrometers has tended to reduce their attractiveness in high frequency astronomy where maximum bandwidth is essential.

For interference removal at low frequencies, in contrast, spectrometer requirements are reversed from those above. As radio sources tend to be bright at low frequencies, wide observing bandwidth is not needed for adequate sensitivity. As bandwidth after a certain point must be obtained by adding more parallel hardware, the cost of spectrometers at the limits of a particular digital technology is essentially proportional to the bandwidth. The cost of a spectrometer with 50 kHz bandwidth should therefore be 1/100 of one with 5 MHz bandwidth.

Wide dynamic range is essential for interference removal. Interfering signals can be received at levels far higher than background noise. Therefore, quantization of the incoming signals must be relatively fine to preserve information over the entire range of received signals. Also, the number of bits of accuracy retained in arithmetic calculations must be sufficient to not cause degradation of signal-to-noise ratio.

The requirements of low bandwidth and wide dynamic range give the FFT spectrometer an advantage in cost and complexity over the correlation spectrometer for low frequency interference removal.

2.2 FFT Basics

The fast Fourier transform emerged from obscurity in 1965 with the publication of a paper by Cooley and Tukey [35]. Since that time the FFT has found widespread application in all areas of data and signal processing. The derivation and properties of the FFT are well known and are described in many papers and texts such as [36], [38], [39], [40], [41], [42] and [43]. Some relevant aspects of the FFT are discussed below.

2.2.1 Calculation of the Cross and Auto Spectra

A method will be described which allows both the cross and auto spectra of two real series to be calculated with one FFT operation. Let $f(n)$ and $g(n)$ for $0 \leq n \leq N-1$ be two real series corresponding to digitized samples of radio signals from two antennas forming an interferometer. Assume $f(n)$ and $g(n)$ have discrete Fourier transforms (abbreviated DFT) given by $F(m)$ and $G(m)$ for $0 \leq m \leq N-1$.

$$\begin{aligned} F(m) &= \sum_{n=0}^{N-1} f(n) \exp(-j 2\pi nm/N) \\ G(m) &= \sum_{n=0}^{N-1} g(n) \exp(-j 2\pi nm/N) \end{aligned} \quad (2.1)$$

Note that $F(m)$ and $G(m)$ are complex.

The two real series $f(n)$ and $g(n)$ may be combined into one complex series $x(n)$ as follows:

$$x(n) = f(n) + j g(n)$$

Then by the linearity property, the DFT $X(m)$ of $x(n)$ will be

$$X(m) = F(m) + j G(m) \quad (2.2)$$

Symmetry properties for the DFT's of purely real or imaginary series may be used to find $F(m)$ and $G(m)$ from $X(m)$. The symmetry property for real series states that

$$\begin{aligned} F(N-m) &= F^*(m) \\ G(N-m) &= G^*(m) \end{aligned} \quad (2.3)$$

Therefore

$$\begin{aligned} X(N-m) &= F(N-m) + j G(N-m) \\ &= F^*(m) + j G^*(m) \\ X^*(N-m) &= F(m) - j G(m) \end{aligned} \quad (2.4)$$

Adding equations 2.4 and 2.2 and solving for $F(m)$ gives

$$F(m) = \frac{1}{2} [X(m) + X^*(N-m)] \quad (2.5)$$

Similarly, subtracting gives

$$G(m) = -j/2 [X(m) - X^*(N-m)] \quad (2.6)$$

From the above results, expressions for the cross and auto spectra are readily found. First of all, express $X(m)$ in terms of its real and imaginary components

$$X(m) = X_r(m) + j X_i(m)$$

The cross power spectrum of $f(n)$ and $g(n)$ is given by

$$\begin{aligned}
FG^*(m) &= F(m) G^*(m) \\
&= \left(\frac{1}{2} [X(m) + X^*(N-m)] \right) (-j/2 [X(m) - X^*(N-m)])^* \\
&= \left(\frac{1}{2} [X(m) + X^*(N-m)] \right) (j/2 [X^*(m) - X(N-m)]) \\
&= j/4 [X(m)X^*(m) - X(N-m)X^*(N-m)] \\
&\quad + j/4 [-X(m)X(N-m) + X^*(m)X^*(N-m)] \\
&= j/4 \{X_R^2(m) + X_I^2(m) - X_R^2(N-m) - X_I^2(N-m)\} \\
&\quad + j/4 \{-[X_R(m) + j X_I(m)] [X_R(N-m) + j X_I(N-m)] \\
&\quad \quad + [X_R(m) - j X_I(m)] [X_R(N-m) - j X_I(N-m)]\}
\end{aligned}$$

which after some algebraic manipulation produces

$$\begin{aligned}
FG^*(m) &= \frac{1}{2} [X_R(m)X_I(N-m) + X_I(m)X_R(N-m)] \\
&\quad + j/4 [X_R^2(m) + X_I^2(m) - X_R^2(N-m) - X_I^2(N-m)] \quad (2.7)
\end{aligned}$$

The real components of $FG^*(m)$ are the in-phase or co spectrum whereas the imaginary components are the quadrature spectrum.

The auto spectrum of $f(n)$ is given by

$$\begin{aligned}
FF^*(m) &= F(m) F^*(m) \\
&= \frac{1}{4} [X(m) + X^*(N-m)] [X^*(m) + X(N-m)] \\
&= \frac{1}{4} [X(m)X^*(m) + X(N-m)X^*(N-m) \\
&\quad + X(m)X(N-m) + X^*(m)X^*(N-m)] \\
&= \frac{1}{4} \{X_R^2(m) + X_I^2(m) + X_R^2(N-m) + X_I^2(N-m) \\
&\quad + [X_R(m) + j X_I(m)] [X_R(N-m) + j X_I(N-m)] \\
&\quad + [X_R(m) - j X_I(m)] [X_R(N-m) - j X_I(N-m)]\}
\end{aligned}$$

which after algebraic manipulation gives

$$\begin{aligned}
FF^*(m) = \frac{1}{4} \{ & X_r^2(m) + X_i^2(m) + X_r^2(N-m) + X_i^2(N-m) \\
& + 2X_r(m)X_r(N-m) - 2X_i(m)X_i(N-m) \}
\end{aligned} \tag{2.8}$$

Similarly,

$$\begin{aligned}
GG^*(m) = \frac{1}{4} \{ & X_r^2(m) + X_i^2(m) + X_r^2(N-m) + X_i^2(N-m) \\
& - 2X_r(m)X_r(N-m) + 2X_i(m)X_i(N-m) \}
\end{aligned} \tag{2.9}$$

The above equations demonstrate the algebra used by the FFT processor to simultaneously calculate the cross and auto spectra of two real series with one FFT operation.

2.2.2 Leakage and Windowing

A problem which occurs during use of the DFT for spectral analysis is the phenomenon of leakage. An excellent discussion of leakage and the measures called windowing or smoothing used to correct it is contained in Harris [44].

The DFT may be viewed as a spectral decomposition in an N-dimensional orthogonal vector space. The basis vectors are of course N/2 equally spaced sinusoidal and cosinusoidal functions. Leakage occurs because there are a finite number of basis vectors whereas a physical signal, even though bandlimited, may have an infinite number of spectral components. Those components which do not precisely match any of the basis vectors (or equivalently are not precisely periodic in the finite observation interval employed) will exhibit non-zero projections on all of the basis vectors of

the DFT. The non-zero projections on DFT spectral components which may be far from the frequency of the actual signal are called leakage.

Windowing may be used to reduce the undesirable effects of spectral leakage. Data prior to DFT processing is multiplied by a weighting function, or window function, which goes smoothly from zero at the end points of the data to 1.0 in the center of the data. The effect of windowing is to reduce the order of discontinuities at the boundaries of the data, as from one viewpoint it is discontinuities between the periodic extensions of the data which give rise to leakage.

There are a large number of different window functions from which to choose, all having somewhat different characteristics and different effects on signals being processed. Harris describes many of these windows and gives a number of figures of merit for them which are useful for comparisons. One of Harris' conclusions is that a window called the Kaiser-Bessel is a superior choice for tone detection using the DFT. The Fourier transform of this window has a highly concentrated central lobe and very low sidelobe levels. For the problem of removing interference from the radio spectrum, it is crucial that a maximum amount of interference energy be concentrated into a few points and a minimum remain in the sidelobes. For this reason, the Kaiser-Bessel window was chosen for use with the interference-excising correlator.

The coefficients for the Kaiser-Bessel window are defined by

$$w(n) = \frac{I_0[\pi\alpha\sqrt{1.0 - (2n/N)^2}]}{I_0[\pi\alpha]}, \quad 0 \leq |n| \leq N/2 \quad (2.10)$$

where I_0 is the modified Bessel function given by

$$I_0(x) = \sum_{k=0}^{\infty} \left[\frac{(x/2)^k}{k!} \right]^2 \quad (2.11)$$

The choice of the parameter α allows a trade off between sidelobe level and main-lobe width. An intermediate value of $\alpha=2.5$ was chosen for this project. The highest window sidelobe level is then -57 dB and the 3 dB bandwidth of the main lobe is 1.57 bins, where one bin is equal to the difference in frequency between DFT spectral components.

For the FFT processor, the window coefficients $w(n)$ had to be quantized with 8 bits of accuracy. There was concern that quantization would affect the sidelobe levels. A Fourier transform of the quantized version of the window showed that there was indeed some effect, but it was not serious. For an unquantized window the sidelobe levels decrease at a rate of -6 dB per octave with frequency. The quantized window, however, exhibited sidelobes which did not decrease monotonically with frequency, but stayed relatively constant and varied from -70 dB to -80 dB relative to the main lobe level. These sidelobes are one of the factors limiting the dynamic range of the FFT processor.

2.2.3 The Effects of Windowing

Windowing has a number of effects on signals being processed. Three parameters describing the most important of these effects are coherent gain, equivalent noise bandwidth, and equivalent integration time.

The coherent gain (CG) is the gain for a purely sinusoidal signal, and is equal to the dc gain or simply the sum of the window terms. Generally, CG is expressed relative to N , the gain of a rectangular window $\{w(n)=1.0$ for all $n\}$. Thus

$$CG = 1/N \sum_{n=0}^{N-1} w(n) \quad (2.12)$$

Because the width of the main lobe of the Fourier transform of a window function is generally larger than that of a rectangular window, another effect is apparent when broadband noise is analyzed. The amplitude of a given spectral estimate contains contributions from neighboring spectral components, resulting in an increase in the equivalent noise bandwidth (ENBW) of each estimate. ENBW may be defined as the width of a rectangular filter, with the same coherent gain, which would accumulate the same noise power as the windowed spectral estimate. An expression for ENBW is found to be [44]

$$ENBW = \frac{N \sum_{n=0}^{N-1} w^2(n)}{\left[\sum_{n=0}^{N-1} w(n) \right]^2} \quad (2.13)$$

For a Kaiser-Bessel window with $\alpha=2.5$, the coherent gain is 0.44 and the equivalent noise bandwidth is 1.65. The major consequence of having an ENBW greater than 1.0 is a reduction in the signal-to-noise ratio for the detection of a tone in the presence of noise. For the above window the change in SNR relative to a rectangular window with ENBW=1.0 is $-10 \log 1.65 = -2.17$ dB. Therefore, in order to have low sidelobe levels one must pay a small price with poorer SNR.

Another result of using windowing is an effective reduction of integration time and a consequent decrease in the sensitivity of the FFT spectrometer. The decrease in sensitivity occurs because points near the ends of the data are not weighted as heavily as points near the center. Some of the information in the sample is therefore discarded.

For the analysis of Gaussian noise, the result is a decrease in the stability (i.e. an increase in the variance) for estimates of noise level. The increased variance does not occur for *individual* spectral components but rather for the *average* of a number of components. Windowing causes a certain amount of correlation between spectral components which are near one another. As components are then not independent (as they would be without windowing) the variance of the average of N components is greater than $1/N$ times the variance of each individual component.

The correlation between components of spectra of white Gaussian noise due to windowing has been calculated by Persson [45] and by Durrani [46]. Their results indicate

that the correlation coefficient $\rho(k_1 - k_2)$ between power spectrum components separated by $k_1 - k_2$ bins is given by

$$\rho(k_1 - k_2) = \left[\frac{\sum_{n=0}^{N-1} w^2(n) \cos [2\pi n(k_1 - k_2)/N]}{\sum_{n=0}^{N-1} w^2(n)} \right]^2 \quad (2.14)$$

The above result holds as long as neither component is near the frequencies 0 or $N/2$. For a Kaiser-Bessel window with $\alpha=2.5$, the correlation coefficients evaluated as above are given in Table 2.1.

An original derivation of the effect which correlation has upon the spectral average when used as an estimate of noise level is presented below. Consider an average \bar{Y} of K components $Y(k)$, $J \leq k \leq J+K$ each with variance σ_Y^2 and with a correlation $\rho(k_1, k_2) = \rho(k_1 - k_2)$ as above between any two components $Y(k_1)$ and $Y(k_2)$. Assume $J > 0$ and $J+K < N/2$ to avoid problems with the correlation coefficients at 0 and $N/2$.

$$\bar{Y} = \left(1/K\right) \sum_{k=J}^{J+K} Y(k)$$

and the variance of \bar{Y} will be

$$V[\bar{Y}] = \left(1/K^2\right) \left[\sum_{k=J}^{J+K} V[Y(k)] + 2 \sum_{k_1 > k_2} \text{Cov}[Y(k_1), Y(k_2)] \right]$$

where the double sum is over all pairs (k_1, k_2) with $k_1 > k_2$.

The covariance is

Table 2.1. Spectral Correlation Coefficients for Kaiser-Bessel Window

Lag Value ($k_1 - k_2$)	$\rho(k)$
1	0.544
2	0.0810
3	0.00250
4	0.711×10^{-5}
5	0.241×10^{-10}
6	0.0

$$\text{Cov}[Y(k_1), Y(k_2)] = \rho(k_1 - k_2) V[Y(k)]$$

and hence

$$\begin{aligned}
 V[\bar{Y}] &= \left(1/K^2\right) \left[\sum_{k=J}^{J+K} V[Y(k)] + 2 \sum_{k_1 > k_2} \rho(k_1 - k_2) V[Y(k)] \right] \\
 &= \left(1/K^2\right) \left[K \sigma_Y^2 + 2 \sum_{k_1 > k_2} \rho(k_1 - k_2) \sigma_Y^2 \right] \\
 &= \left(\sigma_Y^2 / K^2\right) \left[K + 2 \sum_{k_1 > k_2} \rho(k_1 - k_2) \right]
 \end{aligned}
 \tag{2.15}$$

The double sum may be evaluated by noting that for K components there will be $K - (k_1 - k_2)$ pairs a distance $k_1 - k_2$ apart. Letting $k = k_1 - k_2$

$$V[\bar{Y}] = \left(\sigma_Y^2 / K^2 \right) \left[K + 2 \sum_{k=1}^{K-1} (K-k) \rho(k) \right] \quad (2.16)$$

Only a few terms in the summation are required, as $\rho(k)$ for most windows goes to zero rapidly as k increases.

For the FFT processor in this project an average of 108 spectral components is employed. With a rectangular window and white Gaussian input, all spectral components are uncorrelated and hence $\rho(k)=0$ for $k \geq 1$.

$$V[\bar{Y}]_{\text{Rect.}} = \frac{\sigma_Y^2}{K^2} K = \frac{\sigma_Y^2}{K} = \frac{\sigma_Y^2}{108}$$

With the Kaiser-Bessel window and $\rho(k)$ as given Table 2.1,

$$\begin{aligned} V[\bar{Y}]_{\text{K.B.}} &= \frac{\sigma_Y^2}{108^2} \left[108 + 2(107)(.544) + 2(106)(.081) + 2(105)(.0025) \right] \\ &= \frac{\sigma_Y^2}{108^2} (242.1) = \frac{\sigma_Y^2}{108} \frac{242.1}{108} = \frac{\sigma_Y^2}{108} 2.24 \end{aligned}$$

The variance of \bar{Y} is increased by a factor of 2.24 when the window is used. An equivalent integration time (EIT) may be defined as the reduction in integration time producing the same increase in the variance of the power spectrum average for white Gaussian noise as the use of a particular window function does. For a Kaiser-Bessel window with $\alpha=2.5$, $EIT=1/2.24=0.446$.

An alternate derivation of EIT, based upon the time-domain correlation of two windowed Gaussian series and producing identical results to the derivation above, is presented in Appendix 1. It is found that EIT is given by a simple function of the window coefficients.

$$EIT = \frac{\left[\sum_{n=0}^{N-1} w^2(n) \right]^2}{N \sum_{n=0}^{N-1} w^4(n)} \quad (2.17)$$

The loss of information due to windowing could be overcome through the use of overlapped processing as suggested by Welch [47]. However, overlapping increases the number of transforms required and therefore necessitates either a faster FFT processor or a reduction in sampling rate and bandwidth. As the decrease in variance with overlapping would not be as large as the increase in variance due to reduced bandwidth, the most efficient use of the FFT processor is with nonoverlapped processing.

2.2.4 FFT Quantization Errors

The finite word lengths necessary in digital computations generally introduce quantization errors during signal processing. In the case of the FFT, there are two sources of error: coefficient quantization errors due to inexact representation of the sine and cosine basis vectors, and arithmetic roundoff errors produced by rounding after additions or multiplications.

2.2.4.1 Coefficient Quantization Errors

The effect of quantization errors in the sine and cosine FFT basis vectors is to convolve the Fourier transform of the input signal with a pattern of spurious sidelobes. The spurious sidelobes can be found by taking the Fourier transform of the quantized version of the basis vectors. James [48] and Tufts, et al, [49] have investigated spurious sidelobes in FFT's.

In addition to the number of bits used for coefficients, James noted that the spurious sidelobe levels are dependent upon whether or not coefficients identically equal to 1.0 are represented exactly. The use of fixed point binary coefficients generally results in a truncated version of 1.0. This problem is analogous to the fact that 8 bit binary twos complement numbers may be used for all integers between -128 and +127, but cannot represent +128. Improved performance in an FFT processor can be obtained if special measures are taken to recognize the coefficient 1.0 and ensure its exact representation.

For 8 bit FFT coefficients (7 magnitude bits plus 1 sign bit) the largest spurious sidelobe found by James for a sinusoidal input signal is 56 dB below the main lobe. The levels of these sidelobes are therefore somewhat higher than those resulting from a quantized window function as described in Section 2.2.2. The sidelobes due to FFT coefficient quantization errors are a major factor in limiting the dynamic range of the FFT processor.

2.2.4.2 Arithmetic Roundoff Errors

A second source of error in digital FFT's is roundoff following arithmetic operations. Roundoff is necessitated by the finite numbers of bits available for storage in digital machines. Analyses of roundoff errors in references such as [50], [51], [52], [53], [54], [55] and [43] have shown that the combined effect of many roundoff errors during an FFT can be represented by an addition of white noise to the FFT results. The level of this roundoff noise depends upon a number of factors including how often rounding is performed, the number of bits used in digital representations, and the accuracy of the FFT coefficients. Another important factor is the type of arithmetic employed. Floating point arithmetic allows a wider dynamic range for digital signals and therefore generally produces less roundoff noise than fixed point arithmetic where no exponents are used. An intermediate form of arithmetic called block floating point uses a common exponent for blocks of numbers and produces an amount of roundoff noise between that of fixed and floating point operations.

With fixed point arithmetic, Oppenheim and Weinstein [52] show that roundoff noise is constant whereas with floating point or block floating point the noise level increases as signal levels increase. For floating point arithmetic and a Gaussian input signal, roundoff noise variance is directly proportional to input signal variance.

Roundoff noise levels are very sensitive to the

rounding procedure employed. Simple truncation, for instance, produces high noise levels. Much better results are obtained with conventional rounding where if a fractional part is greater than $1/2$ the number is rounded upwards or if less than $1/2$, downwards. However, Weinstein [51] noted that the case where the fractional part is exactly equal to $1/2$ is quite important. If this case is always rounded in one direction, a slight correlation is introduced between the roundoff error and the sign of the number. This correlation contradicts the assumption generally made in analyzing roundoff errors that the noise and signal are independent, and is enough to cause higher than expected noise levels. A "randomized" rounding procedure which randomly rounds this intermediate case upwards or downwards with equal probability corrects the situation.

FFT roundoff noise places a lower limit on the dynamic range of an FFT processor.

2.2.5 Arithmetic Overflow

A problem which occurs during fixed point digital signal processing is arithmetic overflow. The addition of two large fixed point numbers may produce a sum which exceeds the maximum representable by a given number of bits. If it is allowed to happen, overflow causes large errors.

Overflow is not generally a problem with floating point numbers because of the wide dynamic range possible. With

fixed point processing, however, precautions must be taken. The simplest precaution is to never allow numbers to grow large enough to produce overflow. A common method is to divide the results of all additions by 2. An FFT of 2^L samples is calculated in L separate stages. In a fixed point FFT processor, the results of each stage of computation may be scaled by 2 to ensure that overflows do not occur.

However, scaling by 2 at each stage may not be necessary, particularly if large sinusoidal signals which would cause some FFT components to grow during computation are not present. A better approach to fixed point processing is to scale only when necessary. The result is block floating point processing, where all computations are scaled an equal number of times. The number of scalings forms a common exponent for all FFT results. The reduction in the number of scalings compared with fixed point processing produces more accurate results and lower levels of roundoff noise.

Most block floating point methods work by scaling the results of a particular stage only if an actual overflow is detected. A problem with this method is that a number of unscaled computations may be completed and the results stored in memory before the overflow occurs and the necessity of scaling is realized. As the previously computed results for the stage have been rounded before storage, a scaling by 2 followed by a second rounding will introduce additional error and lead to higher levels of roundoff

noise. To correct this problem, results would have to be stored with some of the fractional bits intact in order for correct rounding to be accomplished later on. In addition to the extra memory required for this storage, the FFT processor must remember which results have been scaled and which have not. Considerable extra hardware is therefore required.

A simpler implementation of block floating point developed by the author involves the anticipation of possible overflows prior to the beginning of a stage of computation. For instance, if some of the results of the previous stage had an absolute value greater than one-half the maximum allowable then the addition of two such numbers could produce an overflow. If the possibility of overflow exists, all results for the stage could be scaled and the overflow avoided. If overflow would not have occurred then all new results will be less than one-half the maximum and scaling will not be necessary for the following stage. Such a block floating point scheme is less difficult to implement than one based on the actual occurrence of overflows and avoids the problems of rounding described above.

2.2.6 Overflow Correction

The basic equation employed during FFT computation has the form

$$C_r = A_r + B_r W_r - B_i W_i$$

as described in Section 2.3.1. The coefficients W_r and W_i represent points of cosine and sine functions respectively, and have a maximum combined value when $|W_r| = |W_i| = 0.707$. If it is assumed that the data samples A_r, B_r and B_i all have maximum fixed point values of 1.0, then C_r can have a maximum value of

$$C_{r_{\max}} = 1.0 + (0.707)(1.0) - (-0.707)(1.0) = 2.414$$

In such a case, scaling by 2 would not be sufficient to prevent overflow. Even with scaling, overflow during an FFT is a possibility. However, it will occur very infrequently.

The most drastic consequence of overflow is a reversal of the sign of the number. If overflows can be detected and the maximum allowable number with the correct sign substituted then the errors caused by overflows can be reduced appreciably. In signal processing where overflows may occur but with low probability, such an overflow correction technique performs well in controlling errors.

2.3 Design of the FFT Processor

Design and construction of the fast Fourier transform processor occupied a large part of the time spent on the thesis project. When the project began in 1976 there were a few commercial FFT processors being marketed. None of these machines were capable of real time processing with a bandwidth of more than about 20 kHz, and very few had cross spectral capability. In addition, all were extremely

expensive and consumed considerable amounts of power.

The availability of a number of new signal processing integrated circuits made the construction of a specialized FFT processor appear feasible, and this course was chosen. The design goal was a minimum of 50 kHz real time bandwidth, divided into 128 channels. Each channel would then be $50 \text{ kHz}/128=390 \text{ Hz}$ in width, which is somewhat greater than the minimum expected bandwidth to be observed which is about 100 Hz for marine CW transmissions.

For a bandwidth of 50 kHz the sampling rate must be 100 kHz, and for 128 channels the number of samples per FFT must be 256. For real time operation the processor would have to calculate a 256 point FFT in $256 \times 1/100 \text{ kHz}=2.56 \text{ msec}$. A 256 point FFT can be computed in $\log_2 256=8$ stages, each stage consisting of 128 butterfly operations. The time available for each butterfly is then $2.56 \text{ msec}/(8 \times 128)=2.5 \text{ } \mu\text{sec}$. A butterfly processor consisting of four multipliers and six adders and operating at the above rate forms the heart of the FFT processor designed for the project. An in-place, decimation-in-time FFT algorithm is used. A two-section input buffer allows a new set of 256 samples to be collected while the previous set of samples is Fourier transformed. Eight-bit block floating point arithmetic was chosen for the FFT processor as a compromise between a simple, low power and low cost machine and one with wide dynamic range.

2.3.1 The FFT Algorithm

The discrete Fourier transform of a series $x(n)$, $0 \leq n \leq N-1$, is defined by

$$X(m) = \sum_{n=0}^{N-1} x(n) W^{mn} \quad (2.18)$$

where $W = \exp(-j2\pi/N)$. This equation may be rewritten in matrix form as [40]

$$\bar{X} = [W] \bar{x}$$

where \bar{X} and \bar{x} are column vectors of length N and $[W]$ is an $N \times N$ matrix.

The fast Fourier transform can be viewed as a matrix factorization of $[W]$. In general if N is the product of L prime factors, then $[W]$ can be factored into the product of L simpler matrices where many of the terms become zero, ± 1 or $\pm j$.

Matrix factorization of $[W]$ works particularly well if N is a power of 2. In this case, $[W]$ can be factored into $L = \log_2 N$ matrices

$$[W] = [W_1][W_2][W_3] \dots [W_L]$$

where each row of the new matrices contains only *two* non-zero terms, one of which is unity with the other being $W^k = \exp(-j2\pi k/N)$, $0 \leq k \leq N-1$. A peculiarity of this factorization is that in order for the matrices $[W_\ell]$ to be no larger than $N \times N$, either the input vector \bar{x} or the output vector \bar{X} cannot remain in its natural order. Rather, the terms must be

permuted in a fashion called bit-reversed order. The sequence of the terms can be found by representing the indices i of each term, $0 \leq i \leq N-1$, as a binary integer and then reversing the order of the bits.

There are two possible factorizations of $[W]$ which result in $N \times N$ matrices as above when $N=2^L$. The factorizations correspond to the FFT algorithms known as decimation-in-time and decimation-in-frequency. The decimation-in-time algorithm was chosen for this project.

The basic arithmetic computation for a radix-2 decimation-in-time FFT is given by

$$\begin{aligned} C &= A + W^k B \\ D &= A + W^{k+N/2} B = A - W^k B \end{aligned} \quad (2.19)$$

where A and B are complex input values and C and D are complex results. Note that

$$\begin{aligned} W^{k+N/2} &= \exp\left[-j\frac{2\pi}{N}(k+N/2)\right] \\ &= \exp\left(-j\frac{2\pi}{N}k\right) \exp(-j\pi) \\ &= -\exp(-j2\pi k/N) = -W^k \end{aligned}$$

The operation in equation 2.19 is called a butterfly operation from its graphical representation in Figure 2.1.

Let

$$\begin{aligned} A &= A_r + jA_i \\ B &= B_r + jB_i \\ W^k &= W_r + jW_i \end{aligned}$$

Then the butterfly operation can be expressed as

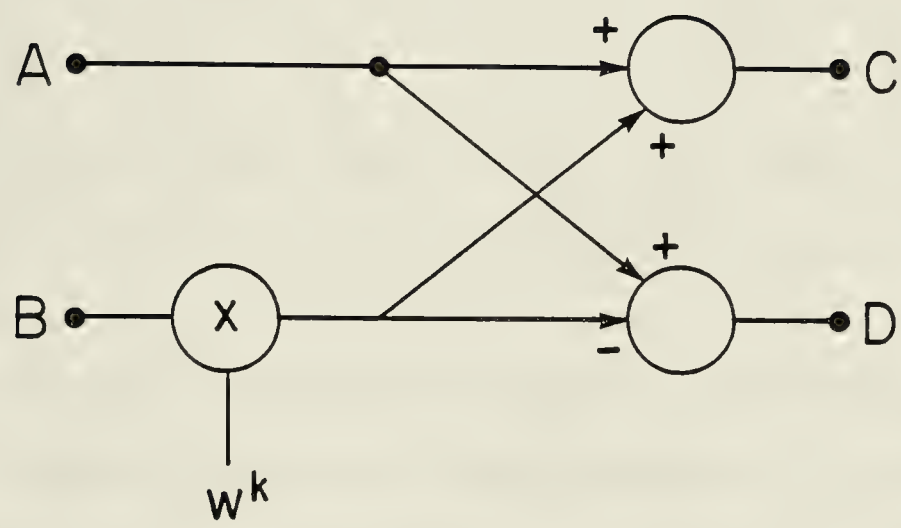


FIGURE 2.1 Complex Butterfly Computation for Decimation-in-Time FFT

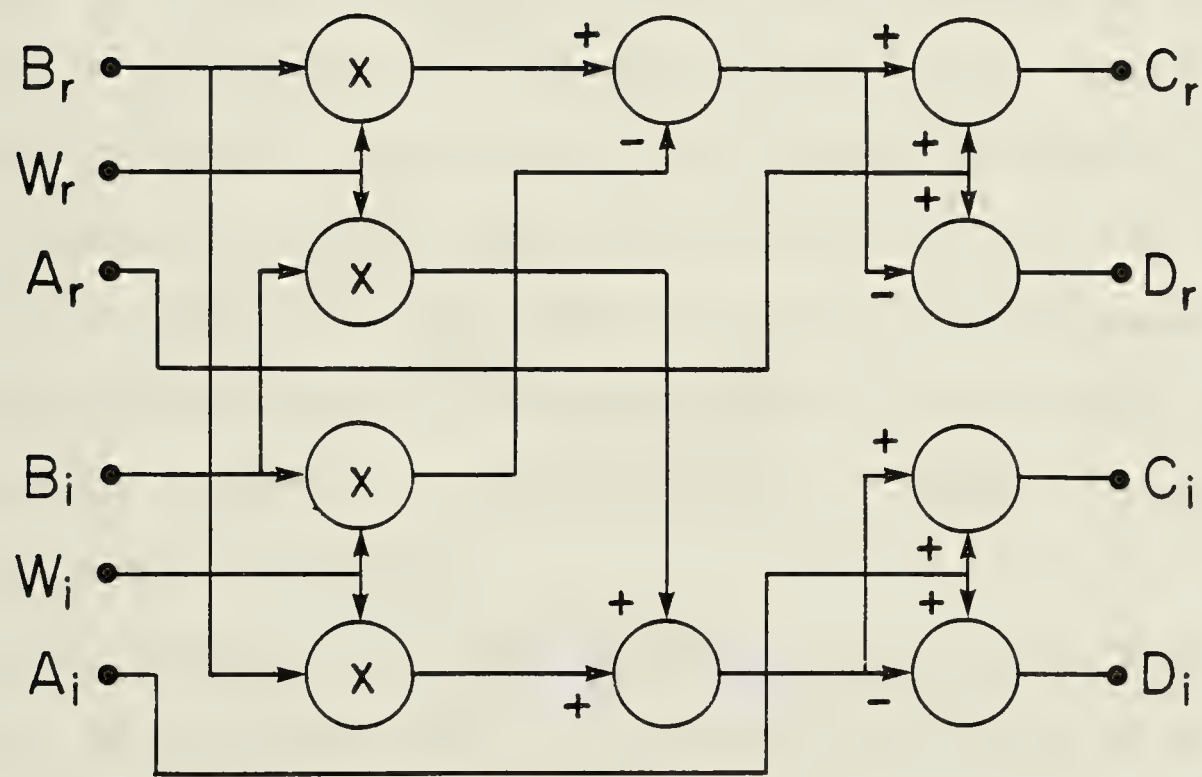


FIGURE 2.2 Real Butterfly Computation for Decimation-in-Time FFT

$$\begin{aligned}
C &= C_R + jC_i = (A_R + B_R W_R - B_i W_i) + j(A_i + B_R W_i + B_i W_R) \\
D &= D_R + jD_i = (A_R - B_R W_R + B_i W_i) + j(A_i - B_R W_i - B_i W_R) \quad (2.20)
\end{aligned}$$

In terms of real rather than complex operations, the butterfly computation can be performed with four multiplications and six additions as shown in Figure 2.2 [56].

2.3.2 FFT Addressing

An FFT is performed by executing a sequence of butterfly operations as described above. It is necessary, of course, to supply the correct data A and B plus the correct coefficient W^k for each operation, and to store the results C and D in some form of memory. This control of memory access is provided by a scheme of memory addressing. The addressing scheme outlined below is an original method developed by the author.

To illustrate how addressing can be accomplished, the example of an 8-point FFT in Figure 2.3 [37] is given. The dots or nodes in Figure 2.3 represent variables stored in memory locations. Lines entering each node from the left represent additive contributions to that variable, while arrows with a factor W^k beside them represent multiplication by the factor. The 8-point FFT is computed in $\log_2 8 = 3$

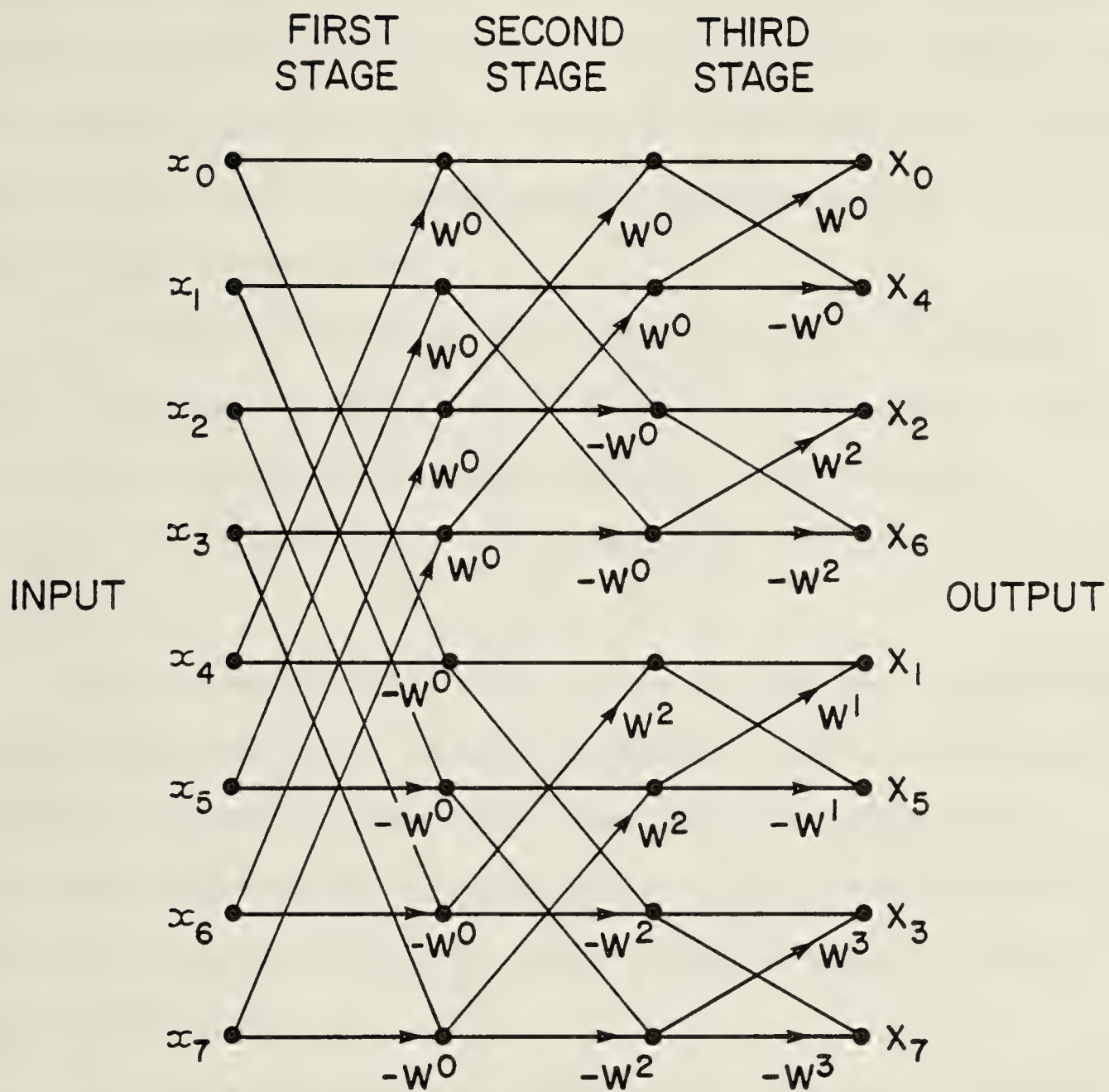


FIGURE 2.3 Butterfly Diagram for an 8-Point Decimation - in - Time FFT

stages with each stage consisting of $8/2=4$ butterfly operations. Note that the results are in bit-reversed order. Only 8 complex memory locations are required for the above FFT because the results C and D of each operation can be stored back into the same memory locations from which the data A and B were read.

A simple pattern in the addressing of the memory locations can be noted from Table 2.2 which shows the binary representations of the addresses for each butterfly in Figure 2.3. The A and B addresses are different in only one bit.

The column of this bit starts as the most significant column for the first stage and moves right one column per stage to finally become the least significant column. Disregarding this particular column, the remaining bits form a binary counter which is incremented by one for each butterfly operation.

A simple pattern is also present for the integer k corresponding to the coefficient W^k , as shown in Table 2.3. The exponent k follows the pattern of a bit-reversed binary count, with the counting rate doubling with each stage of the FFT. One method of obtaining the required coefficients W^k during the FFT is to store the coefficients in a read-only memory in bit-reversed order, and to address the memory with a variable-rate binary counter where the rate is determined by the number of the stage of the FFT being computed.

Table 2.2. Memory Addresses for an 8-Point Decimation-in-Time FFT

Data	First Stage Address	Second Stage Address	Third Stage Address
A	0 0 0	0 0 0	0 0 0
B	1 0 0	0 1 0	0 0 1
A	0 0 1	0 0 1	0 1 0
B	1 0 1	0 1 1	0 1 1
A	0 1 0	1 0 0	1 0 0
B	1 1 0	1 1 0	1 0 1
A	0 1 1	1 0 1	1 1 0
B	1 1 1	1 1 1	1 1 1

↑

Counts

Alternates

↑

Counts

Alternates

↑

Counts

Alternates

Table 2.3. Powers of W for Coefficients in 8-Bit Decimation-in-Time FFT

First Stage	Second Stage	Third Stage
0 0	0 0	0 0
0 0	0 0	1 0
0 0	1 0	0 1
0 0	1 0	1 1

2.3.3 Layout of the FFT Processor

A block diagram of the FFT processor appears in Figure 2.4. The processor can be broken down into six stages:
1) analog-to-digital conversion; 2) windowing; 3) fast

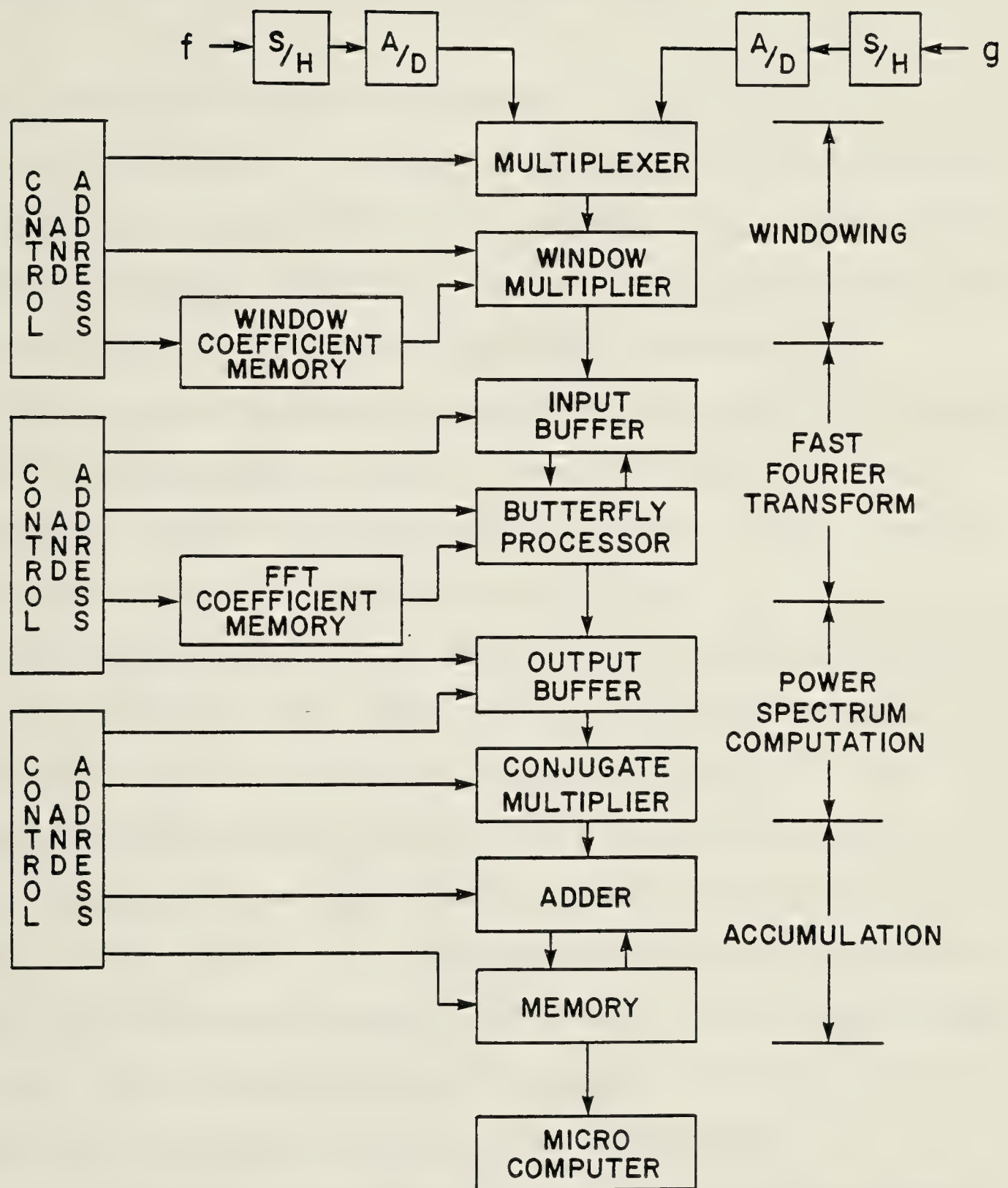


FIGURE 2.4 Block Diagram of the FFT Processor

Fourier transformation; 4) power spectrum computation; 5) accumulation; and 6) the microcomputer.

2.3.3.1 Analog-to-Digital Conversion

The intermediate frequency outputs of the receivers are bandlimited to between 416.7 kHz and 468.8 kHz (3 dB points) by 8-pole Chebyshev bandpass filters. These filters provide sharp cutoff at the bandpass edges and an asymptotic roll-off in the stopband of 48 dB/octave to prevent aliasing of out-of-band signals. The 52.1 kHz bandpass IF output centered on 442.75 kHz is sampled at a rate of 104.2 kHz by A/D converters with a resolution of 8 bits.

Because the frequencies being sampled are relatively high, the times at which samples are taken must be very accurate to ensure that errors due to variation in the sampling time are small. A measure of this variation is given by the aperture uncertainty specification of a sample-and-hold amplifier. Aperture uncertainty is defined to be the difference between the maximum and minimum delays from the time a sample-and-hold command is given to the point when the output ceases to follow the input.

The aperture uncertainty time of the sample-and-hold amplifiers used in this project was 2 nanoseconds. The maximum expected error in the sampled signal due to aperture uncertainty, assuming a full scale signal at 450 kHz, can be found by noting that the maximum rate of change of the signal in bits/sec will be

$$\begin{aligned}
& \frac{d}{dt} \frac{1}{2} (2^8 \text{bits}) \sin (2\pi \times 450 \times 10^3 \times t) \Big|_{t=0} \\
&= (128)(2\pi \times 450 \times 10^3) \cos (2\pi \times 450 \times 10^3 \times t) \Big|_{t=0} \\
&= 3.62 \times 10^8 \text{ bits/sec.}
\end{aligned}$$

Hence the uncertainty will be

$$(2 \times 10^{-9} \text{ sec})(3.62 \times 10^8 \text{ bits/sec}) = 0.724 \text{ bits.}$$

The expected error is less than 1 bit.

The A/D converters used in the project had a conversion time of 2.4 μsec , which is much less than the 9.6 μsec between samples.

2.3.3.2 Windowing

Blocks of 256 samples from each receiver are weighted using a Kaiser-Bessel window function to reduce leakage. The windowing stage is diagrammed in Figure 2.5.

Samples $f(n)$ and $g(n)$ from the A/D converters are gated through a multiplexer onto a bidirectional 8-bit Window Data Bus. From this bus, the samples can be read into the Window Register. This register converts the sample into a serial bit stream and passes it one bit at a time to an 8-bit serial/parallel multiplier. Here the two's complement sample is multiplied by an unsigned 8-bit window coefficient from the Window Coefficient Memory.

The resulting 16-bit serial product goes to a serial adder which rounds it to 8 bits. Randomized rounding is used

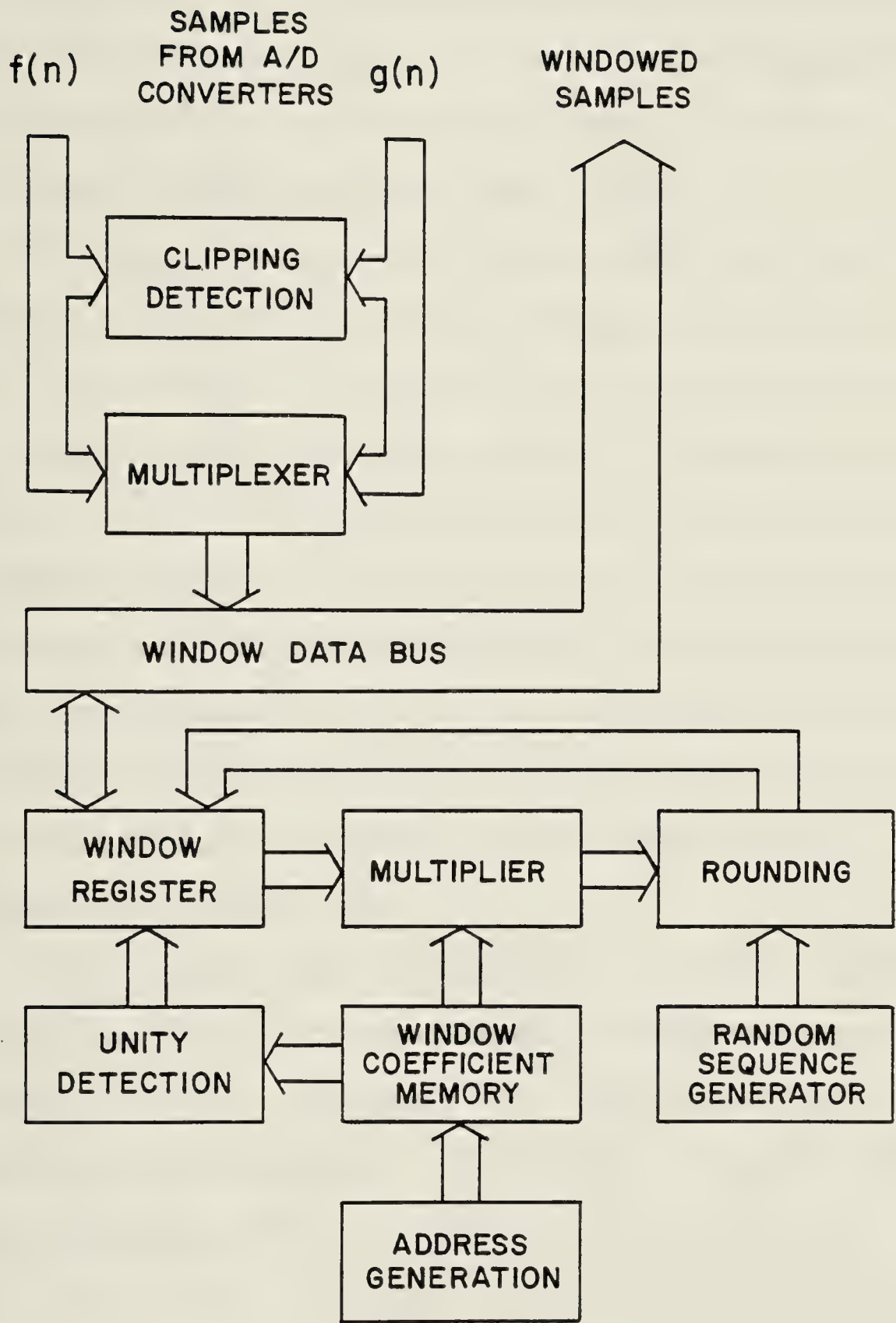


FIGURE 2.5 Windowing Stage

for the case where the fractional part of the product is exactly one-half. The rounding direction is determined from a pseudorandom binary sequence $2^{18}-1$ bits long produced by an 18-stage shift register with feedback through exclusive-OR gates, as described in [57].

The rounded result is clocked back into the Window Register and is then gated via the bus to the Input Buffer of the next stage. A feature of the windowing stage is that multiplication by the coefficient 1.0 is possible even though 1.0 cannot be stored as one of the coefficients in the memory because it requires an extra bit. Because 0.0 is not needed as a window coefficient, a Unity Detection circuit which detects all 0's at the memory's output is used to inhibit the multiplication process. The original sample is then transferred directly to the input buffer, in effect being multiplied by 1.0.

The windowed data is stored in one half of the two-section Input Buffer. Samples from one receiver are stored as the real components of the data to be Fourier transformed while those from the other receiver form the imaginary components.

2.3.3.3 Fast Fourier Transformation

While a new set of 256 samples is being taken, the previous set in the second half of the Input Buffer is fast Fourier transformed by the butterfly processor. A block diagram is shown in Figure 2.6. Address generation circuitry

using the pattern in Section 2.3.2 supplies data from the Input Buffer and FFT sine and cosine coefficients from a read-only memory to the butterfly processor. Butterfly results are calculated as in equation 2.20 and are stored back into the Input Buffer locations from which the data were read.

During the eighth and final stage of the FFT the results are stored in an Output Buffer. Addresses to the Output Buffer are supplied in bit-reversed order, causing the FFT results to be unshuffled and to appear in the Output Buffer in their normal order.

The butterfly processor performs the arithmetic computations for each FFT and as such forms the heart of the FFT processor. Its operation is detailed below.

The Butterfly Arithmetic Unit near the center of Figure 2.6 does a butterfly operation as shown in Figure 2.2. Four 8-bit data words A_r , A_i , B_r and B_i are read into the Data Registers from the Input Buffer. The Data Registers convert the words into serial bit streams for processing by the serial multipliers and adders which perform the arithmetic computations. The devices used are Am25LS14 multipliers and Am25LS15 adders from Advanced Micro Devices.

Computation results C_r , C_i , D_r and D_i are passed to a Rounding stage where they are rounded to 8 bits prior to being transferred back into the Data Registers for conversion to parallel format.

Rounding is an important aspect of the butterfly

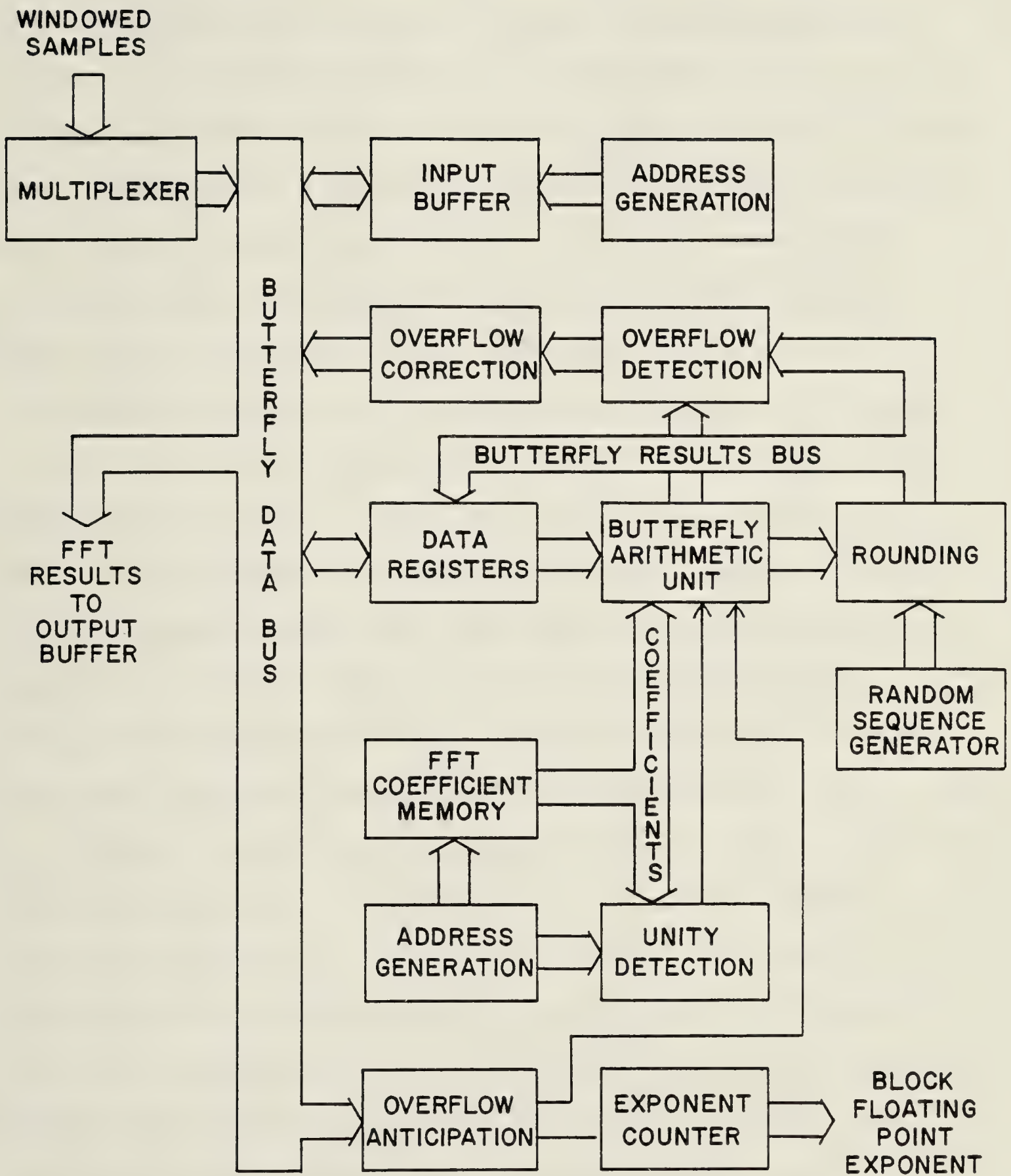


FIGURE 2.6 Butterfly Processor

processor, particularly in view of the limited accuracy of 8-bit computations. In order to keep roundoff noise to a minimum, no rounding is done on intermediate results such as products or sums during the butterfly computation. All bits are preserved until the last point prior to the transfer of results back to the Input Buffer. The level of roundoff noise which results is approximately 5 dB below levels predicted in analyses such as [50] and [51] where all intermediate results are assumed to be rounded individually.

In addition to the minimum amount of rounding above, randomized rounding is used for cases where a remainder is exactly $1/2$. Randomized rounding prevents roundoff errors from being correlated with the signs of numbers as they are rounded. A 20-stage shift register with feedback via exclusive-OR gates provides a pseudorandom binary sequence $2^{20}-1$ bits long for the determination of rounding direction.

Special circuitry is used to ensure an exact value for the FFT coefficient $+1.0$. The Unity Detection circuit monitors coefficients from the FFT Coefficient Memory. The coefficient 80_{16} , which normally represents a twos complement -1.0 , is also used for $+1.0$. By examining the addresses supplied to the memory, the Unity Detection circuit can distinguish between -1.0 and $+1.0$ and instructs the Arithmetic Unit to perform multiplications accordingly.

Block floating point operation is implemented using the overflow anticipation method. The Overflow Anticipation circuit monitors the absolute values of numbers as they are

stored in the Input Buffer by an exclusive-OR of the sign bit and the next most significant bit. If numbers larger than one half the maximum absolute value are detected, scaling is performed in the next stage of FFT computation. The Exponent Counter keeps track of the number of scalings so that results can be normalized later on.

If an overflow should occur, the Overflow Detection and Overflow Correction circuits respond by substituting the maximum allowable number of the correct sign for the overflow result.

2.3.3.4 Power Spectrum Computation

The power spectrum computation stage is outlined in Figure 2.7. It consists of the 4-part Output Buffer, two 8-bit busses leading to two registers Y1 and Y2 and connected by transmission gates, an 8-bit parallel multiplier, a 23-bit adder/subtractor and accumulation register, a storage register, and assorted control and addressing circuits.

By gating the correct FFT results from the Output Buffer into registers Y1 and Y2 and adding or subtracting the resultant multiplier products appropriately in the accumulator, all the required auto and cross spectrum components can be computed. The computations are done according to equations 2.7, 2.8 and 2.9, except that scaling by the factors $1/4$ and $1/2$ in these equations is not done and the auto spectra are computed in complementary form.

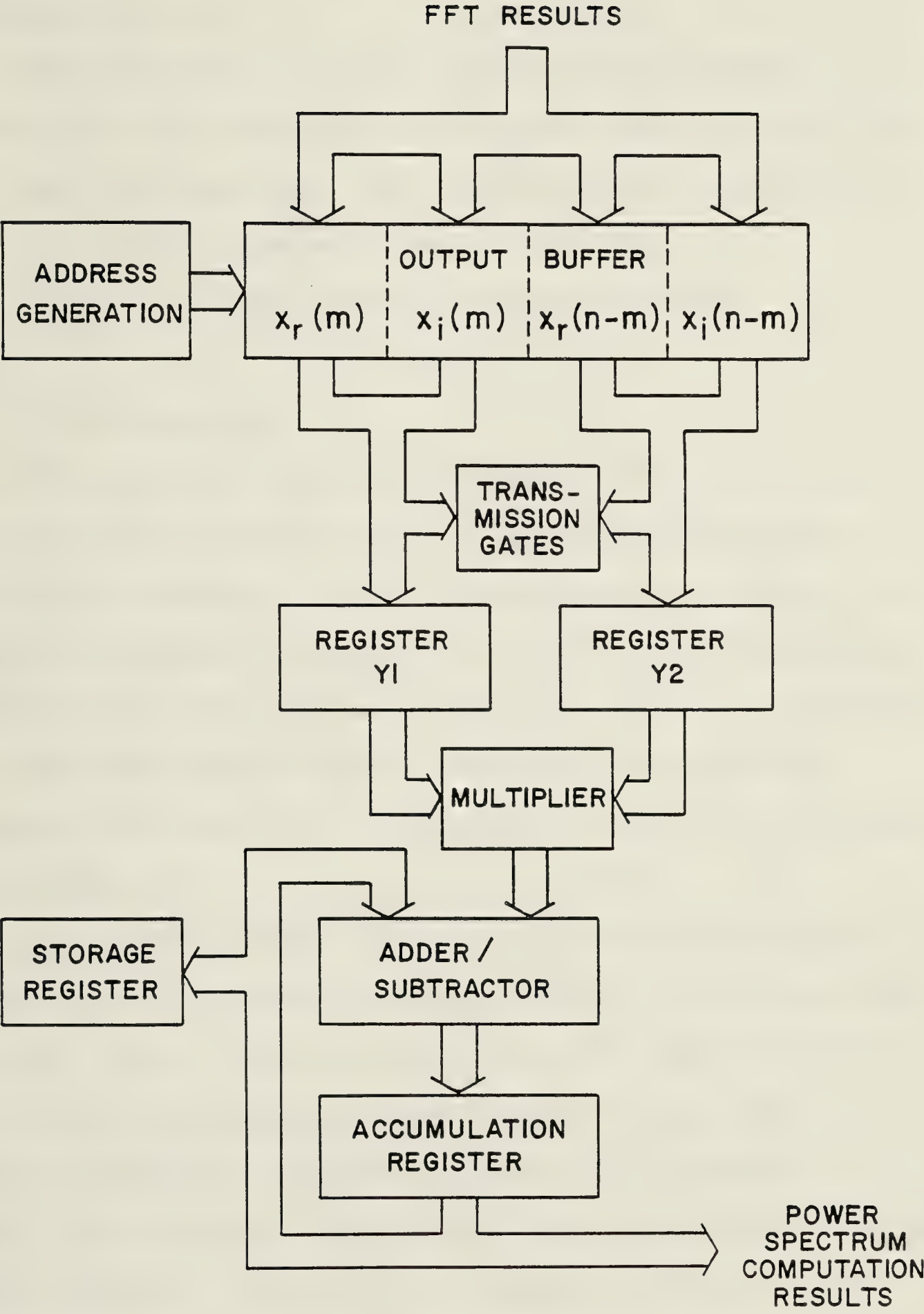


FIGURE 2.7 Power Spectrum Computation

Correction for these discrepancies is made later by the microcomputer.

Control signals for the power spectrum stage are generated with a combination of random logic circuits and fast read-only memories. The multiplier and accumulator sections are implemented using a TDC-1008J multiplier/accumulator from TRW Semiconductors.

2.3.3.5 Accumulation

The process of accumulation is equivalent to the integration or averaging of a large number of spectra. Averaging is commonly used in cross spectral analysis to improve the signal-to-noise ratio when weak signals are combined with high levels of uncorrelated noise. As each FFT requires 2.458 msec, the FFT processor is capable of averaging $(60 \text{ sec/min}) \times (1/2.458 \times 10^{-3} \text{ sec}) = 24,400$ spectra per minute.

A block diagram of the accumulation stage is shown in Figure 2.8. Power spectrum results from the previous stage are first of all scaled in order to align decimal points with those of previously accumulated results. Scaling is necessary because the output of the FFT processor is in block floating point form with a common exponent. The value of the exponent from the FFT processor is used in the scaling step to normalize the power spectra. Scaling is accomplished by simply shifting the power spectra in a 48-bit shift register a number of places according to the

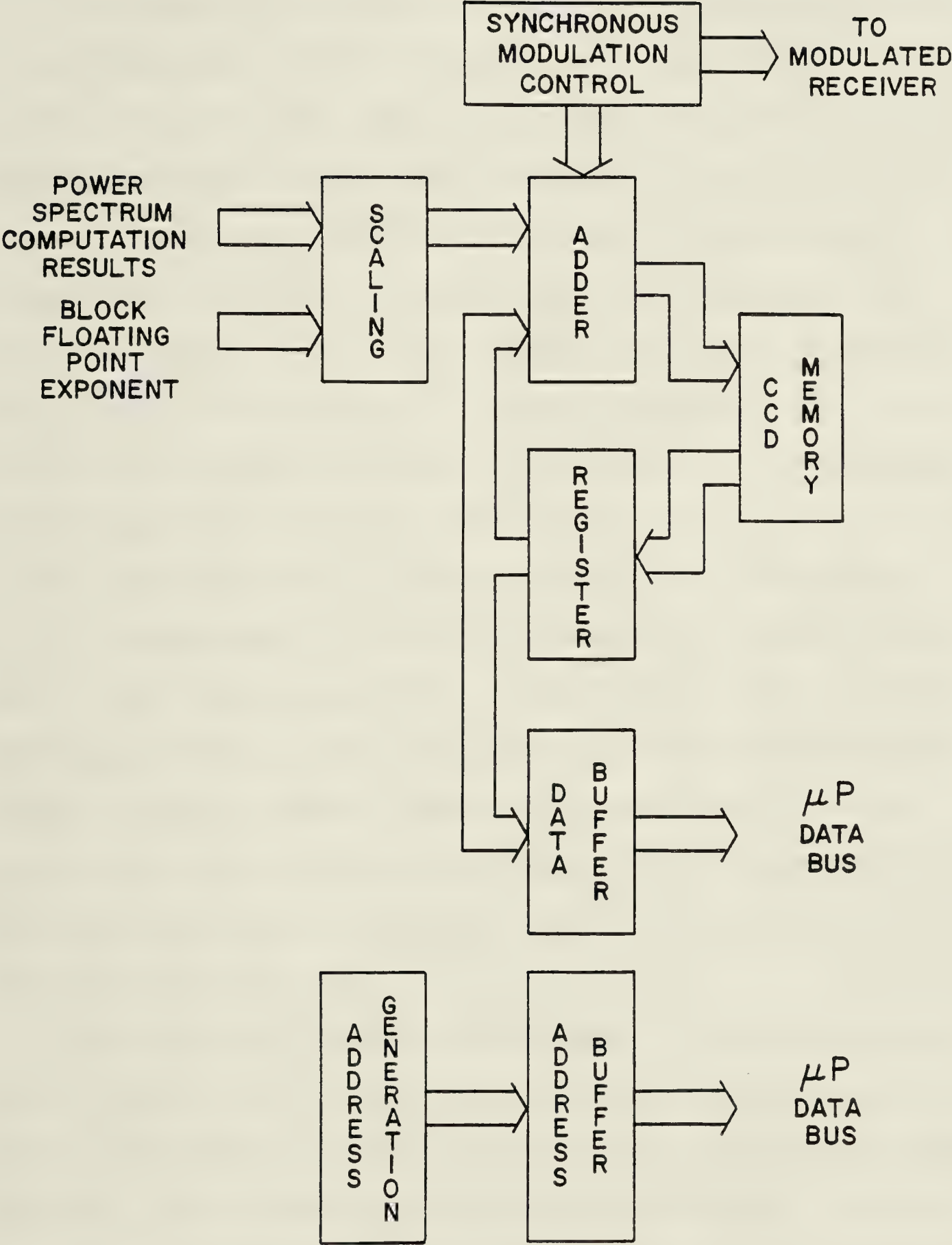


FIGURE 2.8 Accumulation Stage

exponent value.

The speed of the scaling operation is enhanced by using a bidirectional shift register and loading the power spectra in the center of this register so that the total number of shifts required is never more than half the total scaling range. In addition the shift registers are arranged to shift results by two places on each clock cycle because the required number of shifts is always even (i.e. a shift of one bit position in the FFT results produces a shift of 2 places in the power spectrum, as the power is a product). These measures to provide fast scaling are necessary for the accumulation process to keep pace with FFT production.

A scaled power spectrum is passed to a 24-bit adder which adds the new spectrum to the accumulating total of previous spectra. The actual length of the numbers being added is 48 bits which the adder handles in two steps, saving the carry between add cycles. The large number of bits used during accumulation is necessary because of the long accumulation times.

Accumulation results are stored in a charge-coupled device (CCD) shift register memory with a capacity of 3072 bytes. The memory can hold 128 spectral components, each of 48 bits, for the two auto and two cross spectra. The CCD memory has advantages over random access memory of low power consumption, small size and fast read/modify/write capability.

The 24-bit Register in Figure 2.8 serves to latch old

CCD contents for input to the adder during accumulation and also to hold accumulation results during data transfers to the microcomputer. Data transfers occur after a specific number of spectra have been added. The CCD contents are then zeroed and a new accumulation begins.

Results are transferred directly to the microcomputer's memory using a direct memory access (DMA) technique. The FFT processor gains control of the microcomputer data and address busses, and supplies the addresses to write accumulated spectra directly into memory. The complete DMA transfer requires one FFT cycle, or 2.458 msec.

The accumulation stage performs one more function, namely synchronous demodulation. In order to eliminate crosstalk between receivers in radio astronomy, a technique called switching or synchronous modulation and demodulation is commonly employed. The FFT processor accomplishes switching by inverting the phase of the RF signal from one of the antennas with each consecutive FFT. The switching is equivalent to modulation by a bipolar square wave with a frequency of about 203 Hz.

Modulation is accomplished using a diode ring balanced mixer driven by current sources of equal amplitude but opposite sign. The rise and fall times of the square wave are carefully controlled to reduce problems of ringing in the receiver filters and other undesired modulation of the incoming signals. The timing of the square wave is adjusted so that receiver and cable delays are compensated for, and

the phase transitions at the A/D converters coincide with the beginnings of new blocks of FFT samples. Further discussion of the modulation circuit is contained in Section 3.4.

In order to undo the above modulation, the accumulation stage performs synchronous demodulation. Rather than adding consecutive spectra, the add is changed to a subtract on alternate spectra for the in-phase and quadrature spectra¹. Crosstalk occurring after the modulation thereby tends to cancel itself.

2.3.3.6 The Microcomputer

The final stage of the FFT processor is the microcomputer. A block diagram of the computer system appears in Figure 2.9.

The microprocessor which forms the central processor of the microcomputer is a Motorola MC6800. The microcomputer can be operated with either of two operating systems. One of these is Motorola's MIKBUG which uses a teletype, and the other is an operating system written by the author for a small console with a 30-key keyboard and 7-segment readouts.

Programs for the microcomputer were written in assembly language on the University's central computing facility. Machine code for the programs was then loaded into the microcomputer via telephone using a modem and acoustic coupler. An audio tape interface allowed local recording and

¹Synchronous modulation is possible for the cross spectra only, as the auto spectra are always positive.

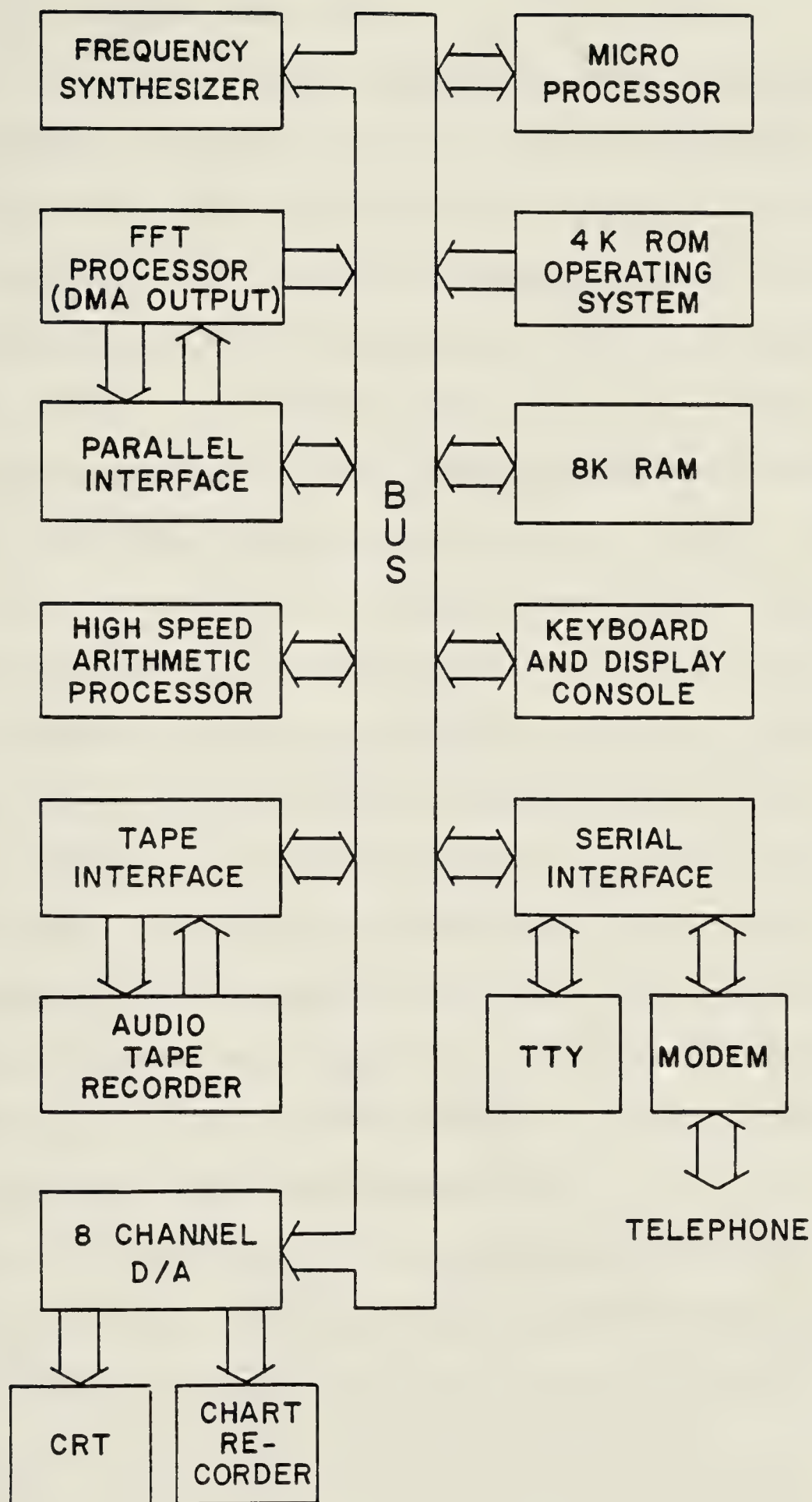


FIGURE 2.9 The Microcomputer

playback of programs and data.

One of the features of the microcomputer is a high speed arithmetic processor. This processor, an Am9511 from Advanced Micro Devices, allowed fast 32-bit floating point arithmetic calculations for robust estimation after spectra were received from the FFT processor. The improvement in speed over software arithmetic was a factor of about 100.

The microcomputer has 64 lines available through Peripheral Interface Adapters for parallel digital input or output. Half of these were required for interfacing to the FFT processor during normal operation. The remaining lines could be connected to various points in the FFT processor via ribbon cables during testing and debugging.

Eight channels of digital-to-analog output were included. These were used to drive the X and Y axes of an oscilloscope to display spectra as they were received, and also to drive chart recorders for a record of fringes and other information such as the number of points being deleted and the amount of clipping encountered.

A serial interface to the programmable frequency synthesizer used for the second local oscillator was provided to allow control over the receiver center frequency.

2.4 General Construction

The FFT processor was designed with two major goals in mind: cost-effectiveness and low power consumption. Power consumption was a consideration in the early stages of the project because initially the FFT processor was to be operated at a remote observing site with no available commercial power.

The processor used a combination of standard TTL, Schottky TTL, low-power Schottky TTL, MOS and CMOS digital integrated circuits. Generally the type of logic consuming the least power was used wherever possible. Schottky TTL was employed in sections with fast clock speeds (up to 20 MHz) and where short propagation delay times were critical.

The circuits were wire-wrapped on a number of approximately 10 inch by 10 inch perforated boards. Wire-wrapping allowed dense packing of the IC's and also easy wiring changes. The circuitry was designed and tested in small sections. High speed sections in particular were kept compact to minimize the lengths of interconnections.

Good grounding is an important consideration in digital design. The best approach is a solid ground plane for low inductance, but this would have been difficult to implement. A satisfactory approximation to a ground plane was the use of two grids consisting of interconnected heavy bus wires to which ground and V_{cc} connections were made. Bypass capacitors at regular intervals on the grid kept noise to a minimum.

A problem commonly encountered in digital systems is RF radiation and consequent electromagnetic interference with communications services. In a radio astronomy environment, electromagnetic interference can be disastrous. Spectrum analyzer measurements showed that the FFT processor and microcomputer produced considerable RF radiation, with harmonics up to many hundreds of megaHertz. The highest levels of RF happened to be right at 22 MHz, creating the spectre of an interference-excising system with a paramount purpose of removing self-inflicted interference.

The solution for this disturbing problem was the placement of the FFT processor and the microcomputer inside a shielded enclosure built from copper screen. All connections passing through the enclosure were low-pass filtered by LC sections, feedthrough capacitors and ferrite beads to prevent RF from escaping. The shielding and filtering were quite successful in eliminating electromagnetic interference problems.

2.5 Laboratory Tests of the FFT Processor

A number of laboratory tests of the FFT processor were conducted in order to verify the correct operation of the hardware and to measure the performance of the completed machine.

2.5.1 Comparisons to Computer Simulations

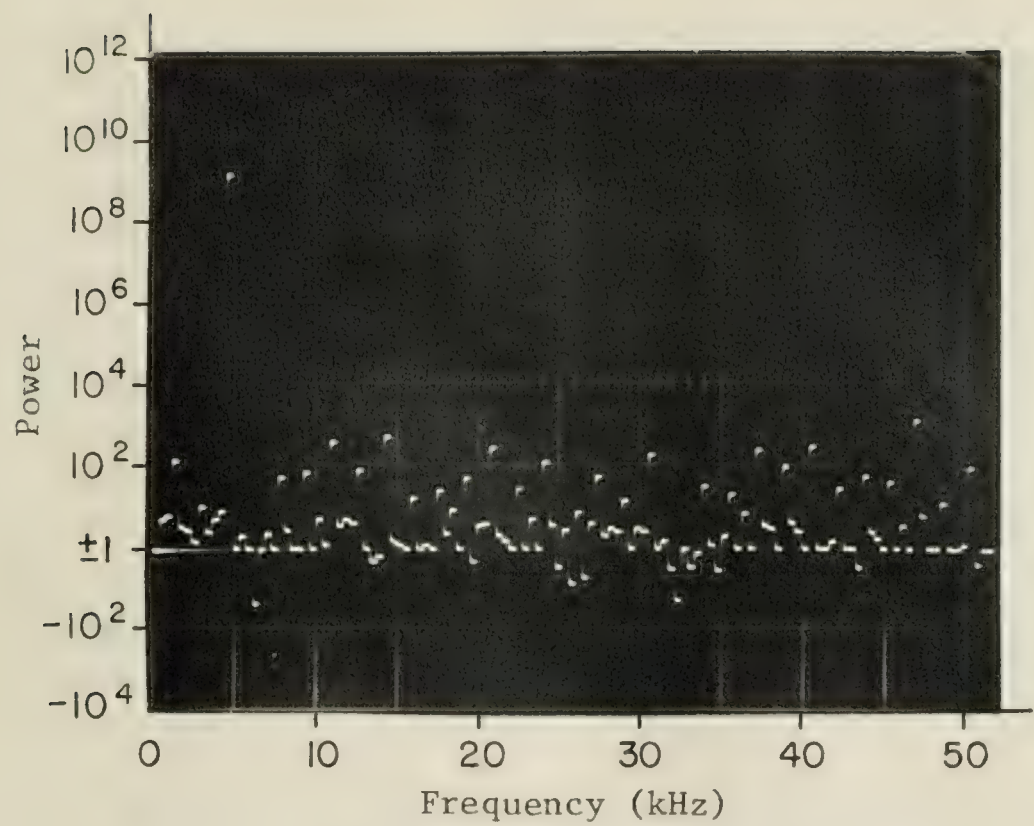
A software model of the FFT processor was generated in FORTRAN for testing purposes. The model could simulate combinations of sinusoidal and Gaussian noise signals and calculate cross and auto spectra using arithmetic identical to that of the FFT hardware. The same signals were then fed to the FFT processor and its results compared to the model's results. By this method, faults in the hardware could be found very easily.

The microcomputer was used as the control element for the FFT hardware during these comparisons. Test points were provided throughout the processor to allow the microcomputer to control hardware operation, to provide simulated data, and to monitor results. Major sections of the hardware could be tested independently or in tandem, allowing faults to be isolated very quickly.

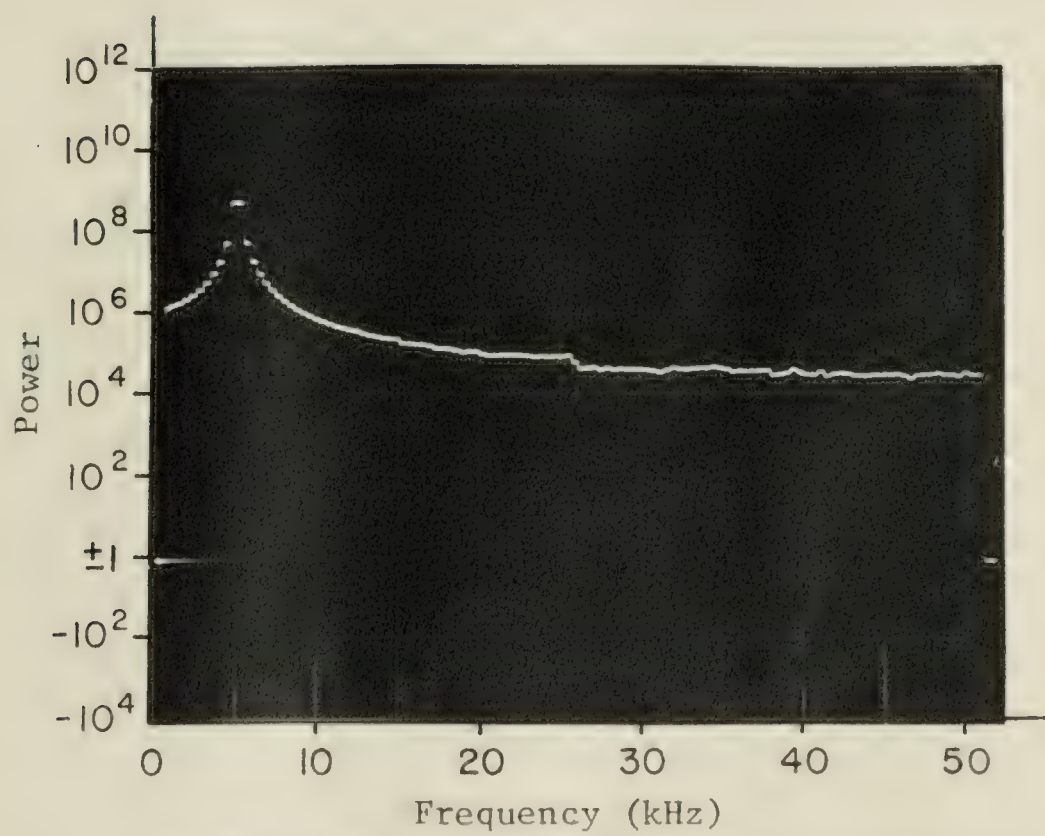
Due to the complexity of the entire machine, the above testing method proved to be invaluable both during the original construction and debugging of the hardware and for maintenance following construction. The software model also allowed aspects of the FFT processor to be tested before a commitment was made to hardware.

2.5.2 Windowing

Four photographs showing the spectrum of a sinusoidal signal as analyzed by the FFT processor appear in Figures 2.10 and 2.11. In photo A of 2.10 a rectangular window was

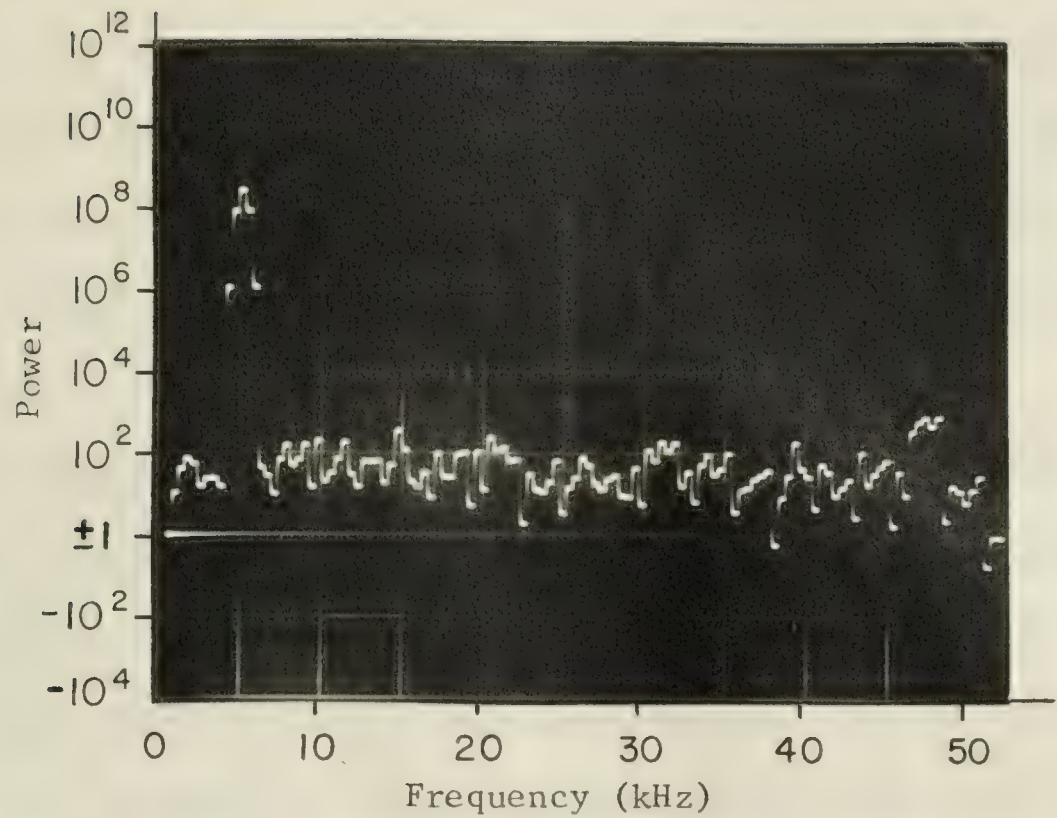


A. Input Frequency = Basis Vector

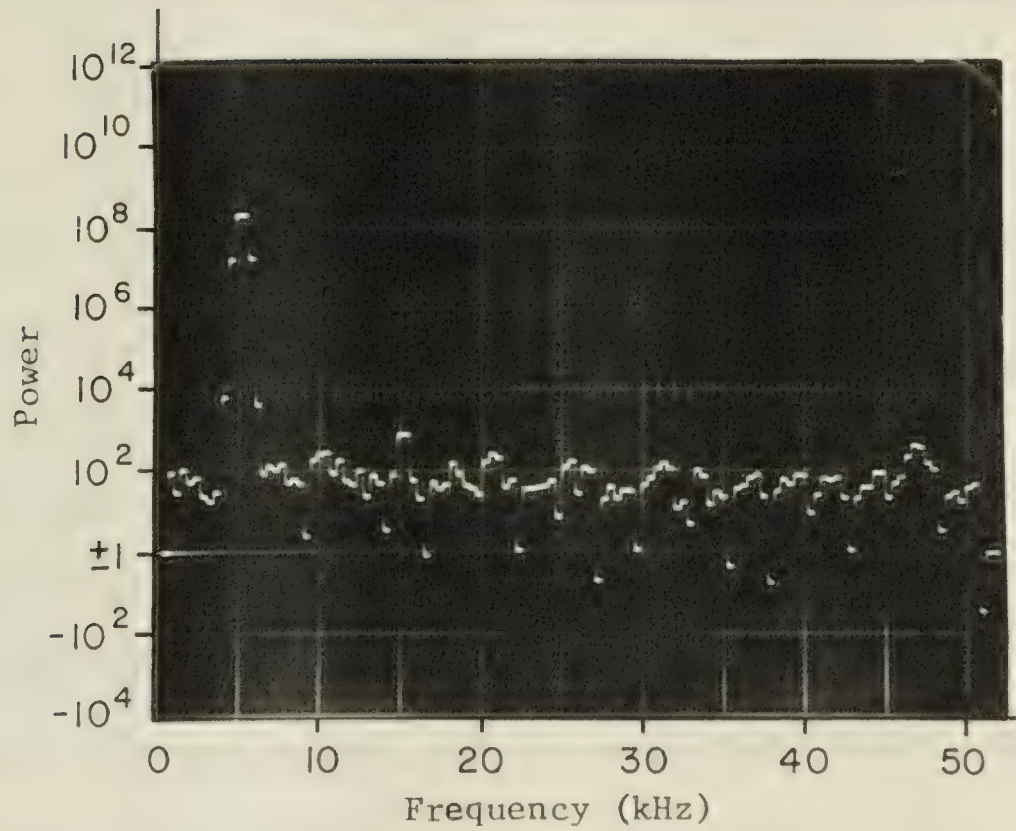


B. Input Frequency Between Basis Vectors

Figure 2.10. FFT Processor Spectrum of Sinusoid Using Rectangular Window



A. Input Frequency = Basis Vector



B. Input Frequency Between Basis Vectors

Figure 2.11. FFT Processor Spectrum of Sinusoid Using
Kaiser-Bessel Window

employed with the frequency of the sinusoid being exactly equal to the frequency of one of the FFT basis vectors. No significant sidelobes were present. In photo B, the input frequency was exactly between two of the FFT basis vectors and sidelobes appeared with the characteristic $(\sin x/x)^2$ amplitudes.

In Figure 2.11 a Kaiser-Bessel window was employed for the same sinusoidal signals as above. Sidelobe levels due to leakage were now controlled. Spurious sidelobes due to FFT coefficient quantization may be seen in 2.10 A and 2.11 A and B. The largest of these occurs at 47 kHz and is between 56 dB and 60 dB below the peak of the signal at 5 kHz.

2.5.3 Phase Relationships of the Co and Quadrature Spectra

Two tests, one with a variable phase sinusoidal source and one with delayed Gaussian noise, were conducted to verify the correct phase relationships of cross spectral components.

The results of the variable phase sinusoid test are illustrated in Figure 2.12. The powers of the peaks of co and quadrature spectra are plotted against the phase difference between the two sinusoids correlated by the processor. As expected, the co and quadrature components are always 90 degrees apart.

For the second test, noise from an audio noise generator was fed in parallel into two 512-stage bucket-brigade analog shift registers. The clock rates of

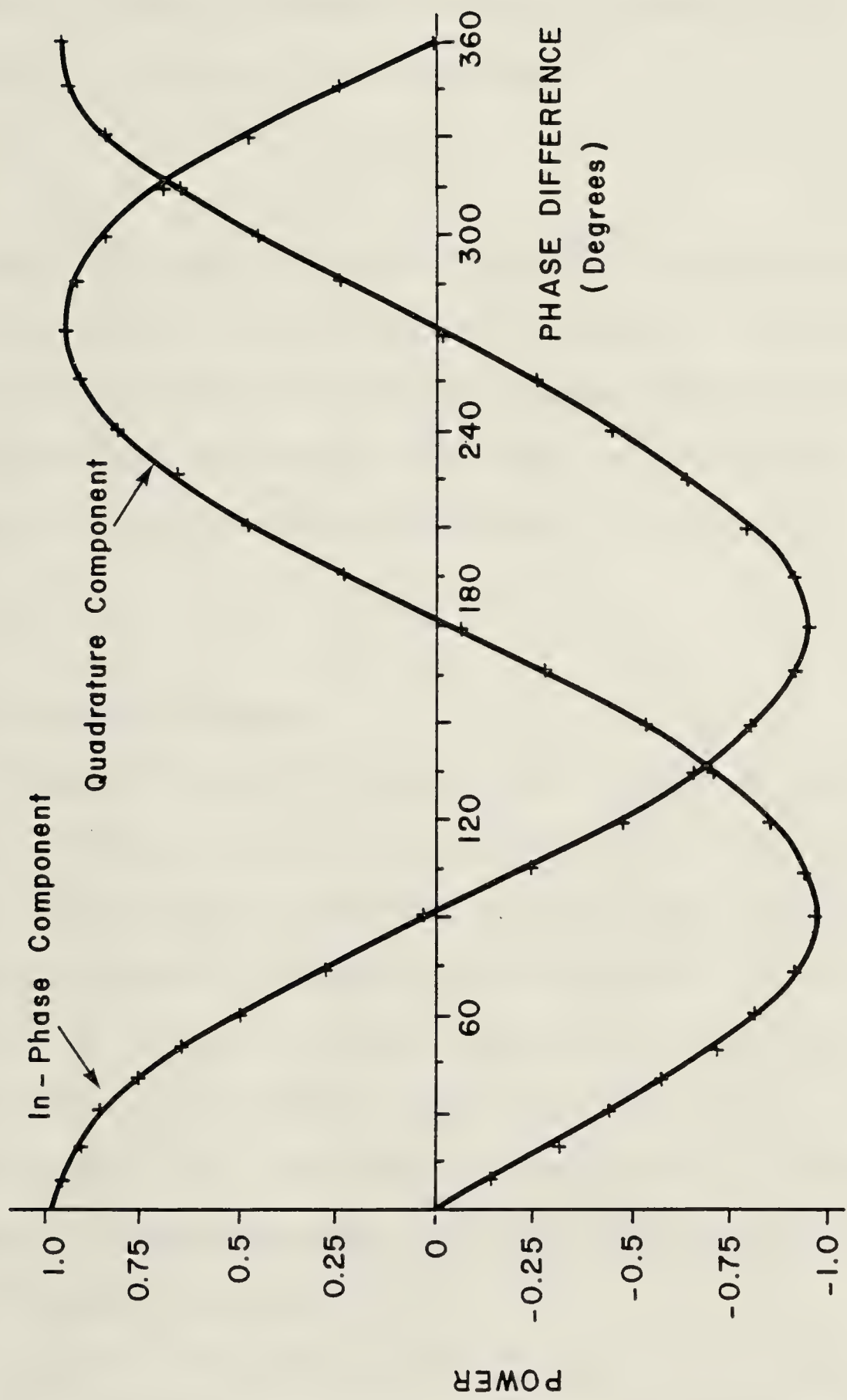


FIGURE 2.12 Power of Cross Spectrum Sinusoidal Components vs Phase Angle

the shift registers could be controlled independently to produce any desired relative delay between the register outputs. A delay τ should produce a phase shift ϕ which varies in proportion to frequency f ,

$$\phi = 2\pi f\tau \quad (2.21)$$

Figures 2.13 and 2.14 show the spectra produced with relative delays of 100 μ sec and 200 μ sec, respectively. The in-phase and quadrature spectra have cosinusoidal and sinusoidal variations of amplitude vs frequency¹, as expected from the phase difference vs frequency in equation 2.21.

2.5.4 Roundoff Noise

Roundoff noise is one of the factors which places a lower limit on the dynamic range of the FFT processor. In a block floating point design, the level of roundoff noise is dependent upon the amount of scaling which occurs during processing and is therefore dependent upon signal levels (particularly sinusoidal signals as their power is concentrated in a few spectral components). Measurements of roundoff noise were made both with and without the presence of sinusoidal signals.

Figure 2.15 shows a plot of equivalent input noise levels for the auto and cross spectra vs actual correlated noise input levels (no sinusoids present). As the input

¹The scale in the figures is logarithmic, hence the peaks appear to be flattened.

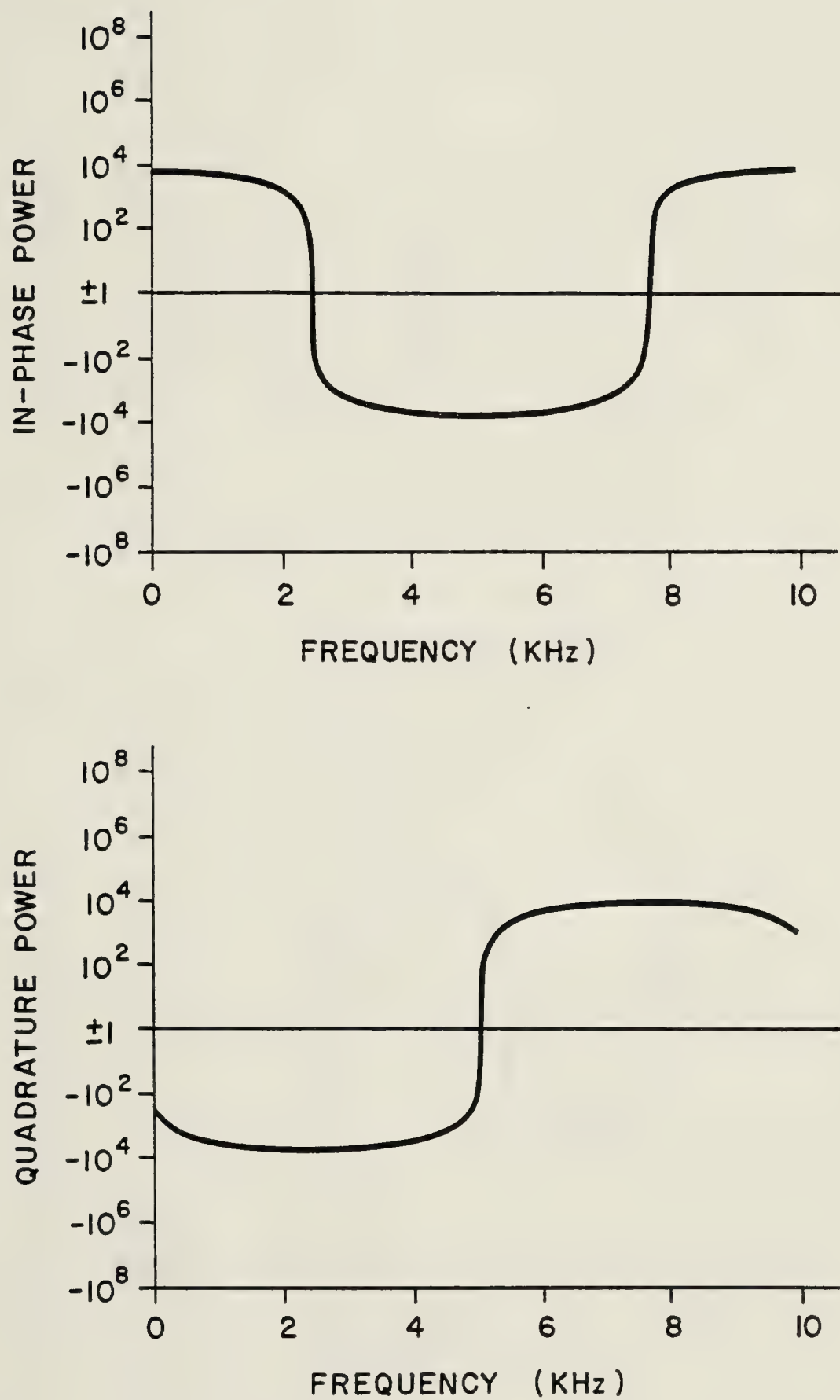


FIGURE 2.13 Cross Spectra of Delayed Noise (Delay = $100\mu\text{sec}$)

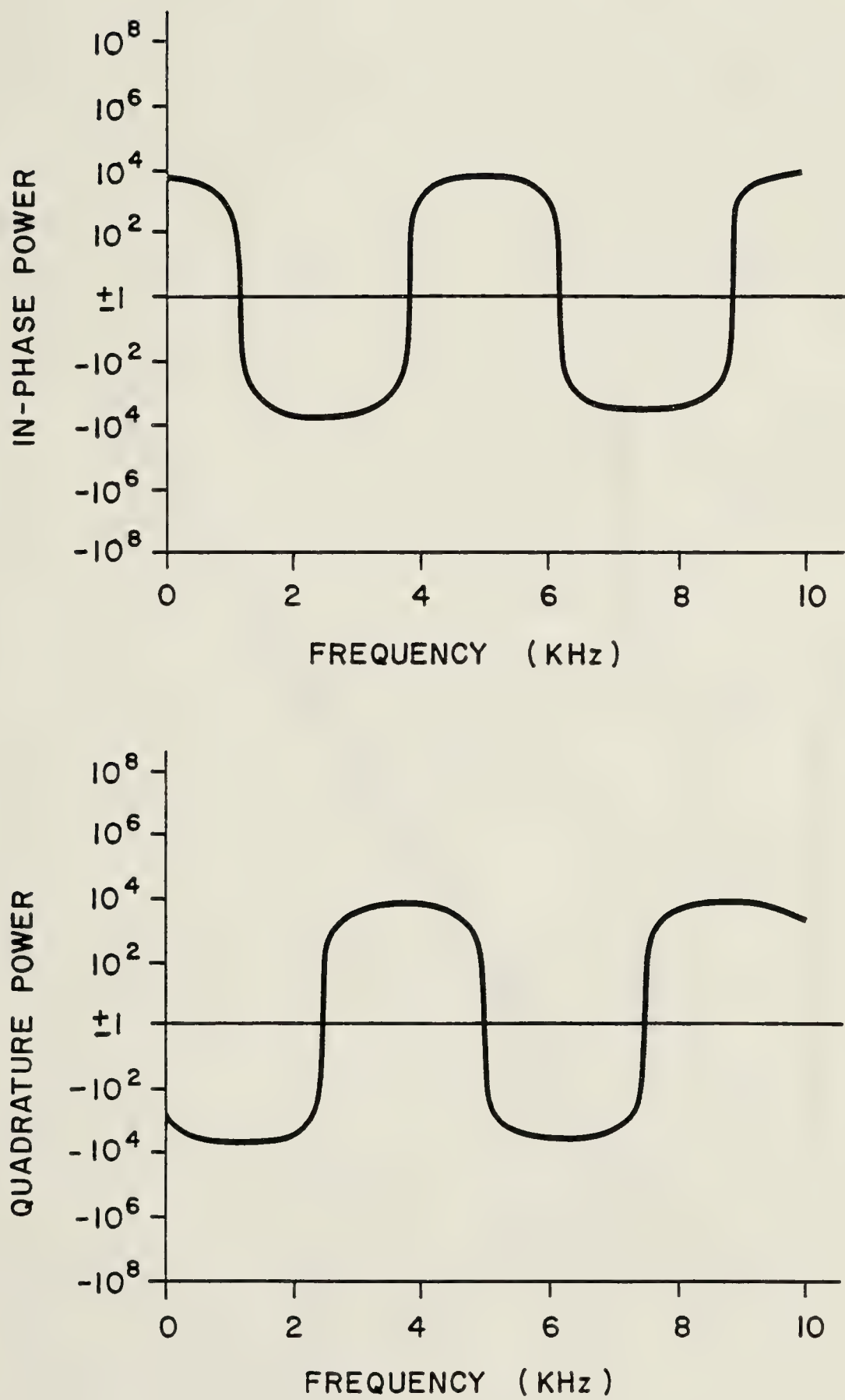


FIGURE 2.14 Cross Spectra of Delayed Noise (Delay = $200\mu\text{sec}$)

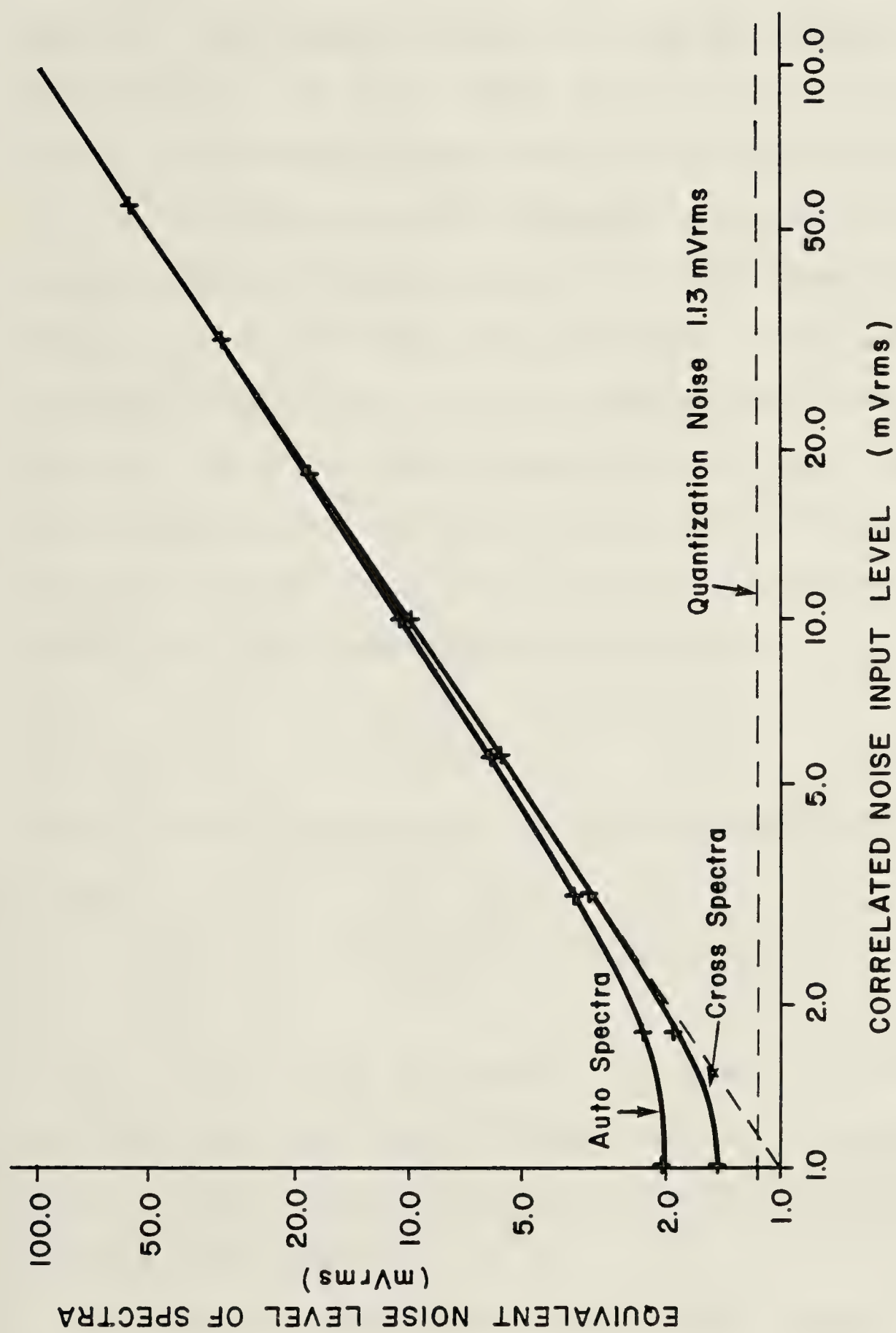


FIGURE 2.15 Equivalent Noise Levels of Spectra vs Correlated Noise Input Level

level decreases, the auto spectra depart from a linear curve (dashed line) much earlier than the cross spectra. The reason is that roundoff noise for the auto spectra is fully correlated and its power has a positive mean value which appears as an additive contribution to the auto spectra.

For the cross spectra, however, roundoff noise is uncorrelated and has zero mean. The cross spectrum therefore more accurately reflects the true input noise level, departing from it only as levels become very small. The curve for the cross spectra approaches a lower limit equal to the quantization noise of the A/D converters. As the maximum allowable input levels are ± 0.5 volts and the number of bits is 8, the quantization step size S is

$$S = \frac{1.0 \text{ volt}}{2^8} = 3.91 \text{ mV.}$$

The well known theoretical rms value of quantization noise is then

$$\sigma_Q = \frac{S}{\sqrt{12}} = 1.13 \text{ mVrms}$$

As the signals being correlated in Figure 2.15 are identical, the quantization noise due to A/D conversion is correlated and appears as an additive contribution to the in-phase cross spectrum.

A number of measurements of roundoff noise in the presence of sinusoidal signals are plotted in Figure 2.16. The noise level is approximately proportional to the sinusoidal level. The method employed in making these

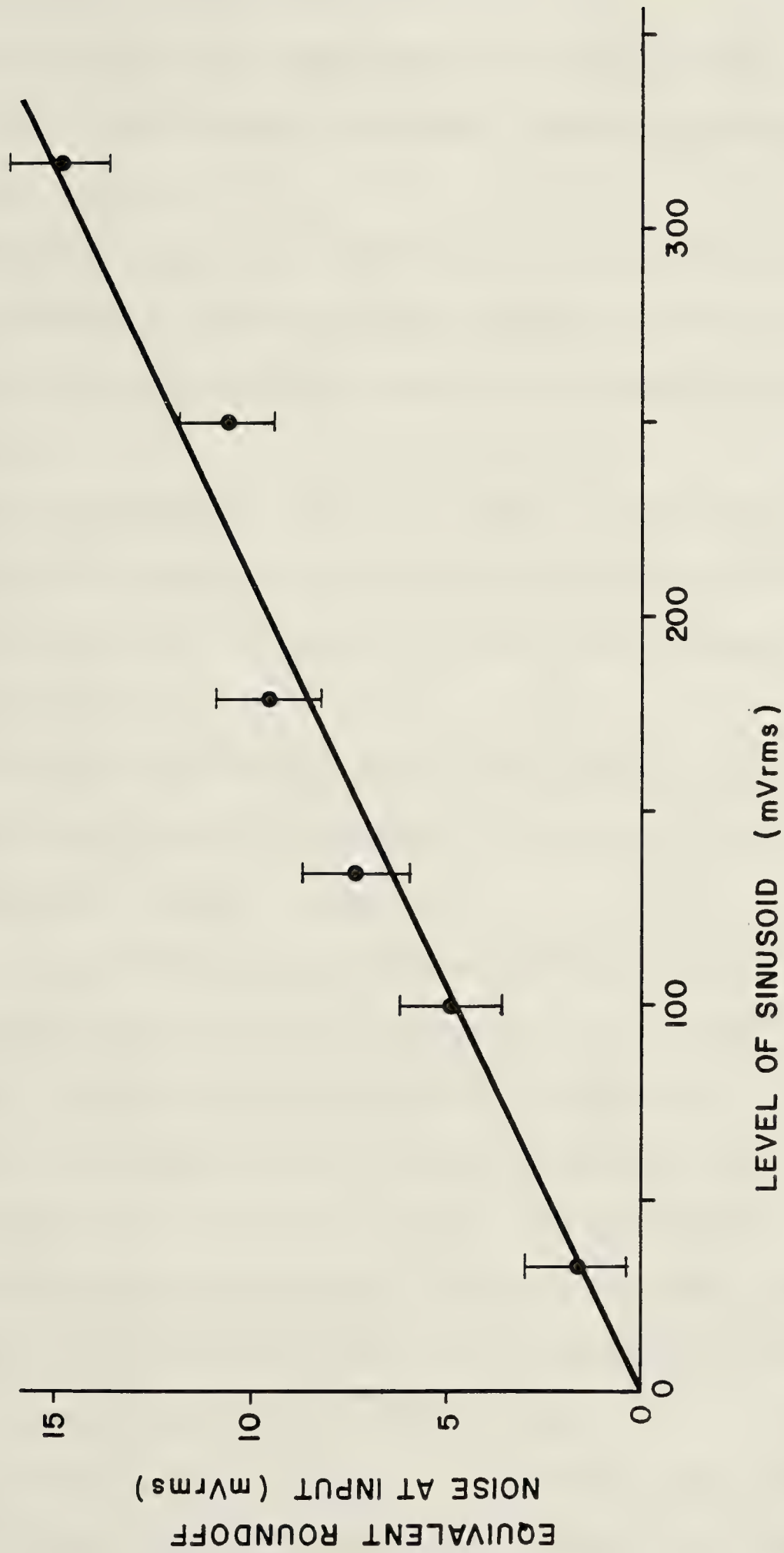


FIGURE 2.16 Roundoff Noise vs Sinusoidal Input Level

measurements is outlined below:

1. The signals analyzed consisted of a common sinusoid to which uncorrelated Gaussian noise was added in two op amp summers.
2. After analysis by the FFT processor, the frequency components containing the sinusoid were deleted from the auto spectra and averages of the remaining components taken.
3. The averages of the auto spectra when analyzing the same level of uncorrelated noise alone were subtracted from the averages in step 2 to find the excess noise due to roundoff.
4. An equivalent input noise level was found which would produce the same changes in the auto spectra as the roundoff noise in step 3.
5. As roundoff noise is not windowed, it exhibits no correlation from one component to another. Its effect on the variance of cross spectral estimates is therefore not as large as that of the windowed input noise found in step 4. This noise level was divided by $4\sqrt{EIT}$ to find an equivalent windowed input noise level which would cause the same increase in variance of cross spectral estimates as the roundoff noise.

The addition of extra noise is necessary because without it, many of the spectral components containing roundoff are so small that they are rounded to zero. A true measurement of the roundoff noise is then impossible.

2.5.5 Correlation Tests

A number of long term correlation tests of two independent noise sources were conducted to investigate the FFT processor's performance as a correlator. A small offset was found to occur when synchronous demodulation or switching was not employed, but otherwise the correlations were as expected from the theory described in other sections of this thesis.

Correlation tests were carried out using two General Radio 1390B random noise generators as noise sources. The number of spectra accumulated per integration was $K=10^5$, equivalent to an integration time of $10^5 \times 2.46 \times 10^{-3} \text{ sec} = 246 \text{ sec}$. An average of 30 trials with $K=10^5$ was taken making the total integration time 123 minutes for each test.

Equivalent levels of correlated input noise for a number of levels of uncorrelated input with and without switching are shown in Table 2.4.

With switching no detectable correlation is present in the cross spectra. Without switching a small offset occurs, probably due to either stray pickup of a common signal by the input lines or a small amount of crosstalk between the A/D converters. The first is more likely because the offset is independent of level.

The relationship between the levels of the auto spectra and the variance of the cross spectra for uncorrelated noise inputs is shown in the results in Table 2.5. As derived in

Section 4.2.3 the product of the means of the auto spectra divided by $2K$ gives an accurate estimate of the variance of the cross spectra.

Finally, in Table 2.6 the variance of the means of 30 cross spectra is compared with the expected variance if all components are independent. The average ratio of the actual variance to the expected variance if all components are independent is 2.25 which is very close to the predicted increase in variance due to windowing found in Section 2.2.3.

Table 2.4. Correlation Test Results

Uncorrelated Input Level (mVrms)	Switching	Equivalent Correlated In-Phase Level (mVrms)	Equivalent Correlated Quadrature Level (mVrms)
100.0	YES	.28±1.54	.85±1.54
31.6	YES	.26±.49	.14±.49
10.0	YES	.07±.15	.04±.15
100.0	NO	1.14±1.54	.39±1.54
31.6	NO	.80±.49	.69±.49
10.0	NO	.75±.15	.53±.15

Table 2.5. Auto Spectrum Levels and Cross Spectrum Variance
(K=10⁵)

Input Level (mVrms)	Auto1 Mean	Auto2 Mean	Auto1 x Auto2 ÷2K	In-Phase Variance	Quadrature Variance
88.6	154300	155300	119800	119900±200	114000±200
28.0	15500	15500	1201	1120±110	1150±110
8.86	1700	1654	14.06	13±3	12±3

Table 2.6. Variance of the Means of the Cross Spectra
($K=10^5$, No. of Components = 120)

Input Level (mVrms)	I or Q	Variance of Cross Spectrum $\div 120$	Variance of Means of 30 Cross Spectra	Ratio
88.6	I	1000	2400 ± 1000	2.4 ± 1.0
	Q	950	2200 ± 900	$2.3 \pm .9$
31.6	I	9.3	24 ± 10	2.6 ± 1.0
	Q	9.6	27 ± 11	2.8 ± 1.1
10.0	I	.11	$.16 \pm .06$	$1.5 \pm .6$
	Q	.10	$.19 \pm .08$	$1.9 \pm .8$
			Average	$2.25 \pm .4$

3. Receivers

A block diagram of the receiving system used for the project appears in Figure 3.1. The antennas, RF amplifiers, first mixers, first IF amplifiers and first local oscillator were part of a previous project at the Dominion Radio Astrophysical Observatory. This project was the first low frequency earth rotation aperture synthesis mapping of the north polar sky and is described in Dewdney [2].

The present system used the 300 kHz bandwidth outputs of the first IF amplifiers at 5.0 MHz to feed second mixers and second IF amplifiers, forming a sharply bandlimited signal from 416 kHz to 468 kHz suitable for sampling and A/D conversion. The receiving equipment designed and built during the course of the present project is described in this chapter.

3.1 Second Mixers and IF Amplifiers

A schematic of a second mixer and IF amplifier is shown in Figure 3.2.

The mixer consists of an MC1496 balanced modulator. This device was chosen because of its good linearity and high isolation (>60 dB) between RF, IF and local oscillator ports. The high isolation reduces crosstalk between the two receivers via the common local oscillator. Isolation is also improved through the use of a balanced hybrid splitter for second local oscillator distribution.

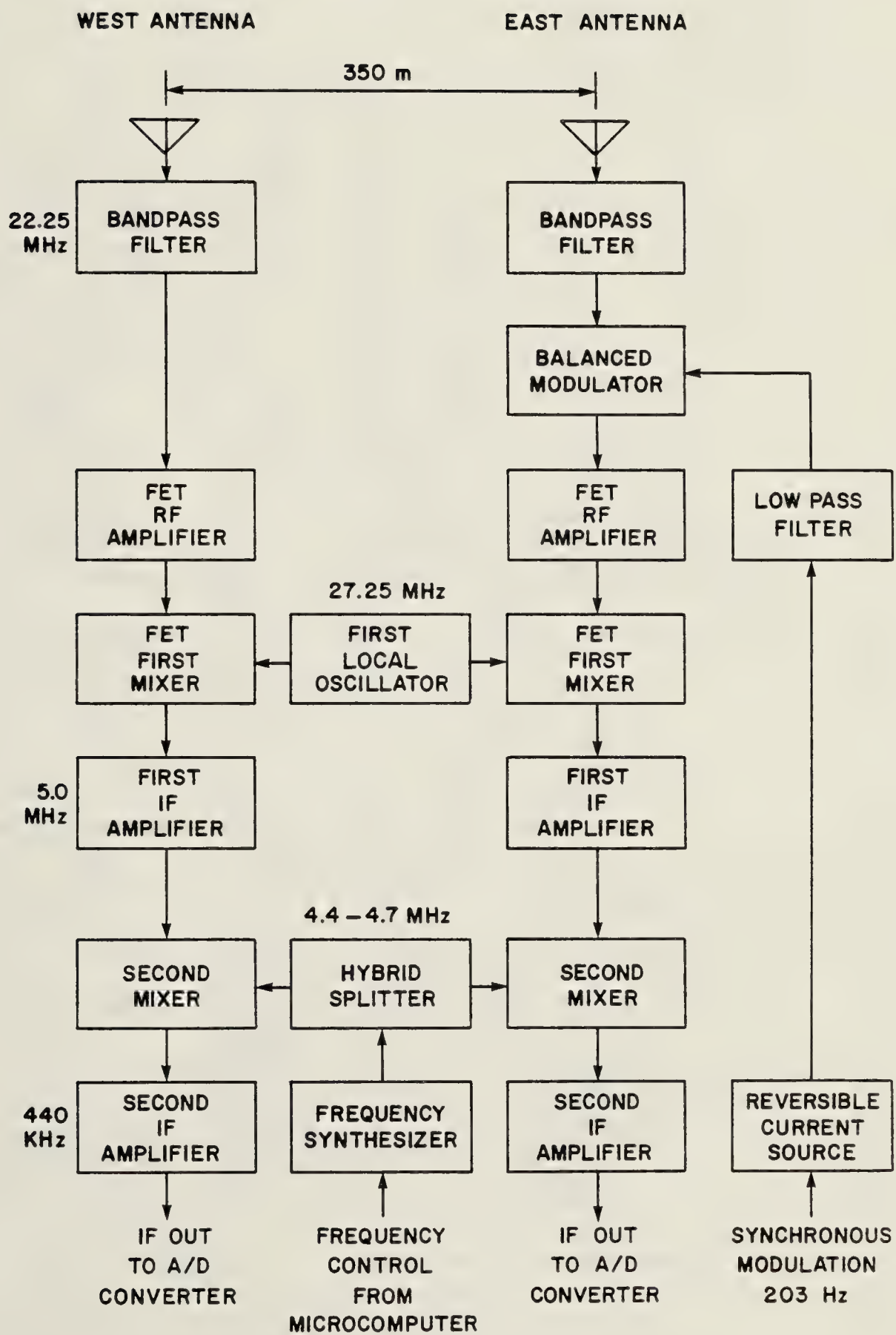


FIGURE 3.1 Receivers

The 440 kHz IF amplifier following the mixer consists of three LM371 cascode amplifier stages and an output buffer stage. Coupling between stages is accomplished via double-tuned tank circuits. The 8 tank circuits form an 8-pole Chebyshev bandpass filter with a design ripple of 0.01 dB.

With the Q of about 150 available in commercial IF transformers at 455 kHz, a Chebyshev filter with 0.01 dB ripple was the best filter characteristic attainable. Sharp cutoff at band edges can be obtained in filters by the addition of zeroes in the transfer function at the edges, as for example in elliptic filters [58]. However, such zeroes cause ripples in the out-of-band response. It was deemed more desirable to minimize the response to out-of-band signals as much as possible rather than having an extremely sharp cutoff. For this reason, a minimum-phase Chebyshev filter seemed most suitable.

In order to achieve a symmetrical bandpass response it was necessary to use inductive coupling for the first two double-tuned circuits and capacitive coupling for the second two. Such a combination is necessary to get the correct number of zeroes in the bandpass transfer function. Very briefly, consider an 8-pole low-pass Chebyshev transfer function [59]

$$G_{LP}(s) = \frac{K_{LP}}{s^8 + a_7s^7 + \cdots + a_1s + a_0}$$

A low-pass to bandpass transformation replaces s with

$(s^2 + \omega^2)/(s BW)$ and produces a bandpass transfer function with 8 zeroes.

$$G_{BP}(s) = \frac{s^8 K_{BP}}{s^{16} + b_{15}s^{15} + \cdots + b_1s + b_0}$$

The correct number of poles can be obtained by cascading the transfer functions of 4 double-tuned stages, each contributing 4 poles. However, with either transformer or inductive coupling a double-tuned stage contributes only one zero. The transfer function is

$$G_L(s) = \frac{sK_L}{s^4 + c_3s^3 + c_2s^2 + c_1s + c_0}$$

A cascade of four such stages would result in an overall $G_{BP}(s)$ with only 4 zeroes. The result is a somewhat skewed frequency response which is particularly noticeable when the filter bandwidth is an appreciable fraction of the center frequency.

A capacitively coupled double-tuned circuit, on the other hand, exhibits 3 zeroes:

$$G_C(s) = \frac{s^3 K_C}{s^4 + d_3s^3 + d_2s^2 + d_1s + d_0}$$

By using two capacitively coupled and two inductively coupled stages, 8 zeroes can be obtained.

The desired filter response was obtained by the choice of component values in the double-tuned stages. The calculations are lengthy and will not be included herein. A short description of the design and tuning procedure follows.

Each tank circuit inductor could be tuned individually to allow pole locations to be adjusted. However, since no identical poles were needed, overcoupling of the double-tuned circuits was used to ensure maximum energy transfer. If the two tank circuits of an overcoupled double-tuned stage are tuned identically, then the actual double-tuned poles occur at different frequencies, with the difference being dependent upon the degree of overcoupling. Element values in the second IF amplifiers were chosen to produce differences in poles of slightly less than the desired values so that tuning could be used to set the poles exactly.

Pole damping to obtain a Chebyshev response was accomplished by resistors marked with asterisks in Figure 3.2. Approximate resistor values were found through calculation but the final selection was made experimentally by physically measuring the Q 's of each tank circuit with all components except the damping resistors connected.

Interaction between the two halves of the double-tuned circuits did not present any problems during tuning of the IF amplifiers. It was possible through careful adjustment of the inductor cores and by some trial-and-error fine adjustment of resistor values to obtain a frequency response with less than 0.1 dB of ripple. Phase matching of the two IF amplifiers was to within 5 degrees.

One problem which was encountered was a lack of mechanical stability in the IF transformer cores. The

amplifier frequency response was found to change, particularly in response to physical shocks or movement. Regular monitoring of the frequency response was necessary to maintain proper tuning.

The final stage of the second IF amplifiers is an output buffer consisting of an LM318 operational amplifier and an LH0002 current driver. This stage is capable of driving a 50 ohm load at high levels (± 10 volts) with low distortion. The required input level for the A/D converters is much less than this (± 0.5 volts).

3.2 RF Amplifier, First Mixer and First IF Amplifier

A schematic of the RF, first mixer and first IF stages is shown in Figure 3.3. The circuit is a modified version of the receivers originally used for the north polar synthesis telescope.

The original receivers used a bipolar transistor in the first stage of the cascode RF amplifier and a bipolar integrated circuit (an MC1550) as the mixer. These bipolar stages were found to produce high levels of intermodulation distortion when observing was attempted during periods of strong interference.

Bipolar transistors are highly susceptible to intermodulation problems because their large-signal i - v characteristic is exponential in nature [60]:

$$I_C = a_{21}[\exp(V_E/V_T) - 1] + a_{22}[\exp(V_C/V_T) - 1]$$

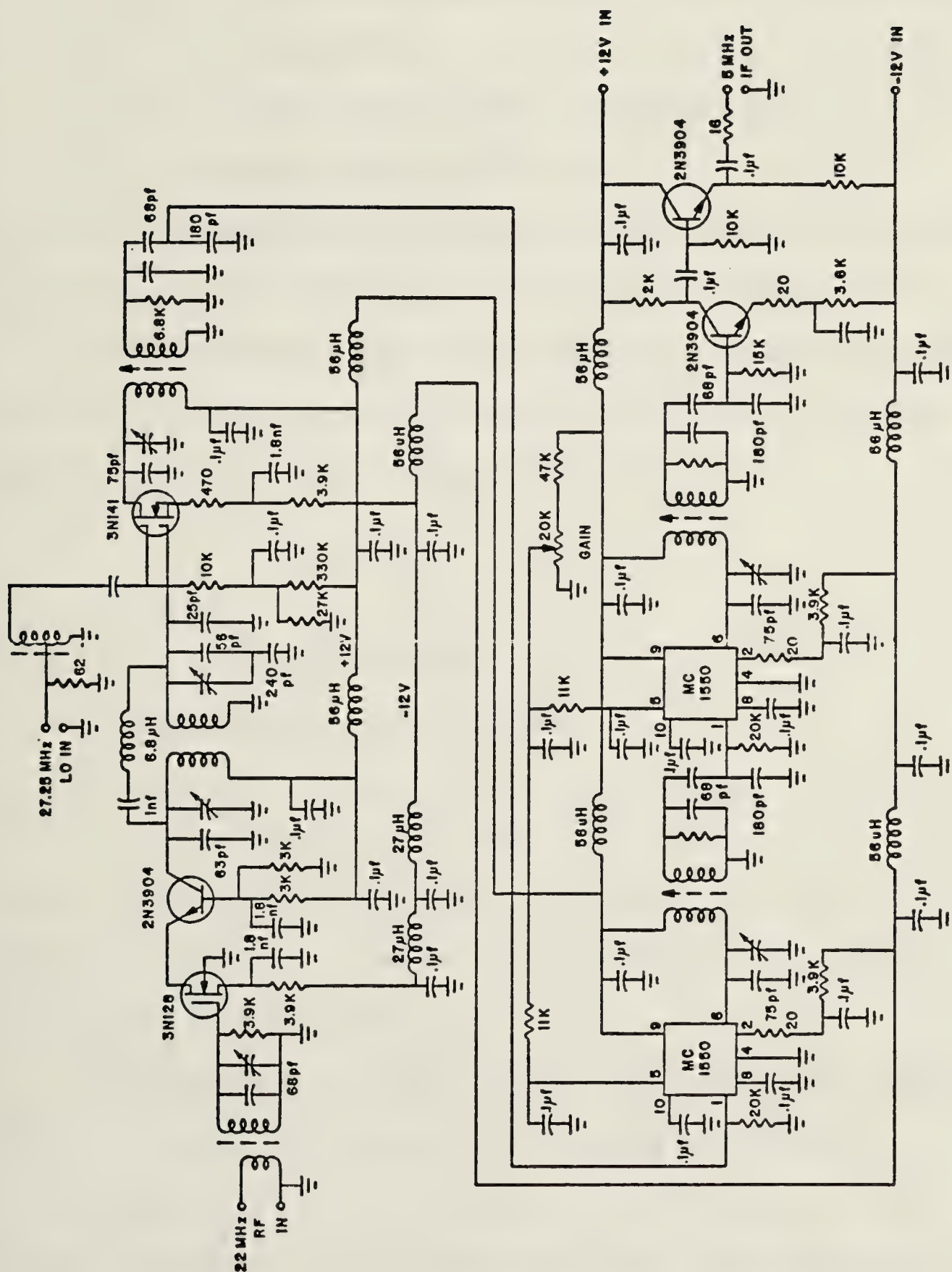


Figure 3.3. RF Amplifier, First Mixer and IF Amplifier

where I_C = collector current

a_{21} , a_{22} = constants depending upon transistor construction

$V_E(V_C)$ = voltage drop across emitter (collector) junction

V_T = voltage equivalent of temperature
= temperature/11600° K/volt

A series expansion of this characteristic contains many odd-order terms which give rise to intermodulation.

Field effect transistors are well known to produce low levels of intermodulation distortion. The i-v characteristic for a FET is a simple square law [61]:

$$I_{DS} = I_{DSS}(1 - V_{GS}/V_P)^2$$

where I_{DS} = saturation drain current

V_{GS} = gate-source voltage

$I_{DSS} = I_{DS} |_{V_{GS}=0}$

V_P = pinch-off voltage

As no terms of higher order than two are present (at least ideally) FET's can amplify or mix high-level signals with little intermodulation.

Replacement of the RF amplifier and mixer stages with FET's as shown in Figure 3.3 reduced problems of intermodulation in the receivers considerably. The third order intermodulation intercept point (as measured in a standard two-tone intermodulation test) was found to increase from -60 dBm to -11 dBm.

The noise temperatures of the two receivers after modification were measured to be 900°K and 1500°K .

The first IF amplifiers consist of two cascode amplifiers (MC1550's) and an output buffer stage. The double-tuned circuits which provide interstage coupling are adjusted for a Butterworth filter response with a bandwidth of 300 kHz centered on 5 MHz. Following front end modifications the responses of the two RF and first IF stages together were adjusted to be matched within ± 0.15 dB in amplitude and ± 1.25 degrees in phase over the central 200 kHz of the pass band, as it was only this region of the first IF output which was actually used.

3.3 Input Bandpass Filters

Most of the RF selectivity of the receivers was provided by the tuned circuits associated with the RF amplifier stage in Figure 3.3. These tuned circuits were adjusted for a 3 dB bandwidth of 600 kHz.

Additional out-of-band rejection was provided by external bandpass filters. These filters had a bandwidth of 5 MHz centered on 22.25 MHz and were specially designed for high rejection at frequencies far below and above the center of the pass band. The filters had a 3-pole Chebyshev response with 0.01 dB ripple and are shown in Figure 3.4.

The filter's rejection at 1 MHz was greater than 100 dB and from 50 MHz to 350 MHz was greater than 50 dB. To obtain good performance over such a wide frequency range required

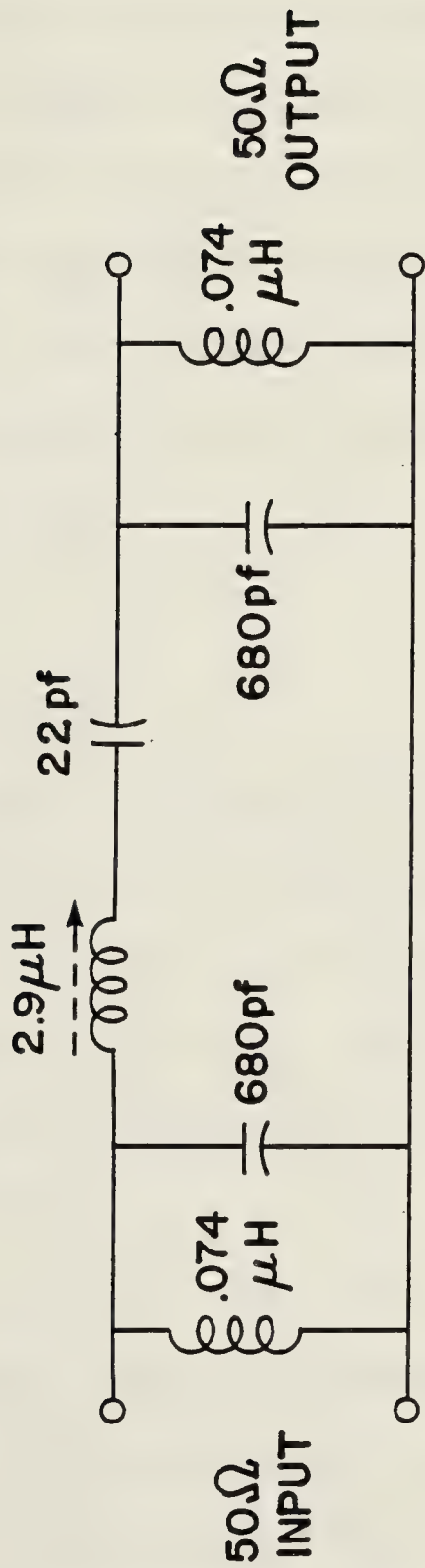


FIGURE 3.4 Input Bandpass Filter

selection of components with low parasitic impedances. For example, the 680 pf capacitors were chip capacitors with extremely low inductance and the 0.074 μ H coils were toroids with high Q and a high self-resonant frequency. High Q inductors limited the insertion loss at 22.25 MHz to 1.0 dB.

Construction was also crucial. Low frequency rejection was found to be highly dependent on good grounding and the use of a solid ground plane. Good high frequency rejection required shielding between the two halves of the filter to prevent radiative coupling.

3.4 Synchronous Modulation

Synchronous modulation of the RF signal from the east antenna was accomplished with a Hewlett Packard 10534A balanced modulator. The diode ring in this modulator was driven through a length of coaxial cable from the observatory building by a reversible current source diagrammed in Figure 3.5.

The phase switch control input was a binary signal from the FFT processor which alternated between +12 V and -12 V at a rate of 203 Hz. The input circuit consisting of an adjustable RC network and back-to-back Zener diodes allowed a variable delay to be introduced. The delay was adjusted to produce phase transitions of 180 degrees at the east receiver A/D input which coincided with the beginnings of new blocks of FFT samples.

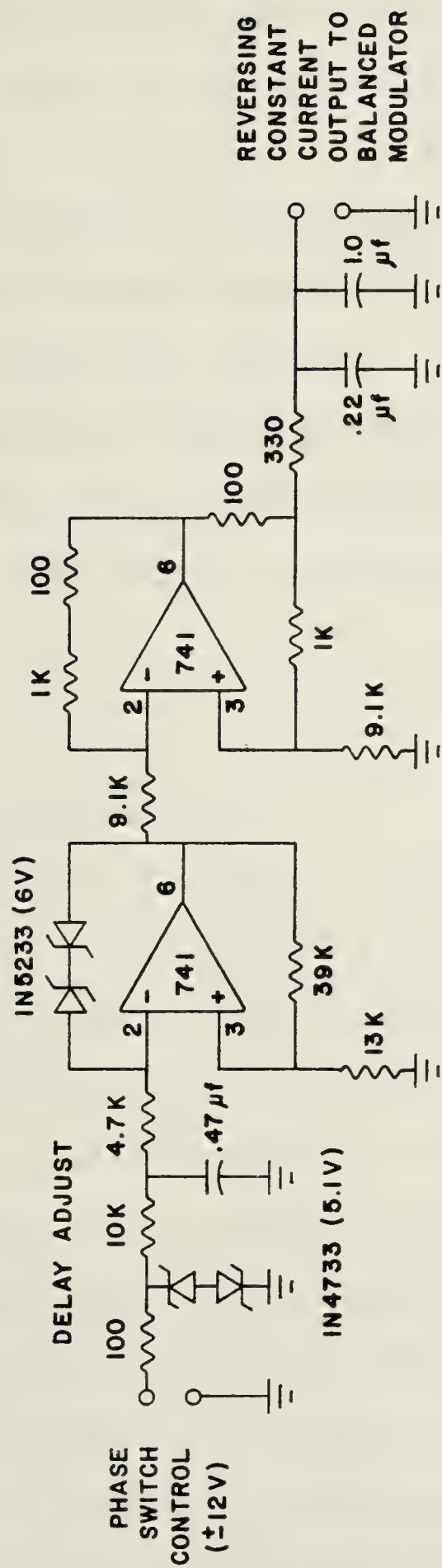


Figure 3.5. Reversible Current Source for Synchronous Modulation

The first op amp formed a Schmitt trigger with its output limited to ± 8.8 volts by feedback through Zener diodes. The second op amp was a voltage-to-current converter which responded to its ± 8.8 volt input with an output of ± 10 ma.

An RC network at the output limited the rise and fall times of the current output to reduce ringing, as the output drives a long length of cable.

A low-pass filter just before the balanced modulator prevented RF signals being conducted by the synchronous modulation cable and introducing crosstalk between the receivers.

3.5 Local Oscillators

The first L.O. was a crystal controlled oscillator at a frequency of 27.25 MHz. This oscillator signal was distributed from a central point via separate buffer stages and cables to the east and west receivers. The RF, first mixer and first IF stages of each receiver were physically located near their respective antennas and were connected via coaxial cable to the second mixers and IF amplifiers which were located in the observatory building.

The second L.O. consisted of a digitally controlled Fluke 6039A frequency synthesizer. A serial digital connection to the microcomputer allowed the frequency of the second L.O. to be changed under computer control. As the synthesizer required about 40 parallel control lines, a

serial-to-parallel interface employing shift registers and a simple binary pulse width modulation scheme was built to reduce the number of control lines needed to only one.

4. Robust Estimation

4.1 Introduction

In this chapter, an estimation procedure well suited to the problem of minimizing the effects of terrestrial interference in the cross power spectrum is derived. Section 4.2 begins by defining the estimation problem and finding the expected probability density functions of the cross and auto spectra. Historical aspects of rejection rules and a branch of statistics known as robust estimation are discussed in Section 4.3, and the concept of robust maximum-likelihood estimation (M-estimation) is introduced. The characteristics and performance of some M-estimators are presented in Section 4.4. A short discussion of adaptive estimation follows in Section 4.5. Finally, Section 4.6 proposes a robust estimation procedure combining rejection rules and M-estimates which the author believes is a good choice for excising terrestrial interference.

4.2 Definition of the Estimation Problem

The underlying assumption which makes the removal of terrestrial interference from the cross power spectrum possible is that the interference will be narrow band and will contaminate only a certain percentage of the components of the spectrum. At least some of the components at any given time will be free of interference and these components, if they can be identified, can be used for

astronomy as if there were no interference at all.

Components with no interference can be expected to exhibit a normal probability distribution, the parameters of which are found below for both the cross and auto spectra. Components containing interference will deviate from the normal distribution, introducing contaminated points and heavier tails in the distribution. Such contamination would be disastrous if a simple mean of all points was used as an estimate of the center of the distribution, as the mean is very sensitive to outlying points. The robust estimation procedures described later in this chapter are designed to provide protection from outlying points when estimating the center of a contaminated normal distribution.

4.2.1 Probability Density Function of Averaged Cross Spectra

This section will show that, in the absence of interference, an averaged cross power spectrum will have a normal probability density function (pdf). Consider the two signals being correlated as two real series $f(n,k)$ and $g(n,k)$, where $0 \leq n \leq N-1$ and $1 \leq k \leq K$. The index n represents points within a block of FFT samples, whereas the index k is incremented with successive FFT's. The FFT's of $f(n,k)$ and $g(n,k)$ for a particular value of k will be called instantaneous FFT's, denoted by $F(m,k)$ and $G(m,k)$, where $0 \leq m \leq N-1$ and F and G are complex.

The instantaneous cross power spectrum, denoted

$FG^*(m,k)$, will be

$$\begin{aligned}
 FG^*(m,k) &= F(m,k) G^*(m,k) \\
 &= F_r(m,k) G_r(m,k) + F_i(m,k) G_i(m,k) \\
 &\quad + j[F_i(m,k) G_r(m,k) - F_r(m,k) G_i(m,k)] \quad (4.1)
 \end{aligned}$$

The subscripts r and i denote real and imaginary components.

Before determining the pdf's of the real and imaginary components above, a number of assumptions will be stated. First, $f(n,k)$ and $g(n,k)$ consist of samples of Gaussian noise bandlimited to exactly the Nyquist frequency. Second, the correlation between $f(n,k)$ and $g(n,k)$ is identical in amplitude and phase at all frequencies. Then $F_r(m,k)$ and $F_i(m,k)$ will be normally distributed with mean 0 and variance σ_F^2 , denoted as $N(0, \sigma_F^2)$, and $G_r(m,k)$ and $G_i(m,k)$ will be $N(0, \sigma_G^2)$. The relationships between the four components above can be seen in the variance-covariance matrix in Table 4.1. Here, ρ_C and ρ_Q refer to the correlation coefficients of the real and imaginary components of the cross power spectrum (the co and quadrature spectra).

From Table 4.1 it is possible to calculate the expected mean and variance for the cross power spectrum. Consider the real part first, $F_r G_r + F_i G_i$. Using results derived in Appendix 2 for the product of two Gaussian variables, the expected mean and variance will be

Table 4.1. Variance-Covariance Matrix for the Complex Spectra of Two Partially Correlated Gaussian Signals

	F_r	F_i	G_r	G_i
F_r	σ_F^2	0	$\rho_C \sigma_F \sigma_G$	$-\rho_Q \sigma_F \sigma_G$
F_i	0	σ_F^2	$\rho_Q \sigma_F \sigma_G$	$\rho_C \sigma_F \sigma_G$
G_r	$\rho_C \sigma_F \sigma_G$	$\rho_Q \sigma_F \sigma_G$	σ_G^2	0
G_i	$-\rho_Q \sigma_F \sigma_G$	$\rho_C \sigma_F \sigma_G$	0	σ_G^2

$$\begin{aligned}
 E[F_r G_r + F_i G_i] &= E[F_r G_r] + E[F_i G_i] \\
 &= \rho_C \sigma_F \sigma_G + \rho_Q \sigma_F \sigma_G = 2\rho_C \sigma_F \sigma_G
 \end{aligned} \tag{4.2}$$

$$\begin{aligned}
 V[F_r G_r + F_i G_i] &= E[(F_r G_r + F_i G_i)^2] - E^2[F_r G_r + F_i G_i] \\
 &= E[F_r^2 G_r^2 + F_i^2 G_i^2 + 2F_r G_r F_i G_i] - 4\rho_C^2 \sigma_F^2 \sigma_G^2 \\
 &= E[F_r^2 G_r^2] + E[F_i^2 G_i^2] + 2E[F_r G_r F_i G_i] - 4\rho_C^2 \sigma_F^2 \sigma_G^2 \\
 &= \sigma_F^2 \sigma_G^2 (1 + 2\rho_C^2) + \sigma_F^2 \sigma_G^2 (1 + 2\rho_Q^2) \\
 &\quad + 2\sigma_F^2 \sigma_G^2 (\rho_C^2 - \rho_Q^2) - 4\rho_C^2 \sigma_F^2 \sigma_G^2 \\
 &= \sigma_F^2 \sigma_G^2 (2 + 4\rho_C^2 + 2\rho_C^2 - 2\rho_Q^2 - 4\rho_C^2) \\
 &= 2\sigma_F^2 \sigma_G^2 (1 + \rho_C^2 - \rho_Q^2)
 \end{aligned} \tag{4.3}$$

Similarly, for the imaginary part of the cross power spectrum,

$$E[F_i G_r - F_r G_i] = 2\rho_Q \sigma_F \sigma_G \tag{4.4}$$

$$V[F_i G_r - F_r G_i] = 2\sigma_F^2 \sigma_G^2 (1 + \rho_Q^2 - \rho_C^2) \quad (4.5)$$

Although the mean and variance of the spectra will be as derived above, the pdf will not necessarily be Gaussian. However, our concern is with the average of many instantaneous cross spectra, for which the pdf as shown below will tend to be Gaussian.

Let the average over K instantaneous cross spectra be

$$P_X(m) = P_C(m) + jP_Q(m) = \frac{1}{K} \sum_{k=1}^K FG^*(m,k) \quad (4.6)$$

In the absence of interference, each instantaneous cross spectrum will be independent and by the Central Limit Theorem of statistics, $P_C(m)$ and $P_Q(m)$ will tend to be normally distributed. The mean and variance of $P_C(m)$ will be

$$\begin{aligned} E[P_C(m)] &= \frac{1}{K} \sum_{k=1}^K E[F_r G_r + F_i G_i] \\ &= \frac{1}{K} \sum_{k=1}^K 2\rho_C(k) \sigma_F(k) \sigma_G(k) \end{aligned} \quad (4.7)$$

$$V[P_C(m)] = \frac{1}{K^2} \sum_{k=1}^K 2\sigma_F^2(k) \sigma_G^2(k) [1 + \rho_C^2(k) + \rho_Q^2(k)] \quad (4.8)$$

Note that σ_F , σ_G , ρ_C and ρ_Q have now become functions of k in order to allow for the variation of these parameters with time. In practice, ρ_C and ρ_Q may change significantly during one averaging interval determined by K , due to the movement of discrete radio sources through the lobes of the antenna beam formed by the interferometer. σ_F and σ_G will

change much more slowly, as they reflect the total power being received by the beam of each individual antenna from the entire sky. σ_F and σ_G may be considered to remain constant over the averaging interval. This is fortunate, as otherwise the requirement for identically distributed variables during summation for the Central Limit Theorem would be violated and the normality of the cross power spectra could not be expected.

Taking σ_F and σ_G as constant,

$$E[P_C(m)] = 2\sigma_F \sigma_G \frac{1}{K} \sum_{k=1}^K \rho_C(k) = 2\sigma_F \sigma_G \overline{\rho_C} \quad (4.9)$$

$$V[P_C(m)] = 2\sigma_F^2 \sigma_G^2 \frac{1}{K^2} \sum_{k=1}^K [1 + \rho_C^2(k) + \rho_Q^2(k)] \quad (4.10)$$

Now ρ_C and ρ_Q were defined as the correlation coefficients of the instantaneous co and quadrature spectra. A complex correlation coefficient ρ_X may be defined as

$$\rho_X = \rho_C + j\rho_Q \quad (4.11)$$

where the magnitude of ρ_X is equal to the fraction of the total power received by either antenna (assuming identical antenna patterns) which is correlated, $0 \leq |\rho_X| \leq 1$, and the phase of ρ_X determines how the correlated power is distributed between the co and quadrature spectra. It follows that

$$0 \leq \rho_X(k) \rho_X^*(k) = \rho_C^2(k) + \rho_Q^2(k) \leq 1 \quad (4.12)$$

$$K \leq \sum_{k=1}^K [1 + \rho_C^2(k) + \rho_Q^2(k)] \leq 2K \quad (4.13)$$

and

$$2\sigma_F^2 \sigma_G^2 / K \leq V[P_C(m)] \leq 4\sigma_F^2 \sigma_G^2 / K \quad (4.14)$$

At this point, an assumption may be made about decametric antennas which will place $V[P_C(m)]$ close to the lower limit in equation 4.14. Practical decametric antennas generally have relatively broad beam widths, thus the total correlated power received from a discrete source will generally be small ($|\rho_X| < 0.1$) relative to background noise received from the rest of the sky. Hence $\rho_C^2(k) + \rho_Q^2(k) \ll 1$ and

$$V[P_C(m)] \approx 2\sigma_F^2 \sigma_G^2 / K \quad (4.15)$$

The probability density function of $P_C(m)$ is then found to be a normal distribution described as $N(2\sigma_F\sigma_G\bar{\rho}_C, 2\sigma_F^2\sigma_G^2/K)$. Similarly, the pdf of $P_Q(m)$ is $N(2\sigma_F\sigma_G\bar{\rho}_Q, 2\sigma_F^2\sigma_G^2/K)$.

4.2.2 Probability Density Function of Averaged Auto Spectra

The instantaneous auto power spectra of the two signals will be

$$FF^*(m,k) = F(m,k)F^*(m,k) = F_r^2(m,k) + F_i^2(m,k) \quad (4.16)$$

$$GG^*(m,k) = G(m,k)G^*(m,k) = G_r^2(m,k) + G_i^2(m,k) \quad (4.17)$$

As F_r is independent of F_i and G_r is independent of G_i for the case of no interference, the pdf's of FF^* and GG^* will correspond to σ_F^2 and σ_G^2 , respectively, times a chi-square distribution with two degrees of freedom, $\chi^2(2)$. The

averaged auto spectra will be

$$P_F(m) = \frac{1}{K} \sum_{k=1}^K FF^*(m,k) \quad (4.18)$$

$$P_G(m) = \frac{1}{K} \sum_{k=1}^K GG^*(m,k) \quad (4.19)$$

and will consist of the sums of the squares of $2K$ independent, normal variables. If σ_F^2 and σ_G^2 are assumed to remain constant over the averaging interval, then $P_F(m)$ and $P_G(m)$ will have pdf's corresponding to σ_F^2/K and σ_G^2/K , respectively, times $\psi^2(2K)$, a chi-square distribution with $2K$ degrees of freedom. For large K , $\psi^2(2K)$ will converge to a normal distribution $N(2K, 4K)$, and so the pdf of $P_F(m)$ will be

$$\frac{\sigma_F^2}{K} N(2K, 4K) = N\left(2K \frac{\sigma_F^2}{K}, 4K \frac{\sigma_F^4}{K^2}\right) = N\left(2\sigma_F^2, \frac{4\sigma_F^4}{K}\right) \quad (4.20)$$

and the pdf of $P_G(m)$ will be

$$\frac{\sigma_G^2}{K} N(2K, 4K) = N\left(2\sigma_G^2, \frac{4\sigma_G^4}{K}\right) \quad (4.21)$$

4.2.3 Estimating the Variance of the Cross Spectra

In the discussion of robust estimation later in this chapter, it will be found that an accurate estimate of the variance of a distribution is invaluable when attempting to estimate the distribution's center. It will now be shown that the auto spectra can be used to provide an accurate estimate of the variance of the cross spectra.

First of all, it can easily be demonstrated that the sample variance is a poor estimator of the cross spectrum variance. From Section 4.2.1, the pdf of $P_C(m)$ is $N(2\sigma_F\sigma_G\overline{P}_C, 2\sigma_F^2\sigma_G^2/K)$. The usual sample variance for $P_C(m)$ would be

$$S^2 = \frac{1}{M-1} \sum_{m=1}^M (P_C(m) - \overline{P}_C)^2 \quad (4.22)$$

where $\overline{P}_C = (1/M) \sum_{m=1}^M P_C(m)$. As the $P_C(m)$ are independent for Gaussian noise, S^2 will have a pdf corresponding to $\sigma_C^2/(M-1)$ times $\chi^2(M-1)$, where σ_C^2 is the variance of $P_C(m)$. The expected value of S^2 will then be σ_C^2 (because S^2 is an unbiased estimator of σ_C^2 [62]) and the expected variance of S^2 will be

$$V[S^2] = 2(M-1) \left[\frac{\sigma_C^2}{M-1} \right]^2 = 2 \frac{\sigma_C^4}{M-1} \quad (4.23)$$

The expected percentage error in S^2 can be found by taking the ratio of the expected standard deviation of S^2 to the expected mean.

$$\begin{aligned} \% \text{ Error for Sample Variance} &= 100 \frac{\sqrt{V[S^2]}}{E[S^2]} = 100 \sqrt{\frac{2\sigma_C^4}{M-1}} \frac{1}{\sigma_C^2} \\ &= 100 \sqrt{\frac{2}{M-1}} \end{aligned} \quad (4.24)$$

For example, if there are 100 spectral points, $M=100$, the expected error in the sample variance will be $100(\sqrt{2/99})=14.2\%$. Clearly, this error is quite large and a better estimate of the cross spectrum variance is desirable.

A better estimate can be found by noting from equations 4.15, 4.20, and 4.21 that

$$\begin{aligned}
\sigma_C^2 &= 2\sigma_F^2 \sigma_G^2 / K = (2\sigma_F^2)(2\sigma_G^2) / 2K \\
&= E[P_F(m)] \cdot E[P_G(m)] / 2K \approx \overline{P_F}(m) \overline{P_G}(m) / 2K
\end{aligned} \tag{4.25}$$

The expected error of this estimate is determined by first finding the error in $\overline{P_F}(m)$ and $\overline{P_G}(m)$.

$$\overline{P_F}(m) = \frac{1}{M} \sum_{m=1}^M P_F(m) \tag{4.26}$$

As $P_F(m)$ is distributed as $N(2\sigma_F^2, 4\sigma_F^4/K)$, the variance of $\overline{P_F}(m)$ will be $(1/M)4\sigma_F^4/K$ and the percentage ratio of the standard deviation to the mean will be

$$\begin{aligned}
\% \text{ Error for } \overline{P_F}(m) &= 100 \frac{\sqrt{V[\overline{P_F}(m)]}}{E[\overline{P_F}(m)]} = 100 \frac{\sqrt{\frac{4\sigma_F^4}{MK}}}{\frac{2\sigma_F^2}{2}} \\
&= \frac{100}{\sqrt{MK}}
\end{aligned} \tag{4.27}$$

A typical value of K such as 10,000 (corresponding to an averaging interval of 25 seconds) will result in a very small percentage error. The result for $\overline{P_G}(m)$ is identical and the overall expected error in σ_C^2 , which is derived from the product of two quantities with small percentage errors, will be twice that error or

$$\% \text{ Error for } \sigma_C^2 = \frac{200}{\sqrt{MK}} \tag{4.28}$$

For $M=100$ and $K=10,000$ the resulting error will be 0.2%. Even if a single point from each auto spectrum is used (i.e. $M=1$), the percent error is only 2%. Hence, the auto spectra can provide a much better estimate of the variance of the cross spectra than the sample variance.

4.2.4 Some Practical Considerations

Two assumptions were made in Section 4.2.1 before deriving the normal distributions of the cross spectra and also the auto spectra. These assumptions must be justified.

The first assumption was that the signals being correlated consist of Gaussian noise bandlimited to exactly the Nyquist frequency. Because ideal filters do not exist, in practice it is necessary to bandlimit an analog signal to less than one-half the Nyquist frequency in order to prevent aliasing. The spectrum of the signals is then not flat, but rolls off on the ends. In order to have a true normal distribution in the spectra, the frequency response of the receiving system and anti-aliasing filters must be flat. The simplest way to attain a flat spectrum is to discard the end points which are affected by the roll-off.

The second assumption was that the correlation between the two signals is identical in amplitude and phase at all frequencies. This requirement first of all means that the frequency response of the receiving system and anti-aliasing filters must be very flat in the center of the spectrum (disregarding the roll-off on the ends mentioned above), and that the phase response of the two channels must be very closely matched. Also, the propagation delays from the antennas to the correlator must be identical as a time difference will cause a linear phase shift across the spectrum. Finally, the signals received at the two antennas themselves must have a correlation which is identical in

amplitude and phase across the portion of the spectrum being observed. Identical amplitude of correlation is relatively assured because at decametric wavelengths the strength of known radio sources changes very slowly as a function of frequency, and can be assumed to be constant over a small bandwidth such as 50 kHz. Identical phase, however, will not always be the case as there will generally be a time delay between the arrival of the signal at the two antennas. In Section 5.4 it will be shown that the maximum phase shift across the spectrum for the system during field trials was quite small and could be ignored.

The measures taken to ensure the flatness of the spectra and phase matching are discussed in Chapter 3 on receiver design and Section 5.6 on field testing. These precautions assure that the cross and auto spectra will be normally distributed in the absence of interference, and allow the robust estimation techniques described in the remainder of this chapter to operate with maximum efficiency.

4.3 A Survey of Robust Estimation

4.3.1 A Brief History

Perhaps since the time that the sample mean was first used as an estimate of the center of a set of measurements, practical people have realized that measurements which are grossly in error should not be included in the calculation of the mean. However, use of the sample mean has become so

entrenched that its users rarely consider that it is an optimum estimate only for errors which are independently, identically and normally distributed. Unfortunately, such normally distributed errors are often not the case. In the introduction to his survey of robust estimation, Ershov [63] mentions many reports of engineering measurements, industrial data, clinical medicine results and other situations where from 1 to 20% of data points may be considered to be anomalous, or "outliers" (i.e. not part of a normal distribution). In [64] Tukey quotes Geary: "Normality is a myth; there never has been, and never will be, a normal distribution."

Gauss himself [65] introduced the normal or Gaussian distribution as that distribution of errors which was best suited in the sense of least squares to the sample mean, rather than vice versa. Before this, in the first published work on least squares, Legendre [66] notes that sample values which appear to be anomalous should be rejected before using least squares methods (and, in particular, the sample mean).

A dogma of normality, and the sacredness of the sample mean, were helped by the Central Limit Theorem, which states that the sum of many small, independent elementary errors is approximately normal. Over the years, the sample mean has come to be used automatically in most situations, often without regard to whether or not it may be appropriate. Anscombe [67], on questioning the assumption of normality,

remarked: "The disposition of the present-day statistician theorists to suppose that all error distributions are exactly normal can be ascribed to their ontological perception that normality is too good not to be true."

Good statisticians and engineers have always been careful to exclude grossly outlying observation in mean calculations, and published accounts such as [68], [69], [70], [71], [72] have proposed rules for rejecting outliers. But it was not until the 1960's that a serious effort began to find estimation procedures with predictable properties which would provide immunity from erroneous observations.

Section 4.3.2 outlines a history of rejection rules and literature on the performance of tests for outliers. Section 4.3.4 describes work since 1960 in the area known as robust estimation. Curiously, the literature on robust estimation does not generally encompass tests for outliers although the two topics are very closely related and overlap in some of their objectives.

More detailed and quite interesting discussions of the historical development of ideas in robust statistical methods can be found in [63], [73], [74], [75], [76] and [77].

4.3.2 Tests for Outliers

In 1936, Pearson and Chandra Sekar [72] published an analysis of a rejection criterion attributed to Thompson [78]. Thompson's proposal was to reject observations y_n for

which

$$|y_n - \bar{y}| > \tau S \quad (4.29)$$

where \bar{y} and S are the sample mean and standard deviation and τ is chosen such that, for a normal population, the probability of rejection is small. This test has come to be known as the Studentized deviate test. Pearson and Chandra Sekar point out a number of drawbacks of this test, namely that for small sample sizes it is only suitable if there is a single outlying observation and for larger sample sizes there is a fixed limit, depending upon sample size, to the number of outlying points which can possibly be rejected.

The possibility is then suggested of applying the Studentized deviate test in a sequential fashion, as follows: (1) apply the rejection criterion to the n observations; (2) if $k \geq 1$ outliers are rejected, apply the criterion again to the remaining $n-k$ observations, recalculating \bar{y} and S each time; (3) repeat until no more observations are rejected. Pearson and Chandra Sekar note two disadvantages of this process: (a) if there are more outliers of a given amplitude than can be rejected for the sample size being considered, rejection will not occur and the process will stop; (b) care must be taken in choosing the rejection levels τ_1, τ_2 , etc., to reduce the risk of rejecting points which belong to a normal distribution.

In 1950, Grubbs [79] proposed a test using the ratios of the sum of squares of deviations for a reduced sample to

the sum of squares for the complete sample,

$$D_n = S_n^2 / S^2$$

$$\text{where } S^2 = \frac{1}{n} \sum_{i=1}^n (y_{(i)} - \bar{y})^2, \quad \bar{y} = \frac{1}{n} \sum_{i=1}^n y_{(i)}$$

$$S_n^2 = \frac{1}{n-1} \sum_{i=1}^{n-1} (y_{(i)} - \bar{y}_n)^2, \quad \bar{y}_n = \frac{1}{n-1} \sum_{i=1}^{n-1} y_{(i)} \quad (4.30)$$

and the $y_{(i)}$ are ordered sample values, $y_{(1)} \leq y_{(2)} \leq \dots \leq y_{(n)}$. A similar test statistic D_1 is found by omitting the smallest sample $y_{(1)}$ rather than the largest $y_{(n)}$. Prescott [80] shows that Grubbs' criterion is algebraically related to the Studentized deviate test and produces identical results, so in effect it is really the same test.

Kudo [81] demonstrated in 1956 that the Studentized deviate test is an optimum test for the case where there is exactly one observation which deviates from a common normal distribution, the variance of which is unknown. Furthermore, if the variance σ^2 is known, the optimum test is

$$|y_n - \bar{y}| > \tau \sigma \quad (4.31)$$

where τ is again a constant which depends upon the sample size and is chosen to keep the probability of rejecting points belonging to the normal distribution small.

Other rejection procedures have been proposed but have been found to be unsatisfactory due to insensitivity or difficulties when more than one outlier is present. These tests include Dixon's [82] criterion, David, Pearson and Hartley's [83] criterion, and the skewness and kurtosis criteria of Ferguson [84]. A graphical comparison of the

behavior of all of the above tests when more than one outlier is present is given by Prescott [80].

The conclusion arrived at by Prescott is that the most satisfactory rejection procedure for more than one outlier is a version of the sequentially applied Studentized deviate test introduced by Rosner [85]. For his method, one first of all selects a maximum number k of observations which one is prepared to regard as being outliers. The Studentized deviate test (or equivalently Grubbs' test) is applied k times, each time rejecting the largest observation whether or not the rejection criterion is satisfied. The rejection procedure is then carried out in reverse, starting with the $n-k$ remaining observations and reincluding one additional observation at a time, in the opposite order to that in which they were rejected, until an actual outlier is identified. This point plus all of those beyond it in the order of reinclusion are then regarded as outliers. Rosner's method overcomes, at least for up to k outlying points, the Studentized deviate test's disadvantage of not identifying any outliers if too many of the same amplitude are present.

4.3.3 Rejection of Outliers in Robust Estimation

Some statisticians working in robust estimation seem to harbor a strange distaste for rejection rules. Huber [73] cites a criticism of outlier rejection by Anscombe [86] and states: "The traditional philosophy behind rejection procedures is highly objectionable." Huber's main objection

appears to be that the performance of rejection procedures is not easily amenable to analysis. Ershov, in his survey paper [63], says: "The fundamental deficiency in the procedures for rejecting anomalous data is the fact that they become complicated and not practically suitable for any significant amount of anomalous values (for example, 5 to 20%), as well as distributions with heavy tails." However, Rosner's method (which Ershov includes as a reference) appears to be neither complicated nor unsuited to many anomalous values.

Robust statisticians then proceed to include among their methods their own versions of rejection rules, under various guises, and to expound at length upon the merits of these procedures. A number of robust estimation techniques which may be called disguised rejection rules are described below.

4.3.3.1 The α -Trimmed Mean

The α -trimmed mean consists of throwing away the $[\alpha n]$ largest and smallest observations of a sample and taking the mean of the remaining observations. $[\]$ denotes the largest integer in the quantity in brackets, and $0 \leq \alpha \leq 0.5$. The estimate is then

$$c_t(\alpha, n) = \frac{1}{n - 2[\alpha n]} \sum_{i=[\alpha n]+1}^{n-[\alpha n]} y_{(i)} \quad (4.32)$$

where $y_{(i)}$ are the ordered samples, $y_{(1)} \leq y_{(2)} \leq \dots \leq y_{(n)}$.

The α -trimmed mean has a long history dating from its

use in certain provinces of France for calculating a mean annual harvest [87] to Poincaré [71]. Bickel [88] investigates the properties of this estimate and its close cousin, the Winsorized mean. The α -trimmed mean was included in the extensive study of robust estimation carried out at Princeton University in 1972 [89].

Major drawbacks of the α -trimmed mean are that the trimming proportion α cannot be chosen properly unless one has information on the distribution of contaminating points (outliers), and that because equal numbers of observations are trimmed from both sides of the sample the estimate does not perform well if the contamination is one-sided or asymmetric.

If α has its maximum value of 0.5, the α -trimmed mean becomes the median of the sample. The median is a relatively robust estimate of the center of a contaminated distribution (it is much less sensitive to outliers than the mean). For this reason the median is often used as an initial estimate of location for the iterative robust methods to be described later.

4.3.3.2 Skipped Estimates

Tukey [90] proposed a class of estimates based on the rejection of outliers and called skipped estimates in the Princeton robustness study [89]. Some of these estimates were found to be among the best of the 68 different estimates considered but they have received surprisingly

little attention since that study. As an example of this type of estimate, the one designated 5T4 (one of the better ones) will be described below.

First of all, from the ordered observations $y_{(i)}$, $y_{(1)} \leq y_{(2)} \leq \dots \leq y_{(n)}$, the first and third quartiles are found. These are designated h_1 and h_2 .

$$h_1 = \begin{cases} y_{([n/4])} & , n \text{ not a multiple of } 4 \\ \frac{1}{2} (y_{(n/4)} + y_{(1+n/4)}) & , n \text{ a multiple of } 4 \end{cases} \quad (4.33)$$

$$h_2 = \begin{cases} y_{(n+1-[(n+3)/4])} & , n \text{ not a multiple of } 4 \\ \frac{1}{2} (y_{(n+1-n/4)} + y_{(n-n/4)}) & , n \text{ a multiple of } 4 \end{cases} \quad (4.34)$$

h_1 is the value below which the smallest quarter of the observations lies, and h_2 is the value above which the largest quarter lies. The interquartile range, $h_2 - h_1$, is used as an estimate of the scale (dispersion) of the data.

Two points t_1 and t_2 further from the center of the data than h_1 and h_2 are then found:

$$t_1 = h_1 - 1.5(h_2 - h_1) \quad (4.35)$$

$$t_2 = h_2 + 1.5(h_2 - h_1) \quad (4.36)$$

The estimation procedure for 5T4 is as follows: (1) Delete all points less than t_1 and greater than t_2 . (2) If k points were deleted in (1), delete a further L points from each end of the sample where

$$L = \min[\max(1, 2k), 0.3n - k/2] \quad (4.37)$$

(3) Take the mean of the remaining samples as the estimate.

Though it is very simple and easy to calculate, even by hand, this estimate was found to perform well in the Princeton study and later in a study by Wegman and Carroll [91]. It is superior to the α -trimmed mean because the decision of how many points to delete is made on the basis of the number of outlying points detected in the sample itself, rather than being fixed beforehand. The disadvantages of the 5T4 estimate are that the interquartile range, used as an estimate of scale, is not the best (see Hampel [92]), and also that the estimate of the center of the distribution used in rejecting outliers, namely the center of the interquartile range, is also not particularly good. In addition, the rejection of an additional L points based on the number k originally deleted may or may not be appropriate. It is not surprising, then, that in [91] the 5T4 estimate was generally inferior to another class of estimates called M-estimates, described in Section 4.3.5.

4.3.4 Maximum Likelihood Estimation

One of the most important estimation techniques in statistics is the method of maximum likelihood reviewed in this section.

The likelihood L of an observed sample x_1, x_2, \dots, x_n

from random variables X_1, X_2, \dots, X_n is defined to be the joint probability of x_1, x_2, \dots, x_n if X_1, X_2, \dots, X_n are discrete random variables, or the joint density function evaluated at x_1, x_2, \dots, x_n if X_1, X_2, \dots, X_n are continuous random variables. A maximum likelihood estimator produces an estimate of a parameter such that the likelihood (i.e. joint probability or joint density) of the sample is maximized.

To illustrate, assume some density function $f(x)$ is displaced by an unknown amount θ to form a density $f(x-\theta)$. To find a maximum likelihood estimate of the location parameter θ from a sample of independent observations x_1, x_2, \dots, x_n , first of all note that the likelihood function $L(\theta)$ will be the joint probability of x_1, x_2, \dots, x_n for some value of θ , and will be given by the product of the individual probabilities.

$$L(\theta) = \prod_{i=1}^n f(x_i - \theta) \quad (4.38)$$

Because it is simpler to deal with sums rather than products, it is often convenient to maximize the logarithm of $L(\theta)$ rather than $L(\theta)$ itself.

$$\begin{aligned} \ln L(\theta) &= \sum_{i=1}^n \ln f(x_i - \theta) \\ &= - \sum_{i=1}^n \rho(x_i - \theta) \end{aligned} \quad (4.39)$$

where $\rho(x) = -\ln f(x)$. The maximum is found by setting the derivative with respect to θ equal to 0 and solving for θ .

$$\begin{aligned}\frac{d}{d\theta} \ln L(\theta) &= -\sum_{i=1}^n \frac{d}{d\theta} \rho(x_i - \theta) \\ &= \sum_{i=1}^n \psi(x_i - \theta)\end{aligned}\quad (4.40)$$

where $\psi(x) = -\rho'(x)$. The solution of

$$\sum_{i=1}^n \psi(x_i - \theta) = 0 \quad (4.41)$$

which maximizes $L(\theta)$ is the maximum likelihood estimate of θ and is frequently denoted as $\hat{\theta}$.

It is easily shown that the maximum likelihood estimate for the normal distribution is the sample mean. Dropping some irrelevant multiplicative constants gives

$$f(x) = \frac{1}{\sqrt{2\pi\sigma}} \exp\left[\frac{-x^2}{2\sigma^2}\right]$$

$$\rho(x) = \frac{x^2}{2}$$

$$\psi(x) = x$$

$$\sum_{i=1}^n \psi(x_i - \theta) = \sum_{i=1}^n (x_i - \theta) = \sum_{i=1}^n x_i - n\theta = 0$$

Therefore,
$$\hat{\theta} = \frac{1}{n} \sum_{i=1}^n x_i = \bar{x}$$

The importance of the function $\psi(x)$ for robust maximum likelihood estimation will become clear later. For now, consider the significance of $\rho(x)$. First of all, the sample mean is known as a least squares estimator because $\rho(x)$ has the form $\rho(x) = x^2/2$. The estimate $\hat{\theta}$ minimizes the sum of the squares of the deviations from $\hat{\theta}$, i.e. $\hat{\theta}$ maximizes $-\sum_{i=1}^n \rho(x_i - \theta)$. A maximum likelihood estimator may also be thought of as maximizing a correlation between the

non-displaced sample density function $f(x)$ and the function $-\rho(x)$.

To illustrate this idea of a correlation being maximized, consider the case of an infinite sample size, $n \rightarrow \infty$. Maximizing the log of the likelihood function,

$$\ln L(\theta) = -\sum_{i=1}^n \rho(x_i - \theta) \quad (4.42)$$

as $n \rightarrow \infty$ will be accomplished if the expected value of $-\rho(x_i - \theta)$ is maximized. x_i may be replaced by a continuous variable x , and the expected value is

$$E[-\rho(x - \theta)] = \int_{-\infty}^{\infty} -\rho(x - \theta) f(x) dx \quad (4.43)$$

The integral has the form of a correlation, $R(\theta)$, between the function $-\rho(x) = \ln f(x)$ and $f(x)$. The correlation will have its maximum value for $\theta = \hat{\theta}$.

The purpose of demonstrating this connection between maximum likelihood estimation and correlation is to contrast the estimation problem to the optimum receiver problem in communications theory. It is well known [93] that the optimum receiver for a signal in the presence of noise is one which correlates the signal plus noise with a duplicate of the signal alone. The correlation will then be a maximum compared to the correlation with all other signals of equal energy. However, for maximum likelihood estimation one attempts to maximize the correlation between a probability density function $f(x)$ and its logarithm rather than a copy of $f(x)$ itself. For example, if one correlates a normal

distribution with a $-\rho(x)$ having the same Gaussian form, the resulting estimator performs rather poorly (c.f. the MEL estimate used in the Princeton study [89]). There is an intrinsic difference in the nature of the two problems. The optimum receiver problem attempts to detect the *presence or absence* of a particular waveform, whereas the estimation problem attempts to determine the *location* of a density function as accurately as possible.

4.3.5 Robust M-Estimators

One of the major advances in robust estimation occurred in 1964 when Huber published a paper [94] introducing a class of maximum likelihood type estimators, subsequently known as M-estimators. These estimators are solutions $\hat{\theta}$ to the general maximum likelihood estimation equation 4.41,

$$\sum_{i=1}^n \psi(x_i - \theta) = 0$$

for various forms of the function ψ . Huber showed that under quite general conditions (normally encountered in practice) $\hat{\theta}$ converges to an asymptotic value θ_a defined by

$$\int_{-\infty}^{\infty} \psi(x - \theta_a) f(x) dx = 0 \quad (4.44)$$

for a given density function $f(x)$. If $f(x)$ is symmetric and $\psi(x)$ is an odd function, then θ_a is the center of $f(x)$. Also, as $n \rightarrow \infty$, $n^{0.5}(\hat{\theta} - \theta_a)$ is asymptotically normal with asymptotic mean 0 and asymptotic variance σ_m^2 given by

$$\sigma_m^2 = \frac{\int_{-\infty}^{\infty} [\psi(x-\theta_a)]^2 f(x) dx}{[\int_{-\infty}^{\infty} \psi'(x-\theta_a) f(x) dx]^2} \quad (4.45)$$

Scale invariant versions of M-estimators are obtained by dividing by the standard deviation σ (or an estimate of σ). The estimation equation then becomes

$$\sum_{i=1}^n \psi \left[\frac{x_i - \theta}{\sigma} \right] = 0 \quad (4.46)$$

This equation is usually solved iteratively from some initial estimate θ_1 of θ (such as the median) using the Newton-Raphson method. Thus,

$$\theta_{k+1} = \theta_k + \frac{\sigma \sum_{i=1}^n \psi \left[\frac{x_i - \theta_k}{\sigma} \right]}{\sum_{i=1}^n \psi' \left[\frac{x_i - \theta_k}{\sigma} \right]} \quad (4.47)$$

Some of the commonly used ψ functions recommended by Hogg [95] are given below:

1. Huber Proposal 2

$$\psi(x) = \begin{cases} -k, & x < -k \\ x, & -k \leq x \leq k \\ k, & x > k \end{cases} \quad (4.48)$$

A good value for k is 1.5.

2. Hampel

$$\psi(x) = (\text{sign } x) \cdot \begin{cases} |x|, & 0 \leq |x| < a \\ a, & a \leq |x| < b \\ a \frac{c - |x|}{c - b}, & b \leq |x| < c \\ 0, & c \leq |x| \end{cases} \quad (4.49)$$

Reasonably good values of the constants are $a=1.7$, $b=3.0$, and $c=6.4$ which correspond to an estimate known as the Hampel 25A.

3. Wave of Andrews

$$\psi(x) = \begin{cases} \sin\left(\frac{x\pi}{k}\right), & |x| \leq k \\ 0 & , |x| > k \end{cases} \quad (4.50)$$

with $k=5.0$ or 6.0 .

4. Biweight of Tukey

$$\psi(x) = \begin{cases} x[1-(x/k)^2]^2, & |x| \leq k \\ 0 & , |x| > k \end{cases} \quad (4.51)$$

with $k=5.0$ or 6.0 .

Because the last three ψ functions above go to zero for $|x|$ beyond specified limits (a desirable property because extreme outliers are rejected completely), there may sometimes be convergence problems with their associated estimates. For instance, if the initial estimate of θ used is not close to the bulk of the data there may be too few points within the limits of the ψ function for proper convergence. These problems can generally be avoided by assuring that the initial estimate of θ is reasonably close to the final value. Hogg [95] recommends that Huber's function (which does not suffer from convergence problems) with $k=1.5$ be used for several iterations to provide an initial value for estimators (2), (3) or (4).

4.3.6 Other Robust Estimators

Besides M-estimators, there are two other general classes of robust estimators called L-estimators and R-estimators. L-estimators consist of linear combinations of order statistics (i.e. observations are weighted according to their rank rather than their actual value). R-estimators are based entirely upon the ranks of observations rather than their actual values. Both of these classes of estimates are described in [89], [73], [63] and [95]. It has been shown ([96], [97]) that M-estimates can generally be found which are asymptotically equivalent to L- and R- estimates. Also, in Monte Carlo studies such as [89] and [91], M-estimates are generally found to be superior to the L- and R-estimates studied. Therefore, these two classes of estimators will not be considered further herein.

4.4 The Performance of M-Estimators

4.4.1 The Influence Curve

An important tool for studying robust estimators is the influence curve developed by Hampel [92]. The influence curve is essentially the first derivative of an estimator evaluated at some distribution, and can be used to derive asymptotic variances and several other robustness properties which will be explained below.

To define the influence curve, let $F(x)$ denote a probability distribution and $T(F)$ denote some estimation function defined for a subset of all probability

distributions, including F . Consider a probability distribution consisting of a mixture of F and a delta function at some point x , written as $(1-\epsilon)F + \epsilon\delta_x$, $0 < \epsilon < 1$. Then the influence curve $IC_{T,F}(x)$ of the estimator T at the underlying distribution F is defined pointwise by

$$IC_{T,F}(x) = \lim_{\epsilon \rightarrow 0} \frac{T[(1-\epsilon)F + \epsilon\delta_x] - T(F)}{\epsilon} \quad (4.52)$$

The value of the influence curve at a point x is equal to the change produced in the estimate T by the addition of a point mass 1 of value x to the underlying probability distribution.

For M-estimators, the influence curve is very closely related to the ψ function. In particular ([92], [89]), if $f(x)$ is symmetric and ψ is odd, then

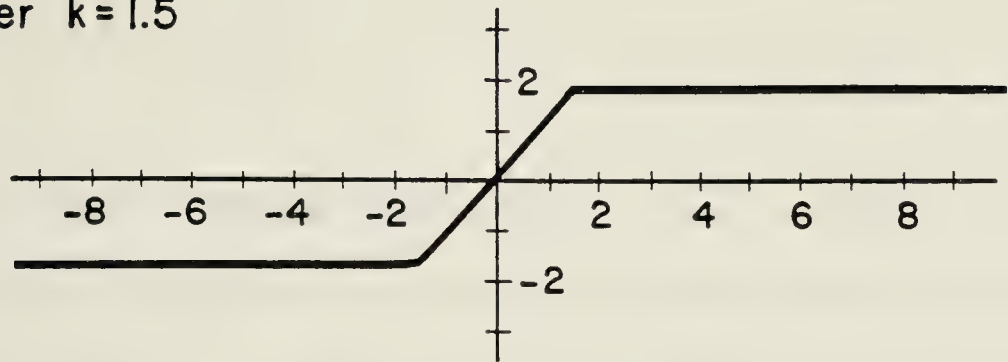
$$IC_{T,F}(x) = \left[\frac{\sigma}{\int_{-\infty}^{\infty} \psi'(y/\sigma) f(y) dy} \right] \psi\left(\frac{x}{\sigma}\right) \quad (4.53)$$

where the term in square brackets is just a scaling factor. The asymptotic variance in this case can be found from the expected value of the square of the influence curve.

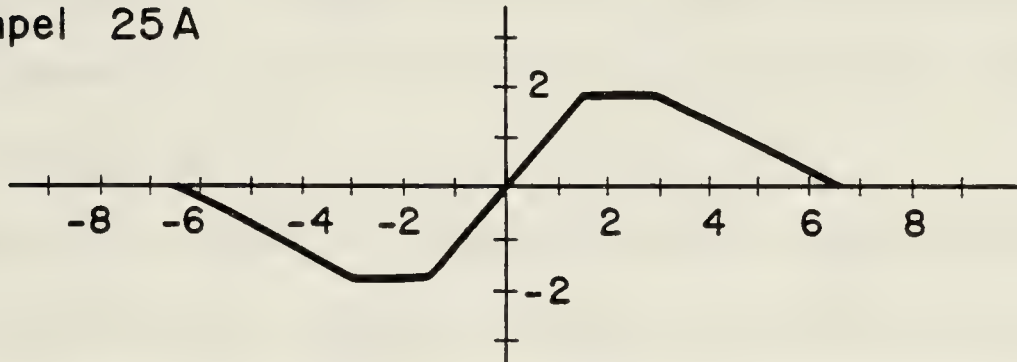
$$\sigma_m^2 = E[IC_{T,F}^2(x)] = \frac{\sigma^2 \int_{-\infty}^{\infty} [\psi(x/\sigma)]^2 f(x) dx}{\left[\int_{-\infty}^{\infty} \psi'(x/\sigma) f(x) dx \right]^2} \quad (4.54)$$

Influence curves for the four M-estimators from Section 4.3.5 are shown in Figure 4.1. A fifth M-estimator, corresponding to a rejection rule which deletes points beyond $\pm k\sigma$ ($k=3.0$ in the figure), is also shown for

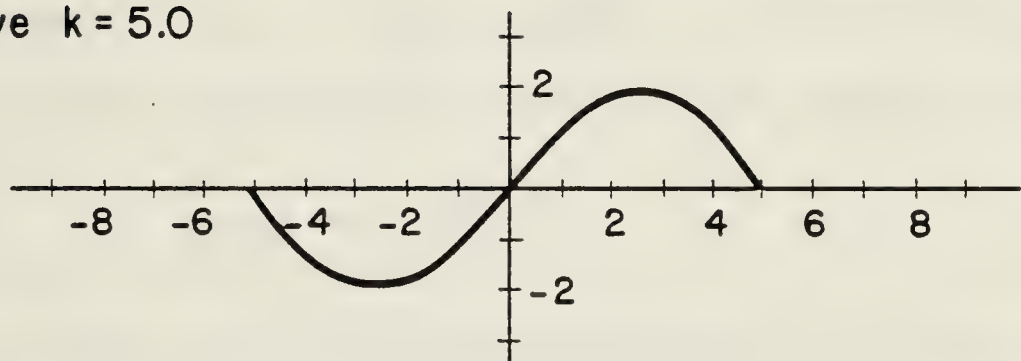
a) Huber $k=1.5$



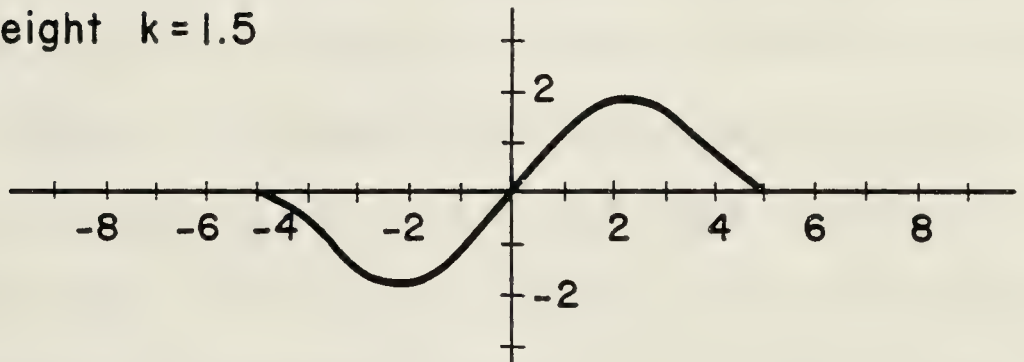
b) Hampel 25A



c) Wave $k=5.0$



d) Biweight $k=1.5$



e) 3σ Rejection Rule

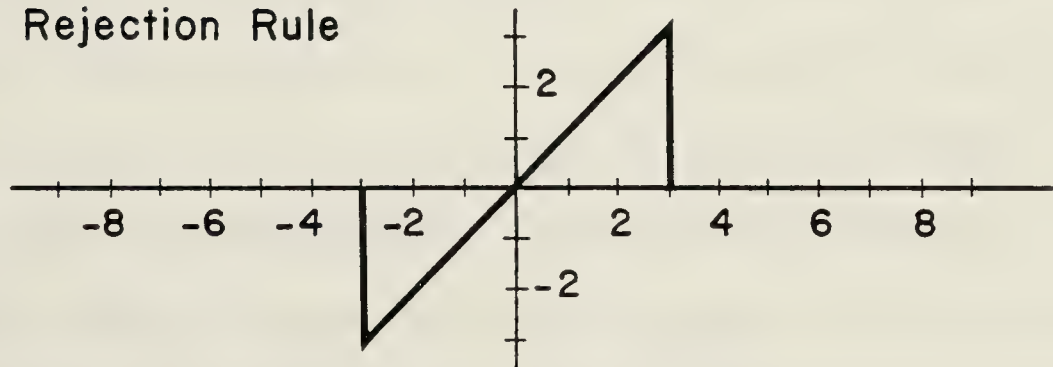


FIGURE 4.1 Influence Curves for Robust M-Estimates

comparison.

4.4.2 Properties of M-Estimators

Three important properties of robust estimators can be derived from their influence curves. These properties are gross-error-sensitivity, local-shift-sensitivity, and rejection point.

Gross-error-sensitivity measures the worst possible effect which a single contaminating point can have on the value of an estimate. It corresponds to the maximum absolute value of the influence curve, and will be denoted GES.

$$\text{GES} = \max |IC(x)| \quad (4.55)$$

Good GES is obtained by placing a bound on the influence curve and making that bound as small as possible (the influence curve of the mean, in contrast, is $IC(x)=x$ and is unbounded). In general, the goal of limiting the influence curve (and hence limiting errors due to outliers) conflicts with the goal of having an asymptotically efficient (i.e. smallest variance) estimator. As the bound is made smaller, the efficiency relative to a most efficient estimate such as a maximum likelihood estimate generally decreases.

Fortunately, the price which must be paid in efficiency is very small (a few percent) to obtain far greater gains in protection from the effects of outliers. The beneficial trade-off is what makes robust estimators practical and attractive.

A second property of robust estimates is called local-shift-sensitivity, denoted as LSS, and is a measure of the worst possible effect on the estimate of a small change in the value of a single observation divided by the size of the change. The LSS is found to be the maximum absolute value of the first derivative of the influence curve.

$$\text{LSS} = \max \left| \frac{d}{dx} \text{IC}(x) \right| \quad (4.56)$$

A large value for LSS does not imply that an estimate will necessarily be inaccurate, but means that the estimate is very sensitive to changes in the distribution of observations near some particular values of x and as a result could behave erratically. This fact is particularly relevant when one considers that for a finite sample size the distribution function will not be smooth but can exhibit local grouping of points. Contamination may also cause local grouping. A very high local shift sensitivity turns out to be the major disadvantage of rejection of outlier estimates.

The third property of estimators is the rejection point, which is the point beyond which the value of the influence curve becomes zero. All observations beyond the rejection point are rejected completely. A low rejection point is desirable to eliminate as many outliers as possible, but its attainment conflicts with the requirements for high asymptotic efficiency and a small local-shift-sensitivity. Generally, a compromise must be reached.

4.4.3 Comparison of Some Estimators

The numerical properties of the M-estimates discussed above for a standard normal distribution are summarized in Table 4.2. The mean and median are included for comparison purposes. Figures for estimators a, b, d, and e were taken from [92]. No published figures for the remainder were available, so they were calculated numerically by computer using equation 4.54 for σ_m^2 and equation 4.53 for the influence curve.

4.4.3.1 3σ Rejection Rule

A 3σ rejection rule, which takes the mean of all observations within $\pm 3\sigma$ of the center, has low asymptotic variance and a low rejection point. However, GES is the largest for any of the estimates considered and LSS is ∞ , indicating extremely high sensitivity of the estimate to observations close to the rejection point. This estimate could be expected to behave badly in the presence of low-level contamination, but would perform well for contamination greater than 3σ .

4.4.3.2 Huber's M-Estimator

The Huber estimate has low asymptotic variance, low GES, and low LSS. In fact, the Huber estimate can be shown to have the smallest asymptotic variance of any estimate with a given gross-error-sensitivity (i.e. it is a minimax estimate [94]). Its disadvantage is an infinite rejection

Table 4.2. Numerical Properties of Some Robust M-Estimates

Estimate	σ_m^2	GES	LSS	Rejection Point
a) Mean	1.000	∞	1.00	∞
b) Median	1.571	1.25	∞	∞
c) 3σ Rejection	1.026	3.08	∞	3.00
d) Huber $k=1.5$	1.037	1.73	1.15	∞
e) Hampel 25A	1.026	1.86	1.10	6.41
f) Wave $k=5$	1.026	1.95	1.22	5.00
g) Biweight $k=5$	1.041	1.83	1.28	5.00
h) Biweight $k=4$	1.100	1.68	1.46	4.00
i) Biweight $k=3$	1.295	1.67	1.94	3.00

point, which as mentioned in Section 4.3.5 aids in its convergence to the true center of a distribution regardless of the initial estimate used, but which degrades its performance in the presence of large contamination.

4.4.3.3 Hampel's Redescending M-Estimate

As seen from their influence curves, a Hampel estimate is simply a Huber estimate which redescends to zero rather than staying constant. Thus, a Hampel estimate overcomes the

Huber's deficiency by having a finite rejection point (at the expense of slightly increased σ_m^2 for the same GES). Hampel estimates are therefore recognized as being good in all respects ([89], [92]). By varying the constants a , b , and c various performance factors may be traded off with one another. For instance, the rejection point may be improved at the expense of some of the other factors.

4.4.3.4 Wave M-Estimate

The use of a smoothly changing ψ function such as the biweight or wave has some slight advantages over one composed of straight line segments like the Hampel. For instance in Table 4.2 the wave has the same variance and a slightly higher GES than the Hampel, but it must be noted that the region for which the influence curve is a maximum is much smaller than that for the Hampel. The wave has a lower rejection point which is paid for mainly by a larger LSS.

4.4.3.5 Biweight M-Estimate

The wave and biweight estimates are very similar and as Hogg [95] suggests, almost interchangeable. The performance of the biweight with $k=5.0$ is very close to that of the wave with $k=5.0$. Both of these estimates have very good qualities and in the opinion of the author of this thesis are the best choices for most applications.

4.5 Adaptive Estimation

Three versions of the biweight are shown in Table 4.2 with values of the parameter k of 5.0, 4.0, and 3.0. Note that as the rejection point is decreased, the variance σ_m^2 increases. LSS also increases but GES is actually reduced somewhat.

The asymptotic variance σ_m^2 is the variance for very large sample sizes ($n \rightarrow \infty$). Because the actual variance of any estimate varies with the sample size as $1/n$, for $n \rightarrow \infty$ the actual variance should approach zero. The interpretation of σ_m^2 in Table 4.2 is that σ_m^2 is the variance for a very large but finite sample size, *relative* to the variance of the mean (the optimum estimate for a normal distribution). If one is dealing with a large enough sample size the expected variance may be small enough that one would, in some situations, tolerate an increased variance in order to gain greater protection from outliers which are relatively close to the center of the distribution (within a few σ). Such a situation would occur if there was evidence or suspicion of low-level contamination, and one wished to minimize its effects on the estimate. In such a case, a biweight parameter of $k=4.0$ or 3.0 might be more appropriate than $k=5.0$.

Adaptive estimation consists of choosing which estimate to use *after* looking at the data and making some decision about the nature of the contamination. If one could through some choice of reliable statistics determine that there was

a significant amount of close-in contamination and could then choose the value of biweight parameter which would produce the most accurate estimate in the presence of this contamination, then adaptive robust estimation would be a major improvement over estimation based on a single biweight ψ function.

A few relatively simple forms of adaptive estimators have been suggested and evaluated in [89], [98], [99], [91], and [100]. These estimators have not been spectacularly successful, for though they may be better than non-adaptive estimators in worst-case situations, they are generally somewhat worse in "run-of-the-mill" cases. The problem appears to be a difficulty in judging the nature of close-in contamination. Often the adaptive procedure will select a non-optimum ψ -function (i.e. one for more contamination than is actually present), and consequently overall performance tends to suffer. However, most authors express much hope that adaptive procedures can be improved (little effort seems to have been expended in this area as of yet) and so adaptive estimation should bear considerable attention in the future. Adaptive estimation would be of the greatest benefit in cases of asymmetric contamination. If outliers are concentrated on one side of the center of a distribution but are close enough to not be rejected, they will cause the estimate of the center to be biased in the direction of the contamination. A natural criterion for judging the performance of an estimate is the mean squared error

considered by Jaeckel [96], who shows that the mean squared error with asymmetric contamination can be minimized by trading off increased variance for decreased bias. This could be accomplished by reducing the value of the parameter k for a biweight estimate.

Asymmetric contamination is a major problem in the developing theory of robust estimation. An observation by Hogg is mentioned in [91]: "In particular, as Hogg has suggested in private communication, although a sample may be drawn from a symmetric population the sample may have significant asymmetries." For the rejection of terrestrial interference considered herein, asymmetry is very likely because one contaminating signal may affect a large number of points in the spectrum, first of all through leakage and secondly through a large occupied bandwidth (e.g. amplitude modulation). As of yet, no consensus has been reached on how robust estimation should handle asymmetric situations. Some discussion of the problem is contained in [96], [101] and [102].

4.6 An Estimation Procedure

There is no one estimation procedure which is optimum for all situations. Each of the methods described in Section 4.3.5 has some disadvantages. A combination of procedures, or "hybrid" approach, can be used to overcome some of the individual disadvantages and is most appropriate where a wide range of contaminating signals must be handled.

However, even a very complex hybrid procedure is unlikely to work in all conceivable cases. A practical compromise is to keep the estimation procedure as simple as possible, yet able to handle the most commonly encountered contamination in a highly efficient manner and less common contamination with reasonable efficiency. Provisions should be made for difficult cases to be at least recognized and perhaps recorded. In this way one could evaluate the estimator's performance and note improvements which could be made in the handling of difficult contamination.

The estimation procedure described below is not claimed to be the best possible, nor is it the only way to achieve comparable results. Rather, it is one of many possible combinations, but one which the author believes will work well for the problem of contamination of the radio spectrum with terrestrial interference. Possible additions and improvements to the procedure are mentioned in Section 4.6.5.

4.6.1 Estimation of Variance

As described in Section 4.2.3 the variance of the cross spectra may be estimated from the auto spectra. The auto spectra will be contaminated by the same interference as the cross spectra, hence some form of robust estimation is again required. The first decile (see below) is proposed as a simple but effective estimator.

The auto spectra are different from the cross spectra

in that the auto spectra are always positive and the contamination is entirely one-sided. Interference may increase the power received at some frequencies, but can never reduce the power below the level of background noise. With no interference, the dispersion of the auto spectra will be very small relative to the mean. From equation 4.20 the probability density with no interference (and assuming a perfectly flat frequency response) will be $N(2\sigma_F^2, 4\sigma_F^4/K)$. The ratio of the standard deviation to the mean is then

$$\frac{\sigma_{P_F}}{\bar{P}_F} = \frac{\sqrt{4\sigma_F^4/K}}{2\sigma_F^2} = \frac{1}{\sqrt{K}} \quad (4.57)$$

which will be .01 or less for a typical K of 10^4 or more. Almost any estimate of the mean, as long as it is not drastically affected by interference, will provide reasonable accuracy.

In addition, the variance of the cross spectra need not be known with extreme accuracy. Good robust estimators (especially those with small local-shift-sensitivity) are relatively insensitive to small changes in the estimate of scale used (this corresponds to the notion of "qualitative robustness" discussed in Hampel [92]). Accuracy of the scale estimate to within a few percent would appear to be more than adequate.

The estimator proposed for the centers of the auto spectra is the first decile (i.e. the point below which 10% and above which 90% of the observations are found). This

estimate is robust in the presence of single-sided contamination and, as will be shown, has sufficient accuracy for the required purpose.

4.6.2 Accuracy of the First Decile as an Estimator

Let λ represent some fraction, $0 < \lambda < 1$, of the cumulative area under a standard normal curve, $f(x)$. Let α_λ represent the value of x at which the area λ has been accumulated, as shown in Figure 4.2.

$$\lambda = \int_{-\infty}^{\alpha_\lambda} \frac{1}{\sqrt{2\pi}} \exp(-x^2/2) dx \quad (4.58)$$

If n independent observations, y_1, y_2, \dots, y_n from an $N(0,1)$ distribution are ordered to form n order statistics, $y_{(1)} \leq y_{(2)} \leq \dots \leq y_{(n)}$, then the expected value of the k 'th order statistic, $y_{(k)}$, will be α_λ as above with $\lambda = (k-1/2)/n$. It is known [103] that the asymptotic distribution of order statistics approaches a normal distribution given by $N(\alpha_\lambda, \lambda(1-\lambda)/nf^2(\alpha_\lambda))$. The mean and standard deviation of this distribution is evaluated for $n=100$ and various values of λ in Table 4.3.

When using an order statistic $P_{(k)}$ corresponding to the first decile ($k=[\lambda n]+1$) to estimate the center of the auto spectra, the estimate will from Table 4.3 typically underestimate the mean by $1.3 \sigma_{P_F}$ and have a standard deviation of $0.17 \sigma_{P_F}$. From equation 4.57, the ratio of the standard deviation σ_{P_F} to the mean \bar{P}_F is $1/\sqrt{K}$. A small correction factor of $1/(1-1.3/\sqrt{K})$ will correct for the

$$f(x) = \frac{1}{\sqrt{2\pi}} e^{-x^2/2}$$

$$\lambda = \int_{-\infty}^{\alpha_\lambda} f(x) dx$$

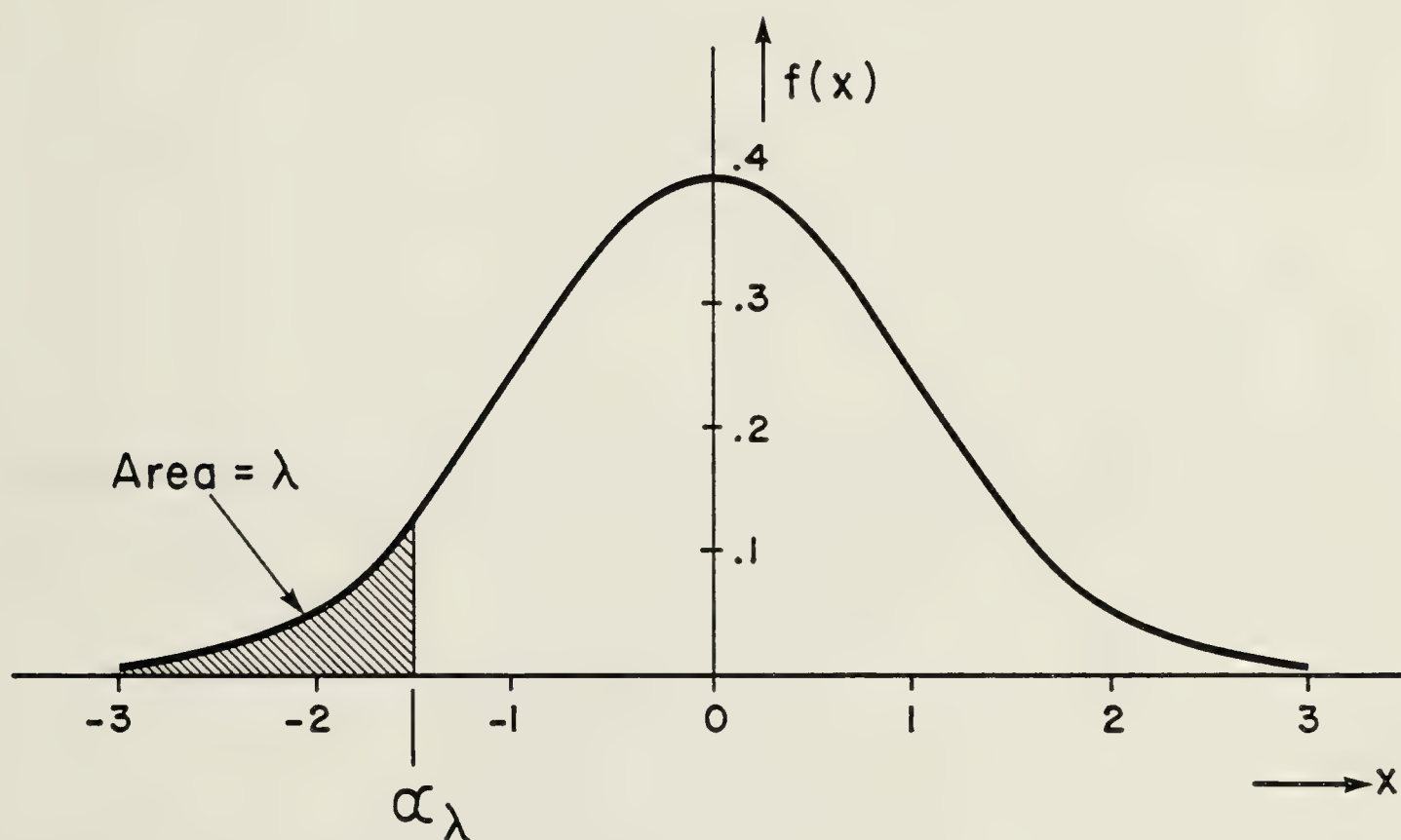


FIGURE 4.2 Cumulative Area Under a Standard Normal Curve

Table 4.3. Asymptotic Expected Value and Standard Deviation of Quantiles of the Normal Curve

Quantile	Expected Value	Standard Deviation
λ	α_λ	$f^{-1}(\alpha_\lambda) \sqrt{\lambda(1-\lambda)/n}$
0.1	-1.3	0.17
0.2	-0.85	0.14
0.5	0.0	0.13

underestimation and provide an unbiased estimate \overline{P}_{EST} of the mean \overline{P} . Thus

$$\begin{aligned} \overline{P}_{EST} &= \frac{1}{(1-1.3/\sqrt{K})} P_{([\alpha n]+1)} \\ &\approx (1+1.3/\sqrt{K}) P_{([\alpha n]+1)} \quad \text{for } K \gg 1 \end{aligned} \tag{4.59}$$

The standard deviation of \overline{P}_{EST} will be

$$\begin{aligned} \sigma_{EST} &= (1+1.3/\sqrt{K}) 0.17 \sigma_{P_F} = (1+1.3/\sqrt{K}) 0.17 \overline{P}/\sqrt{K} \\ &= 0.0017 \overline{P} \quad \text{for } K = 10^4 \end{aligned} \tag{4.60}$$

If no interference is present the first decile plus the correction factor above provides a very accurate estimate of the means of the auto spectra.

If there is interference, the estimate is affected only slightly. For example, if 50% of the points of an auto spectrum contain interference and are larger than they

should be, then the remaining 50% will still belong to a normal distribution and the order statistic $P_{([\alpha n]+1)}$ which previously corresponded to the first decile will now correspond to the second decile ($\lambda=0.2$) of a normal distribution. The new estimate with the old correction factor will be

$$\begin{aligned}\bar{P}_{EST} &= (1+1.3/\sqrt{K}) P_{([0.2n]+1)} \\ &= (1+1.3/\sqrt{K}) (1-0.85/\sqrt{K}) \bar{P} = 1.0044 \bar{P}\end{aligned}\quad (4.61)$$

for $K=10^4$. The error with 50% contamination is only 0.44%. The first decile is therefore insensitive to even large amounts of interference and will serve as a very simple but accurate estimation for the means of the auto spectra, and hence the variance of the cross spectra.

It must be noted that this estimator will be affected by any anomalies, especially dips, in the frequency response of the auto spectra. The spectra must either be flat or any ripples must be corrected for before the first decile will function properly as the auto mean estimator.

An alternative to the first decile which would provide better accuracy would be an M-estimator such as a biweight. However, the additional computational complexity of an M-estimator is not warranted in this case.

4.6.3 Location Estimation

The estimation procedure used to find the location parameters (centers) of the cross spectra described below is

a hybrid of three different procedures. A Huber estimator with $k=1.5$ is combined with a 6σ rejection rule to obtain a reliable initial estimate for a final biweight M-estimate. The rejection rule takes advantage of expected sidelobe levels to reject additional contaminated points on each iteration, and combines rejections from both the co and quadrature cross spectra.

Prior to estimation, all spectra must be as flat as possible. First of all, end points affected by roll-off are deleted. Ten points are deleted from each end leaving a total of $n=108$ spectral components of the original 128. The auto spectra are corrected for amplitude ripples, and the cross spectra are corrected for amplitude ripples and, if possible, phase ripples.

The steps in the estimation procedure are as follows:

1. Order the components of the auto spectra according to magnitude. Find the location parameters of the auto spectra, θ_F and θ_G , using the first decile plus the appropriate correction factor as the estimate. The order statistic which most closely approximates the first decile is found using

$$k = [\lambda n] + 1 = [(0.1)(108)] + 1 = 11$$

where $[\]$ is the largest integer function. Thus,

$$\theta_F = P_{F(11)}(1 + 1.3/\sqrt{K}) \quad (4.62)$$

$$\theta_G = P_{G(11)}^{(1+1.3/\sqrt{K})} \quad (4.63)$$

The standard deviations of the cross spectra are then estimated as

$$\sigma_x = \sigma_C = \sigma_Q = \sqrt{\frac{\theta_F \theta_G}{2K}} \quad (4.64)$$

2. Find the medians M_C and M_Q of both the co and quadrature spectra. Do not disturb the order of the spectral components in doing so. Use the medians as initial estimates of the location parameters of the spectra (i.e. let $\theta_C = M_C$ and $\theta_Q = M_Q$). Calculate the standard deviations about the location parameters:

$$S_C = \left[\frac{\sum_{i=1}^n (P_C(i) - \theta_C)^2}{n} \right]^{1/2} \quad (4.65)$$

$$S_Q = \left[\frac{\sum_{i=1}^n (P_Q(i) - \theta_Q)^2}{n} \right]^{1/2} \quad (4.66)$$

If both $S_C \leq 1.25\sigma_x$ and $S_Q \leq 1.25\sigma_x$, conclude that there is no significant interference and proceed to biweight estimation, step 10.

3. If either S_C or S_Q is greater than $1.25\sigma_x$, outliers may be present. Starting with the spectrum (co or quadrature) with the largest standard deviation, proceed to delete outliers. Find the spectral component corresponding to the largest standardized deviate from the location estimate:

$$D_{\max} = \max_{(i)} \frac{|P_C(i) - \theta_C|}{\sigma_x} \quad (4.67)$$

If $D_{\max} \geq 6.0$, delete this observation from the sample.

Delete adjacent spectral components which will also be contaminated due to leakage. If $D_{\max} \geq 10.0$, delete two adjacent observations on each side. Otherwise, delete one adjacent observation on each side.

4. Repeat step 3 a maximum of 5 times on the reduced sample. Stop after 5 iterations or if no more points are found with $D \geq 6.0$.
5. For the other spectrum, first of all delete the spectral components corresponding to those deleted in steps 3 and 4 from the first spectrum. Then proceed as in steps 3 and 4 to delete additional points. The combined components rejected from both spectra upon completion of this step are considered to be contaminated with interference and are subsequently rejected from both the co and quadrature spectra.
6. Use a Huber M-estimator (equation 4.48) with $k=1.5$ to estimate the location parameters of the remaining components in both spectra. Use the Newton-Raphson method of 4.47.

$$\theta_{k+1} = \theta_k + \sigma_x \frac{\sum_{i=1}^n \psi \left[\frac{P(i) - \theta_k}{\sigma_x} \right]}{\sum_{i=1}^n \psi' \left[\frac{P(i) - \theta_k}{\sigma_x} \right]} \quad (4.68)$$

Exclude deleted observations from the summations and start with the medians from step 2 as initial estimates of θ . Iterate until either the change in θ is less than some fraction of σ_x (.01, for example) or until some fixed number of iterations have been completed. The

resulting estimates of θ_C and θ_Q should be reasonably accurate.

7. If either of the estimates has changed by more than $0.1\sigma_x$, indicating considerable asymmetric contamination, go back to step 3 and repeat the rejection and Huber estimation using the new estimates of θ_C and θ_Q . Reininclude all observations prior to starting rejection, as some previously rejected points may now not be identified as outliers. Continue steps 3 to 7 until the estimates become stable. This should normally happen after very few iterations.
8. Calculate the standard deviations of the remaining points after deletion as in equations 4.65 and 4.66. If both $S_C \leq 1.25\sigma_x$ and $S_Q \leq 1.25\sigma_x$, conclude that no significant interference remains undeleted and proceed to biweight estimation, step 10.
9. If either S_C or S_Q are larger than $1.25\sigma_x$, some interference which should be deleted may remain. Note whether or not the maximum of 5 outliers was detected in steps 4 and 5 for either the co or quadrature spectrum. If less than 5 were detected, proceed to step 10. Otherwise, return to step 3 and proceed to delete up to another 5 points (plus adjacent observations) from both spectra. Continue on from step 4 to recalculate new estimates of θ_C and θ_Q . Repeat steps 4 through 9 until either (a) the criteria in step 8 are satisfied or (b) no more points meeting the rejection criterion in step 3

remain.

10. Use a biweight M-estimator with $k=5.0$ to find final estimates of θ_c and θ_q from the spectral components remaining after the largest outliers have been rejected in steps 1 through 9. Starting with the last Huber estimate from step 6, use Newton-Raphson iterations until θ changes by less than $0.01\sigma_x$.

4.6.4 Evaluation of the Estimation Procedure

The above procedure is quite conservative and will operate successfully to minimize the effects of interference in the majority of cases. Steps 1 to 9 together provide a very good initial estimate for step 10, a biweight M-estimate. A Huber estimator is used in step 6 because of its good convergence properties, while the iterative rejection procedure removes large and easily distinguishable outliers to overcome the Huber estimate's infinite rejection point.

The procedure should not break down except in extreme situations. One such possibility would be one-sided contamination of more than 50% of the spectral components, in which case the median would be unreliable as an initial estimate of location. With symmetric contamination the procedure should work properly with even more than 50% of the points being contaminated.

4.6.5 Possible Improvements

Two possible improvements would be to provide a more reliable initial estimate than the median to reduce the likelihood of breakdown when more than 50% of points are contaminated, and to use some form of adaptive estimation to reduce the mean squared error when considerable low-level interference is present.

One way of increasing the reliability of the initial estimate would be to note that there is a certain range beyond which the centers of the cross spectra are not expected to be found. Other a priori information, such as the values of estimates for previous spectra, might also be used. A correlation of the histogram of the cross spectra with the expected normal distribution could be employed to initially locate the center of the distribution.

4.7 Summary

The cross and auto spectra are shown to have normal probability distributions with interference causing contamination and therefore heavier tails. The expected means and variances of the underlying normal distributions are found. It is shown that the location parameters of the auto spectra will provide a reliable estimate of the variance of the cross spectra.

Published literature in the areas of rejection rules and robust estimation is reviewed. M-estimators are singled out as the best class of estimators, and properties of a

number of M-estimators are described.

The order statistic corresponding to the first decile is proposed as a simple but effective estimator for the location parameters of the auto spectra and thereby the variance of the cross spectra. The performance of this estimate is discussed.

An estimation procedure for the centers of the cross spectra consisting of a combination of an outlier rejection test, a Huber M-estimator and a biweight M-estimator is presented and evaluated. Some possible future improvements to this procedure, including the addition of an adaptive biweight M-estimate, are suggested.

5. Field Trials

5.1 Introduction

Field testing of the complete interference excising system was carried out between Nov. 12, 1979 and Jan. 6, 1980 at the Dominion Radio Astrophysical Observatory (DRAO) in Penticton, British Columbia. Reasons for the choice of DRAO were the availability of a large 22.25 MHz T-array radio telescope and the expertise and experience of DRAO's staff from a long-standing program of research in low frequency radio astronomy.

The timing of the observations, by chance rather than design, coincided with an approximate maximum in the 11-year sunspot cycle. Due to increased solar and hence ionospheric activity, terrestrial interference and also scintillation and refraction of radio signals were expected to be quite bad.

The part of the year from November to January is ideal for low frequency astronomy as a result of the long winter nights. Electron density in the F layer of the ionosphere reaches a low value a few hours after sunset and remains low until sunrise. Hence there is a long period during the night with low levels of terrestrial interference. During the day, however, electron densities reach maximum values (due to the winter anomaly) and so daytime interference is at its worst. The diurnal variation in electron density, with steep gradients at sunrise and sunset, is reflected in graph (d)

of Figure 1.1.

The interference excising system was not expected to handle the very high levels of interference during the winter day, and so the periods of transition at sunset and sunrise were of particular interest as a test of the system. Late fall was deemed a good time for testing because the strong radio source Cassiopeia A has an upper transit in the evening and a lower transit in the morning, and could be expected to provide easily observable fringes from which interference could be excised at these times.

5.2 Antennas

The antennas were originally part of a 22.25 MHz T-shaped array telescope at the Dominion Radio Astrophysical Observatory [104]. The major arm of the T was oriented east-west and had a length of 1300 m (96λ at 22.25 MHz). The minor arm extended 312 m north from the center of the east-west arm. A photograph of the junction point, facing west down the east-west arm and showing the north-south arm going off to the right, appears in Figure 5.1.

The array consisted of 624 full-wave dipoles strung between wooden poles. A reflecting ground screen of additional wires was situated a distance $\lambda/8$ below the dipoles.

The basic array element consisted of a pair of full-wave dipoles as pictured in Figure 5.2. For the north polar sky synthesis project [2], sets of four such basic



Figure 5.1. A View of the DRAO
22.25 MHz Telescope

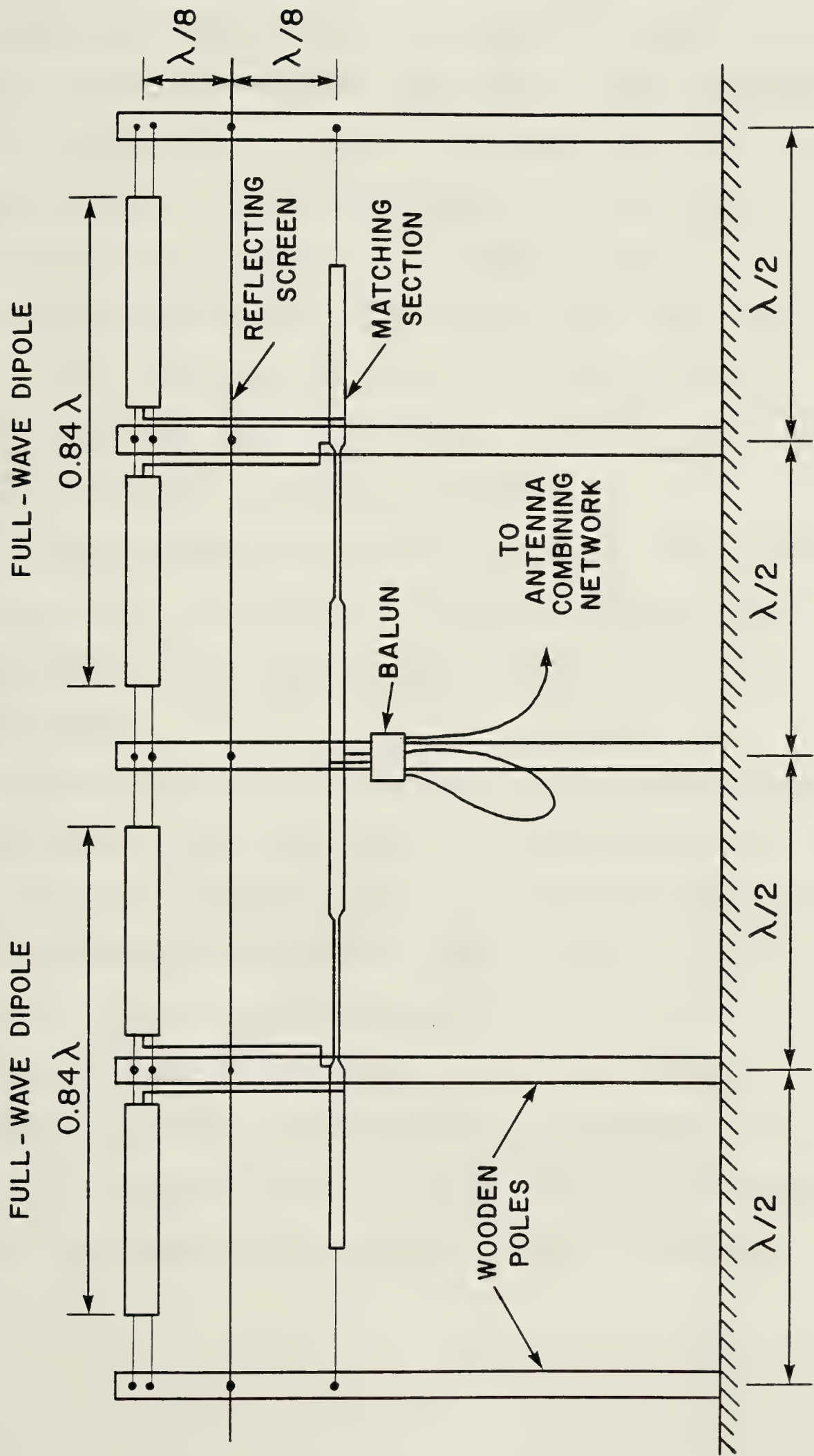


FIGURE 5.2 Basic Array Element for 22.25 MHz Telescope

elements in the east-west arm were combined together to form 48 sub-arrays, each 2λ by 2λ , as shown in Figure 5.3. An additive combining network plus precise cable lengths for each of the four basic elements allowed control of the north-south pointing and beam shape for each sub-array.

For the polar synthesis telescope the sub-array beams were centered on the north celestial pole. The 3 dB beam width in both the E-plane (east-west) and H-plane (north-south) was about 24 degrees, and the beam width between first nulls was about 60 degrees.

For the interference-excising project two of the sub-arrays near the center of the east-west arm and a distance 350 m (26λ) apart were chosen to form an interferometer.

As the sub-array beam pattern had an approximate null for Cassiopeia A during transit, fringes from Cassiopeia A were initially not very strong. The antennas were changed part way through the observations. Instead of using the sub-arrays, signals were taken from just one of the four dipole-pair elements. A single element provided an antenna pattern centered on the zenith with an E-plane 3 dB beam width of 24 degrees and an H-plane width of 96 degrees. Signals from Cassiopeia A were then much improved.

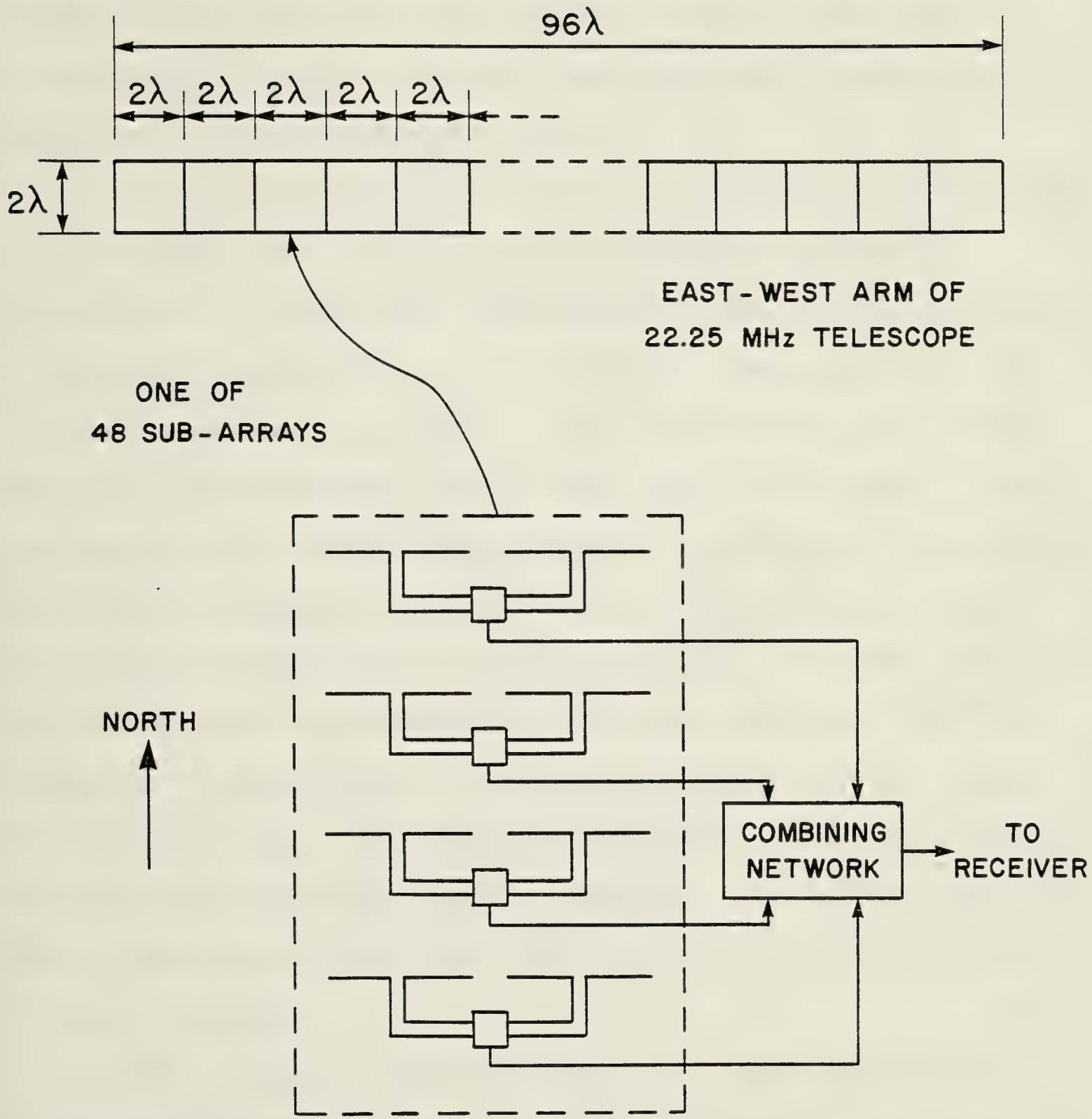


FIGURE 5.3 Sub-arrays of Polar Synthesis Telescope

5.3 Cable Lengths and Losses

One of the requirements for an interferometer is accurate knowledge of the phases of signals from the antennas. To determine phase, the electrical lengths of all cables in a system must be known.

The only unknown cable lengths in the project (and also the longest) were for the cables between the first IF amplifiers (located near the antennas) and the second mixers (located in the observatory building). Measurement of the cable lengths was assisted by the availability of a number of cable runs between the building and the antennas. Three cables, all of unknown length, were connected at the antenna end via a resistive Y splitter as in Figure 5.4. A signal generator transmitted an accurately known frequency down one of the cables. Measurement of the amplitudes and relative phases of the signals at the terminated ends of all three cables were made. The generator frequency was then changed slightly and the measurements repeated. The signal generator was connected to the other two cables in turn and the above process repeated.

From the amplitude measurements it was possible to determine the loss of each cable individually, and from the phase measurements at different frequencies the electrical lengths of each cable could be calculated. The length calculations were similar to those for a cable measurement procedure known as the "extended probe" method [2].

The losses and electrical lengths at 5.0 MHz measured

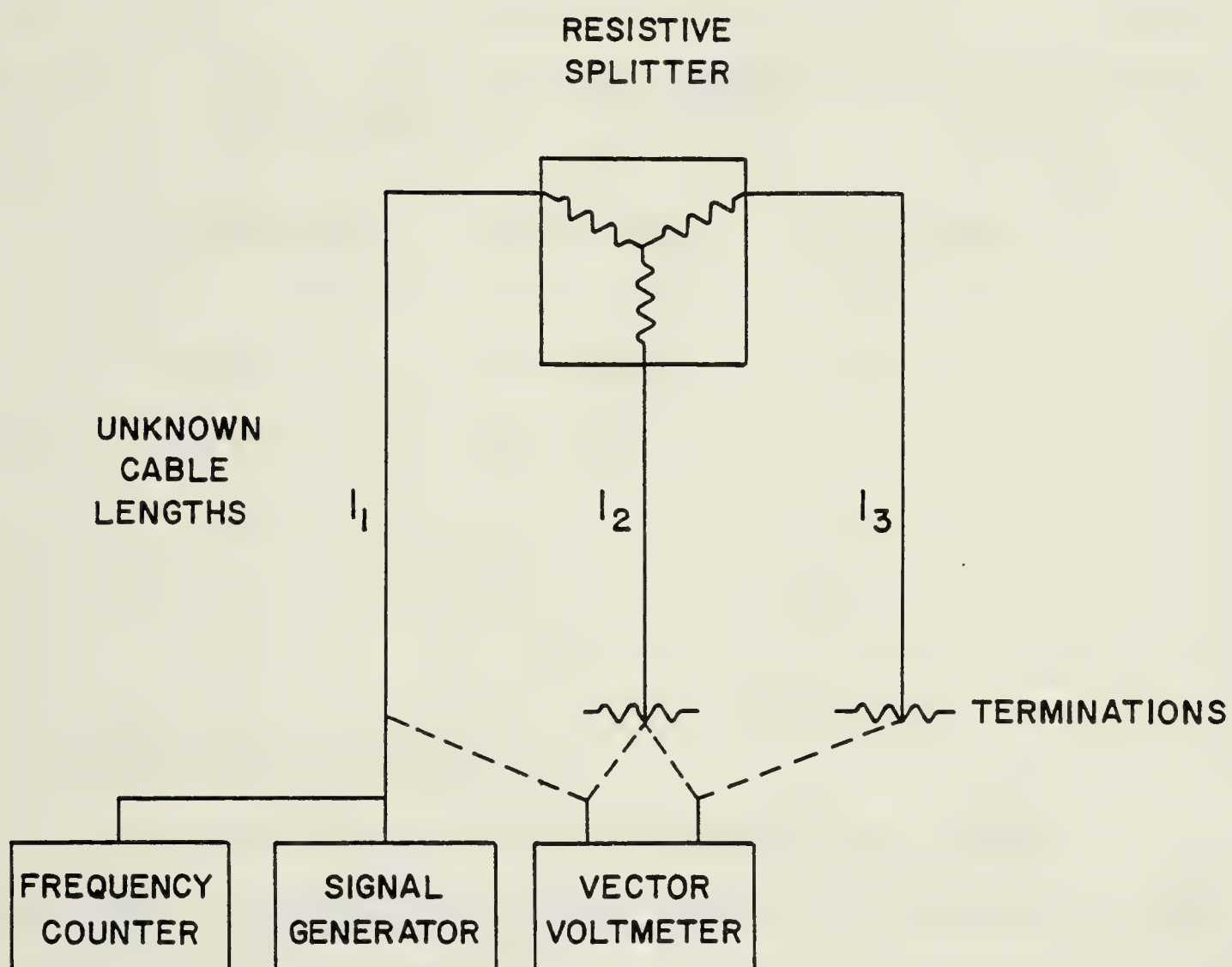


FIGURE 5.4 Connections for Measurement of Cable Lengths and Losses

for the cables to the east and west receivers are given in Table 5.1. The difference in losses is due to the use of low-loss heliax for a large part of the cable to the east receiver, rather than RG-8 as used for the west receiver.

Table 5.1. Losses and Electrical Lengths of Receiver Cables at 5.0 MHz

Receiver	Cable Loss	Electrical Length
West	12.0 dB	11.4 λ
East	8.4 dB	11.0 λ

5.4 Bandwidth Decorrelation

A possible problem which may occur with radio telescopes is bandwidth decorrelation. If there is a large relative delay between two signals being correlated, a phase shift results across the bandwidth of the signals, thereby reducing sensitivity.

Because the 52 kHz bandwidth of the FFT processor is small, bandwidth decorrelation is not serious. At the first null of the antennas in the east-west direction the position of a source would be $\theta = 30$ degrees from the zenith. With a baseline of $D_\lambda = 26$ wavelengths, the delay τ_1 between the signal's arrival at the two antennas is

$$\begin{aligned}\tau_1 &= \frac{D_\lambda \sin \theta}{v} \\ &= \frac{26 \sin 30^\circ}{22 \times 10^6 / \text{sec}} = 0.59 \times 10^{-6} \text{ sec}\end{aligned}$$

An additional delay τ_2 due to the difference of 0.4λ in the lengths of the IF cables should be added.

$$\tau_2 = \frac{0.4}{5 \times 10^6 / \text{sec}} = 0.08 \times 10^{-6} \text{ sec}$$

The phase shift ϕ across a bandwidth of $BW = 52 \text{ kHz}$ for a delay of $\tau = 0.67 \times 10^{-6}$ seconds will be

$$\begin{aligned}\phi &= 2\pi BW \tau \\ &= 2\pi \times 52 \times 10^3 / \text{sec} \times 0.67 \times 10^{-6} \text{ sec} \times 180/\pi \\ &= 12.5^\circ\end{aligned}$$

This small phase shift will not produce any significant bandwidth decorrelation over the field of view of the antennas.

If bandwidth decorrelation were a problem, it could be corrected for by adding a compensating amount of phase shift to the in-phase and quadrature spectra. The amount of compensation would be calculated to produce zero decorrelation for a desired point in the sky.

5.5 System Operation

The component parts of the entire system, including antennas, receivers, FFT processor and microcomputer were interconnected as outlined in the previous chapters. Figure

5.5 shows the equipment in the observatory building. The two second mixers and IF amplifiers were rack mounted above and below the Fluke synthesizer at right center of the photo. The FFT processor and microcomputer were enclosed in a shielding cage (end removed) to the left. A view of the FFT processor from above in Figure 5.6 shows the circuit boards in a rack at the back and the keyboard and readout console at the front.

For the receivers the major operating considerations were frequency response and gain adjustment. As mentioned previously, the frequency responses of the second IF amplifiers were found to change due to mechanical instability of the IF transformer cores. Frequent monitoring and adjustment was therefore necessary. Receiver gains were set to provide a noise level of between 30 and 60 mVrms into the A/D converters. This level ensured that signal levels were above roundoff noise, even in the presence of strong sinusoidal interference. The largest sinusoid which would not cause significant clipping was about 300 mVrms.

Most aspects of the system's operation were controlled by the microcomputer. For example, the microcomputer controlled the second local oscillator frequency and the integration time. For many of the observations the second LO was sequenced through four values: 4.483 MHz, 4.533 MHz, 4.583 MHz and 4.633 MHz. The resulting receiver center frequencies were 22.325 MHz, 22.275 MHz, 22.225 MHz and 22.175 MHz.

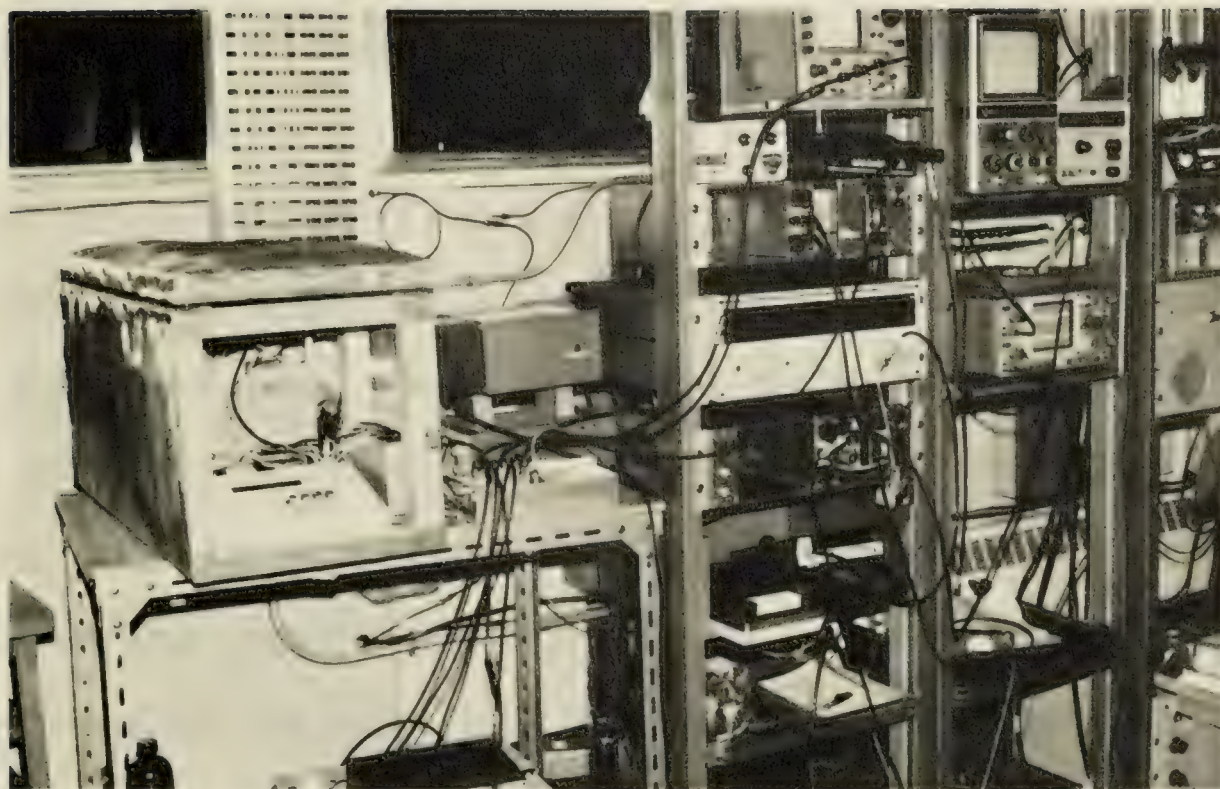


Figure 5.5.
Equipment Layout in
the Observatory Building

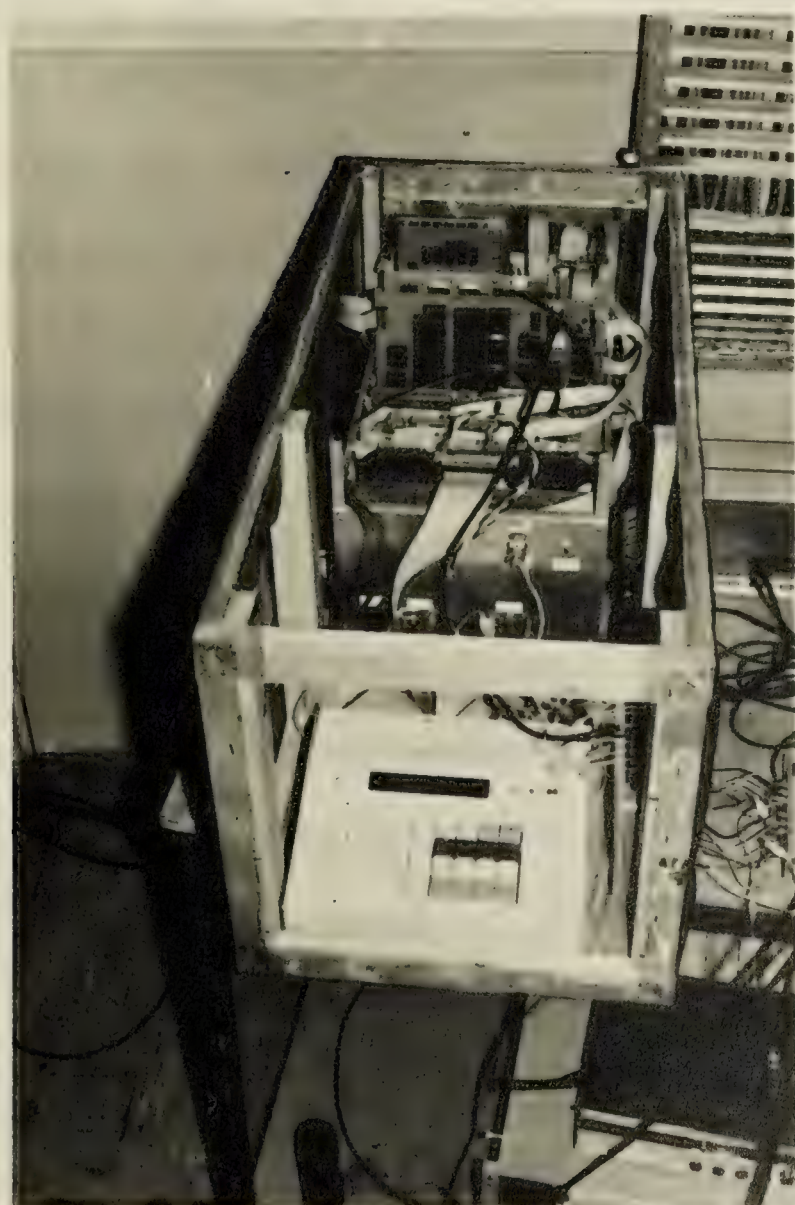


Figure 5.6.
The FFT Processor

A major function of the microcomputer was the recording of observation results. In order for detailed analysis of the observations to be carried out at a later time, the raw spectra from the FFT processor were recorded on magnetic tape. Spectra directly from the FFT processor consisted of 48 bit integers. These were converted by the microcomputer to 32 bit floating point numbers with a sign bit, a 7 bit twos complement exponent and a 24 bit unsigned mantissa. To reduce the amount of data stored on tape, spectra were recorded as 16 bit floating point numbers by truncating the mantissa to 8 bits. A header containing an identifying file number, the time of recording, the accumulation time, the local oscillator frequency and the number of clips counted during A/D conversion was recorded with each spectrum. A checksum for error detection was also included.

The microcomputer employed a 4σ rejection procedure for robust estimation of the centers of the in-phase and quadrature spectra. Estimation results were recorded on a two-pen chart recorder so that fringes could be observed as they were received. A second multiple-input chart recorder was used for the number of points deleted during robust estimation, the local oscillator frequency and the amount of clipping. An assembly language listing of the microcomputer program used during the observations is included in Appendix 3.

A problem encountered with the microcomputer during the observations was eventually traced to the Am9511 Arithmetic

Processing Unit. This device was discovered on occasion to refuse to clear its BUSY flag. As a result, the microcomputer would get hung up in a loop waiting for arithmetic computations. A program modification which timed Am9511 operations and reissued commands if the device remained BUSY for too long was partially successful in overcoming this problem. However, further testing revealed that the device was operating incorrectly in other ways. Correct operation was found to be highly dependent on clock frequency which the manufacturer claimed could be anything from 0.3 to 3 MHz but which actually exhibited only a few windows a few tens of cycles wide near 3 MHz within which the device would work properly. The windows were dependent on temperature and would slowly drift, causing the author considerable consternation.

This strange behavior appeared to be the result of a manufacturing defect. A second device (from the same manufacturing lot) performed in a similar manner. This integrated circuit was a relatively new and highly complex LSI chip, so manufacturing difficulties were not unexpected.

The problem was finally alleviated by the simple addition of a heat sink to the IC. Though not called for in the manufacturer's information, the heat sink kept the IC's temperature sufficiently stable so that it would continue to operate satisfactorily once the clock frequency was set. Fortunately, spectra stored on tape were not affected by the difficulties with the arithmetic unit.

5.6 Data Analysis

The spectra from the tapes were analyzed on the University of Alberta's computing facilities. The FORTRAN program used for robust estimation is listed in Appendix 4. Analysis results presented in the next chapter were plotted by the computer on a CalComp plotter.

Prior to robust estimation, a correction was made to the spectra to force the frequency response to be as flat as possible. This correction was necessary because of ripples in the frequency response of the receivers.

An accurate reference for amplitude corrections was provided by the auto spectra. Auto spectra containing no interference were chosen, and fifth order polynomials fitted to estimate the receiver amplitude responses. All of the auto spectra received on the same night were then divided by these reference polynomials to produce a flat frequency response.

The cross spectra were divided by the square root of the product of the polynomials for the two receivers in order to correct for amplitude ripples. Unfortunately a good reference for the relative phases of the two receivers was not available. Therefore, no correction could be made for differences in the phase responses of the receivers.

The amplitude ripples found in the spectra before correction ranged from 0.15 dB to 2.4 dB, with the median amount of ripple being 0.88 dB. Spectra of strong fringes were examined for evidence of phase ripples, but no

detectable ripples were found.

6. Observation Results

This chapter describes observation results obtained using the interference excising correlator at the Dominion Radio Astrophysical Observatory in Penticton, British Columbia during the period from November 12, 1979 to January 6, 1980. Section 6.1 contains a number of plots of in-phase and quadrature fringes both before and after interference has been removed. Some examples of raw spectra and their histograms are included. A number of plots of morning and evening observations are given, illustrating the range of interference levels encountered.

Some of the fringes are plotted in terms of amplitude and phase in Section 6.2 in order to demonstrate the presence of scintillation. Variations in the amplitude of the fringes are compared to similar variations noted in the auto spectra. The performance of the first decile as an estimator for the auto spectra is investigated in Section 6.5. The subsequent section describes an attempt at daytime observation employing an experimental frequency-changing scheme.

An empirical probability distribution for interference amplitude is given in Section 6.5. The probability of interference is found to exhibit a power-law relationship to interference level.

The chapter concludes with some general comments on the observations.

6.1 Plots of the Observations

6.1.1 Examples with No Interference Removed

Figures 6.1 and 6.2 show records of fringes from which interference has not been removed (i.e. the sample mean is used as the estimate of the centers of the co and quadrature spectra). In 6.1 fringes from Cassiopeia A (lower transit time 6:44¹, fringe period 17.0 min. at transit) are evident until 6:25 when interference obliterates them. Figure 6.2 contains small fringes from Jupiter (transit time 4:00, fringe period 8.9 min.) with high levels of terrestrial interference at 5:30 and after 7:00. The peaks are truncated at ± 100 , but some of those shown were actually as large as ± 1000 . The interference peaks are periodic because the system is scanning sequentially through four adjacent 50 kHz regions of the spectrum between 22.15 and 22.35 MHz. Records of terrestrial interference such as these are commonly encountered in low frequency radio astronomy.

¹All times in this chapter are Pacific Standard Time.

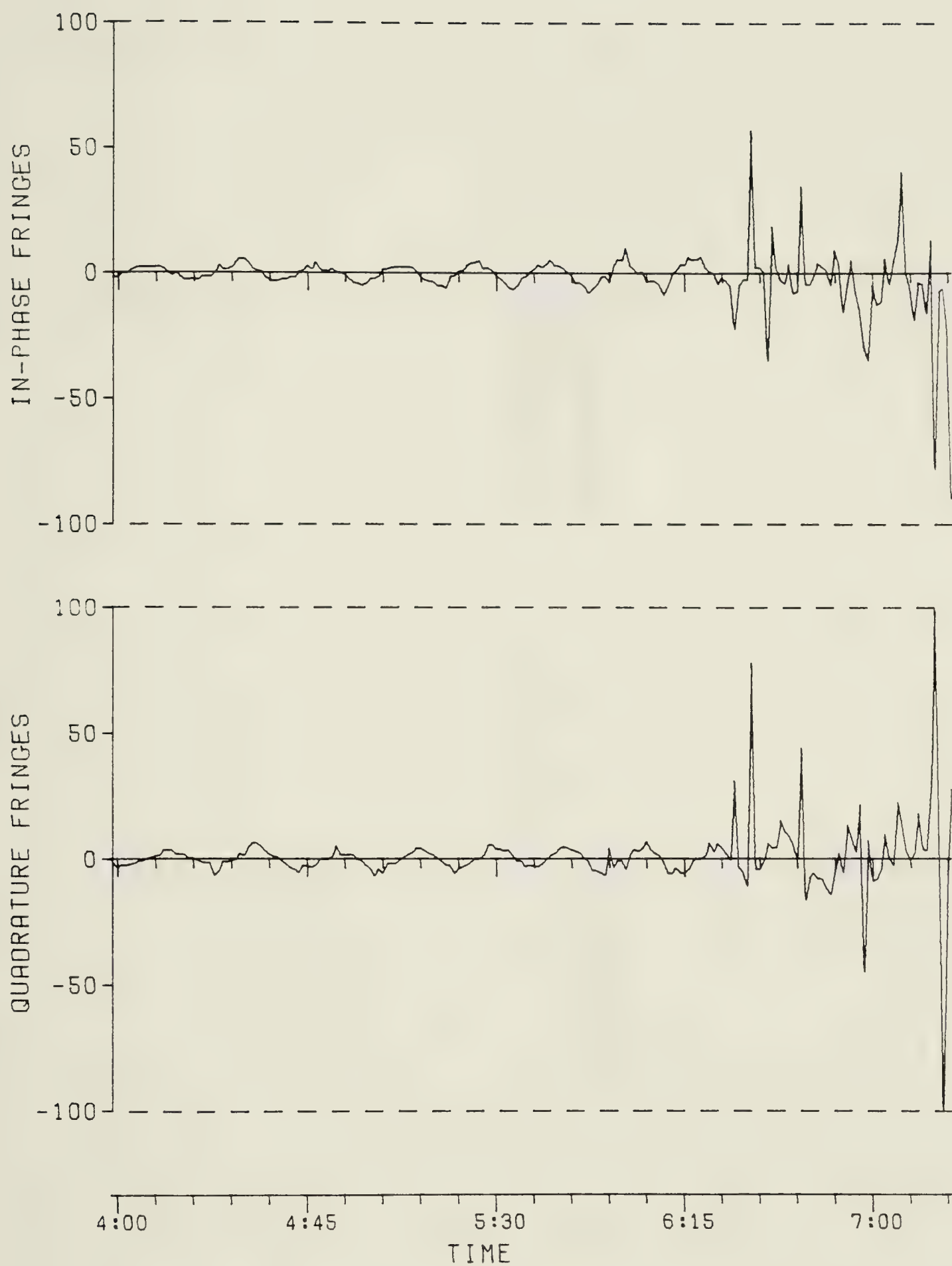


Figure 6.1. Fringes with Interference

November 29, 1979

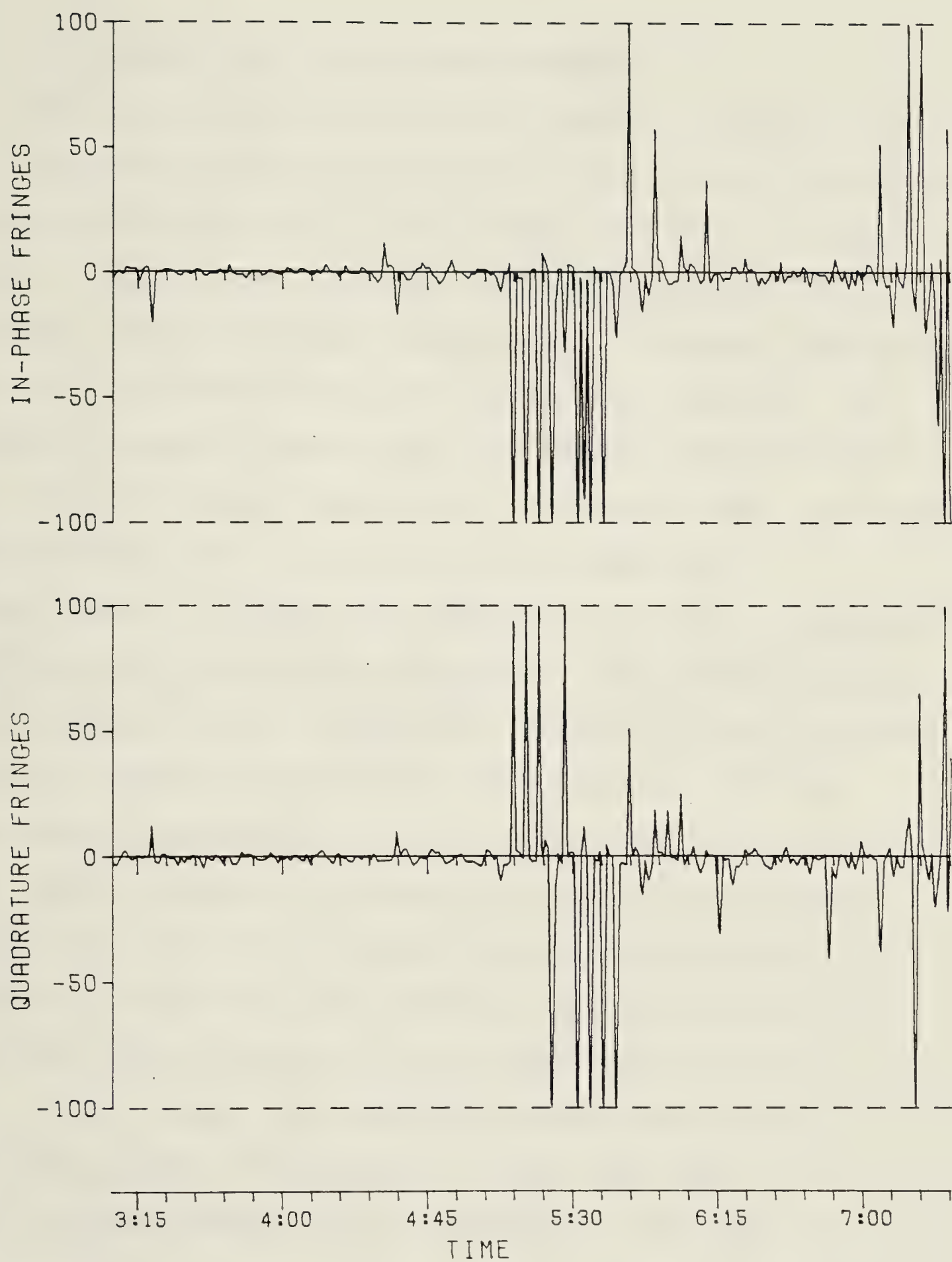


Figure 6.2. Fringes with Interference
January 4, 1980

6.1.2 Examples with Interference Removed

The same records as above are shown in Figures 6.3 and 6.4 following interference removal via the robust estimation method of Section 4.6.3. Four traces are shown in these plots. Traces A and B are the in-phase and quadrature fringes. The solid lines are the robust estimates, while the x's are the sample means (no interference removed). The central regions of these plots are linear, whereas beyond ± 10 the plots become logarithmic in order to show the actual magnitude of the fringes when contaminated with interference. It should be remembered that the x's represent the means of 108 spectral components, only a few of which contain interference. Therefore, in order to cause the mean to have a magnitude of 10^3 the interference, if it is contained predominantly in a single channel (as is usual), must have a magnitude of about 10^5 and is thus at least 40 dB larger than the fringes (which are less than ± 10). Figure 6.4 contains some examples of interference of this amplitude being successfully rejected from the spectra.

Trace C shows the expected standard deviation σ_x of the underlying normal distribution as derived from the auto spectra using the estimation technique of Section 4.6.2. An approximate idea of the expected error in the fringes due to fluctuation noise can be obtained by dividing the value of trace C by $\sqrt{(n)(EIT)}$, where n is the number of spectral components containing no interference and EIT gives the loss

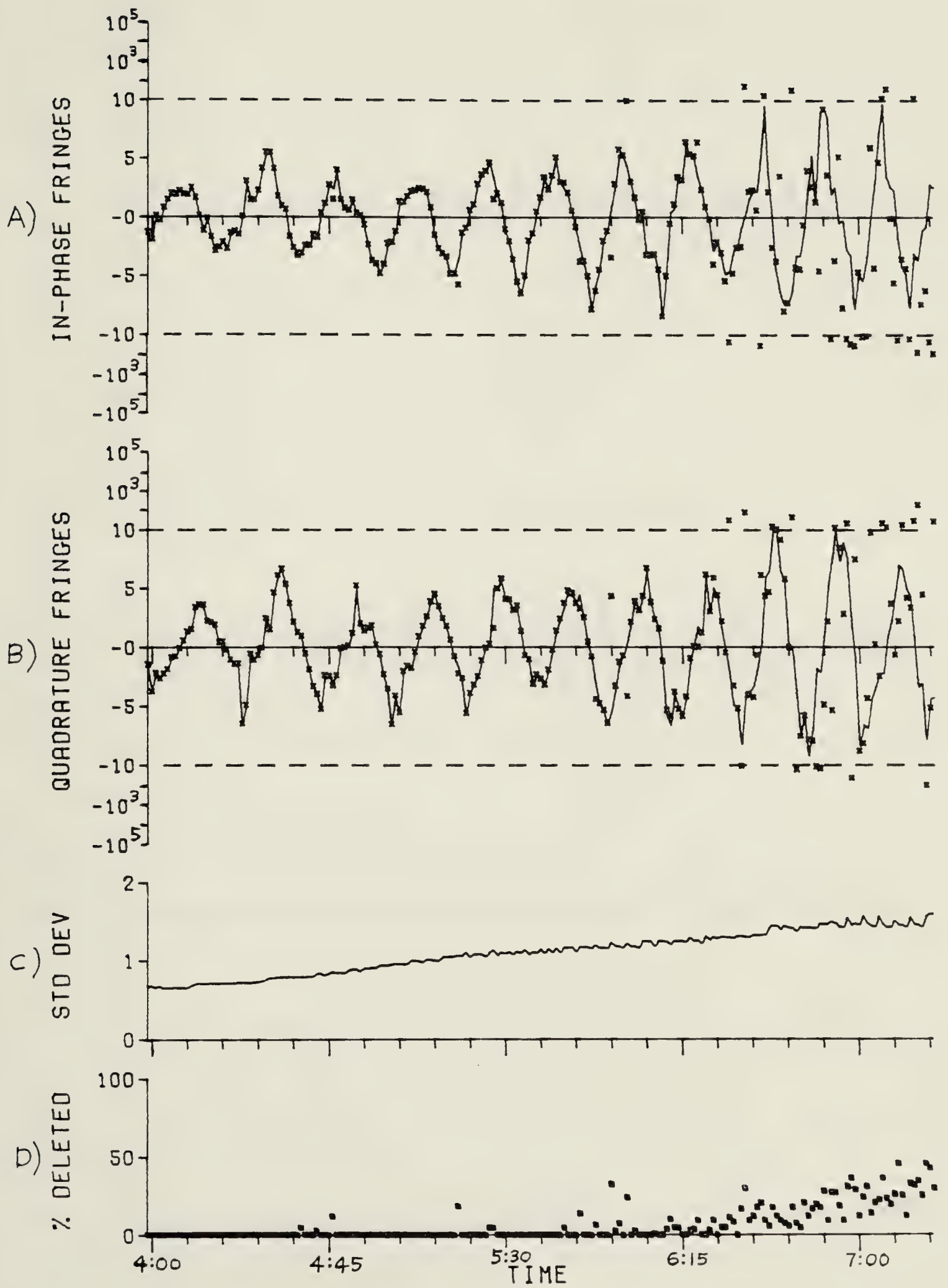


Figure 6.3. Fringes after Interference Removal
November 29, 1979

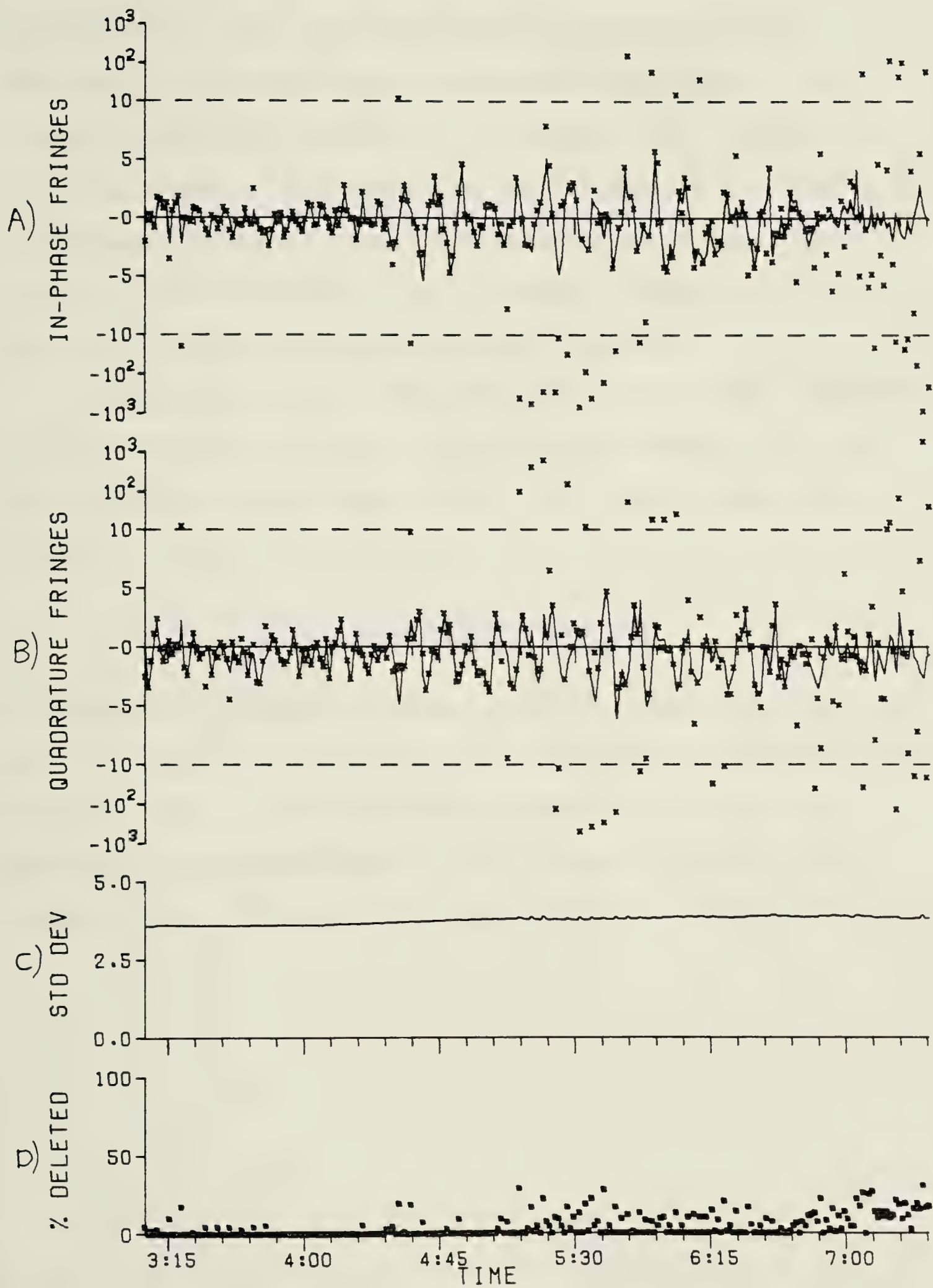


Figure 6.4. Fringes after Interference Removal
January 4, 1980

in stability of the estimate due to windowing. Trace D represents the percentage of components deleted by the robust estimation procedure (i.e. beyond $\pm 5\sigma_x$ from the final estimate). This trace may be thought of as showing the percentage of points positively identified as outliers. Close-in contamination is not included though its effects are still minimized by the biweight estimator.

From Table 4.2 the efficiency of the biweight estimator relative to the mean from a normal distribution is 1.041. The expected standard deviation σ_f of the fringes due to fluctuation noise will then be

$$\sigma_f = \sigma_x \left[\frac{1.041}{(100 - \%Deleted)(108)(EIT)} \right]^{1/2} \quad (6.1)$$

For example, if %Deleted=0 and EIT=0.44 then $\sigma_f = .148\sigma_x$. In most of Figure 6.3 only small percentages of the points are deleted, thus $\sigma_f = (0.148)(1.0) = 0.148$ which is very small compared to the magnitude of the fringes. Similarly in Figure 6.4, $\sigma_f = 0.53$ which is small relative to the fringes.

6.1.3 Examples of Spectra and their Histograms

Three examples of in-phase cross spectra and their histograms are given in Figures 6.5, 6.6 and 6.7. The examples correspond to cases of no interference, low-level interference, and strong interference. Each figure shows four consecutive in-phase spectra and their histograms. The spectra are all from observations on November 28-29 in Figure 6.3. The spectra and histograms are linear between the dotted lines but become logarithmic beyond the dotted lines in order to show the complete range of points necessary.

Figure 6.5 shows four spectra from between 5:09 and 5:13. In each case the histograms have a Gaussian shape with a standard deviation σ_x of about 1, which is as expected from the levels of the auto spectra (trace C in Figure 6.3). The centers of the four spectra change because the fringe from Cassiopeia A at this time is just passing through zero.

Low to moderate interference appears in the spectra of Figure 6.6, taken from between 6:24 and 6:28. A central Gaussian distribution ($\sigma_x=1.3$) is present with a few outlying points.

Large amounts of interference are seen in Figure 6.7 from between 7:15 and 7:19. The underlying Gaussian distribution ($\sigma_x=1.5$) has been badly contaminated with interference. Between 25 and 45% of points are identified as outliers by the estimation procedure for these spectra

(trace D in Figure 6.3), but there are sufficient numbers of non-contaminated points for the centers of the underlying normal distributions to be accurately determined.

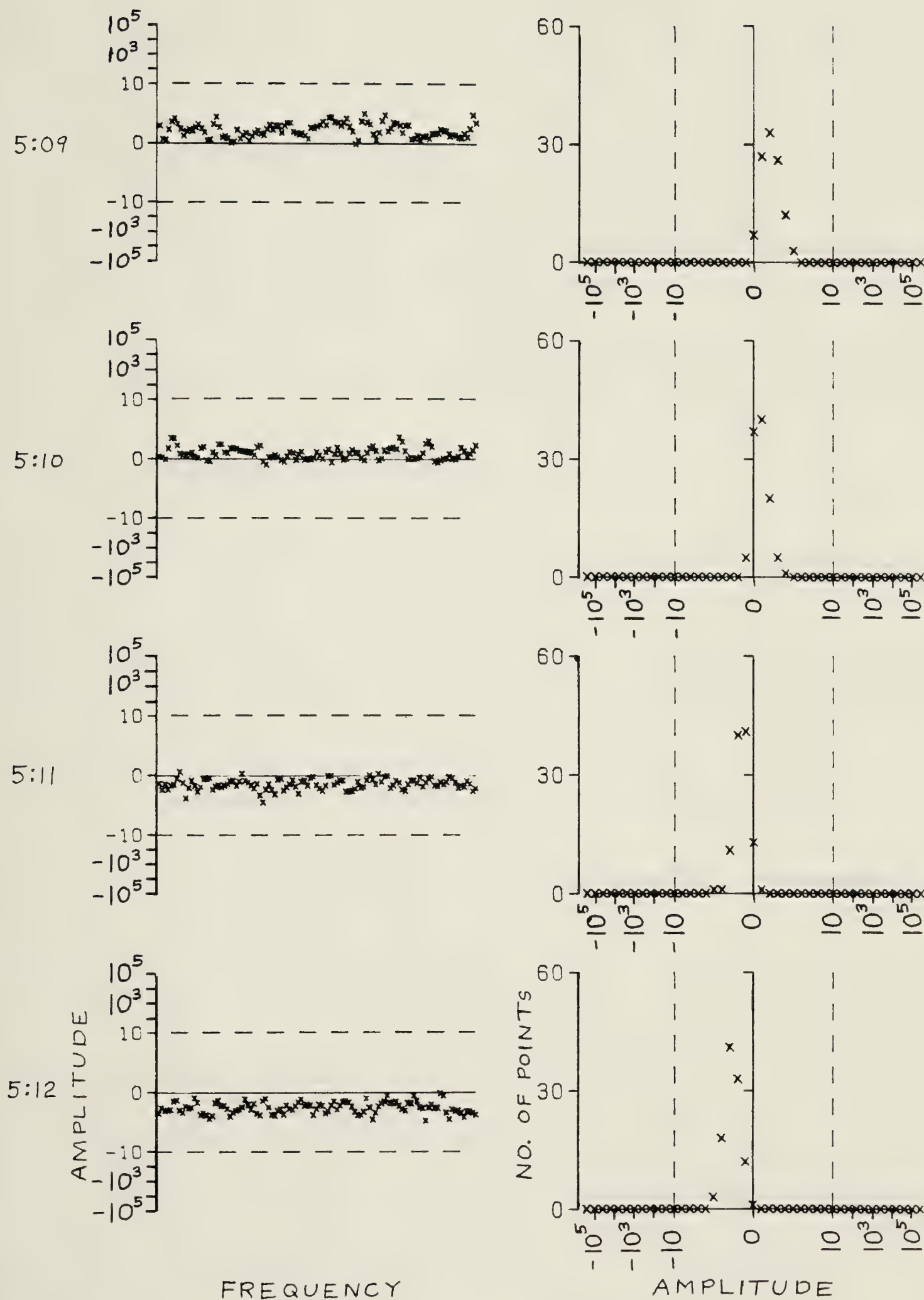


Figure 6.5. Spectra and Histograms

November 29, 1979

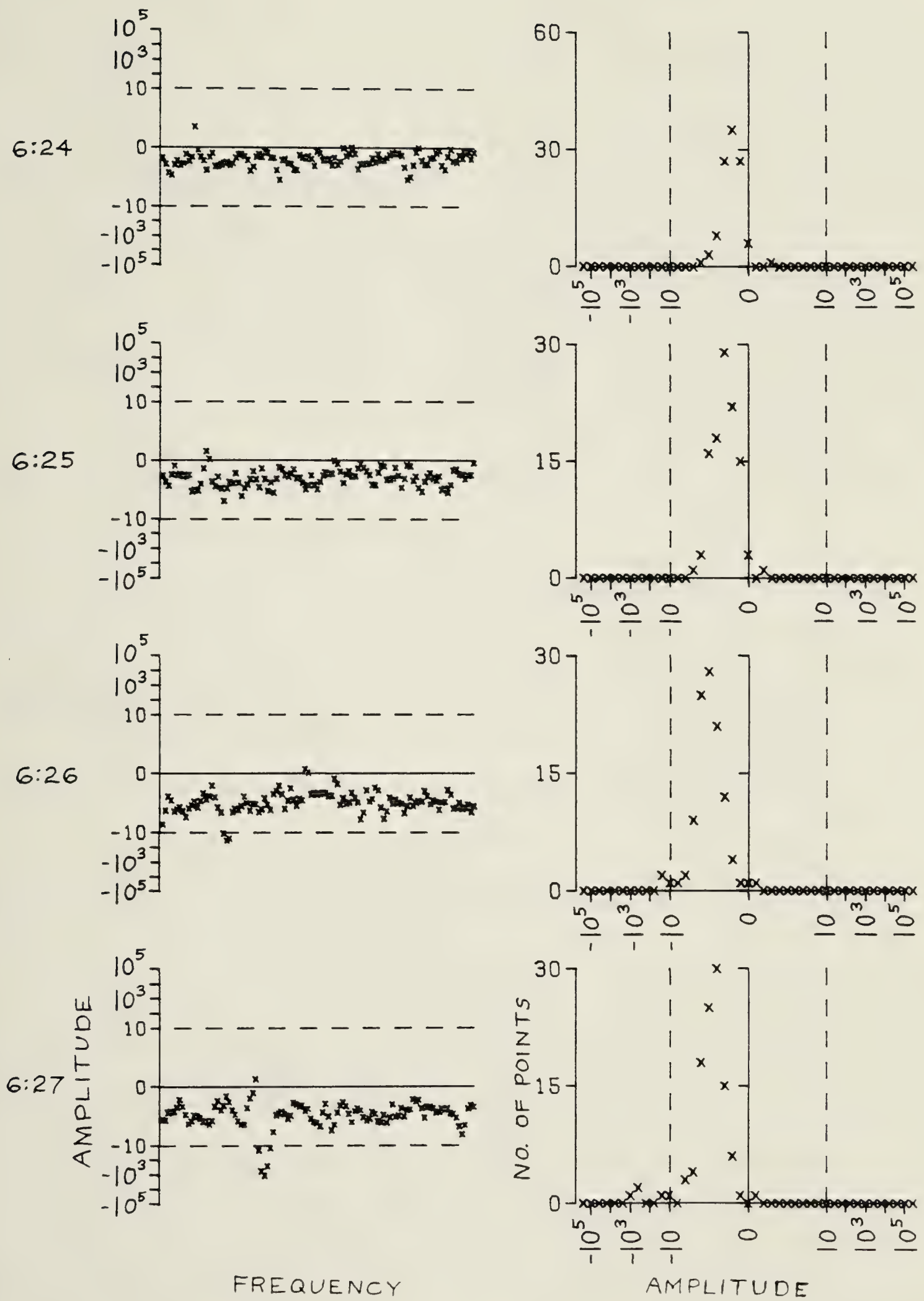


Figure 6.6. Spectra and Histograms

November 29, 1979

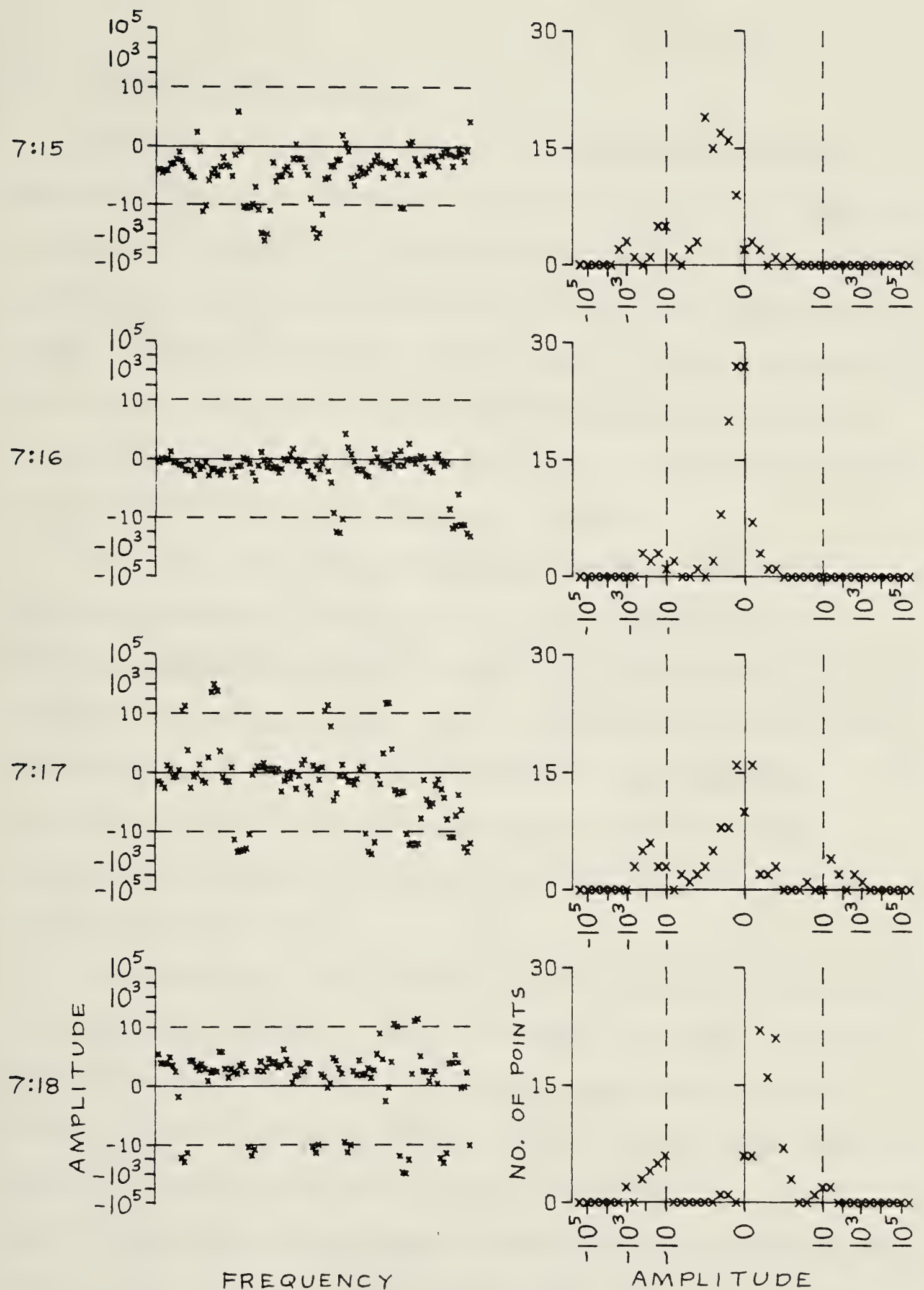


Figure 6.7. Spectra and Histograms
November 29, 1979

6.1.4 Morning Observations

Figures 6.3 and 6.4 were both examples of morning observations, with increasing interference at the approach of sunrise. Figure 6.8 is another example, in this case continuing until after sunrise.. Fringes from Cassiopeia A (lower transit time 6:48) can be seen. A rapid increase in both levels and numbers of interfering signals begins at about 6:00, as would be expected due to the rapid increase in ionospheric electron density at sunrise.

At 7:30, something unexpected happens. The fringe estimates begin to swing wildly, the standard deviation estimates jump erratically, and up to 100% of the observations are deleted. The estimates have broken down completely. The cause of this behavior was sweeping narrow-band signals which appeared over most of the shortwave spectrum at the same time nearly every morning during the observations.

The sweeping signals were strong and easily observable on a spectrum analyzer. They continued throughout the day and gradually diminished as evening approached, usually becoming undetectable by about 16:00. Two or three separate sweeping signals were often seen simultaneously. Some started above 30 MHz and swept slowly down to below 15 MHz, while others appeared and disappeared rapidly and moved about the spectrum very unpredictably. The most troublesome swept signal at 22 MHz was one which recurred regularly with

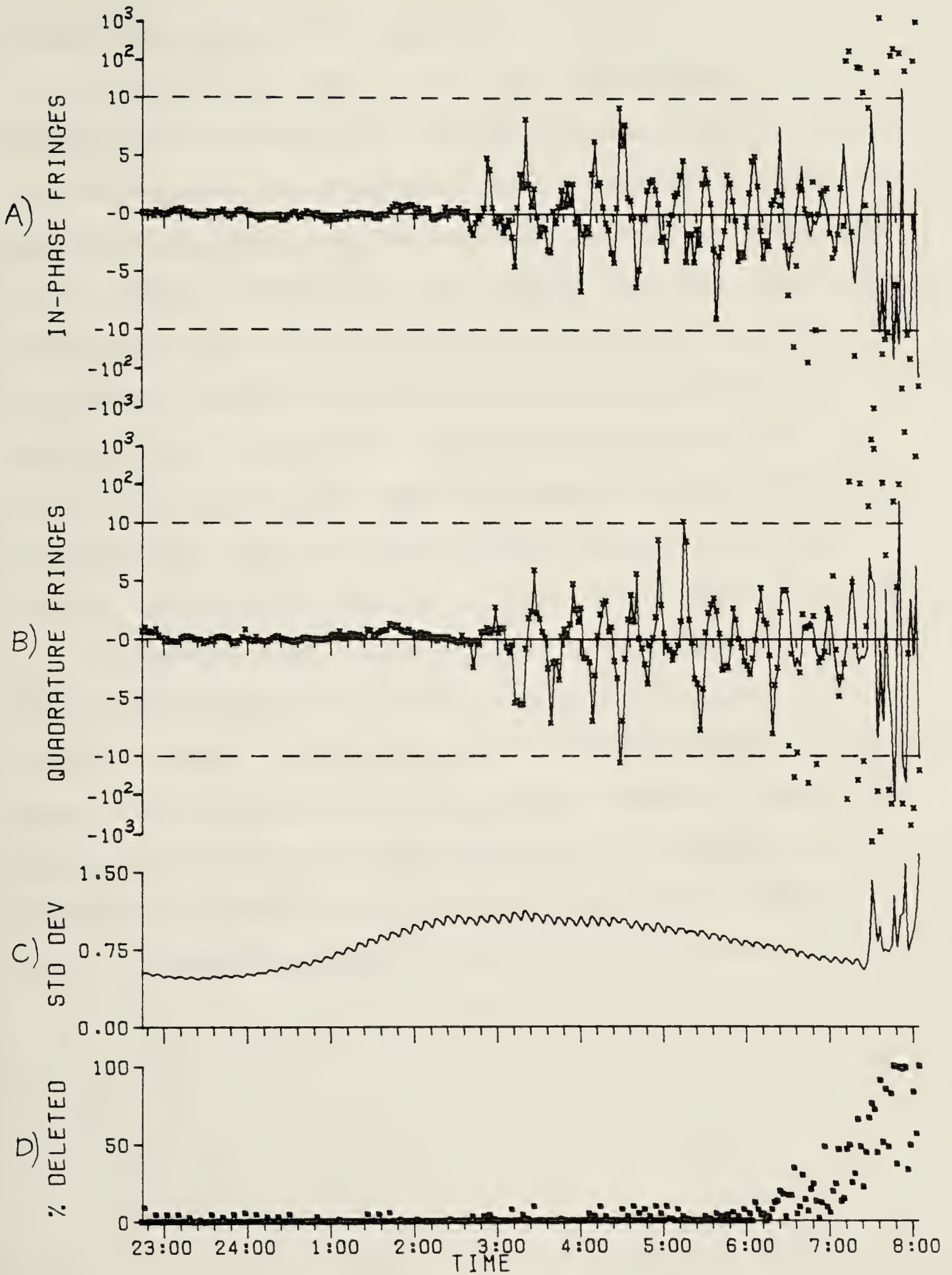


Figure 6.8. Fringes after Interference Removal

November 27-28, 1979

a repetition period of 10 seconds.

Enquiries were made to the local Department of Communications office as to the source and legality of such sweeping signals. Monitoring stations eventually identified two locations producing the signals: Denver, Colorado and San Francisco, California. The signals were believed to be ionospheric soundings which are conducted worldwide for ionospheric research and radio propagation studies. A discussion of ionospheric sounding is contained in Davies [17]. Local Department of Communications officials indicated that the observed sweeping signals might be illegal, though confirmation of this has not been received.

The presence of sweeping signals made observations beyond 7:30 and during the day impossible. Before 7:30, however, normal interference was excised successfully in all cases, as illustrated by the previous examples. Generally, the removal of interference consistently allowed from 60 to 90 minutes (occasionally much more) additional observing time in the mornings during the field testing period.

6.1.5 Evening Observations

In the evenings it was necessary to wait until some time after sunset before observations could begin. Strong interference caused the receivers to overload until ionospheric electron densities decayed sufficiently to reduce interference levels. After interference decreased, heavy scintillation was observed for a number of hours. Scintillation was apparent in all of the fringes observed during the field trials, and was always severe in the evenings.

6.1.5.1 November 28

One record of evening fringes from Cassiopeia A is shown in Figure 6.9. Transit time is 18:48 and the fringe period at transit is 17.0 minutes. A large amount of interference is initially present, with the strengths and numbers of interfering signals decreasing slowly over 1 1/2 hours. Here again the received frequency is being sequentially scanned through four adjacent 50 kHz regions of the spectrum between 22.15 and 22.35 MHz. From the first half of trace D it may be noted that one of the four regions regularly has little or no interference present while the others have much more. The region of least interference is between 22.15 and 22.2 MHz.

From trace C the expected standard deviation varies from 19 to 6, implying a standard deviation of the fringes

due to fluctuation noise of from 2.9 to 0.9 or slightly more if a significant number of points are deleted. Most of the scatter in the fringes is therefore due to fluctuation noise. The fringes are relatively noisy because the antenna pattern at this time is centered on the north celestial pole and has an approximate null for Cassiopeia A at upper transit.

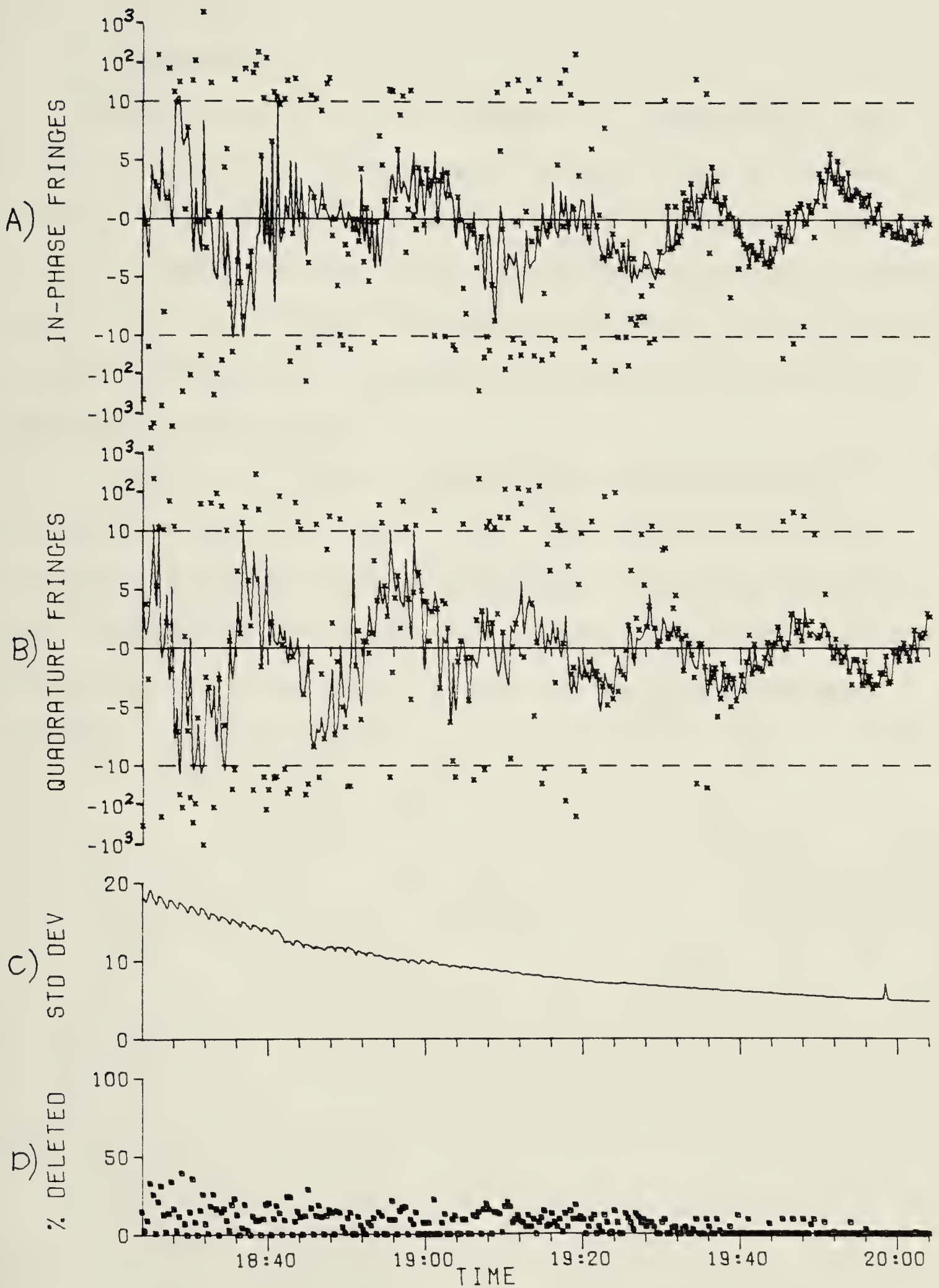


Figure 6.9. Fringes after Interference Removal

November 28, 1979

6.1.5.2 December 4

A second evening record appears in Figure 6.10. The antenna pattern has been changed to have a maximum at the zenith, thus the signal from Cassiopeia A (transit time 18:17) is much stronger as evidenced by an expected standard deviation of $\sigma_x = 0.8$, or fluctuation noise of $\sigma_f = 0.12$. The receiving frequency is constant for this record and is centered on 22.225 MHz.

A relatively constant amount of interference is received between 19:00 and 19:50, after which reception becomes quiet. There are many spikes in the fringes which are too large to be due to fluctuation noise. These appear to be due to strong scintillation and will be discussed further in Section 6.2.1.

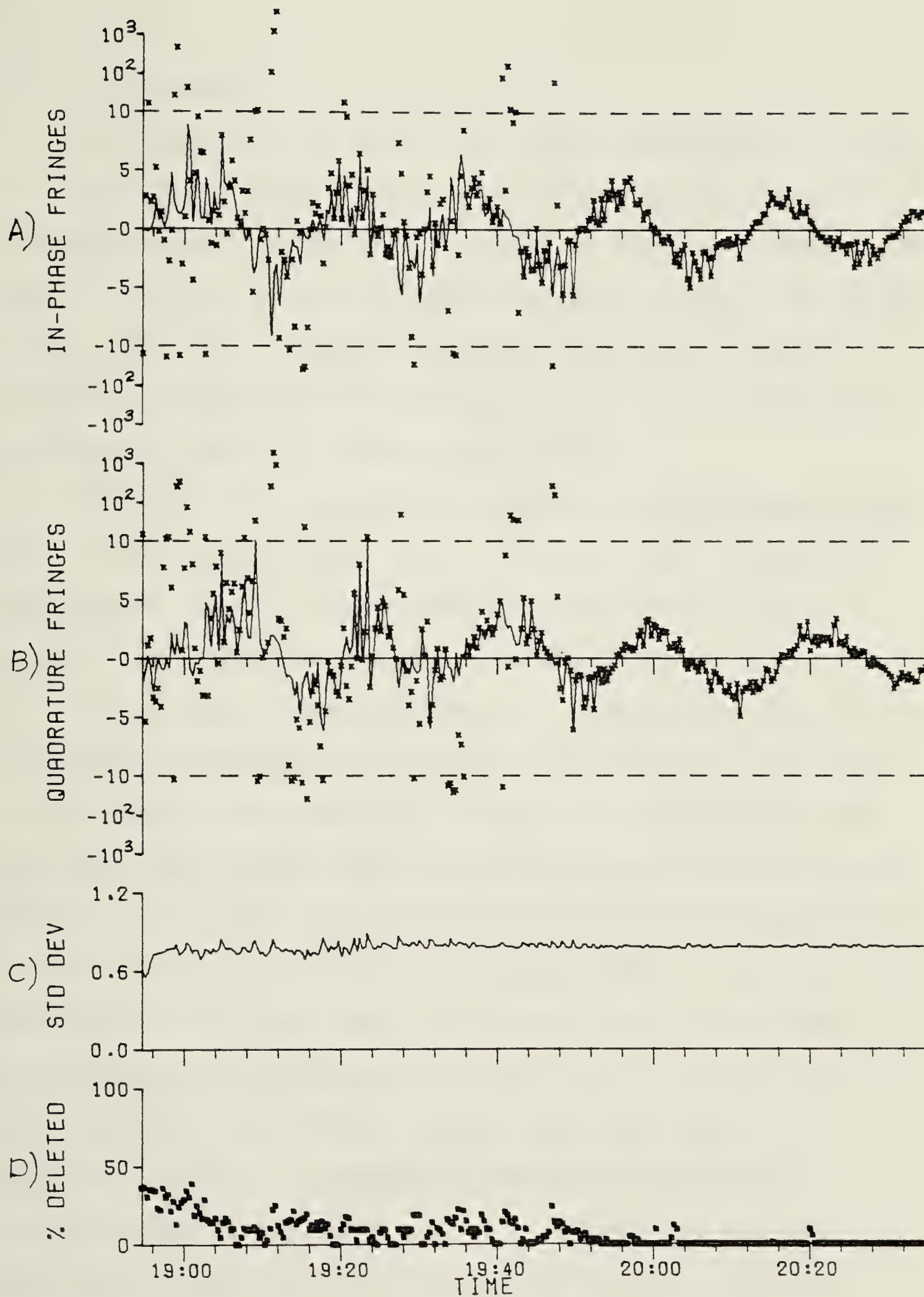


Figure 6.10. Fringes after Interference Removal

December 4, 1979

6.1.5.3 December 5

A record showing severe evening interference is shown in Figure 6.11. Very strong interference approaching 10^5 in some cases with up to 75% of points deleted continues from 18:15 to 20:00. A single interferer would have to be 60 dB larger than the fringes to produce the levels shown. A considerable amount of clipping at the A/D converters was recorded a number of times until 19:45.

The receiver frequency was again being scanned across four frequencies between 22:15 and 22:35 MHz. For most of the record, trace D shows one frequency which is usually free of any interference (22.15 to 22.2 MHz).

The fringes from Cassiopeia A (transit time 18:13) are virtually unrecognizable for most of the record. For the first half of the record the fringes are being distorted because high interference levels are exceeding the dynamic range of the system. Periods of excessive clipping produce harmonics and contaminate the entire spectrum. Large single interferers such as those 60 dB above the fringe level produce spurious sidelobes (a result of FFT coefficient quantization) and thereby contaminate the rest of the spectrum. Finally, intermodulation distortion in the receivers was observed directly on a spectrum analyzer monitoring the first I.F. outputs during the time this record was made. Two very strong, steady shortwave signals were observed below 22.15 MHz which were clearly overloading

the first mixer and producing intermodulation products throughout the first I.F. pass band. It was only after 19:30 that the level of these two signals decreased sufficiently to allow normal observations to begin.

After 20:00 the interference has become quite small. However, much larger variations are present in the fringes than would be expected due to fluctuation noise. These variations appear to be due to scintillation.

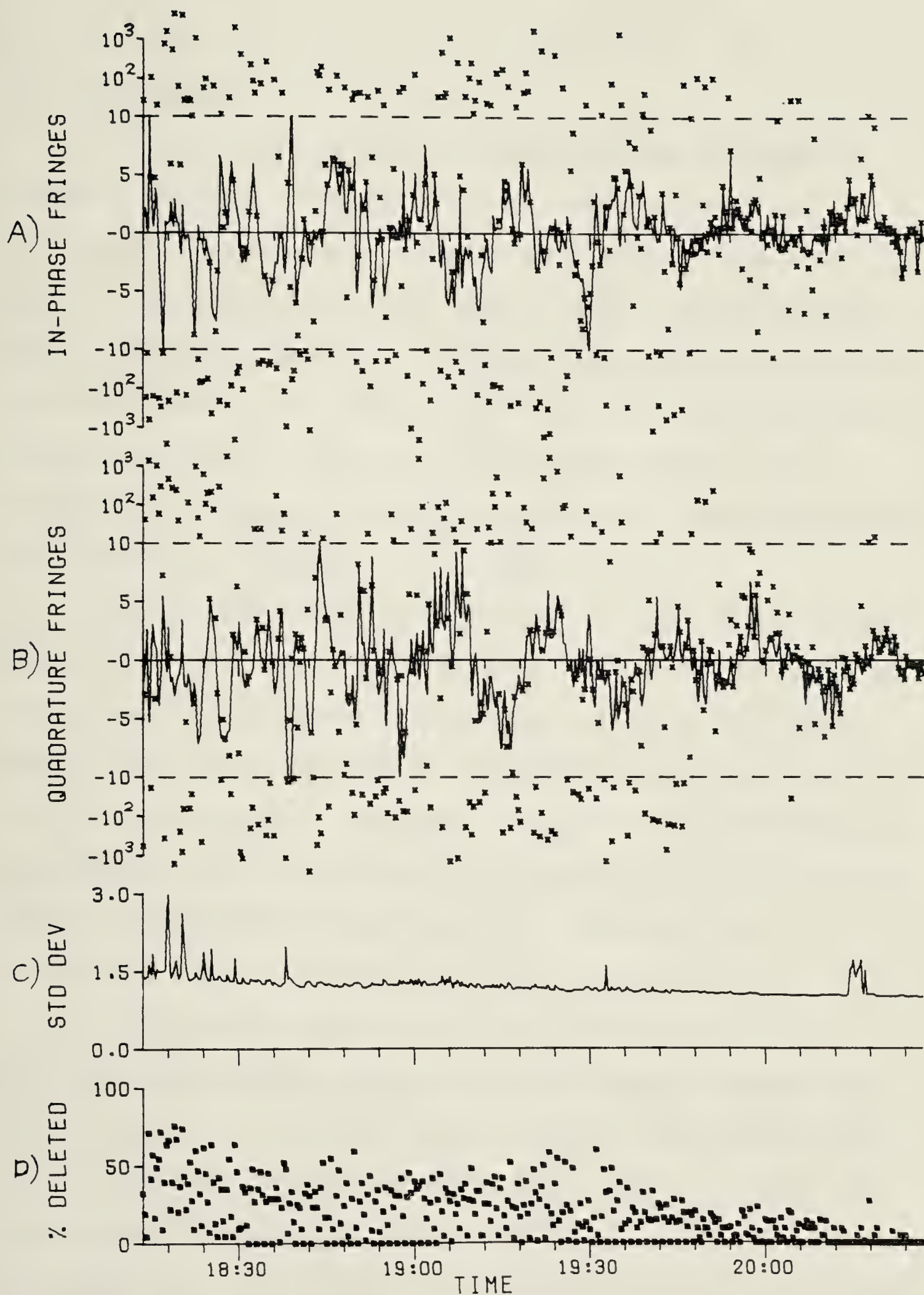


Figure 6.11. Fringes after Interference Removal

December 5, 1979

6.1.5.4 December 6

A final record of evening observations is shown in Figure 6.12. The received frequency was centered on 22.175 MHz. Considerable interference occurs from 18:06 until 19:15 with 10% to 30% (and in one instance 70%) of points being deleted. No clipping at the A/D converters was recorded during this record, but from 18:12 to 18:36 there is an increase in the levels of the auto spectra, as evidenced by trace C, which may be due to intermodulation or some form of broadband interference.

Fringes from Cassiopeia A (transit time 18:09) appear after 19:15. However, these fringes are badly distorted by scintillation. At a few points, such as at 19:12, large peaks occur. Examinations of the spectra for these points do not show any signs of the peaks being due to interference, hence they seem to be a result of severe scintillation and possibly momentary focussing of the radiation from Cassiopeia A on the antennas by the ionosphere.

An interesting observation for this record is the extreme rapidity with which the interference disappeared. In a space of 20 minutes interference goes from occupying 40% of the spectrum to zero percent. Also, on this night the interference remained at zero from this time until 5:30 the next morning. Scintillation continued until at least 21:00. The absence of interference during the night was unusual and was seen only twice (December 5-6 and December 6-7) during

fifteen nights of observing between November 19 and January 6.

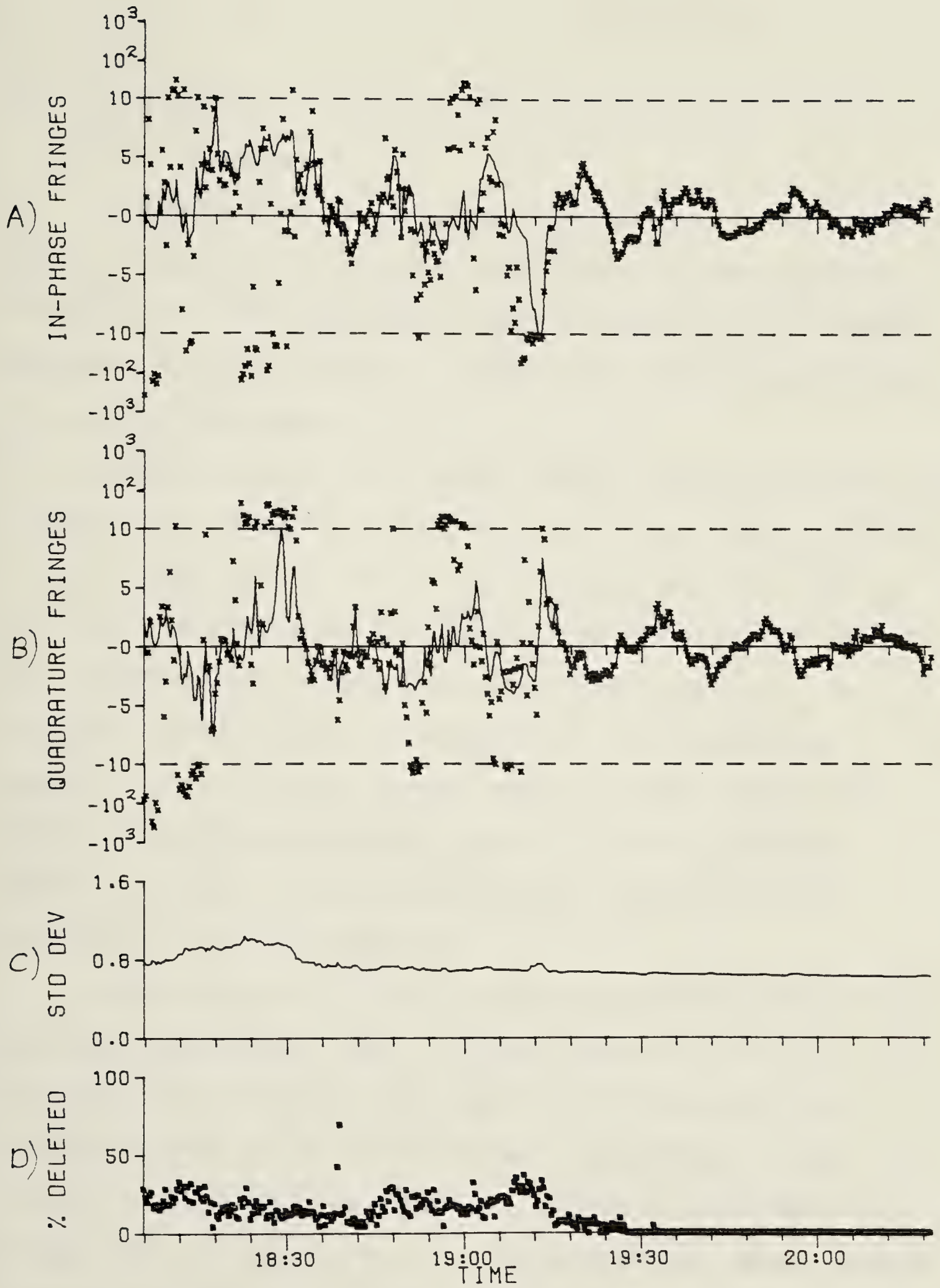


Figure 6.12. Fringes after Interference Removal

December 6, 1979

6.2 Scintillation

6.2.1 December 4

In Figure 6.13 the in-phase and quadrature fringes from part of Figure 6.10 are plotted in terms of amplitude and phase rather than real and imaginary components. The phase changes in a linear manner, as expected, but the amplitude fluctuates considerably.

Nearly identical amplitude fluctuations can be observed riding on top of both auto spectra as illustrated in Figure 6.14. Traces A and B are of the two auto spectra, showing only the variations on the tops of the spectra. In trace D the amplitude of the cross spectra from Figure 6.13 is redrawn. Trace C is most interesting, as it shows the geometric mean of the fluctuations in A and B. There is a striking similarity between C and D; in fact, they are almost identical. The same pattern of fluctuations is observed on the auto spectra.

The conclusion is that a single broadband source with a rapidly varying amplitude is being received by both antennas. The source is Cassiopeia A and the amplitude variations are due to scintillation. According to the presently accepted view of scintillation as described by Briggs [23], irregularities in the ionosphere impose random phase variations on an incoming wavefront. At the earth's surface, these phase variations are converted by constructive and destructive interference into a combination

of both phase and amplitude variations. Evidently, the 350 meter baseline used for the above observations is short enough that phase variations appear nearly simultaneously at both antennas, as do the amplitude variations in Figure 6.14. Therefore, the phase difference in Figure 6.13 changes in a fairly linear fashion.

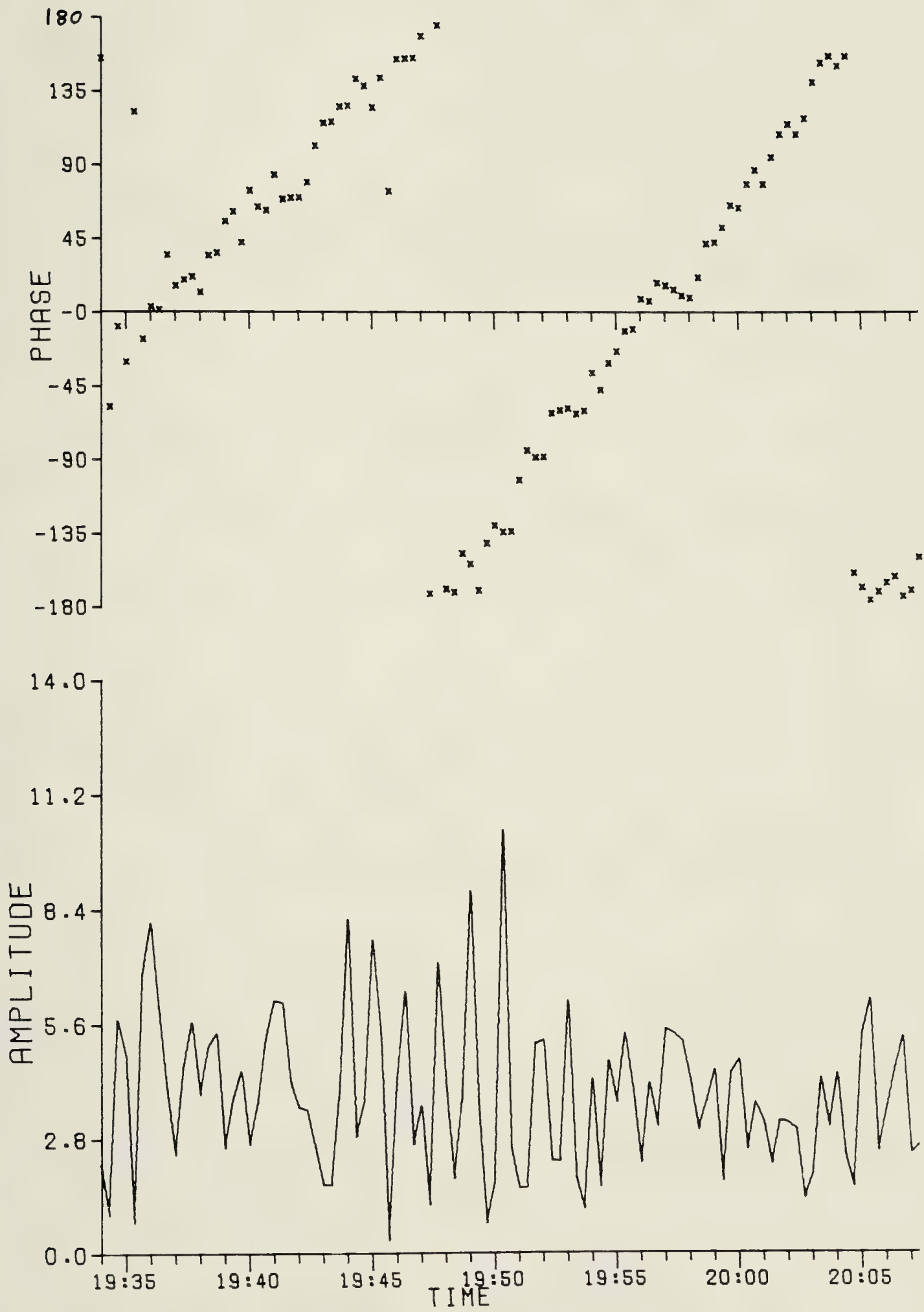


Figure 6.13. Fringe Phase and Amplitude
December 4, 1979

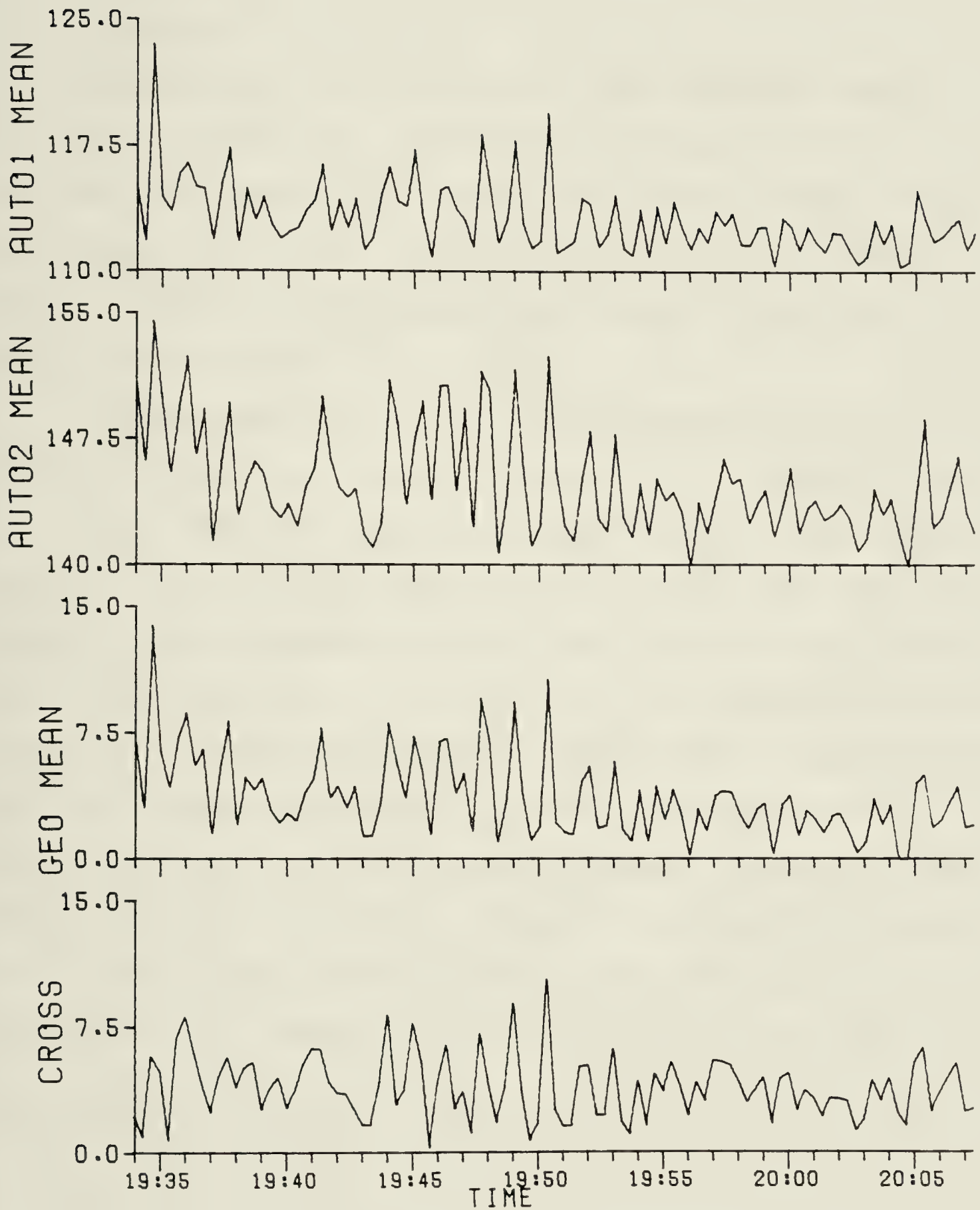


Figure 6.14. Auto Spectra, their Geometric Mean,
and Cross Spectrum Amplitude
December 4, 1979

6.2.2 December 6

Two more plots of fringe amplitude and phase appear in Figures 6.15 and 6.16. These plots correspond to two portions of Figure 6.12. In 6.15, both amplitude and phase variations are evident. This is also true in 6.16, where there is good correspondence between peaks in both the amplitude and phase fluctuations.

The auto spectra for 6.16 and the geometric mean of their variations are shown in Figure 6.17. As before, there is a close similarity among all four traces in this figure. However, on very close examination it may be seen that the peaks in trace B generally lead those in trace A by a very short time (approximately 20 seconds). The difference in the timing of the peaks is caused by ionospheric irregularities drifting between Cassiopeia A and the antennas with a velocity of at least $350\text{m}/20\text{sec}=17.5\text{m/sec}$ from west to east. The drifting of ionospheric irregularities has been observed in a similar manner since studies of the structure of the ionosphere first began (e.g. Booker [105], Briggs [23]).

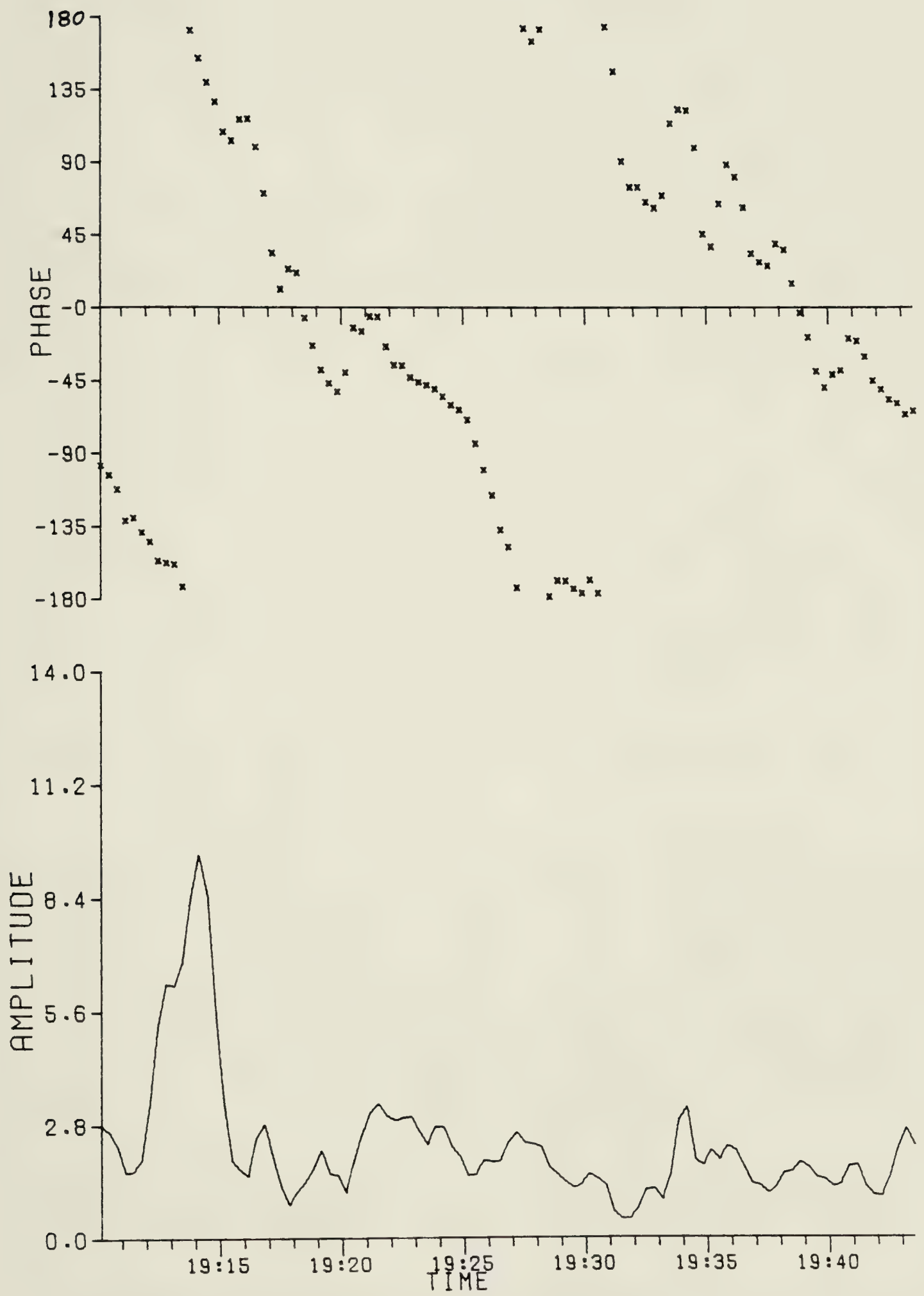


Figure 6.15. Fringe Phase and Amplitude
December 6, 1979

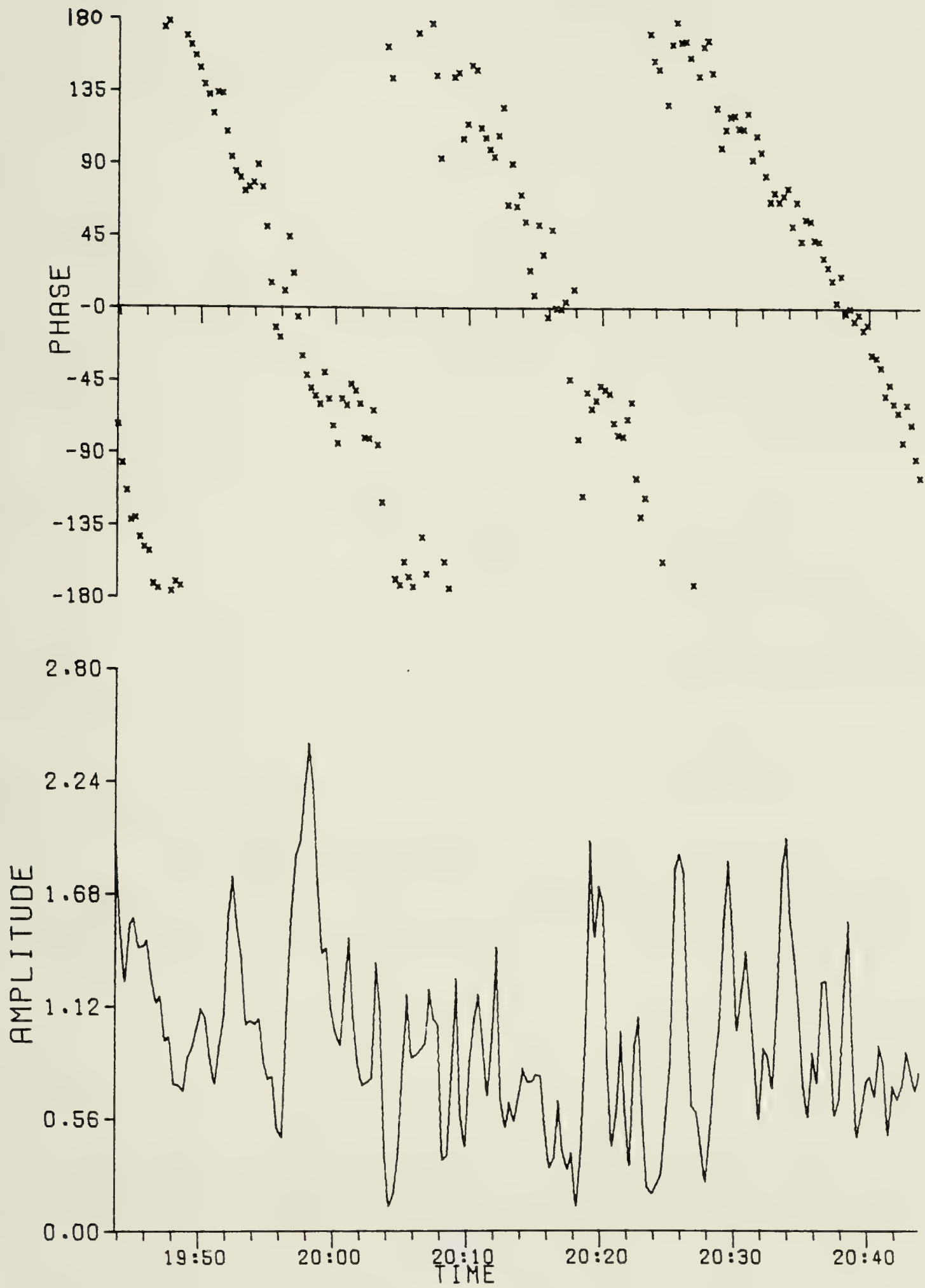


Figure 6.16. Fringe Phase and Amplitude
December 6, 1979

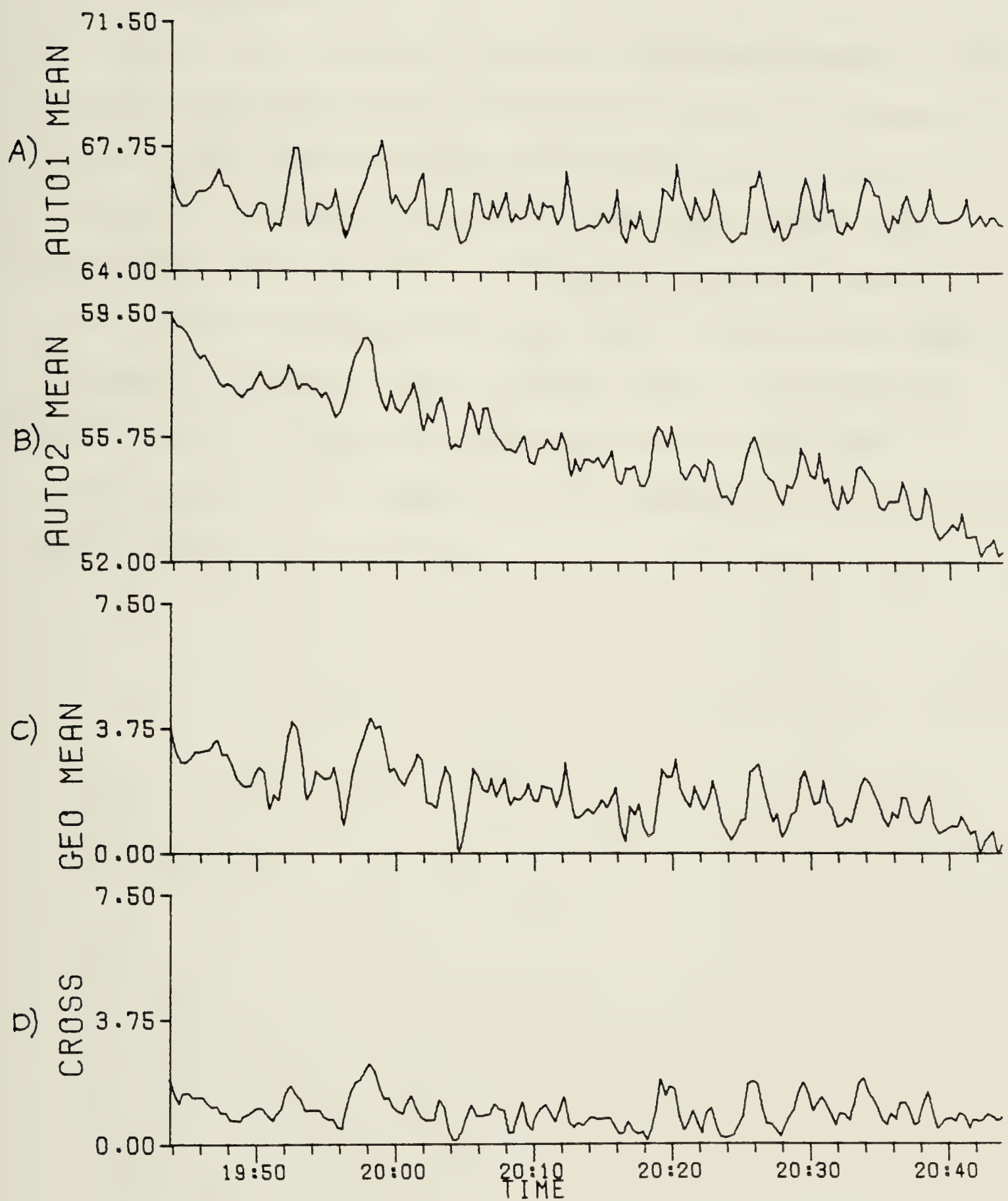


Figure 6.17. Auto Spectra, their Geometric Mean,
and Cross Spectrum Amplitude
December 6, 1979

6.2.3 November 28

A fourth record of fringe amplitude and phase, in this case corresponding to the fringes in Figure 6.3, appears in Figure 6.18. These fringes are from the lower transit of Cassiopeia A during the morning. Once again there are amplitude variations while the phase is quite linear. Scintillation is therefore occurring in the morning when ionospheric electron density should be at a minimum. As Cassiopeia A is just above the horizon at this time scintillation is increased by the long path the signals must take through the ionosphere.

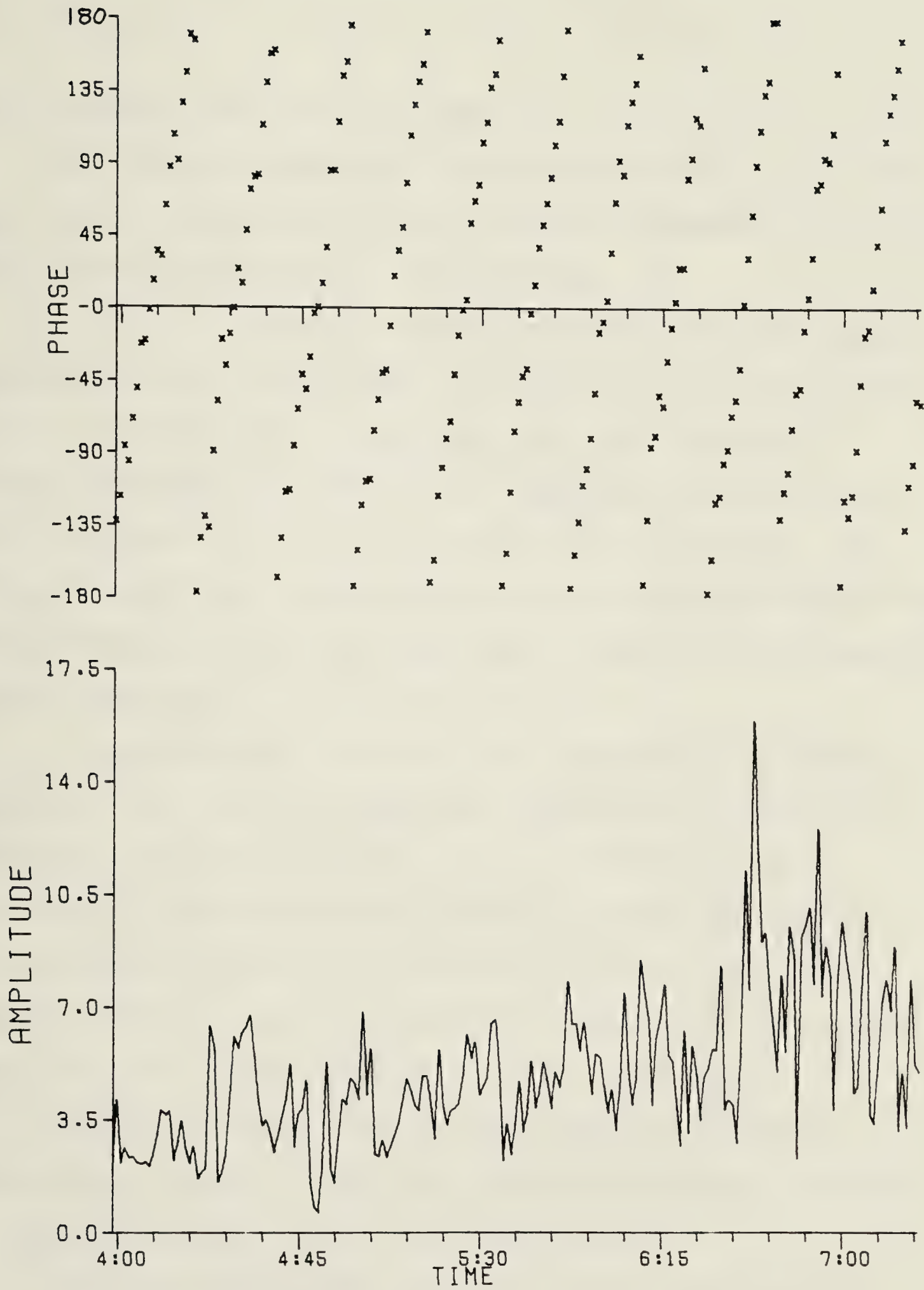


Figure 6.18. Fringe Phase and Amplitude

November 29, 1979

6.3 Estimation for the Auto Spectra

Two examples demonstrating the performance of the first decile as an estimator for the location parameter of an auto spectrum are presented in this section.

Figure 6.19 shows estimates for one of the auto spectra associated with the fringes in Figure 6.10. In trace A, the solid line represents an estimate derived from a $\pm 3\sigma$ rejection procedure. The x 's are uncorrected estimates of the first decile (i.e. the eleventh order statistic, $P_{(11)}$). Trace B gives the standard deviation of the points remaining after iterative $\pm 3\sigma$ rejection, and C gives the percentage of points deleted.

A comparison of the solid line and the x 's in trace A indicates that the first decile is consistently below the rejection estimate by about 2.0, or $2.0/100=2\%$. The integration time during this record is 20 seconds, which corresponds to $K=8137$. The correction factor required in equation 4.63 is then $(1+1.3/\sqrt{8137})=1.014$. After correction, the first decile estimates of θ_F will therefore be $(1-0.02)(1.014)=0.994$ times the 3σ rejection estimates, producing a bias of -0.6% . The slight discrepancy is due to a small amount of ripple in the auto spectrum.

The expected standard deviation of the auto spectrum from equation 4.58 is $100/\sqrt{8137}=1.11$. From trace B, the standard deviation after deletions is actually about 1.5, as would result if a ripple of something less than 1% were

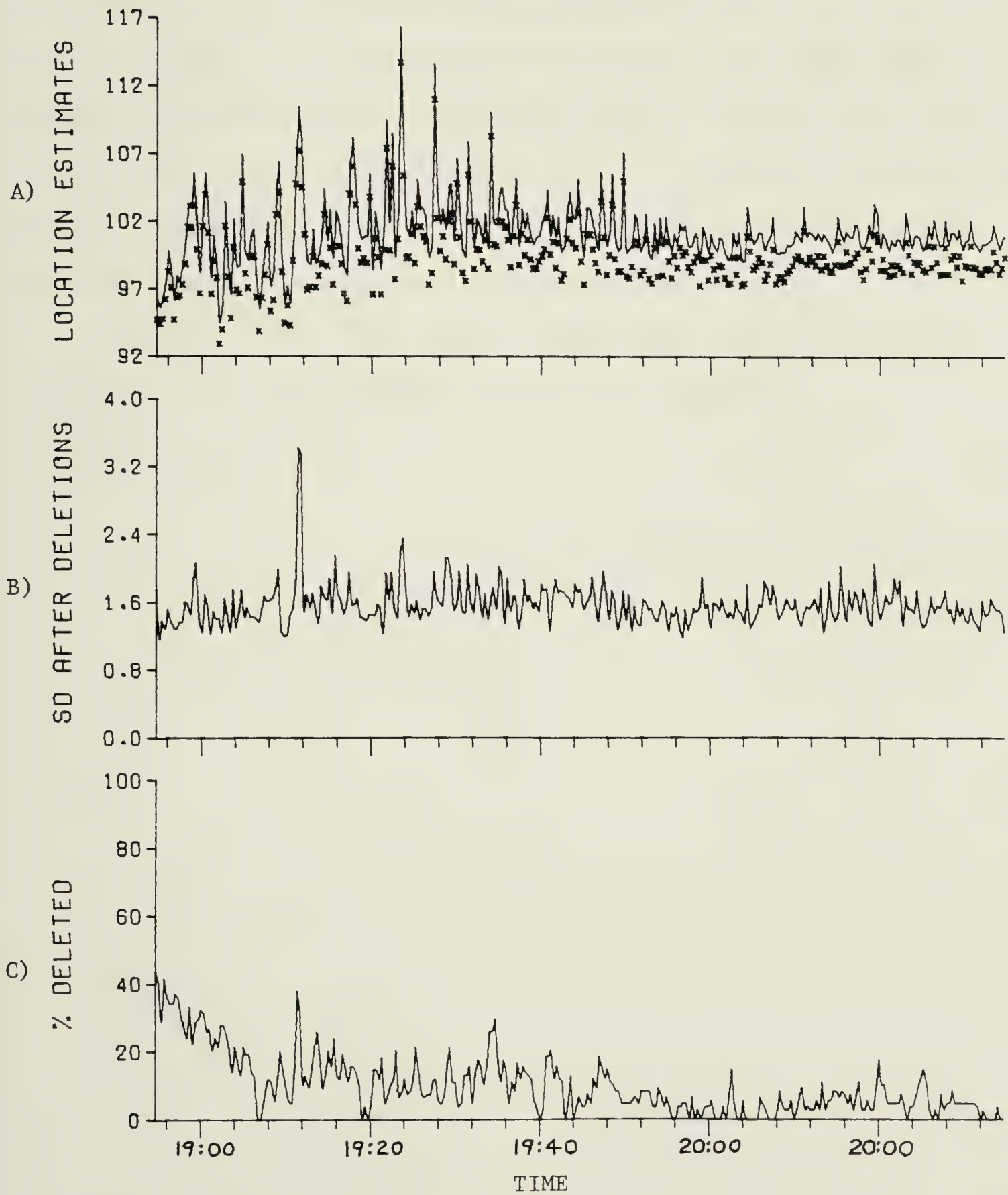


Figure 6.19. Auto Spectrum Estimates
December 6, 1979

present in the auto spectrum. The fluctuations in the level of the auto spectrum are due to scintillation of Cassiopeia A, as shown in Figure 6.13.

A second example of auto spectrum estimation is given in Figure 6.20, corresponding to the fringes in 6.4. In this example, the first decile estimates are less than the rejection estimates by about 10.0, or $10.0/830=1.2\%$. The correction factor with $K=24411$ is $(1+1.3/\sqrt{24411})=1.0083$. The final estimate is then $(1-0.012)(1.0083)=0.996$ times the correct value, resulting in an error of -0.4% .

Overall, the first decile performs very well as an estimator for the centers of the auto spectra.

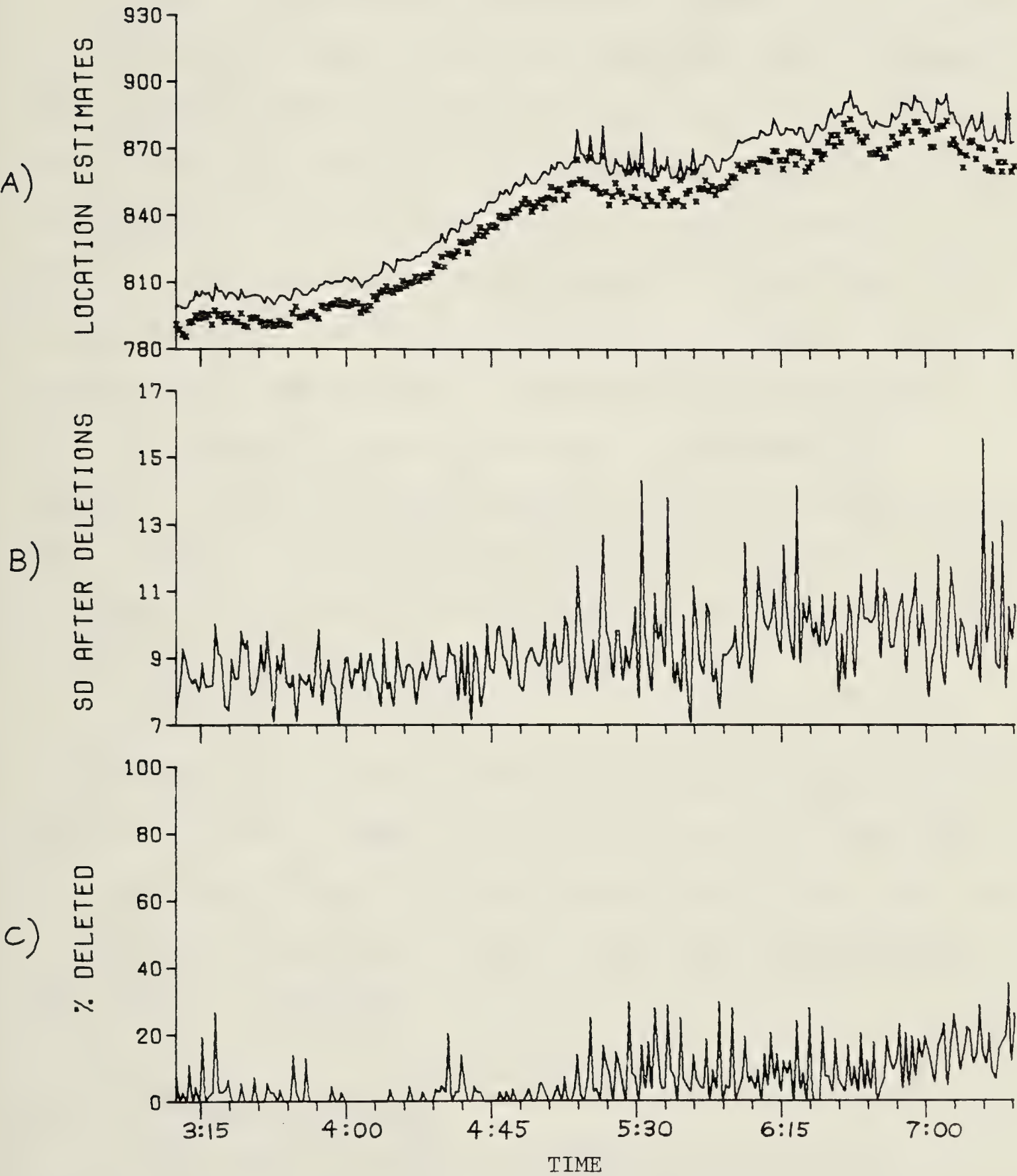


Figure 6.20. Auto Spectrum Estimates
January 4, 1980

6.4 An Attempt at Daytime Observation

From an interference standpoint, daytime in the winter of a sunspot maximum is the worst possible time to attempt low frequency astronomy. Indeed, the levels of interference were found to be very high in the daytime. Intermodulation distortion in the receivers initially made daytime observations impossible. Modifications to the RF and first mixer stages of the receivers detailed in Chapter 3 were undertaken to improve their intermodulation performance.

An attempt at daytime observation was made on January 6, 1980. The major objective of this attempt was to test a scheme of automatically changing the receiver center frequency if excessive interference was encountered in order to look for a quieter part of the spectrum.

A fortunate circumstance was the absence of sweeping interference on the day of the test, probably because the day was a Sunday. Sweeping interference was not detectable on a spectrum analyzer at any time during the day, as it had invariably been during the days of previous observations which were all weekdays.

6.4.1 Frequency Changing

A very simple method of frequency changing was employed. The spectrum between 22.15 and 22.35 MHz was divided into four 50 kHz slots, any of which could be selected for observing. Changes were always made in order,

starting from the highest slot, 22.325 MHz, through 22.275, 22.225 and 22.175 MHz and then back to 22.325 MHz.

The center frequency was changed on either of two conditions; 1) an excessive amount of clipping occurred at the A/D converters due to very large interference; 2) more than 40% of spectral components were deleted due to a large number of small interferers. The above scheme was easy to implement and seemed adequate to test the merits of having a frequency-changing capability.

6.4.2 Daytime Results

The results of the daytime test were mixed. Interference levels were high enough that, even with the improved receivers, serious intermodulation was at times noticeable on the spectrum analyzer. In addition, interference of a broadband nature (100 kHz or more) was sometimes seen. However, there were also times when two of the 50 kHz slots, centered on 22.175 and 22.225 MHz, were virtually free of interference.

Some fringes from Cygnus A (transit time 12:56) were seen between 10:00 and 14:00, but these were interspersed with periods of severe interference which the system could not remove completely. The fringes were extremely irregular in both amplitude and phase. A portion of the daytime observations can be seen in Figure 6.21.

The ability to change frequencies was of very limited value. The two higher slots, 22.275 and 22.325 MHz,

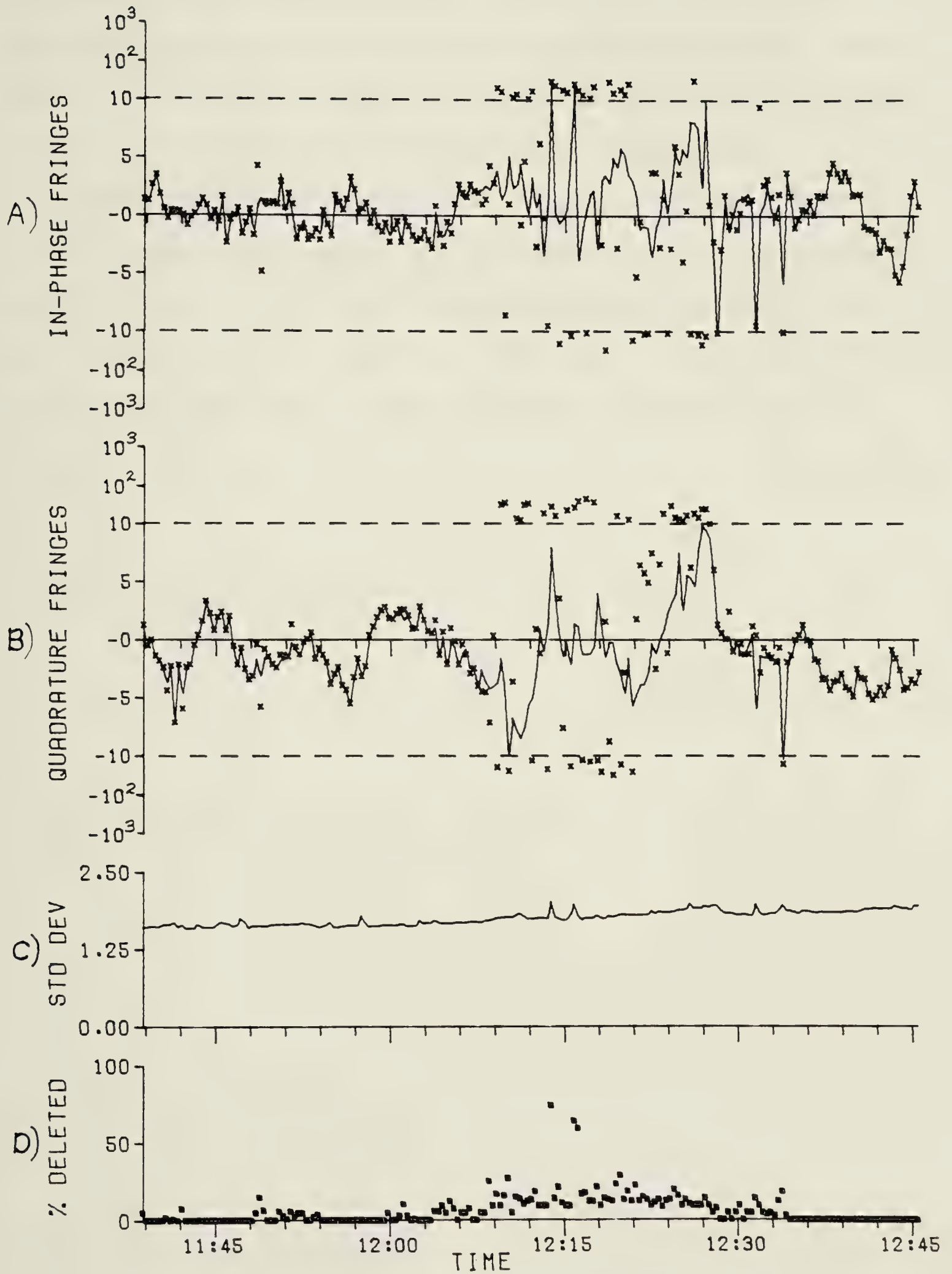


Figure 6.21. Fringes after Interference Removal
January 6, 1980

contained strong interference at all times. The system therefore spent more than 99% of its time in the two lower slots. The system changed between these two frequencies only three times during an eight hour observing period.

Frequency changing would be of the greatest advantage if there were many regions of the spectrum from which one could choose, with an equal and independent probability of interference at any frequency. Such was not the case during the daytime test above, hence frequency changing was of little benefit.

6.5 A Probability Distribution for Interference

A very important point in predicting the success of interference excising is some knowledge of how interference tends to be distributed in amplitude. In particular it is desirable to know to what degree very small and undetectable interference can be expected to be present.

An analysis of the records of the observations made at the Dominion Radio Astrophysical Observatory was conducted to determine whether or not the distribution of interference followed a pattern. The analysis consisted of producing histograms of the magnitude of deviations of cross spectral components from the centers of the spectra. The fringes found by robust estimation were subtracted from the co and quadrature spectra to center the spectra about zero, and then the rms deviation ($\sqrt{\text{co}^2 + \text{quadrature}^2}$) of each component of the spectrum was found. The rms deviations of many hours of observing were tabulated to form each histogram.

Because interference varied over a range of about 60 dB, it was impractical to perform tabulation in a linear manner. Instead, a tabulation with equal sized intervals was performed on the logarithms of the rms deviations. In effect, the size of the intervals or bins into which spectral components were collected then increased in proportion to the amplitude of the components. The number of counts in each bin was then divided by the size of the bin to restore linearity.

A histogram of results from part of the night of December 6-7 when almost no interference was received appears in Figure 6.22. The dashed line represents a Rayleigh distribution, which is the expected distribution with no interference. Only 0.031% of the 38,700 points tabulated in this histogram were found to deviate significantly from the Rayleigh distribution.

A second histogram, this time with considerable interference, is shown in Figure 6.23. This histogram corresponds to the first two-thirds of the record in Figure 6.10. There is now interference extending for over four decades past the end of the Rayleigh distribution. The most important feature is the nearly linear manner in which the histogram decreases over the four decades of interference. A power-law relationship between the probability of interference and its magnitude is suggested.

Five additional histograms containing interference are presented. Figure 6.24 shows a period of considerable interference from the evening of January 4, while 6.25 is a period of very small interference later the same night. Figure 6.26 is from the daytime observations of January 6. Figures 6.27 and 6.28 are from the evening observations of December 5, but for different center frequencies (22.175 and 22.325 MHz, respectively). For 6.28, spectra from periods of excessive clipping have been excluded to prevent distortion products from contaminating the histogram.

In each case above, the probability of interference is

functionally related to amplitude by a power law. The slopes of the linear portions of the histograms vary from -1.23 to -1.33, with the average being -1.3. It therefore appears that the probability density function for interference has the form

$$f(p) = \alpha p^{-1.3} \quad (6.2)$$

over the range of amplitudes shown in the histograms, where p is the interference power and α is a constant of proportionality which varies with the degree of interference being received. The above power law does not hold true beyond a normalized count of about 10^{-4} in most of the histograms, perhaps due to there being too few points to count accurately and also due to limits on the system's dynamic range. Also, the power law cannot hold as p approaches zero, as $f(p)$ would go to infinity.

Unfortunately, the behavior of $f(p)$ as p becomes small is masked by the Rayleigh distribution of fluctuation noise. Because fluctuation noise is contained in all spectral components, the combined distribution is actually a convolution of the Rayleigh distribution and the interference distribution. The interference distribution alone, without fluctuation noise, includes a delta function at its center which represents components with zero interference. The very regular nature of the interference distribution for a number of decades beyond the Rayleigh distribution suggests that the power law may hold for

interference at lower levels as well. It is only contaminated points near the junction of the interference distribution and the Rayleigh distribution which are important, because smaller interference will not affect location estimates significantly and larger interference is rejected by the robust estimation procedure. The power law should perform reasonably well for predicting average numbers of interferers near the junction point.

It must be emphasized that the power law found above is derived from the long term behavior of interference (over a few hours, at least) and as such is only a statistical average. Over the short term, interference is less predictable and the power law loses much of its significance. Also, the proportionality factor α in equation 6.2 is not a constant, but will exhibit its own statistical distribution reflecting ionospheric activity. A determination of the dependence of α on such factors as the time of day, the season and the solar cycle would require a long term program of observations and data collection.

A relative idea of the range of α encountered during the observations can be found by measuring the distance between the peak of the Rayleigh distribution and the junction point of the Rayleigh and linear sections of the curves in the histograms. The junction point varies from a factor of $10^{1.0}$ below the peak in Figure 6.24 to $10^{2.8}$ below in Figure 6.25, implying a change in α by a factor of $10^{1.8}=63$ between these records. Over this range of α the

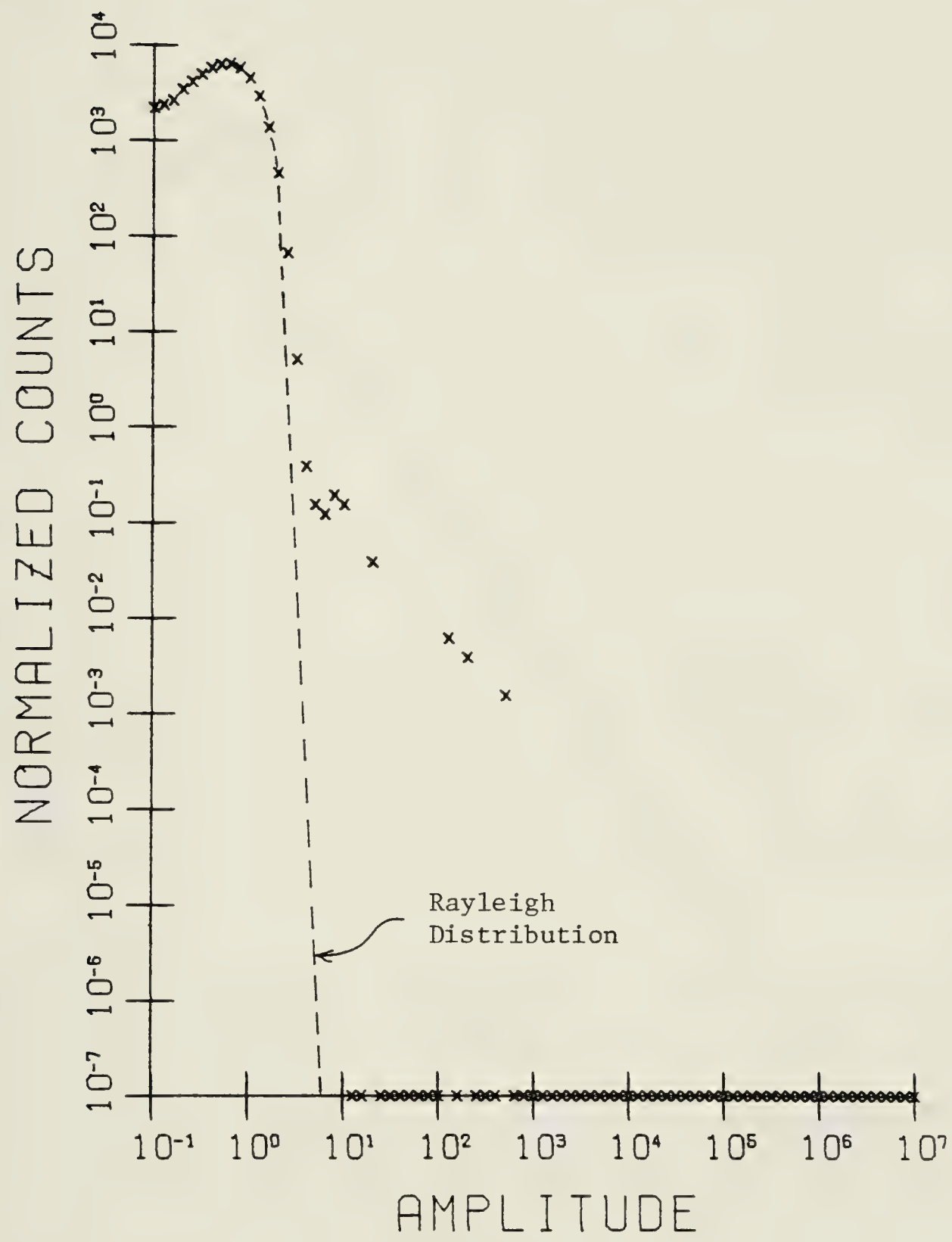


Figure 6.22. Histogram of Cross Spectrum
Probability vs. Amplitude
December 6-7, 1979

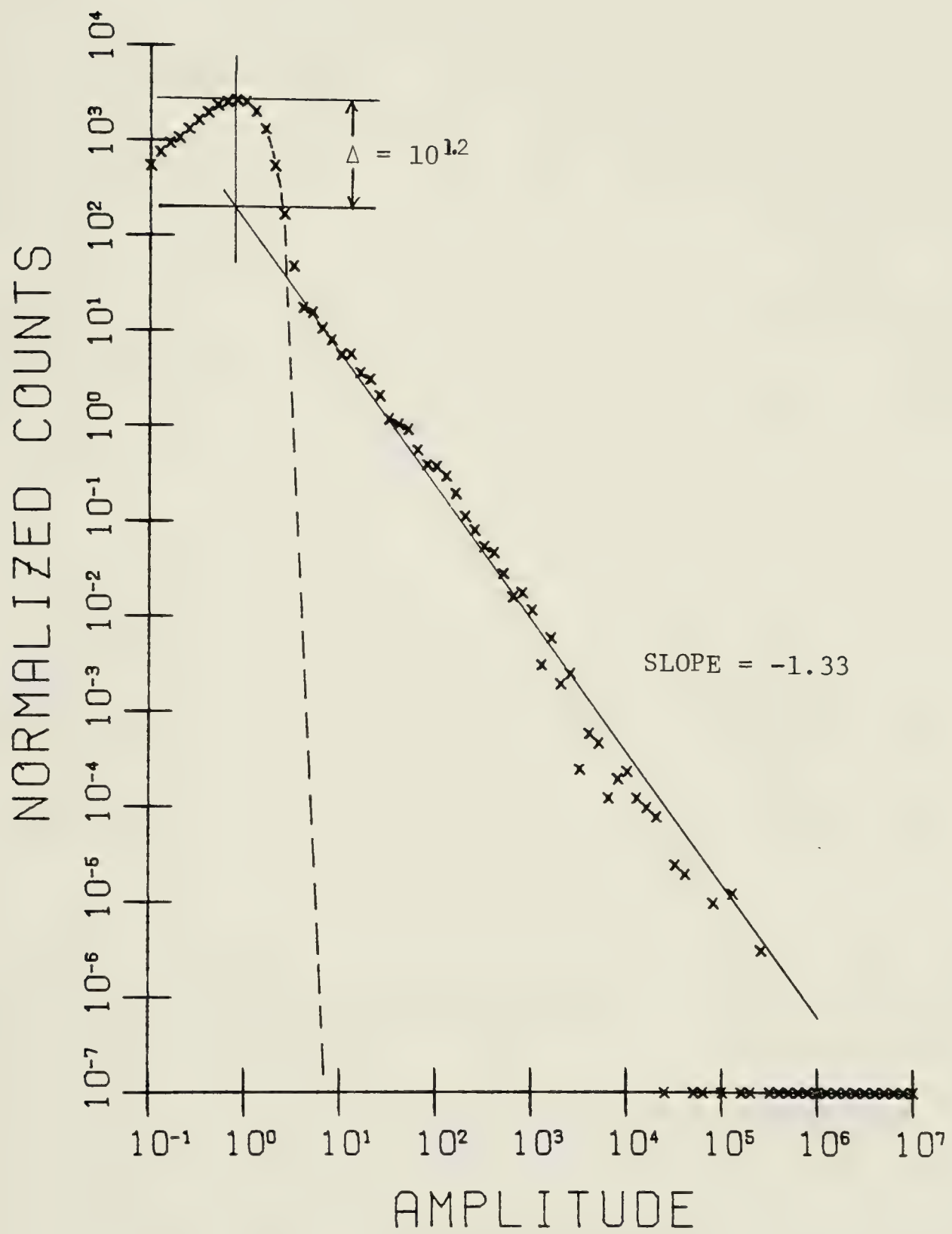


Figure 6.23. Histogram of Cross Spectrum
Probability vs. Amplitude
December 4, 1979

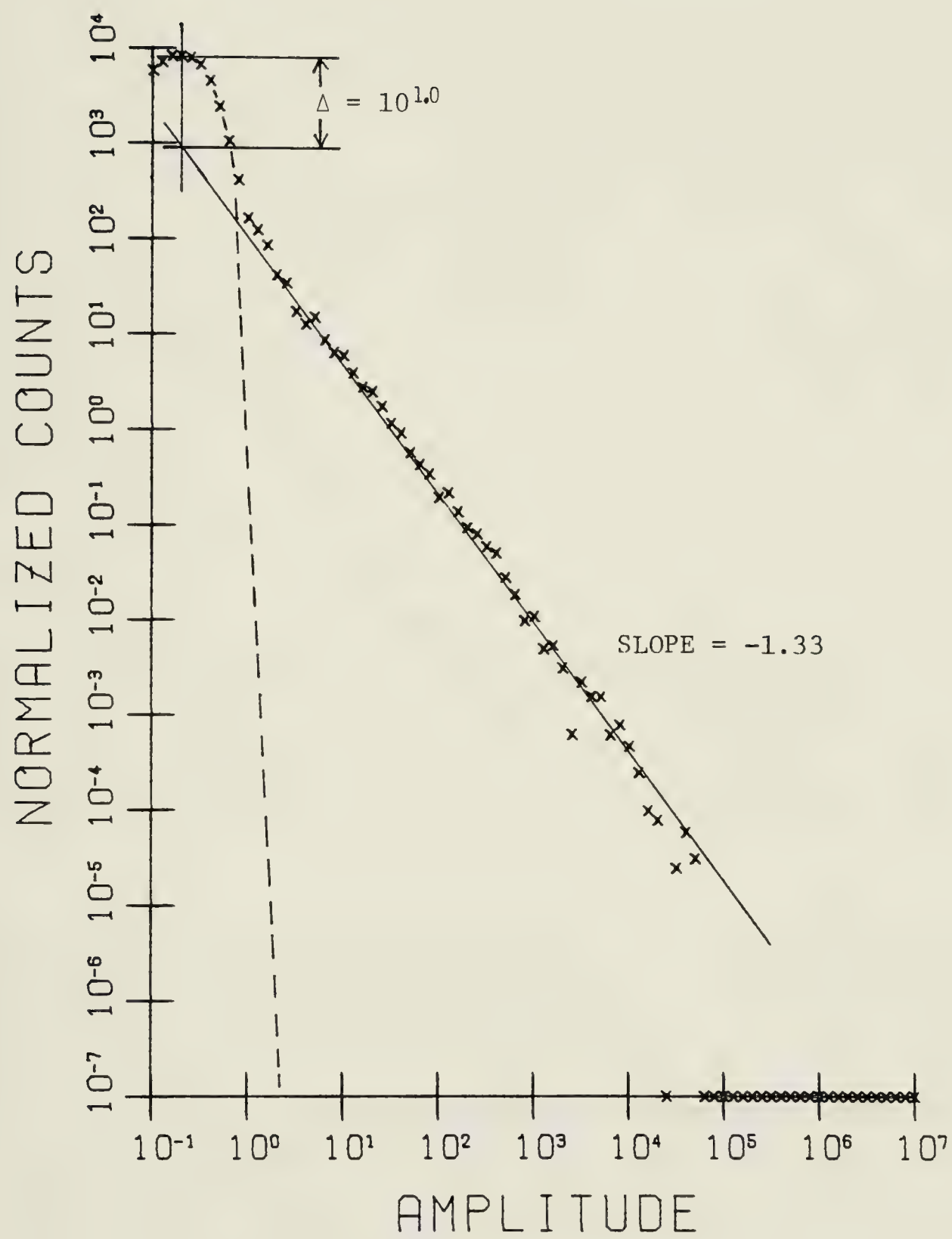


Figure 6.24. Histogram of Cross Spectrum
Probability vs. Amplitude
January 4, 1980
18:30 to 19:30

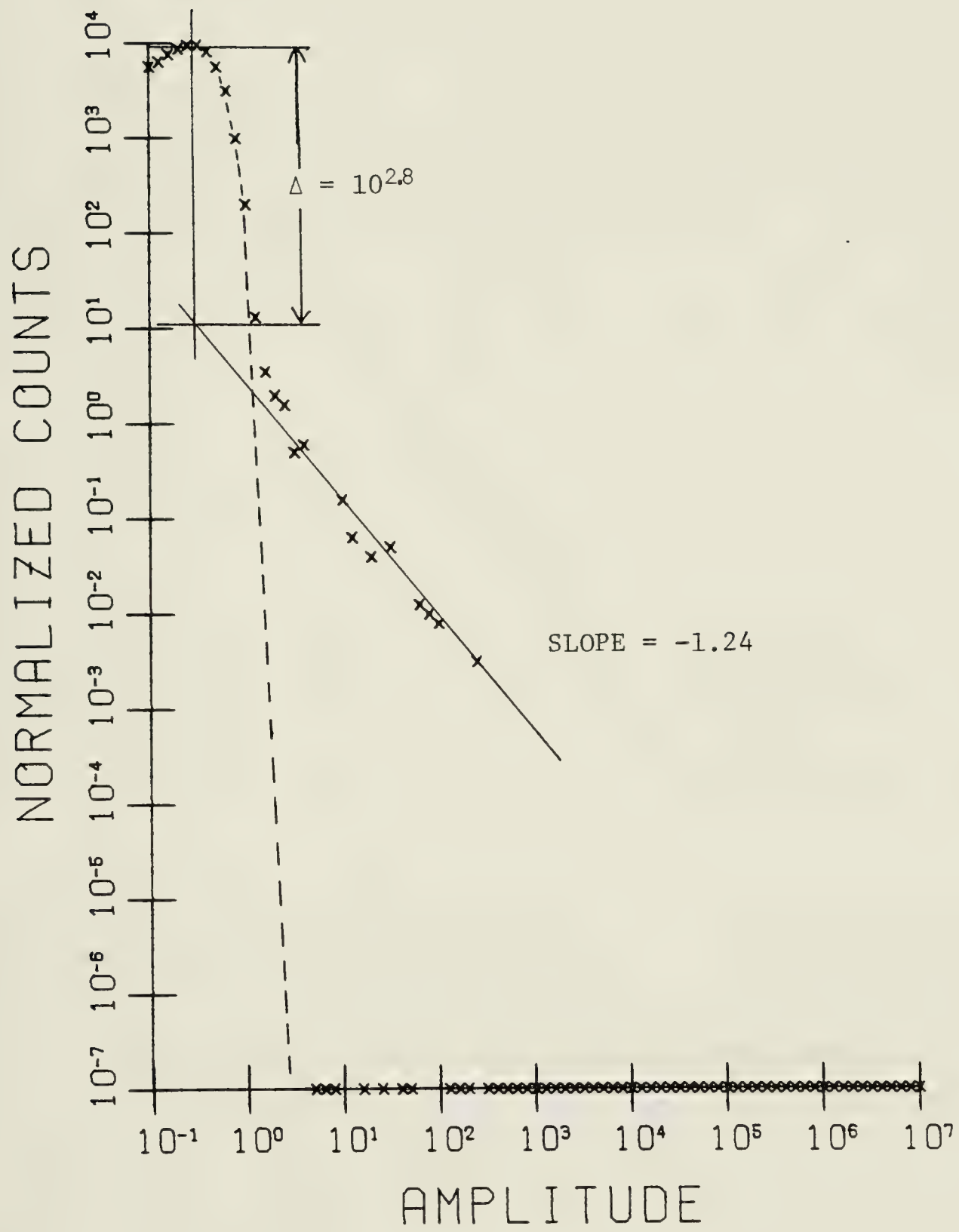


Figure 6.25. Histogram of Cross Spectrum
Probability vs. Amplitude
January 4, 1980
20:00 to 21:00

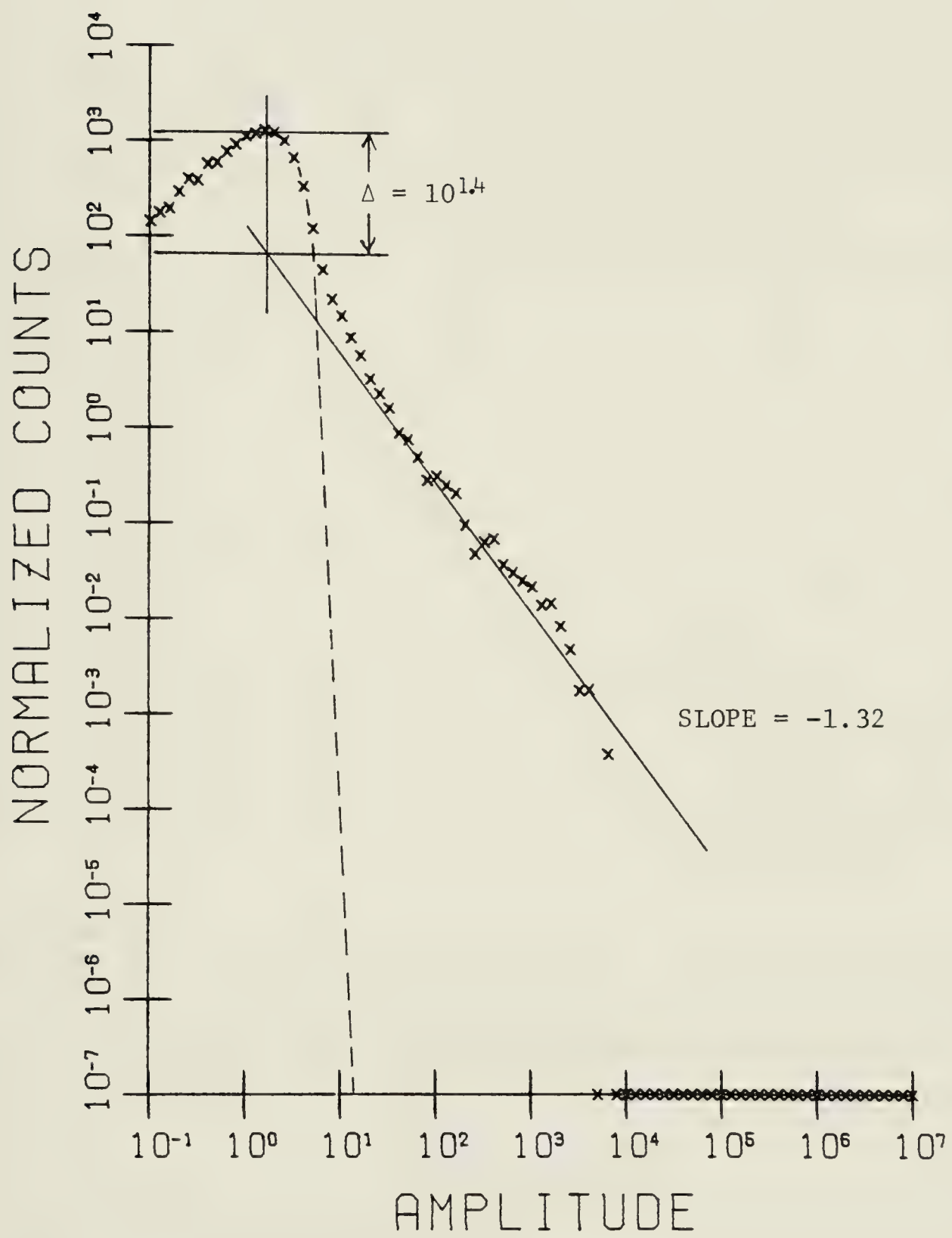


Figure 6.26. Histogram of Cross Spectrum
Probability vs. Amplitude
January 6, 1980

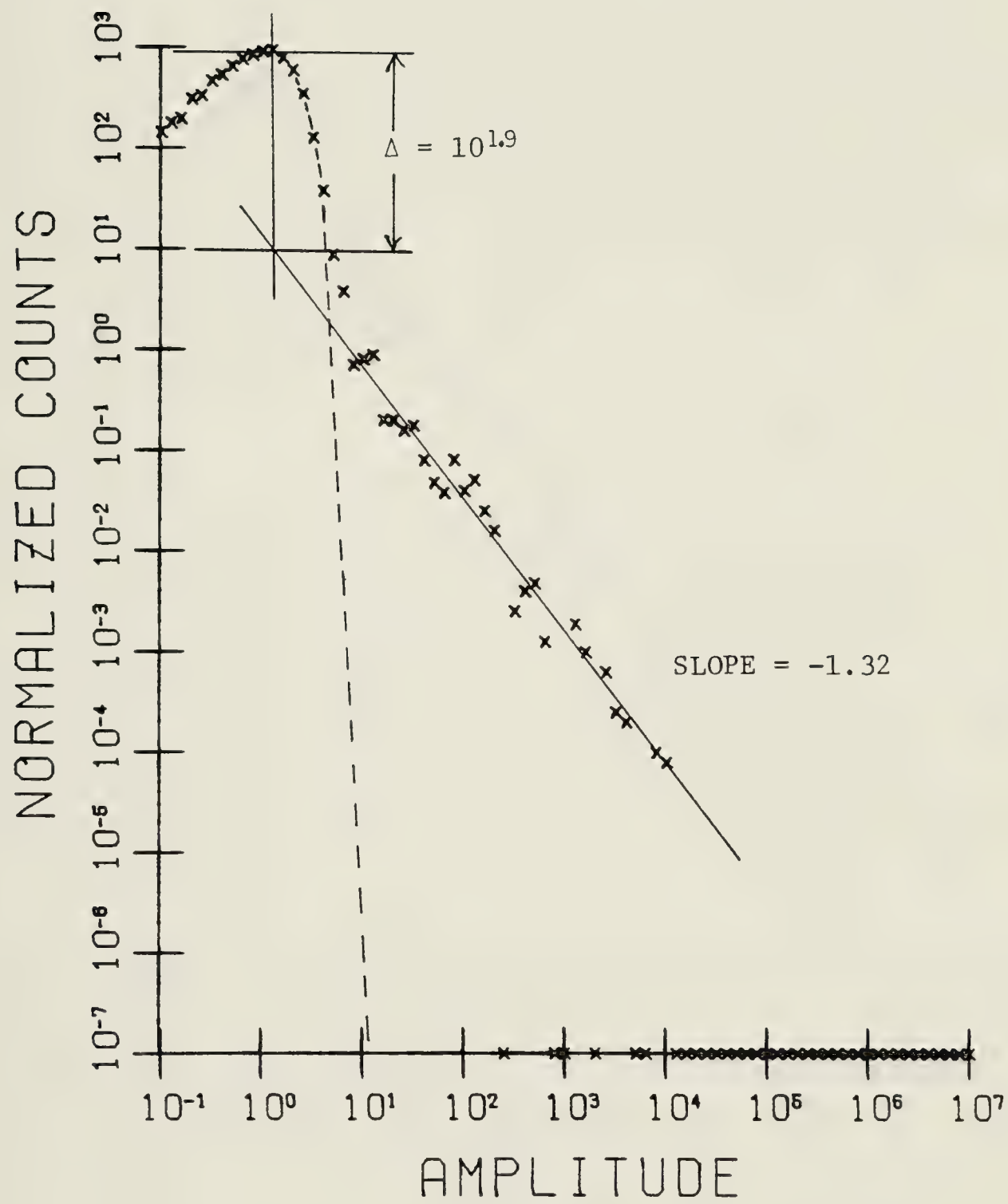


Figure 6.27. Histogram of Cross Spectrum
 Probability vs. Amplitude
 December 5, 1979
 Frequency = 22.175 MHz

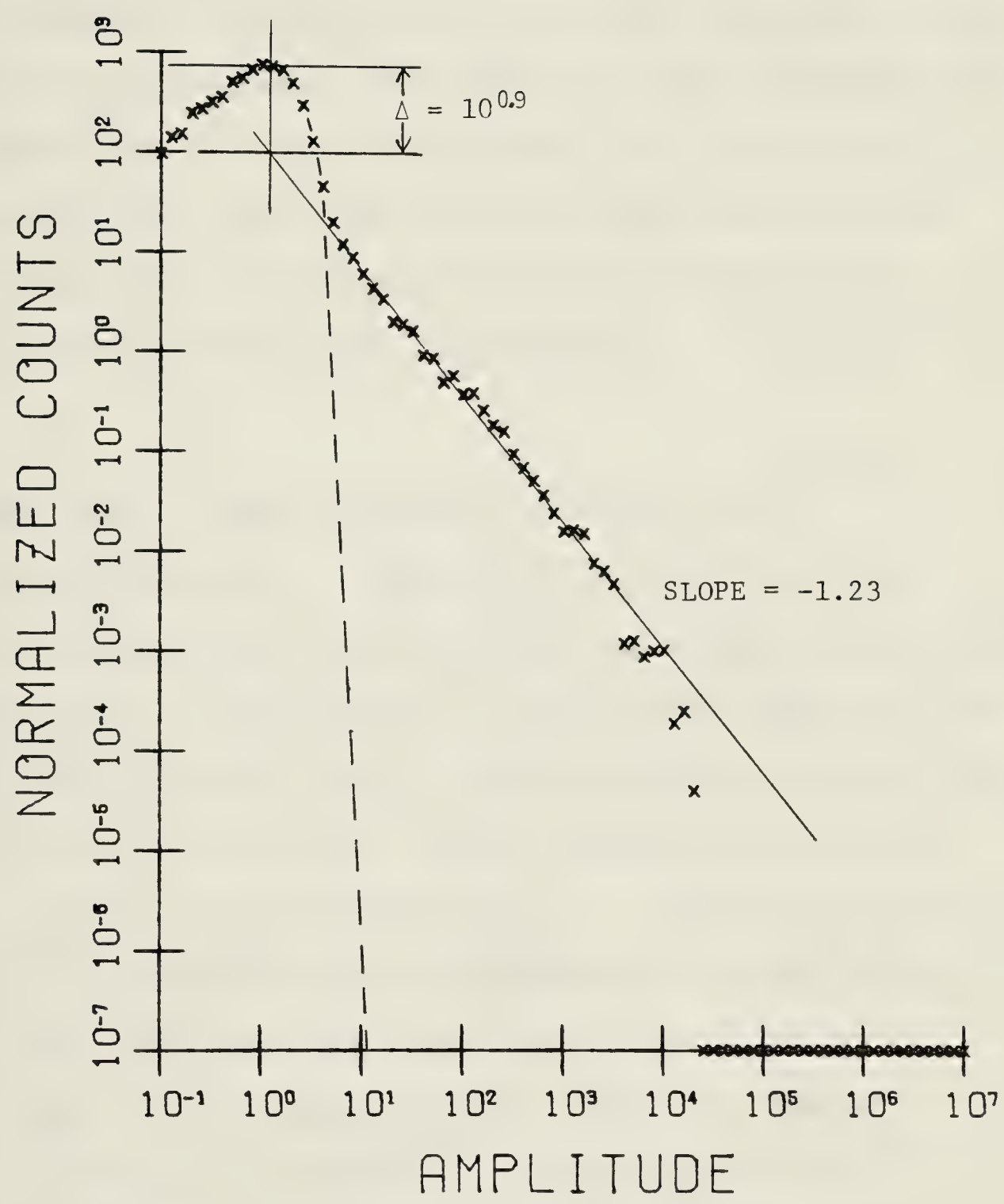


Figure 6.28. Histogram of Cross Spectrum
Probability vs. Amplitude
December 5, 1979
Frequency = 22.325 MHz

power law $f(p) = \alpha p^{-1.3}$ remains unchanged.

It must be noted that the value of α , or alternatively the incidence of interference, is strongly dependent upon the observing frequency. This fact is clearly demonstrated by a comparison of Figures 6.27 and 6.28, which were tabulated at the same times but at frequencies 150 kHz apart. The values of α are different by a factor of approximately 10 for these two figures.

6.6 Comparison to the Log-Normal Distribution

A previous study by Wheeler [31] found that the statistical distribution of interfering signal powers could be approximately described by a log-normal function. The interference distributions in the preceding section also fit portions of log-normal curves reasonably well. The author stresses that the fitting of his own observations or others to a curve such as a log-normal or power law is purely empirical and should not be extrapolated or generalized to any degree without further evidence.

The fitting of interference distributions to a log-normal function has one serious drawback, namely a somewhat arbitrary choice of function parameters. To illustrate this difficulty, two log-normal curves with different parameters are shown in Figure 6.29. The expression for a log-normal density function is given in equation 1.7. Over a range of p from 10^{-2} to 10^8 (ten decades) the two curves in Figure 6.29 are nearly identical,

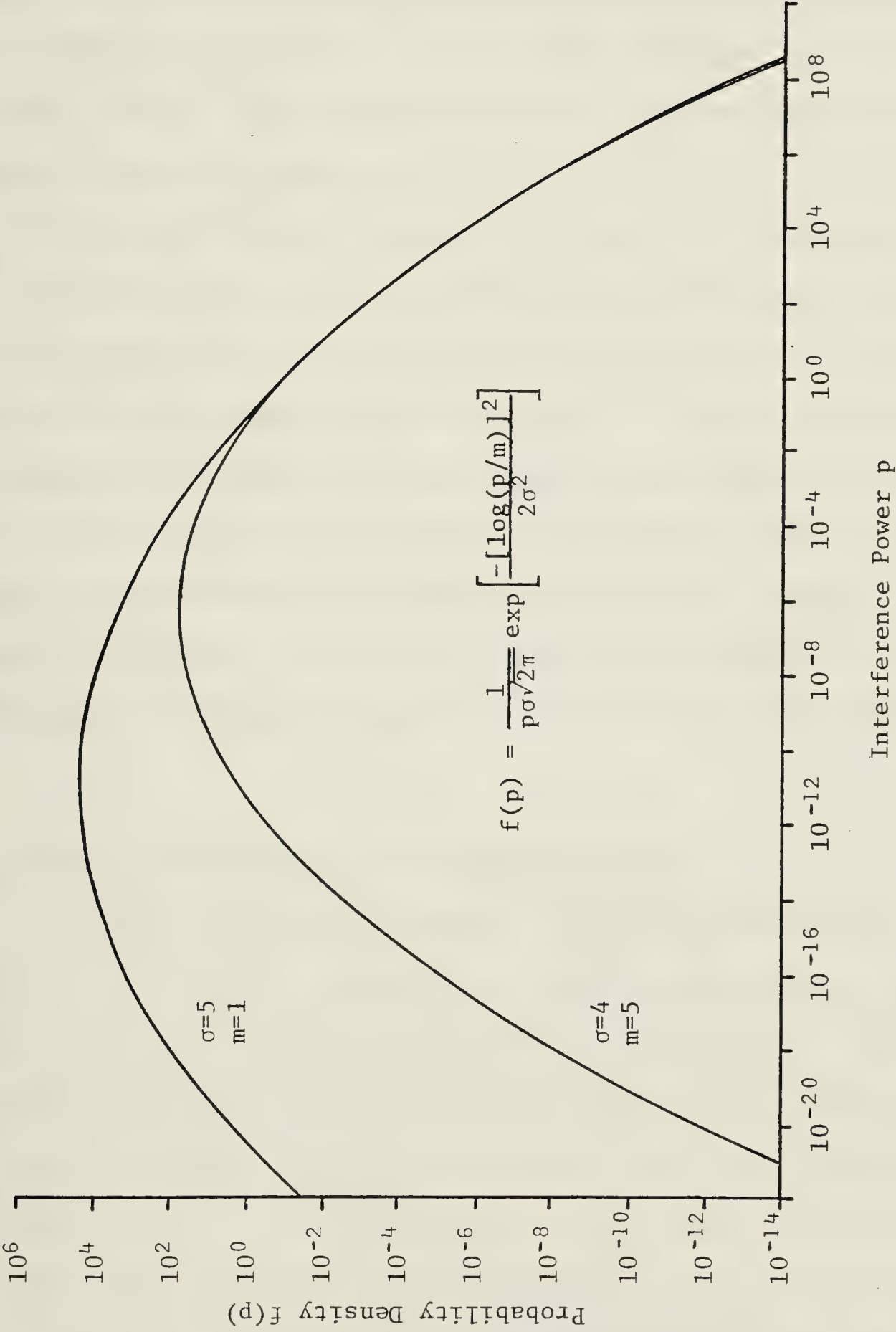


Figure 6.29. Log-Normal Curves

with a slope (on the log-log plot) ranging from -1.0 to -2.0. A portion of either curve over a selected four decade range within this region would undoubtedly fit the observed data, which has a fairly linear slope of about -1.3.

However, there are no unique choices of parameters m and σ which produce the desired fit.

Note that the two curves in Figure 6.29 diverge sharply as p becomes small. Measurements of interference levels down to extremely low values of p would be necessary to determine whether any particular distribution is truly representative. The author believes that the equipment designed for this interference excising project may be the most sensitive ever used for measurements of interfering signal levels.

Wheeler's method, for example, was not as sensitive because averaging to reduce background noise was not possible.

6.7 General Comments on the Observations

A number of general comments on the observations may be made. First of all, terrestrial interference during the observations was extremely common. In addition to mornings and evenings, a great deal of interference was received during the nights. The incidence of nighttime interference changed during the observing period. Between November 20 and November 30, low-level interference was virtually continuous each night. On December 5 and 6, the nights were free from interference. The remainder of the records showed intervals of low-level interference at night lasting from a few

minutes to many hours.

The part of the spectrum chosen by the Dominion Radio Astrophysical Observatory for their 22.25 MHz telescope is extremely good from an interference standpoint. A view of daytime radio transmissions on a spectrum analyzer showed signals to be less common and generally lower in amplitude by as much as 30 dB or more near 22.25 MHz than in neighboring parts of the spectrum. Even within this region of low interference, some frequencies were better than others. As indicated by the results in this chapter, there is a marked difference in the incidence of interference across the 200 kHz band from 22.15 to 22.35 MHz. There was consistently less interference in the lower half of this band, and the 50 kHz region from 22.15 to 22.20 MHz generally had the least of all.

Scintillation was continually present during the observations. As both the incidence of terrestrial interference and scintillation are strongly correlated with solar activity, the amounts of both experienced during the field testing were not unexpected.

Overall, the interference excising system performed very well as long as interference levels were not too large. Generally this was the case for periods of from 60 to 90 minutes in both the mornings and evenings when interference was increasing or decreasing. In addition numerous occasions of low-level interference were encountered during the night. Interference was removed successfully on these occasions.

7. Conclusions

What are the conclusions to be reached following this project? First of all, interference detection and removal through spectral analysis and robust estimation has a great deal of promise for enhancing the quality of low frequency observations and for extending the amount of time during which observations may be conducted. Second, the very important aspect of the distribution of interference amplitudes requires more investigation before a definitive answer as to how much improvement is possible can be given. This chapter begins by outlining the performance of the present system and noting additions or changes which could be made. The question of the distribution of interference is then examined, and recommendations for further research are made.

7.1 System Performance

A number of comments about the receivers, the FFT processor and the robust estimation method may be made.

Overall, the receivers worked well but could certainly be improved upon. In particular, dynamic range and frequency response stability were two problem areas. During the reception of strong interference, the avoidance of nonlinear operation in any stage of the receivers is crucial. A calibration system which would have allowed the monitoring of both amplitude and phase response of the system would

have been desirable for maintaining proper filter tuning and for allowing correction of residual response ripples.

The FFT processor, though not designed for large interfering signals, was certainly adequate for the majority of signals encountered during the observations. Improvements in dynamic range could be made through the use of more than 8 bits for FFT processing, but the benefits such as the incremental gain in observing time and quality should be weighed against the cost. An increase in spectral resolution, as discussed further on, would undoubtedly be beneficial. The calculation of auto spectra as well as cross spectra is quite valuable for robust estimation.

Careful containment of electromagnetic interference generated by the digital circuitry is most essential. An oscilloscope probe connected to the FFT processor and brought outside the shielded enclosure was enough to radiate detectable RF interference. Electromagnetic interference produced by digital equipment at low frequencies could be a serious problem to radio astronomy.

The robust estimation procedure developed for the project worked very well. Some possible improvements, such as the use of adaptive estimation, have already been mentioned. Additional possibilities could include the identification of specific modulation types and the deletion of an appropriate amount of bandwidth, or the use of past spectral information to determine if some frequencies should be weighted less heavily than others due to a higher

probability of interference.

A major difficulty encountered during the observations was the occasional presence of signals which were not fixed in frequency or were not narrow in bandwidth. Sweeping signals from ionospheric sounding were one such problem. If sweeping signals could be readily identified and were present only intermittently, as they appeared to be during the field tests, then it should be possible to operate between the sweeps. A more serious potential problem could be spread-spectrum communications systems used by the military. The author does not know to what extent such systems are presently in use or at what frequencies, but attempts should be made to find out.

The interference power distribution observed during the field trials is quite interesting due both to its consistency (a power law $f(p) = \alpha p^{-1.3}$) and its variability (a wide range of α depending upon frequency and time of day, and varying considerably from one day to the next). The relatively weak dependence of the probability of interference upon interference power (as compared to an exponential dependence, for example) suggests that if α is large enough for significant interference to be present, then the largest of the interfering signals should certainly be detectable via spectral analysis. Also, if the number of detectable interfering signals is not too large, then it is unlikely that there will be many just below the detection limit which could produce significant errors in observation

results. The obvious conclusion is that an interference detection and removal system as described in this thesis will be extremely successful if the number of interfering signals is small. If the amount of interference is too large then errors due to undetected interference will at some point begin to dominate.

The results in this thesis show the interference excising system operating on occasion with up to 50% of channels being deleted because of interference. More typically, successful operation is possible with 20 to 30% of the overall bandwidth being rejected. The nominal increase in observing time without disruption from interference in the mornings and evenings is from 60 to 90 minutes. In addition, night-time interference was noted on the majority of nights and was removed with no difficulty.

7.2 Recommendations for Further Research

This thesis has demonstrated that interference excising is highly successful during the winter nights of a solar maximum. However, it is not successful during the days. The main question which arises is how well such a scheme can operate during a solar minimum when conditions are more favorable for astronomy. As typical critical frequencies during the summer day of a solar minimum are nearly the same as those during the night of a solar maximum, it is conceivable that interference excising could allow very long periods of continuous, interference-free observing during

the summer and possibly the winter of a solar minimum. Further research should therefore include the use of the present or a similar system in conjunction with a large decametric telescope to evaluate its performance during the next solar minimum in 1984-86.

As the probability of interference appears to be highly dependent on frequency, studies could be undertaken to identify other regions of the spectrum below 22.25 MHz where an interference excising system of the type described herein would be most effective. In particular, spectral regions with very narrowband signals and phase-coherent carriers should be sought.

Far more about the probability distribution of interfering signals needs to be known. Is it similar at all frequencies and for all classes of signals? How does it vary from day to day, season to season, and over the sunspot cycle? And, most importantly from an interference excising viewpoint, how is interference distributed below the threshold of detectability where it can produce observation errors? In order to answer this question, more sensitive measurements of interfering signals are required. The simplest method would be higher resolution spectral analysis, perhaps down to a few Hertz. The basic question to be asked is does the interference distribution turn over at some point (like the log-normal curve) and if so, at what point?

There is a massive amount of literature on ionospheric

radio propagation which would shed a great deal of light upon and perhaps even answer some of the above questions.

The decreasing costs of digital electronics and the improving performance of signal processing IC's makes interference detection and removal quite feasible for decametric telescopes. The ability to avoid terrestrial interference using the methods developed in this thesis will undoubtedly be of much benefit to low frequency radio astronomy.

References

- [1] D. Routledge, "Proposal for a Canadian decametric telescope," Unpublished proposal for submission to the N.R.C. Associate Committee on Astronomy, December 1973.
- [2] P.E. Dewdney, "An aperture synthesis radiotelescope and a deep sky survey at 22 MHz," Ph.D. thesis, University of British Columbia, August 1978.
- [3] J.D. Kraus, *Radio Astronomy*, New York: McGraw-Hill, 1966.
- [4] CCIR Report AM/2, "Ionospheric limitations to ground-based radio astronomy," December 1976.
- [5] A.H. Bridle and C.R. Purton, "Observations of radio sources at 10.03 MHz," *Astronomical Journal*, vol. 73, no. 8, pp. 717-726, Oct. 1968.
- [6] S.Ya. Braude, O.M. Lebedeva, A.V. Megn, B.P. Ryabov and I.N. Zhouck, "The spectra of discrete radio sources at decametric wavelengths - I," *Mon. Not. R. Astr. Soc.*, vol. 143, pp. 289-300, 1969.
- [7] G.R.A. Ellis and P.A. Hamilton, "Cosmic radio noise survey at 4.7 Mc/s," *Astrophys. Journ.*, vol. 143, no. 1, pp. 227-235, 1966.
- [8] G. Reber, "Cosmic static at 144 meters wavelength," *Journal of the Franklin Institute*, vol. 285, no. 1, pp. 1-12, Jan. 1968.
- [9] B.Y. Mills, "Cross-type radio telescopes," *Proc. IRE Australia*, vol. 24, pp. 132-140, February, 1963.
- [10] M. Ryle and A. Hewish, "The synthesis of large radio telescopes," *Mon. Not. R. Astr. Soc.*, vol. 120, pp. 220-230, 1960.
- [11] E.B. Fomalont, "Earth-rotation aperture synthesis," *Proc. IEEE*, vol. 61, no. 9, pp. 1211-1218, 1973.
- [12] K. Davies, *Ionospheric Radio Propagation*, National Bureau of Standards Monograph 80, Washington: U.S. Government Printing Office, 1966.
- [13] *ibid*, p. 71.

- [14] *ibid*, p. 153.
- [15] *ibid*, p. 253.
- [16] *ibid*, p. 150.
- [17] *ibid*, pp. 101-158.
- [18] E.C. Jordan and K.G. Balmain, *Electromagnetic Waves and Radiating Systems*, New Jersey: Prentice-Hall, 1968, p. 676.
- [19] *ibid*, p. 678.
- [20] C.G. Little and H. Leinbach, "The riometer - a device for the continuous measurement of ionospheric absorption," *Proc. IRE*, vol. 47, no. 2, pp. 315-320, February 1959.
- [21] E. Chvojková, "Propagation of radio waves from cosmical sources," *Nature*, vol. 181, p. 105, January 1958.
- [22] F.G. Smith, "Ionospheric refraction of 81.5 Mc/s radio waves from radio stars," *Journ. Atmos. Terr. Phys.*, vol. 2, p. 350, 1952.
- [23] B.H. Briggs, "Ionospheric irregularities and radio scintillations," *Contemp. Phys.*, vol. 16, pp. 469-488, 1975.
- [24] K. Davies, *Ionospheric Radio Waves*, Waltham, Mass.: Blaisdell, 1969, p. 365.
- [25] K.A. Norton, "Transmission loss in radio propagation," *Proc. IRE*, vol. 41, pp. 146-152, January 1953.
- [26] N. Smith and M.B. Harrington, "The variability of sky-wave field intensities at medium and high-frequencies," National Bureau of Standards Report CRPL-1-6, April 15, 1948.
- [27] CCIR Report 539, "The protection of radioastronomy observations on the shielded side of the moon," 1974.
- [28] M.D. Papagiannis and M. Mendillo, "Low frequency radio astronomy through an artificially created ionospheric window," *Nature*, vol. 255, no. 5503, pp. 42-44, May 1975.

- [29] C.A. Shain, "The Sydney 19.7-MC radio telescope," *Proc. IRE*, vol. 46, no. 1, pp. 85-88, January 1958.
- [30] P.A. Hamilton and R.F. Haynes, "Observations of the southern sky at 10.02 MHz," *Aust. J. Phys.*, vol. 21, pp. 895-902, 1968.
- [31] J.L. Wheeler, "Frequency-domain interference excising at radio frequencies," *IEEE Trans. Electromagnetic Compatibility*, vol. EMC-19, no. 3, pp. 132-136, August 1977.
- [32] S. Weinreb, "A digital spectrum analysis technique and its application to radio astronomy," *M.I.T. Technical Report 412*, Research Laboratory of Electronics, 1963.
- [33] R.S. Roger, C.H. Costain, J.D. Lacey, T.L. Landecker, and F.K. Bowers, "A supersynthesis radio telescope for neutral hydrogen spectroscopy at the Dominion Radio Astrophysical Observatory," *Proc. IEEE*, vol. 61, no. 9, pp. 1270-1276, Sept. 1973.
- [34] I.R. Linscott, J.W. Erkes, and N.R. Powell, "A fast Fourier transform spectrometer for radio astronomy," presented to the American Astronomical Society, Haverford, Pennsylvania, June 23, 1976.
- [35] J.W. Cooley and J.W. Tukey, "An algorithm for the machine calculation of complex Fourier series," *Math. Comp.*, vol. 19, pp. 297-301, April 1965.
- [36] B. Gold and C.M. Rader, *Digital Processing of Signals*, New York: McGraw-Hill, 1969.
- [37] *ibid*, p. 180.
- [38] W.T. Cochran, et al, "What is the fast Fourier transform," *IEEE Trans. Audio and Electroacoustics*, vol. AU-15, pp. 45-55, June 1967.
- [39] G.D. Bergland, "A guided tour of the fast Fourier transform," *IEEE Spectrum*, vol. 6, pp. 41-52, July 1969.
- [40] E.O. Brigham and R.E. Morrow, "The fast Fourier transform," *IEEE Spectrum*, vol. 4, pp. 63-70, Dec. 1967.
- [41] W.M. Gentleman and G. Sande, "Fast Fourier transforms - for fun and profit," *1966 Fall Joint Computer Conf., AFIPS Proc.*, vol. 29, Washington, D.C.: Spartan Books, 1966.

- [42] D. Childers and A. Durling, *Digital Filtering and Signal Processing*, St. Paul: West Publishing Co., 1975.
- [43] A. Oppenheim and R. Schaffer, *Digital Signal Processing*, New Jersey: Prentice-Hall, 1975.
- [44] F.J. Harris, "On the use of windows for harmonic analysis with the discrete Fourier transform," *Proc. IEEE*, vol. 66, no. 1, pp. 51-83, 1978.
- [45] J. Persson, "Variability and covariability of modified spectral estimators," *IEEE Trans. Acoust. Speech and Signal Proc.*, vol. ASSP-22, no. 2, pp. 158-160, April 1975.
- [46] T.S. Durrani, "Joint density functions for digital spectra," *IEEE Trans. Acoust. Speech and Signal Proc.*, vol. ASSP-22, no. 5, pp. 314-320, October 1974.
- [47] P.D. Welch, "The use of fast Fourier transform for estimation of power spectra: a method based on time averaging over short, modified periodograms," *IEEE Trans. Audio Electroacoust.*, vol. AU-15, pp. 70-73, June 1967.
- [48] D.V. James, "Quantization errors in the fast Fourier transform," *IEEE Trans. Acoust. Speech and Signal Proc.*, vol. ASSP-23, no. 3, pp. 277-283, June 1975.
- [49] D.W. Tufts, H.S. Hersey, and W.E. Moiser, "Effects of FFT coefficient quantization on bin frequency response," *Proc. IEEE (Lett.)*, vol. 60, pp. 146-147, Jan. 1972.
- [50] P.D. Welch, "A fixed-point fast Fourier transform error analysis," *IEEE Trans. Audio Electroacoustics*, vol. AU-17, pp. 151-157, June 1967.
- [51] C.J. Weinstein, "Roundoff noise in floating point fast Fourier transform computation," *IEEE Trans. Audio Electroacoustics*, vol. AU-17, no. 3, pp. 209-215, Sept. 1969.
- [52] A.V. Oppenheim and C.J. Weinstein, "Effects of finite register length in digital filtering and the fast Fourier transform," *Proc. IEEE*, vol. 60, no. 8, pp. 957-976, 1972.
- [53] T. Kaneko and B. Liu, "Accumulation of round-off error in fast Fourier transforms," *J. Assoc. Computing Machinery*, vol. 17, pp. 637-654, Oct. 1970.

- [54] Tran-Thong and B. Liu, "Fixed-point fast Fourier error analysis," *IEEE Trans. Acoust. Speech and Signal Proc.*, vol. ASSP-24, no. 6, pp. 563-573, Dec. 1976.
- [55] M. Sundaramurthy and V. Umapathi Reddy, "Some results in fixed-point fast Fourier transform error analysis," *IEEE Trans. Computers*, vol. C-26, no. 3, pp. 305-308, March 1977.
- [56] *Digital Signal Processing Handbook*, Sunnyvale, California: Advanced Micro Devices, 1976
- [57] D. Lancaster, "Understanding pseudo-random circuits," *Radio-Electronics*, vol. 46, pp. 42-49, April 1975.
- [58] A.S. Sedra and P.D. Brackett, *Filter Theory and Design: Active and Passive*, London: Pitman, 1979, p. 155.
- [59] A. Budak, *Passive and Active Network Analysis and Synthesis*, Boston: Houghton Mifflin Company, 1974, p. 520.
- [60] J. Millman and C.C. Halkias, *Electronic Devices and Circuits*, New York: McGraw-Hill, 1967, p. 229.
- [61] *ibid*, p. 392.
- [62] W. Mendenhall and R.L. Scheaffer, *Mathematical Statistics with Applications*, North Scituate, Mass.: Duxbury Press, 1973, p. 263.
- [63] A.A. Ershov, "Stable methods of estimating parameters," *Automation and Remote Control*, vol. 39, pp. 1152-1181, 1979.
- [64] J.W. Tukey, "The future of data analysis," *Ann. Math. Stat.*, vol. 33, pp. 1-67, 1967.
- [65] C.F. Gauss, "Gottingische gelehrte Anzeigen," pp. 321-327, 1821 (reprinted in *Werke*, Bd. 4, p. 98).
- [66] A.M. Legendre, "On the method of least squares," 1805, translated from the French in: *A Source Book in Mathematics* (edited by D. E. Smith), New York: Dover, 1959, pp. 576-579.
- [67] F.J. Anscombe, "Topics in the investigation of linear relationships fitted by the method of least squares," *Journal of the Royal Statistical Society, Series B*, vol. 29, pp. 1-52, 1967.

- [68] B. Pierce, "Criterion for the rejection of doubtful observations," *Astron. J.*, vol. 2, pp. 161-163, 1852.
- [69] W. Chauvenet, *Manual of Spherical and Practical Astronomy*, Philidelphia, 1863.
- [70] S. Newcomb, "Researches of the motion of the moon, II," *Astronomical Papers*, U. S. Nautical Office, vol. 9, pp.1-249, 1912.
- [71] H. Poincaré, *Calcul des Probabilities*, Paris, Gauthiers-Villars, 1912.
- [72] E.S. Pearson and C. Chandra Sekar, "The efficiency of statistical tools and a criterion for the rejection of outlying observations," *Biometrika*, vol. 28, pp. 308-320, 1936.
- [73] P.J. Huber, "Robust statistics: A review," *The Annals of Mathematical Statistics*, vol. 43, pp. 1041-1067, 1972.
- [74] S.M. Stigler, "Simon Newcomb, Percy Daniel and the history of robust estimation," *J. Am. Stat. Assoc.*, vol. 68, pp. 872-879, 1973.
- [75] C. Eisenhart, "The development of the concept of the best mean of a set of measurements from antiquity to the present day," *Am. Stat. Assoc. Presidential Address*, 1971.
- [76] W.J. Dixon, "Rejection of observations," *Contributions to Order Statistics*, A. E. Sarhan and B. G. Greenberg (Eds.), New York: John Wiley and Sons, 1962, pp. 299-342.
- [77] T.S. Ferguson, "Rules for rejection of outliers," *Revue Inst. Int. de Stat.*, vol. 29, pp. 29-43, 1961.
- [78] W.R. Thompson, *Annals of Mathematical Statistics*, vol. VI, pp. 214-219, 1935.
- [79] F.E. Grubbs, "Sample criteria for testing outlying observations," *Ann. Math. Statist.*, vol 21, pp. 27-58, 1950.
- [80] P. Prescott, "Examination of the behavior of tests for outliers when more than one outlier is present," *Appl. Statist.*, vol. 27, pp. 10-25, 1978.

- [81] A. Kudo, "On the testing of outlying observations," *Sankhya*, vol. 17, pp. 67-76, 1956.
- [82] W. J. Dixon, "Analysis of extreme values," *Ann. Math. Statist.*, vol. 21, pp. 488-506, 1950.
- [83] H. A. David, H.O. Hartley and E.S. Pearson, "The distribution of the ratio, on a single normal sample, of range to standard deviation," *Biometrika*, vol. 41, pp. 482-483, 1954.
- [84] T.S. Ferguson, "On the rejection of outliers," *Fourth Berkeley Symp. Math. Statist. Prob.*, J. Neyman (Ed.), Berkeley and Los Angeles: University of California Press, 1961, pp. 253-287.
- [85] B. Rosner, "On the detection of many outliers," *Technometrics*, vol. 17, pp. 221-227, 1975.
- [86] F.J. Anscombe, "Rejection of outliers," *Technometrics*, vol. 2, pp. 123-147, 1960.
- [87] C. Eisenhart, Mendeleev's Expressed Preference (1895) of the 33 1/3%-Trimmed Mean, Memorandum, National Bureau of Standards, Washington, D. C., 1971.
- [88] P.J. Bickel, "On some robust estimates of location," *Ann. Math. Statist.*, vol. 36, pp. 847-858, 1965.
- [89] D.F. Andrews, P.J. Bickel, F.R. Hampel, P.J. Huber, W.H. Rogers and J. W. Tukey, *Robust Estimates of Location: Survey and Advances*, Princeton, New Jersey: Princeton University Press, 1972.
- [90] J.W. Tukey, *Exploratory Data Analysis*, (Limited Preliminary Edition), Reading, Massachusetts: Addison-Wesley, 1970.
- [91] E.J. Wegman and R.J. Carroll, "A Monte Carlo study of robust estimators of location," *Commun. Statist.-Theor. Meth.* vol. A6, pp. 795-812, 1977.
- [92] F.R. Hampel, "The influence curve and its role in robust estimation," *J. Am. Statist. Assoc.*, vol. 69, pp. 383-393, 1974.
- [93] J.M. Wozencraft and I.M. Jacobs, *Principles of Communication Engineering*, New York: John Wiley and Sons, 1965, p. 234.

- [94] P.J. Huber, "Robust estimation of a location parameter," *Ann. Math. Statist.*, vol. 35, pp. 73-101, 1964.
- [95] R.V. Hogg, "Statistical robustness: One view of its use in applications today," *American Statistician*, vol. 33, pp. 108-115, 1979.
- [96] L.A. Jaeckel, "Robust estimates of location: Symmetry and asymmetric contamination," *Ann. Math. Statist.*, vol. 42, no. 3, pp. 1020-1034, 1971.
- [97] J. Jureckova, "Asymptotic Relations of M-Estimates and R-Estimates in Linear Regression Models," *Annals of Statistics*, vol. 5, pp. 464-472, 1977.
- [98] R. V. Hogg, "Adaptive robust procedures: A partial review and some suggestions for future applications and theory," *J. Am. Statist. Assoc.*, vol. 69, no. 348, pp. 909-923, Dec. 1974.
- [99] A.M. Gross, "Confidence interval robustness with long-tailed symmetric distributions," *J. Am. Statist. Assoc.*, vol. 71, no. 354, pp. 409-416, June 1976.
- [100] T. De Wet and J.W.J. van Wyk, "Efficiency and robustness of Hogg's adaptive trimmed means," *Commun. Statist.-Theor. Meth.*, vol. A8, no. 2, pp. 117-128, 1979.
- [101] J.R. Collins, "Robust estimation of a location parameter in the presence of asymmetry," *Annals of Statistics*, vol. 4, pp. 68-85, 1976.
- [102] R.J. Carroll, "On estimating variances of robust estimators when the errors are asymmetric," *J. Am. Statist. Assoc.*, vol. 74, pp. 674-679, Sept. 1979.
- [103] M. Fisz, *Probability Theory and Mathematical Statistics*, New York: John Wiley and Sons, 1963, p. 229.
- [104] C.H. Costain, J.D. Lacey and R.S. Roger, "The 22.25 MHz radio telescope at the Dominion Radio Astrophysical Observatory," *Publications of the Dominion Observatory*, vol. 25, no. 13, pp. 327-335, 1969.
- [105] H.G. Booker, "The use of radio stars to study irregular refraction of radio waves in the ionosphere," *Proc. IRE*, vol. 46, pp. 298-314, January 1958.

Appendix 1 - A Derivation of Equivalent Integration Time

Consider two real Gaussian series f and g with zero means and variances σ_f^2 and σ_g^2 , respectively. Assume that consecutive samples are independent, hence

$$\text{Cov}[f_i, f_j] = E[f_i f_j] = \begin{cases} \sigma_f^2, & i=j \\ 0, & i \neq j \end{cases}$$

$$\text{Cov}[g_i, g_j] = \begin{cases} \sigma_g^2, & i=j \\ 0, & i \neq j \end{cases}$$

Let the covariance of f_i and g_j be nonzero only if $i=j$, thus

$$\text{Cov}[f_i, g_i] = \begin{cases} \rho \sigma_f \sigma_g, & i=j \\ 0, & i \neq j \end{cases}$$

where ρ is the correlation coefficient of f and g .

Define the product P of f and g to be

$$P = \sum_{i=1}^n f_i g_i$$

Finding P is equivalent to correlating the two series. The expected value and variance of P can be found by considering P to be a linear function of a random variable fg . It is well known that the expected value and variance of a weighted sum U of independent terms Y_i are given as follows:

$$U = \sum_{i=1}^n a_i Y_i$$

$$E[U] = \sum_{i=1}^n a_i E[Y_i]$$

$$V[U] = \sum_{i=1}^n a_i^2 V[Y_i]$$

For P , the weights a_i are all 1.0 and so

$$\begin{aligned} E[P] &= \sum_{i=1}^n E[f_i g_i] \\ &= nE[fg] \end{aligned}$$

$$\begin{aligned} V[P] &= \sum_{i=1}^n V[f_i g_i] \\ &= nV[fg] \end{aligned}$$

The relative error RE in P is given by the ratio of $\sqrt{V[P]}$ and $E[P]$:

$$\begin{aligned} RE_P &= \frac{\sqrt{V[P]}}{E[P]} \\ &= \frac{\sqrt{nV[fg]}}{nE[fg]} \\ &= \frac{1}{\sqrt{n}} \frac{\sqrt{V[fg]}}{E[fg]} \end{aligned}$$

This result is as expected for a rectangular window where all points are weighted equally.

Now consider two weighted series f' and g' formed by multiplying f and g by a set of window coefficients w_i :

$$f_i' = w_i f_i$$

$$g_i' = w_i g_i$$

The new product P' is

$$P' = \sum_{i=1}^n w_i^2 f_i g_i$$

with expected value and variance given by

$$\begin{aligned}
 E[P'] &= \sum_{i=1}^n w_i^2 E[fg] \\
 V[P'] &= \sum_{i=1}^n [w_i^2]^2 V[fg] \\
 &= \sum_{i=1}^n w_i^4 V[fg]
 \end{aligned}$$

The relative error for P' is

$$\begin{aligned}
 RE_{P'} &= \frac{\sqrt{\sum_{i=1}^n w_i^4 V[fg]}}{\sum_{i=1}^n w_i^2 E[fg]} \\
 &= \frac{\sqrt{\sum_{i=1}^n w_i^4} \sqrt{V[fg]}}{\sum_{i=1}^n w_i^2 E[fg]}
 \end{aligned}$$

Equivalent integration time (EIT) for a windowed series may be defined as the square of the ratio of the relative error with no window to that with the window:

$$\begin{aligned}
 EIT &= \left[\frac{RE_P}{RE_{P'}} \right]^2 \\
 &= \left[\frac{\frac{1}{\sqrt{n}} \frac{\sqrt{V[fg]}}{E[fg]}}{\frac{\sqrt{\sum_{i=1}^n w_i^4} \sqrt{V[fg]}}{\sum_{i=1}^n w_i^2 E[fg]}} \right]^2 \\
 &= \frac{\left[\sum_{i=1}^n w_i^2 \right]^2}{n \sum_{i=1}^n w_i^4}
 \end{aligned}$$

Some examples of equivalent integration time for a few windows using the above expression are $EIT=1.0$ for a rectangular window, $EIT=0.516$ for a Hanning window, and $EIT=0.444$ for a Kaiser-Bessel window with parameter $\alpha=2.5$.

Appendix 2 - Products of Gaussian Variables

1. Expected Value of the Product of Two Gaussian Variables

Start with two independent standard normal variables x_1 and x_2 . Two partially correlated Gaussian variables y_1 and y_2 may be created as follows:

$$y_1 = \sigma_1 x_1$$

$$y_2 = \sigma_2(\rho x_1 + \sqrt{1-\rho^2}x_2), \quad 0 \leq \rho \leq 1$$

Then

$$E[y_1] = \sigma_1 E[x_1] = 0$$

$$V[y_1] = \sigma_1^2 E[x_1^2] = \sigma_1^2$$

$$E[y_2] = \sigma_2 \rho E[x_1] + \sigma_2 \sqrt{1-\rho^2} E[x_2] = 0$$

$$\begin{aligned} V[y_2] &= \sigma_2^2 \rho^2 V[x_1] + \sigma_2^2 (1-\rho^2) V[x_2] \\ &= \sigma_2^2 (\rho^2 + 1 - \rho^2) = \sigma_2^2 \end{aligned}$$

The expected value of the product of y_1 and y_2 is

$$\begin{aligned} E[y_1 y_2] &= E[(\sigma_1 x_1) \sigma_2 (\rho x_1 + \sqrt{1-\rho^2} x_2)] \\ &= E[\sigma_1 \sigma_2 \rho x_1^2 + \sigma_1 \sigma_2 \sqrt{1-\rho^2} x_1 x_2] \\ &= \sigma_1 \sigma_2 (E[x_1^2] + \sqrt{1-\rho^2} E[x_1 x_2]) \\ &= \sigma_1 \sigma_2 \rho E[x_1^2] = \sigma_1 \sigma_2 \rho \end{aligned}$$

as x_1 and x_2 are independent.

2. Variance of the Product of Two Gaussian Variables

The variance of the product of y_1 and y_2 defined above will be given by

$$V[y_1 y_2] = E[y_1^2 y_2^2] - E^2[y_1 y_2]$$

However ,

$$\begin{aligned} E[y_1^2 y_2^2] &= E[\sigma_1^2 x_1^2 \sigma_2^2 (\rho x_1 + \sqrt{1-\rho^2} x_2)^2] \\ &= E[\sigma_1^2 x_1^2 \sigma_2^2 (\rho^2 x_1^2 + (1-\rho^2) x_2^2 + 2\rho\sqrt{1-\rho^2} x_1 x_2)] \\ &= \sigma_1^2 \sigma_2^2 (\rho^2 E[x_1^4] + (1-\rho^2) E[x_1^2] E[x_2^2] \\ &\quad + 2\rho\sqrt{1-\rho^2} E[x_1^3] E[x_2]) \\ &= \sigma_1^2 \sigma_2^2 (\rho^2 E[x_1^4] + 1-\rho^2) \end{aligned}$$

To find $E[x_1^4]$, define the fourth moment as

$$\begin{aligned} E[x_1^4] &= \int_{-\infty}^{\infty} x_1^4 \frac{1}{\sqrt{2\pi}} \exp(-x_1^2/2) dx_1 \\ &= \frac{2}{\sqrt{2\pi}} \int_0^{\infty} x_1^4 \exp(-x_1^2/2) dx_1 \end{aligned}$$

Using integration by parts, let

$$\begin{aligned} u &= x_1^3 & du &= 3x_1^2 dx_1 \\ dv &= x_1 \exp(-x_1^2/2) & v &= \exp(-x_1^2/2) \end{aligned}$$

Then, using standard integration tables,

$$\begin{aligned} E[x_1^4] &= \frac{2}{\sqrt{2\pi}} [uv - \int_0^{\infty} v du] \\ &= \frac{2}{\sqrt{2\pi}} \left[-x_1^3 \exp(-x_1^2/2) \Big|_0^{\infty} + \int_0^{\infty} 3x_1^2 \exp(-x_1^2/2) dx_1 \right] \\ &= \frac{2}{\sqrt{2\pi}} \left[0 + \frac{3\Gamma\left(\frac{3}{2}\right)}{2\left(\frac{1}{2}\right)^{3/2}} \right] \\ &= \frac{3}{\sqrt{2\pi}} \frac{\sqrt{\pi}}{2} 2^{3/2} = 3 \end{aligned}$$

Hence,

$$\begin{aligned}
 E[y_1^2 y_2^2] &= \sigma_1^2 \sigma_2^2 (3\rho^2 + 1 - \rho^2) \\
 &= \sigma_1^2 \sigma_2^2 (2\rho^2 + 1)
 \end{aligned}$$

Finally,

$$\begin{aligned}
 V[y_1 y_2] &= E[y_1^2 y_2^2] - E^2[y_1 y_2] \\
 &= \sigma_1^2 \sigma_2^2 (2\rho^2 + 1) - \sigma_1^2 \sigma_2^2 \rho^2 \\
 &= \sigma_1^2 \sigma_2^2 (\rho^2 + 1)
 \end{aligned}$$

3. Expected Value of the Product of Four Gaussian Variables

Start with four independent standard normal $N(0,1)$ variables x_1, x_2, x_3 and x_4 . It is desired to create four Gaussian variables F_r, F_i, G_r and G_i with the following variance-covariance matrix:

	F_r	F_i	G_r	G_i
F_r	σ_F^2	0	$\rho_C^{\sigma_F \sigma_G}$	$-\rho_Q^{\sigma_F \sigma_G}$
F_i	0	σ_F^2	$\rho_Q^{\sigma_F \sigma_G}$	$\rho_C^{\sigma_F \sigma_G}$
G_r	$\rho_C^{\sigma_F \sigma_G}$	$\rho_Q^{\sigma_F \sigma_G}$	σ_G^2	0
G_i	$-\rho_Q^{\sigma_F \sigma_G}$	$\rho_C^{\sigma_F \sigma_G}$	0	σ_G^2

These variables will represent real and imaginary components of the complex spectra of two Gaussian series. The desired relationships above can be obtained by letting

$$\begin{aligned}
 F_r &= \sigma_F x_1 \\
 F_i &= \sigma_F x_2
 \end{aligned}$$

$$G_r = \sigma_G(\rho_r x_1 + \rho_i x_2 + \sqrt{1-\rho_r^2-\rho_i^2} x_3)$$

$$G_i = \sigma_G(-\rho_i x_1 + \rho_r x_2 + \sqrt{1-\rho_r^2-\rho_i^2} x_4)$$

Then,

$$E[F_r] = E[F_i] = E[G_r] = E[G_i] = 0$$

$$V[F_r] = E[F_r^2] = \sigma_F^2 E[x_1^2] = \sigma_F^2$$

$$V[F_i] = \sigma_F^2$$

$$V[G_r] = E[G_r^2]$$

$$= \sigma_G^2 E[(\rho_r x_1 + \rho_i x_2 + \sqrt{1-\rho_r^2-\rho_i^2} x_3)^2]$$

$$= \sigma_G^2 E[\rho_r^2 x_1^2 + \rho_i^2 x_2^2 + (1-\rho_r^2-\rho_i^2) x_3^2]$$

because all cross products have an expected value of 0.

$$\begin{aligned} V[G_r] &= \sigma_G^2 (\rho_r^2 E[x_1^2] + \rho_i^2 E[x_2^2] + (1-\rho_r^2-\rho_i^2) E[x_3^2]) \\ &= \sigma_G^2 \end{aligned}$$

Similarly,

$$V[G_i] = \sigma_G^2$$

$$\text{Cov}[F_r, F_i] = E[F_r F_i]$$

$$= \sigma_F^2 E[x_1 x_2] = 0$$

$$\text{Cov}[G_r, G_i] = E[G_r G_i]$$

$$= \sigma_G^2 (-\rho_r \rho_i E[x_1^2] + \rho_r \rho_i E[x_2^2])$$

$$= 0$$

$$\begin{aligned}
\text{Cov}[F_r, G_r] &= E[F_r G_r] \\
&= \sigma_F \sigma_G (\rho_r E[x_1^2] + \rho_i E[x_1 x_2] + \sqrt{1-\rho_r^2-\rho_i^2} E[x_1 x_3]) \\
&= \sigma_F \sigma_G \rho_r
\end{aligned}$$

$$\text{Cov}[F_i, G_i] = \sigma_F \sigma_G \rho_r$$

$$\text{Cov}[F_r, G_i] = -\sigma_F \sigma_G \rho_i$$

$$\text{Cov}[F_i, G_r] = \sigma_F \sigma_G \rho_i$$

With four variables as defined above, it is possible to find the expected value of the product of all four:

$$\begin{aligned}
E[F_r F_i G_r G_i] &= E[\sigma_F^2 \sigma_G^2 x_1 x_2 (\rho_r x_1 + \rho_i x_2 + \sqrt{1-\rho_r^2-\rho_i^2} x_3) \\
&\quad \cdot (-\rho_i x_1 + \rho_r x_2 + \sqrt{1-\rho_r^2-\rho_i^2} x_4)] \\
&= \sigma_F^2 \sigma_G^2 E[x_1 x_2 (-\rho_r \rho_i x_1^2 + \rho_r^2 x_1 x_2 + \rho_r \sqrt{1-\rho_r^2-\rho_i^2} x_1 x_4 \\
&\quad - \rho_i^2 x_1 x_2 + \rho_r \rho_i x_2^2 + \rho_i \sqrt{1-\rho_r^2-\rho_i^2} x_2 x_4 \\
&\quad - \rho_i \sqrt{1-\rho_r^2-\rho_i^2} x_1 x_3 + \rho_r \sqrt{1-\rho_r^2-\rho_i^2} x_2 x_3 \\
&\quad + (1-\rho_r^2-\rho_i^2) x_3 x_4)] \\
&= \sigma_F^2 \sigma_G^2 \left[-\rho_r \rho_i E[x_1^3] E[x_2] + \rho_r^2 E[x_1^2] E[x_2^2] \right. \\
&\quad + \rho_r \sqrt{1-\rho_r^2-\rho_i^2} E[x_1^2] E[x_2] E[x_4] \\
&\quad - \rho_i^2 E[x_1^2] E[x_2^2] + \rho_r \rho_i E[x_1] E[x_2^3] \\
&\quad + \rho_i \sqrt{1-\rho_r^2-\rho_i^2} E[x_1] E[x_2^2] E[x_4] \\
&\quad - \rho_i \sqrt{1-\rho_r^2-\rho_i^2} E[x_1^2] E[x_2] E[x_3] \\
&\quad + \rho_r \sqrt{1-\rho_r^2-\rho_i^2} E[x_1] E[x_2^2] E[x_3] \\
&\quad \left. + (1-\rho_r^2-\rho_i^2) E[x_1] E[x_2] E[x_3] E[x_4] \right] \\
&= \sigma_F^2 \sigma_G^2 (\rho_r^2 - \rho_i^2)
\end{aligned}$$

Appendix 3 - Microcomputer Observing Program

The following is an MC6800 assembly language listing of the program used to control the microcomputer and FFT processor during observations. The program enables DMA transfers after a specified integration time, displays and records the spectra, and performs robust estimation using 4 standard deviation deletions. Estimation results, numbers of points deleted, amounts of clipping, and second local oscillator frequencies are recorded on chart recorders.

M68SAM is the property of Motorola Spd, Inc.
Copyright 1974 by Motorola Inc.

Motorola M6800 Cross Assembler, Release 1.1

00001			NAM	DISP	
00002	0040		ORG	\$0040	
00003	0040	0002	XTEMP RMB	2	TEMP INDEX STORAGE
00004	0042	0002	RESPTR RMB	2	RESULTS POINTER
00005	0044	0002	DATPTR RMB	2	DATA POINTER
00006	0046	0002	DELPTR RMB	2	DELETION POINTER
00007	0048	0002	DISPTR RMB	2	DISPLAY POINTER
00008	004A	0001	SIGN RMB	1	WORKING REGISTERS FOR
00009	004B	0002	LOW RMB	2	FLOATING POINT CONVERSION
00010	004D	0002	HIGH RMB	2	
00011	004F	0001	LS1 RMB	1	
00012	0050	0001	LS2 RMB	1	
00013	0051	0001	LS3 RMB	1	
00014	0052	0002	CHAN RMB	2	CHANNEL POINTER
00015	0054	0001	COUNT1 RMB	1	INTEGRATION COUNTER
00016	0055	0001	COUNT2 RMB	1	
00017	0056	0001	COUNT3 RMB	1	
00018	0057	0001	PASS RMB	1	FIRST FFT INDICATOR
00019	0058	0002	DEL RMB	2	DELETION VECTOR POINTER
00020	005A	0001	NUM RMB	1	COUNTER FOR NO. OF CHANNELS NOT DELETED
00021	005B	0003	HEAD RMB	3	FILE HEADER
00022	005E	0001	FILE RMB	1	FILE NUMBER
00023	005F	0003	TIME RMB	3	TIME OF DAY
00024	0062	0003	INT RMB	3	INTEGRATION COUNT
00025	0065	0003	FREQ RMB	3	SECOND L.O. FREQUENCY
00026	0068	0004	CLIPS RMB	4	CLIPPING COUNTER
00027	006C	0001	ITER RMB	1	INTEGRATION COUNTER
00028	006D	0004	MEAN1 RMB	4	CO SPECTRUM LOCATION ESTIMATE
00029	0071	0001	NUM1 RMB	1	CO SPECTRUM NO. OF CHANNELS DELETED
00030	0072	0004	SDEV1 RMB	4	CO SPECTRUM STD. DEV. ESTIMATE
00031	0076	0004	MEAN2 RMB	4	QUADRATURE SPECTRUM PARAMETERS
00032	007A	0001	NUM2 RMB	1	
00033	007B	0004	SDEV2 RMB	4	
00034	007F	0004	MEAN3 RMB	4	AUTO1 SPECTRUM PARAMETERS
00035	0083	0001	NUM3 RMB	1	
00036	0084	0004	SDEV3 RMB	4	
00037	0088	0004	MEAN4 RMB	4	AUTO2 SPECTRUM PARAMETERS
00038	008C	0001	NUM4 RMB	1	
00039	008D	0004	SDEV4 RMB	4	
00040	0091	0001	CKSM RMB	1	TAPE CHECKSUM
00041	0092	0002	CASPTR RMB	2	TAPE STORAGE POINTER
00042	0094	0004	MAX RMB	4	DELETION MAXIMUM
00043	0098	0004	FACTOR RMB	4	MAX=FACTOR * STD. DEV.
00044	009C	0004	SCALE RMB	4	CRT DISPLAY PARAMETERS
00045	00A0	0002	OFFSET RMB	2	

DISP

Motorola M68SAM Cross-Assembler

Page 2

00046	00A2	0001	PHASE	RMB	1	ADD/SUBTRACT/SWITCH SPECIFIER
00047	00A3	0001	EXP	RMB	1	EXPONENT
00048	00A4	0002	DPTR	RMB	2	SPECTRUM POINTER
00049	00A6	0001	RAMPH	RMB	1	DISPLAY RAMP
00050	00A7	0001	OLDN	RMB	1	OLD NO. OF CHANNELS DELETED
00051	00A8	0001	ITMAX	RMB	1	MAX. NO. OF ITERATIONS
00052	00A9	0001	TMRDEL	RMB	1	ITERATION DELAY COUNTER
00053	00AA	0003	NFREQ	RMB	3	NEXT L.O. FREQUENCY
00054	00AD	0003	FMAX	RMB	3	MAX. L.O. FREQUENCY
00055	00B0	0003	FMIN	RMB	3	MIN. L.O. FREQUENCY
00056	00B3	0003	FINC	RMB	3	FREQUENCY INCREMENT
00057	00B6	0001	DMAFLG	RMB	1	DMA FLAG
00058			*			
00059	0100			ORG	\$0100	
00060	0100	0080	WCOEF	RMB	128	WINDOW COEFFICIENTS
00061			*			
00062		3227	FPSUB	EQU	\$3227	FLOATING POINT SUBTRACION ROUTINE
00063		3370	CLRMEM	EQU	\$3370	SUBROUTINE TO CLEAR MEMORY LOCATIONS
00064		37AC	CRLF	EQU	\$37AC	CARRIAGE RETURN, LINEFEED ROUTINE
00065		3600	FPOUT	EQU	\$3600	FLOATING POINT TTY OUTPUT ROUTINE
00066		3F00	DVCTR1	EQU	\$3F00	DELETION VECTOR 1
00067		3F80	DVCTR2	EQU	\$3F80	DELETION VECTOR 2
00068		4000	LATCH	EQU	\$4000	OUTPUT LATCHES (NOT USED)
00069		5000	TOS	EQU	\$5000	TOP OF AM9511 STACK
00070		5001	CMSTAT	EQU	\$5001	AM9511 COMMAND AND STATUS REGISTER
00071		5008	TIMER	EQU	\$5008	MC6840 TIMER
00072		8004	TTYPIA	EQU	\$8004	TTY OUTPUT REGISTER
00073		8007	RDRCTL	EQU	\$8007	READER CONTROL REGISTER
00074		8008	KEYBD	EQU	\$8008	KEYBOARD REGISTER
00075		8010	ACIACR	EQU	\$8010	ACIA CONTROL REGISTER
00076		8011	ACIATR	EQU	\$8011	ACIA DATA REGISTER
00077		8020	FCNTRL	EQU	\$8020	FFT CONTROL PIA
00078		8021	FFTFLG	EQU	\$8021	CONTROL REGISTER WITH FFT DONE FLAG
00079		8022	PCNTRL	EQU	\$8022	FFT PHASE CONTROL PIA
00080		8023	CLKFLG	EQU	\$8023	CONTROL REGISTER WITH FFT CLOCK FLAG
00081		8042	HZ	EQU	\$8042	1 HZ CLOCK PIA
00082		8600	WINPIA	EQU	\$8600	WINDOW CONTROL PIA
00083		A00F	XTMP	EQU	\$A00F	TEMPORARY INDEX STORGAE
00084		B000	DC0	EQU	\$B000	CO SPECTRUM DISPLAY VALUES
00085		B100	DQUAD	EQU	\$B100	QUADRATURE DISPLAY VALUES
00086		B200	DAUTO1	EQU	\$B200	AUTO1 DISPLAY VALUES
00087		B300	DAUTO2	EQU	\$B300	AUTO2 DISPLAY VALUES
00088		B800	CO	EQU	\$B800	CO SPECTRUM VALUES
00089		BA00	QUAD	EQU	\$BA00	QUADRATURE SPECTRUM VALUES
00090		D202	DAC2	EQU	\$D202	7 D/A CONVERTER REGISTERS
00091		D204	DAC3	EQU	\$D204	
00092		D206	DAC4	EQU	\$D206	
00093		D208	DAC5	EQU	\$D208	
00094		D20A	DAC6	EQU	\$D20A	
00095		D20C	DAC7	EQU	\$D20C	

DISP

Motorola M68SAM Cross-Assembler

Page 3

```

00096      D20E      DAC8      EQU      $D20E
00097      E1D1      OUT       EQU      $E1D1      TTY CHARACTER OUTPUT ROUTINE
00098      *
00099 3000          ORG      $3000
00100          * LOAD WINDOW COEFFICIENTS FROM RAM
00101          * TO WINDOW COEFFICIENT MEMORY
00102 3000 BD 3840 BEGIN JSR      INFREQ
00103 3003 CE 8600 WINDOW LDX      #WINPIA      INITIALIZE WINDOW PIA
00104 3006 86 04          LDA A      #4
00105 3008 C6 FF          LDA B      #$FF
00106 300A 6F 01          CLR      1,X
00107 300C 6F 03          CLR      3,X
00108 300E E7 00          STA B      X
00109 3010 A7 01          STA A      1,X
00110 3012 86 F0          LDA A      #$F0
00111 3014 A7 00          STA A      X
00112 3016 86 F2          LDA A      #$F2
00113 3018 A7 00          STA A      X
00114 301A E7 02          STA B      2,X
00115 301C 86 04          LDA A      #4
00116 301E A7 03          STA A      3,X
00117 3020 CE 00FF        LDX      #WCOEF-1
00118 3023 A6 00 OVER    LDA A      X
00119 3025 B7 8602        STA A      WINPIA+2
00120 3028 86 F6          LDA A      #$F6
00121 302A B7 8600        STA A      WINPIA
00122 302D 86 F2          LDA A      #$F2
00123 302F B7 8600        STA A      WINPIA
00124 3032 7C 8600        INC      WINPIA
00125 3035 7A 8600        DEC      WINPIA
00126 3038 08            INX
00127 3039 8C 0180        CPX      #WCOEF+128
00128 303C 26 E5          BNE      OVER
00129 303E 7F 8603        CLR      WINPIA+3
00130 3041 7F 8602        CLR      WINPIA+2
00131 3044 86 FE          LDA A      #$FE
00132 3046 B7 8600        STA A      WINPIA
00133 3049 86 04          LDA A      #4
00134 304B B7 8603        STA A      WINPIA+3
00135      *
00136      * INITIALIZE PERIPHERALS AND VARIABLES
00137      *
00138 304E 0F          INIT SEI
00139 304F CE 8004        LDX      #TTYPIA      INITIALIZE TTY PIA
00140 3052 6F 01          CLR      1,X
00141 3054 6F 03          CLR      3,X
00142 3056 86 01          LDA A      #1
00143 3058 A7 00          STA A      X
00144 305A C6 07          LDA B      #7
00145 305C E7 01          STA B      1,X

```

DISP

Motorola M68SAM Cross-Assembler

Page 4

```

00146 305E A7 00      STA A X
00147 3060 E7 02      STA B 2,X
00148 3062 86 34      LDA A #$34
00149 3064 A7 03      STA A 3,X
00150 3066 A7 02      STA A 2,X
00151                *
00152 3068 CE 8020     LDX  #$8020  INITIALIZE FFT CONTROL PIA'S
00153 306B CE 8020     LDX  #$8020
00154 306E 86 04      LDA A #4      SET OUTPUTS TO $FF
00155 3070 A7 01      STA A 1,X      BEFORE DEFINING DATA DIRECTION
00156 3072 A7 03      STA A 3,X
00157 3074 C6 FF      LDA B #$FF
00158 3076 E7 00      STA B X
00159 3078 E7 02      STA B 2,X
00160 307A 6F 01      CLR  1,X
00161 307C 6F 03      CLR  3,X
00162 307E C6 1C      LDA B #$1C    DEFINE DATA DIRECTION
00163 3080 E7 00      STA B X
00164 3082 C6 0E      LDA B #$0E
00165 3084 E7 02      STA B 2,X
00166 3086 C6 15      LDA B #$15    SET CONTROL REGISTERS
00167 3088 E7 01      STA B 1,X
00168 308A 5A        DEC B
00169 308B A7 03      STA A 3,X
00170 308D 96 A2      LDA A PHASE  SET ADD/SUB/SWITCH CONTROL
00171 308F A7 02      STA A 2,X
00172 3091 86 1C      LDA A #$1C    DETECT RISING EDGE FOR 1 HZ CLOCK
00173 3093 A7 23      STA A $23,X
00174                *
00175 3095 86 81      LDA A #$81    INIT. MC6840 CLIPPING COUNTER
00176 3097 B7 5009     STA A TIMER+1
00177 309A C6 80      LDA B #$80
00178 309C F7 5008     STA B TIMER
00179 309F F7 5009     STA B TIMER+1
00180 30A2 86 03      LDA A #3
00181 30A4 B7 5008     STA A TIMER
00182                *
00183 30A7 CE B000     LDX  #DC0    INIT SPECTRUM POINTER
00184 30AA DF A4      STX  DPTR
00185                *
00186                *
00187 30AC CE CCCC     LDX  #$CCCC  SCALE=204.8
00188 30AF DF 9C      STX  SCALE
00189 30B1 CE CC08     LDX  #$CC08  PRODUCES 10DB/VOLT ON CRT DISPLAY
00190 30B4 DF 9E      STX  SCALE+2
00191 30B6 CE 0000     LDX  #$0000
00192 30B9 DF 98      STX  FACTOR   FACTOR=3.0
00193 30BB CE C002     LDX  #$C002
00194 30BE DF 9A      STX  FACTOR+2
00195 30C0 CE 0000     LDX  #$0000  OFFSET=0

```

DISP

Motorola M68SAM Cross-Assembler

Page 5

```

00196 30C3 DF :AO          STX    OFFSET
00197                      *
00198 30C5 CE 311C          LDX    #IRQ      SET ADDRESS OF INTERRUPT
00199 30C8 FF A000          STX    $A000     HANDLING ROUTINE
00200 30CB 86 CC            LDA A  #$CC      SET HEADER FOR TAPE STORAGE
00201 30CD 97 5B            STA A  HEAD
00202 30CF CE 040D          LDX    #$040D
00203 30D2 DF 5C            STX    HEAD+1
00204                      *
00205                      * START FFT
00206                      *
00207 30D4 OF              START SEI
00208 30D5 7F 00B6          CLR    DMAFLG
00209 30D8 86 1C            LDA A  #$1C      CLEAR FFT PROCESSOR
00210 30DA B7 8020          STA A  FCNTRL
00211 30DD 86 10            LDA A  #$10      ENABLE FFT PROCESSOR
00212 30DF B7 8020          STA A  FCNTRL
00213 30E2 86 03            LDA A  #3        INIT. PASS COUNTER
00214 30E4 97 57            STA A  PASS
00215 30E6 96 A2            LDA A  PHASE     SET LOAD/ACCUMULATE TO LOAD
00216 30E8 8A 08            ORA A  #8
00217 30EA B7 8022          STA A  PCNTRL
00218                      *
00219 30ED B6 8020 PASS1     LDA A  FCNTRL     WAIT FOR FFT DONE FLAG
00220 30F0 B6 8021 PASS2     LDA A  FFTFLG
00221 30F3 2A FB            BPL     PASS2     WAIT FOR 3 FFT'S
00222 30F5 7A 0057          DEC     PASS
00223 30F8 26 F3            BNE     PASS1
00224 30FA D6 A2            LDA B  PHASE     SET LOAD/ACCUM. TO ACCUM.
00225 30FC BD 3110          JSR     CLK
00226 30FF B6 8020          LDA A  FCNTRL
00227 3102 7F 0054          CLR     COUNT1   CLEAR INTEGRATION COUNTER
00228 3105 7F 0055          CLR     COUNT2
00229 3108 86 02            LDA A  #2
00230 310A 97 56            STA A  COUNT3
00231 310C 0E              CLI
00232 310D 7E 3523          JMP     DISP     ENABLE INTERRUPTS
00233                      *                               GO TO SPECTRUM DISPLAY ROUTINE
00234 3110 B6 8022 CLK       LDA A  PCNTRL     SUBROUTINE TO WAIT
00235 3113 B6 8023 CLK1      LDA A  CLKFLG     FOR FFT CLOCK TRANSITION
00236 3116 2A FB            BPL     CLK1
00237 3118 F7 8022          STA B  PCNTRL
00238 311B 39              RTS
00239                      *
00240                      * INTERRUPT HANDLING ROUTINE;
00241                      *
00242 311C 7D 8021 IRQ        TST     FFTFLG   CHECK FFT INTERRUPT
00243 311F 2B 24            BMI     IRQFFT
00244 3121 B6 8010          LDA A  ACIACR     CHECK TAPE INTERRUPT
00245 3124 2B 0C            BMI     IRQA

```

DISP

Motorola M68SAM Cross-Assembler

Page 6

```

00246 3126 B6 8043      LDA A  HZ+1      CHECK IF 1 HZ INTERRUPTS ENABLED
00247 3129 84 7F        AND A  #$7F
00248 312B 81 5C        CMP A  #$5C
00249 312D 27 06        BEQ      IRQTMR
00250 312F 7E 36F2      JMP      IRQHZ
00251 3132 7E 36A9      JMP      IRQA    IRACIA
00252                  *
00253 3135 B6 5009      IRQTMR LDA A  TIMER+1  ITERATION DELAY ROUTINE
00254 3138 B6 500E      LDA A  TIMER+6  CLEAR INTERRUPT FLAG
00255 313B 7A 00A9      DEC      TMRDEL
00256 313E 2F 01        BLE      NEWIT    IF SUFFICIENT DELAY,BEGIN
00257 3140 3B          RTI              NEW DELETION ITERATION
00258                  *
00259 3141 0E          NEWIT CLI
00260 3142 7E 31EE      JMP      ITER1
00261                  *
00262 3145 B6 8020      IRQFFT LDA A  FCNTRL  FFT INTERRUPT ROUTINE
00263 3148 96 B6        LDA A  DMAFLG
00264 314A 26 1B        BNE      DMA
00265 314C DE 55        LDX      COUNT2  CLEAR INTERRUPT FLAG
00266 314E 08          INX              INCREMENT INTEGRATION COUNTER
00267 314F DF 55        STX      COUNT2
00268 3151 26 03        BNE      NE
00269 3153 7C 0054      INC      COUNT1  COMPARE TO REQUIRED COUNT
00270 3156 9C 63      NE    CPX      INT+1
00271 3158 26 0C        BNE      RET      IF EQUAL, START DMA
00272 315A 96 54        LDA A  COUNT1
00273 315C 91 62        CMP A  INT
00274 315E 26 06        BNE      RET
00275 3160 7C 00B6      INC      DMAFLG
00276 3163 BD 381B      JSR      CHFREQ
00277 3166 3B          RET      RTI
00278                  *
00279 3167 D6 A2      DMA    LDA B  PHASE    SET LOAD/ACCUM. TO LOAD
00280 3169 CA 08        ORA B  #8
00281 316B BD 3110      JSR      CLK
00282 316E 4F          CLR A
00283 316F B7 8020      STA A  FCNTRL  ENABLE DMA TRANSFER
00284 3172 7F 00B6      CLR      DMAFLG
00285                  *
00286 3175 FE 500A      LDX      TIMER+2  READ NUMBER OF CLIPS COUNTED
00287 3178 DF 6A        STX      CLIPS+2
00288 317A FE 500C      LDX      TIMER+4
00289 317D DF 68        STX      CLIPS
00290 317F CE FFFF      LDX      #$FFFF
00291 3182 FF 500A      STX      TIMER+2
00292 3185 FF 500C      STX      TIMER+4
00293                  *
00294 3188 B6 8021      DMA1  LDA A  FFTFLG  WAIT FOR FFT DONE FLAG
00295 318B 48          ASL A

```

DISP

Motorola M68SAM Cross-Assembler

Page 7

```

00296 318C 2A FA      BPL      DMA1
00297 318E B6 8020    LDA A    FCNTRL  CLEAR INTERRUPT FLAG
00298 3191 86 10      LDA A    #$10
00299 3193 B7 8020    STA A    FCNTRL  DISABLE DMA TRANSFER
00300 3196 D6 A2      LDA B    PHASE   SET LOAD/ACCUM. TO ACCUM.
00301 3198 BD 3110    JSR      CLK
00302 319B 7F 0054    CLR      COUNT1  CLEAR INTEGRATION COUNTER
00303 319E 7F 0055    CLR      COUNT2
00304 31A1 86 02      LDA A    #2
00305 31A3 97 56      STA A    COUNT3
00306 31A5 0E         CLI
00307 31A6 86 3C      LDA A    #$3C
00308 31A8 B7 8007    STA A    RDRCTL  START TAPE RECORDER MOTOR
00309 31AB 7F 0091    CLR      CKSM   INIT. CHECKSUM AND
00310 31AE CE 005B    LDX      #HEAD  TAPE OUTPUT POINTER
00311 31B1 DF 92      STX      CASPTR
00312                *
00313 31B3 86 20      LDA A    #$20    SET EXP=32
00314 31B5 97 A3      STA A    EXP
00315 31B7 CE B800    LDX      #C0    CONVERT C0 SPECTRUM FROM
00316 31BA BD 327F    JSR      FPCONV  INTEGER TO FLOATING POINT
00317 31BD 08         INX
00318 31BE 08         INX
00319 31BF 08         INX
00320 31C0 08         INX
00321 31C1 8C BA00    CPX      #QUAD
00322 31C4 26 03      BNE      FP1
00323 31C6 7A 00A3    DEC      EXP      SET EXP=31 TO DIVIDE BY 2
00324 31C9 8C C000    CPX      #QUAD+$600  CONVERT QUADRATURE AND AUTO
00325 31CC 26 EC      BNE      THREE    SPECTRA TO FLOATING POINT
00326 31CE 01         NOP
00327 31CF 01         NOP
00328 31D0 01         NOP
00329                *
00330 31D1 BD 33CA      JSR      ALLCON  PRODUCE LOG DISPLAY VALUES
00331 31D4 86 7F      LDA A    #$7F    SET OLDN=127
00332 31D6 97 A7      STA A    OLDN
00333                *
00334 31D8 CE 3F00    DINIT  LDX      #DVCTR1  INIT. DELETION VECTORS TO 1'S
00335 31DB 86 01      LDA A    #1
00336 31DD A7 00      DINIT1 STA A    X
00337 31DF 08         INX
00338 31E0 8C 3F80    CPX      #DVCTR1+$80
00339 31E3 26 F8      BNE      DINIT1
00340 31E5 7F 006C    CLR      ITER   CLEAR ITERATION COUNTER
00341 31E8 BD 3604    JSR      CLPOUT  OUTPUT NO. OF CLIPS AND L.O. FREQ.
00342 31EB BD 3656    JSR      FRQOUT  TO CHART RECORDER
00343                *
00344 31EE 7C 006C    ITER1  INC      ITER   DELETION ITERATION ROUTINE
00345 31F1 CE 3F00    LDX      #DVCTR1

```

DISP

Motorola M68SAM Cross-Assembler

Page 8

```

00346 31F4 4F          CLR A
00347 31F5 C6 01      LDA B  #1
00348 31F7 A7 00      CLRDV1 STA A  X
00349 31F9 08          INX
00350 31FA 5A          DEC B
00351 31FB 26 FA      BNE     CLRDV1
00352 31FD CE 3F7F    LDX     #DVCTR1+$7F
00353 3200 C6 01      LDA B  #1
00354 3202 A7 00      CLRDV2 STA A  X
00355 3204 09          DEX
00356 3205 5A          DEC B
00357 3206 26 FA      BNE     CLRDV2
00358
00359 3208 86 03      LDA A  #3      DISABLE DELAY TIMER
00360 320A B7 5008    STA A  TIMER
00361
00362 320D CE B800    LDX     #CO      INIT. POINTERS FOR CO SPECTRUM
00363 3210 DF 44      STX     DATPTR
00364 3212 CE 006D    LDX     #MEAN1
00365 3215 DF 42      STX     RESPTR
00366 3217 CE 3F00    LDX     #DVCTR1
00367 321A DF 46      STX     DELPTR
00368 321C BD 33FO    JSR     MEAN      FIND MEAN AND STD. DEV.
00369 321F CE 3F80    LDX     #DVCTR2    OF NON-DELETED CHANNELS
00370 3222 DF 46      STX     DELPTR    DELETE CHANNELS WHICH DEVIATE
00371 3224 BD 34AD    JSR     COMP      FROM MEAN BY TOO MUCH
00372 3227 BD 35BA    JSR     DVAND     COMBINE CO AND QUAD. DELETION VECTORS
00373
00374 322A CE BA00    LDX     #QUAD     INIT. POINTERS FOR QUADRATURE
00375 322D DF 44      STX     DATPTR     SPECTRUM AND PERFORM DELETIONS
00376 322F CE 0076    LDX     #MEAN2
00377 3232 DF 42      STX     RESPTR
00378 3234 CE 3F00    LDX     #DVCTR1
00379 3237 DF 46      STX     DELPTR
00380 3239 BD 33FO    JSR     MEAN
00381 323C CE 3F80    LDX     #DVCTR2
00382 323F DF 46      STX     DELPTR
00383 3241 BD 34AD    JSR     COMP
00384 3244 BD 35CE    JSR     MNOUT     OUTPUT MEANS TO CHART RECORDER
00385 3247 BD 35BA    JSR     DVAND     COMBINE CO AND QUAD. DELETION VECTORS
00386
00387 324A 96 6C      LDA A  ITER      WAIT FOR 3 ITERATIONS BEFORE
00388 324C 81 03      CMP A  #3      SENDING DATA TO TAPE RECORDER
00389 324E 2D 10      BLT     ITER3
00390 3250 26 0A      BNE     ITER2
00391 3252 86 14      LDA A  #$14
00392 3254 B7 8043    STA A  HZ+1
00393 3257 86 3D      LDA A  #$3D
00394 3259 B7 8010    STA A  ACIACR    ENABLE DATA SENDING
00395

```

DISP

Motorola M68SAM Cross-Assembler

Page 9

```

00396 325C D1 A7    ITER2  CMP B  OLDN    WERE MORE CHANNELS DELETED?
00397 325E 27 08          BEQ      ITER4
00398 3260 D7 A7    ITER3  STA B  OLDN
00399 3262 96 6C          LDA A  ITER    HAS MAX. NO. OF ITERATIONS
00400 3264 91 A8          CMP A  ITMAX   BEEN REACHED?
00401 3266 2D 07          BLT      ITER5
00402 3268 BD 35F0  ITER4  JSR     NOUT    OUTPUT NO. OF CHANNELS TO RECORDER
00403 326B BD 3773          JSR     PRINT   PRINT RESULTS ON TTY
00404 326E 3B          RTI
00405                *
00406 326F CE FFFF  ITER5  LDX     #$FFFF  START ITERATION DELAY TIMER
00407 3272 FF 500E          STX     TIMER+6
00408 3275 86 43          LDA A  #$43
00409 3277 B7 5008          STA A  TIMER
00410 327A 86 02          LDA A  #2
00411 327C 97 A9          STA A  TMRDEL
00412 327E 3B          RTI
00413                *
00414                *
00415 327F 7F 004A  FPCONV CLR     SIGN    SUBROUTINE TO CONVERT 48-BIT
00416 3282 DF 4B          STX     LOW      INTEGER TO AM9511 32-BIT FLOATING
00417 3284 96 4B          LDA A  LOW      POINT FORMAT
00418 3286 84 F7          AND A  #$F7
00419 3288 97 4B          STA A  LOW
00420 328A DF 4D          STX     HIGH
00421 328C DE 4B          LDX     LOW
00422 328E A6 01          LDA A  1,X
00423 3290 97 4F          STA A  LS1
00424 3292 A6 03          LDA A  3,X
00425 3294 DE 4D          LDX     HIGH
00426 3296 E6 00          LDA B  X
00427 3298 A7 00          STA A  X
00428 329A D7 50          STA B  LS2
00429 329C A6 01          LDA A  1,X
00430 329E 97 51          STA A  LS3
00431 32A0 A6 02          LDA A  2,X
00432 32A2 A7 01          STA A  1,X
00433 32A4 A6 03          LDA A  3,X
00434 32A6 A7 02          STA A  2,X
00435 32A8 2A 2A          BPL     ZSTRT
00436                *
00437 32AA 70 004F  NEG     NEG     LS1
00438 32AD 25 16          BCS     COM2
00439 32AF 70 0050          NEG     LS2
00440 32B2 25 14          BCS     COM3
00441 32B4 70 0051          NEG     LS3
00442 32B7 25 12          BCS     COM4
00443 32B9 60 00          NEG     X
00444 32BB 25 10          BCS     COM5
00445 32BD 60 01          NEG     1,X

```

DISP

Motorola M68SAM Cross-Assembler

Page 10

```

00446 32BF 25 0E          BCS    COM6
00447 32C1 60 02          NEG    2,X
00448 32C3 20 0C          BRA    SGNST
00449                      *
00450 32C5 73 0050 COM2    COM    LS2
00451 32C8 73 0051 COM3    COM    LS3
00452 32CB 63 00    COM4    COM    X
00453 32CD 63 01    COM5    COM    1,X
00454 32CF 63 02    COM6    COM    2,X
00455 32D1 7C 004A SGNST    INC    SIGN
00456                      *
00457 32D4 96 A3    ZSTRT    LDA    A    EXP
00458 32D6 A7 03          STA    A    3,X
00459 32D8 86 06          LDA    A    #6
00460 32DA E6 02    ZTEST    LDA    B    2,X
00461 32DC 26 2E          BNE     SHIFT1
00462 32DE E6 01          LDA    B    1,X
00463 32E0 E7 02          STA    B    2,X
00464 32E2 E6 00          LDA    B    X
00465 32E4 E7 01          STA    B    1,X
00466 32E6 D6 51          LDA    B    LS3
00467 32E8 E7 00          STA    B    X
00468 32EA D6 50          LDA    B    LS2
00469 32EC D7 51          STA    B    LS3
00470 32EE D6 4F          LDA    B    LS1
00471 32F0 D7 50          STA    B    LS2
00472 32F2 7F 004F    CLR     LS1
00473                      *
00474 32F5 E6 03          LDA    B    3,X
00475 32F7 C0 08          SUB    B    #8
00476 32F9 E7 03          STA    B    3,X
00477 32FB 4A          DEC    A
00478 32FC 26 DC          BNE     ZTEST
00479 32FE 6F 03          CLR     3,X
00480 3300 39          RTS
00481                      *
00482 3301 6A 03    SHIFT    DEC     3,X
00483 3303 78 0051          ASL     LS3
00484 3306 69 00          ROL     X
00485 3308 69 01          ROL     1,X
00486 330A 69 02          ROL     2,X
00487 330C 2A F3    SHIFT1 BPL     SHIFT
00488 330E A6 03          LDA    A    3,X
00489 3310 84 7F          AND    A    #$7F
00490 3312 7D 004A          TST     SIGN
00491 3315 27 02          BEQ     DONE
00492 3317 8A 80          ORA    A    #$80
00493 3319 A7 03    DONE    STA    A    3,X
00494 331B 39          RTS
00495                      *

```

DISP

Motorola M68SAM Cross-Assembler

Page 11

```

00496          *
00497 331C A6 00   LDTOS  LDA A  X      SUBROUTINE TO LOAD FLOATING
00498 331E B7 5000      STA A  TOS      POINT NUMBER FROM LOCATION
00499 3321 A6 01      LDA A  1,X      INDICATED BY X TO TOS
00500 3323 B7 5000      STA A  TOS
00501 3326 A6 02      LDA A  2,X
00502 3328 B7 5000      STA A  TOS
00503 332B A6 03      LDA A  3,X
00504 332D B7 5000      STA A  TOS
00505 3330 39          RTS
00506          *
00507 3331 4F          CL4TOS CLR A      SUBROUTINE TO CLEAR 4 BYTES
00508 3332 B7 5000      STA A  TOS      ON TOS
00509 3335 B7 5000      STA A  TOS
00510 3338 B7 5000      STA A  TOS
00511 333B 4F          CL1TOS CLR A      SUBROUTINE TO CLEAR 1 BYTE
00512 333C B7 5000      STA A  TOS      ON TOS
00513 333F 39          RTS
00514          *
00515 3340 5F          DISCON CLR B      SUBROUTINE TO CONVERT FLOATING
00516 3341 A6 00          LDA A  X      POINT SPECTRUM VALUE TO
00517 3343 27 01          BEQ    D1      LOGARITHMIC CRT DISPLAY VALUE
00518 3345 5C          INC B
00519 3346 B7 5000 D1      STA A  TOS
00520 3349 A6 01          LDA A  1,X
00521 334B 27 01          BEQ    D2
00522 334D 5C          INC B
00523 334E B7 5000 D2      STA A  TOS
00524 3351 A6 02          LDA A  2,X
00525 3353 27 01          BEQ    D3
00526 3355 5C          INC B
00527 3356 B7 5000 D3      STA A  TOS
00528 3359 A6 03          LDA A  3,X
00529 335B 27 01          BEQ    D4
00530 335D 5C          INC B
00531 335E B7 5000 D4      STA A  TOS
00532 3361 5D          TST B
00533 3362 27 47          BEQ    DEXIT
00534 3364 7F 004A        CLR    SIGN
00535 3367 4D          TST A
00536 3368 2A 08          BPL    DPOS
00537 336A 7C 004A        INC    SIGN
00538 336D 86 15          LDA A  #$15      CHSF
00539 336F BD 33A3        JSR    CMD
00540 3372 86 08          DPOS  LDA A  #8      LOG
00541 3374 BD 33A3        JSR    CMD
00542 3377 CE 009C        LDX    #SCALE
00543 337A BD 331C        JSR    LDTOS
00544 337D 86 12          LDA A  #$12      FMUL
00545 337F BD 33A3        JSR    CMD

```

DISP

Motorola M68SAM Cross-Assembler

Page 12

```

00546 3382 86 1F          LDA A  #$1F      FIXS
00547 3384 BD 33A3        JSR      CMD
00548 3387 96 A1          LDA A  OFFSET+1
00549 3389 B7 5000        STA A  TOS
00550 338C 96 A0          LDA A  OFFSET
00551 338E B7 5000        STA A  TOS
00552 3391 86 6D          LDA A  #$6D      SSUB
00553 3393 BD 33A3        JSR      CMD
00554 3396 48            ASL A
00555 3397 2A 03          BPL      D5
00556 3399 BD 3331        JSR      CL4TOS
00557 339C 7D 004A D5     TST      SIGN
00558 339F 27 0A          BEQ      DEXIT
00559 33A1 86 74          LDA A  #$74      CHSS
00560 33A3 B7 5001 CMD     STA A  CMSTAT
00561 33A6 B6 5001 BUSY    LDA A  CMSTAT
00562 33A9 2B FB          BMI      BUSY
00563 33AB 39            DEXIT RTS
00564                      *
00565 33AC BD 3340 CHCON    JSR      DISCON  SUBROUTINE TO CONVERT A SPECTRAL
00566 33AF DE 48          LDX      DISPTR  COMPONENT TO LOG DISPLAY VALUE
00567 33B1 B6 5000        LDA A  TOS
00568 33B4 43            COM A
00569 33B5 A7 00          STA A  X
00570 33B7 B6 5000        LDA A  TOS
00571 33BA 43            COM A
00572 33BB A7 01          STA A  1,X
00573 33BD 08            INX
00574 33BE 08            INX
00575 33BF DF 48          STX      DISPTR
00576                      *
00577 33C1 DE 52 INCHAN    LDX      CHAN     SUBROUTINE TO CONVERT ALL 4
00578 33C3 08            INX               SPECTRA TO LOG DISPLAY VALUES
00579 33C4 08            INX
00580 33C5 08            INX
00581 33C6 08            INX
00582 33C7 DF 52          STX      CHAN
00583 33C9 39            RTS
00584                      *
00585 33CA CE B000 ALLCON   LDX      #$B000
00586 33CD DF 48          STX      DISPTR
00587 33CF CE B800        LDX      #$B800
00588 33D2 DF 52          STX      CHAN
00589 33D4 BD 33AC A1      JSR      CHCON
00590 33D7 8C BCOO        CPX      #$BCOO
00591 33DA 26 F8          BNE      A1
00592 33DC BD 331C A2      JSR      LDTOS
00593 33DF 86 15          LDA A  #$15      CHSF
00594 33E1 BD 33A3        JSR      CMD
00595 33E4 BD 3498        JSR      STTOS

```

DISP

Motorola M68SAM Cross-Assembler

Page 13

```

00596 33E7 BD 33AC      JSR      CHCON
00597 33EA 8C C000      CPX      #$C000
00598 33ED 26 ED        BNE      A2
00599 33EF 39          RTS
00600
00601 33F0 DE 44      *      MEAN      LDX      DATPTR      SUBROUTINE TO FIND MEAN AND
00602 33F2 DF 52          STX      CHAN      STD. DEV. OF SPECTRAL COMPONENTS
00603 33F4 DE 46          LDX      DELPTR      FOR WHICH DELETION VECTOR=1
00604 33F6 DF 58          STX      DEL
00605 33F8 7F 005A      CLR      NUM      DATPTR SPECIFIES BEGINNING OF SPECTRUM
00606 33FB BD 3331      JSR      CL4TOS
00607 33FE BD 3331      JSR      CL4TOS      DELPTR SPECIFIES BEGINNING OF
00608
00609 3401 DE 58      *      DELETION VECTOR
00610 3403 A6 00      M1      LDX      DEL
00611 3405 27 29          LDA A      X      RESPTR SPECIFIES WHERE TO STORE RESULTS
00612 3407 DE 52          BEQ      M2
00613 3409 BD 331C      LDX      CHAN
00614 340C 86 10          JSR      LDTOS
00615 340E BD 33A3      LDA A      #$10      FADD
00616 3411 86 19          JSR      CMD
00617 3413 BD 33A3      LDA A      #$19      XCHF
00618 3416 BD 331C      JSR      CMD
00619 3419 86 17          JSR      LDTOS
00620 341B BD 33A3      LDA A      #$17      PTOF
00621 341E 86 12          JSR      CMD
00622 3420 BD 33A3      LDA A      #$12      FMUL
00623 3423 86 10          JSR      CMD
00624 3425 BD 33A3      LDA A      #$10      FADD
00625 3428 86 19          JSR      CMD
00626 342A BD 33A3      LDA A      #$19      XCHF
00627 342D 7C 005A      JSR      CMD
00628
00629 3430 BD 33C1 M2      INC      NUM
00630 3433 96 59      *      JSR      INCHAN
00631 3435 4C          LDA A      DEL+1
00632 3436 97 59          INC A
00633 3438 84 7F          STA A      DEL+1
00634 343A 26 C5          AND A      #$7F
00635 343C 96 5A          BNE      M1
00636 343E B7 5000      LDA A      NUM
00637 3441 BD 333B      STA A      TOS
00638 3444 86 1D          JSR      CL1TOS
00639 3446 BD 33A3      LDA A      #$1D      FLTS
00640 3449 86 13          JSR      CMD
00641 344B BD 33A3      LDA A      #$13      FDIV
00642
00643 344E 86 17          JSR      CMD
00644 3450 BD 33A3      LDA A      #$17      PTOF
00645 3453 DE 42          JSR      CMD
                                LDX      RESPTR

```

DISP

Motorola M68SAM Cross-Assembler

Page 14

00646	3455	BD	3498	JSR	STTOS	
00647	3458	86	17	LDA A	#\$17	PTOF
00648	345A	BD	33A3	JSR	CMD	
00649	345D	86	12	LDA A	#\$12	FMUL
00650	345F	BD	33A3	JSR	CMD	
00651	3462	96	5A	LDA A	NUM	
00652	3464	B7	5000	STA A	TOS	
00653	3467	BD	333B	JSR	CL1TOS	
00654	346A	86	1D	LDA A	#\$1D	FLTS
00655	346C	BD	33A3	JSR	CMD	
00656	346F	86	12	LDA A	#\$12	FMUL
00657	3471	BD	33A3	JSR	CMD	
00658	3474	86	11	LDA A	#\$11	FSUB
00659	3476	BD	33A3	JSR	CMD	
00660	3479	96	5A	LDA A	NUM	
00661	347B	A7	04	STA A	4,X	
00662	347D	4A		DEC A		
00663	347E	B7	5000	STA A	TOS	
00664	3481	BD	333B	JSR	CL1TOS	
00665	3484	86	1D	LDA A	#\$1D	FLTS
00666	3486	BD	33A3	JSR	CMD	
00667	3489	86	13	LDA A	#\$13	FDIV
00668	348B	BD	33A3	JSR	CMD	
00669	348E	86	01	LDA A	#\$01	SQRT
00670	3490	BD	33A3	JSR	CMD	
00671	3493	08		INX		
00672	3494	08		INX		
00673	3495	08		INX		
00674	3496	08		INX		
00675	3497	08		INX		
00676	3498	B6	5000	STTOS	LDA A TOS	SUBROUTINE TO STORE TOS AT
00677	349B	A7	03		STA A 3,X	LOCATIONS INDICATED BY X
00678	349D	B6	5000		LDA A TOS	
00679	34A0	A7	02		STA A 2,X	
00680	34A2	B6	5000		LDA A TOS	
00681	34A5	A7	01		STA A 1,X	
00682	34A7	B6	5000		LDA A TOS	
00683	34AA	A7	00		STA A X	
00684	34AC	39			RTS	
00685				*		
00686	34AD	DE	44	COMP	LDX DATPTR	SUBROUTINE TO COMPARE CHANNELS
00687	34AF	DF	52		STX CHAN	TO MEAN AND DELETE THOSE BEYOND
00688	34B1	DE	46		LDX DELPTR	FACTOR*SDEV
00689	34B3	DF	58		STX DEL	
00690	34B5	DE	42		LDX RESPTR	
00691	34B7	08			INX	
00692	34B8	08			INX	
00693	34B9	08			INX	
00694	34BA	08			INX	
00695	34BB	08			INX	

DISP

Motorola M68SAM Cross-Assembler

Page 15

```

00696 34BC BD 331C      JSR    LDTOS
00697 34BF CE 0098      LDX    #FACTOR
00698 34C2 BD 331C      JSR    LDTOS
00699 34C5 86 12        LDA    A    #$12      FMUL
00700 34C7 BD 33A3      JSR    CMD
00701 34CA CE 0094      LDX    #MAX
00702 34CD BD 3498      JSR    STTOS
00703                   *
00704 34D0 CE 0094 C1    LDX    #MAX
00705 34D3 BD 331C      JSR    LDTOS
00706 34D6 DE 42        LDX    RESPTR
00707 34D8 BD 331C      JSR    LDTOS
00708 34DB DE 52        LDX    CHAN
00709 34DD BD 331C      JSR    LDTOS
00710 34E0 86 11        LDA    A    #$11      FSUB
00711 34E2 BD 33A3      JSR    CMD
00712 34E5 48          ASL    A
00713 34E6 2A 05        BPL    C2
00714 34E8 86 15        LDA    A    #$15      CHSF
00715 34EA BD 33A3      JSR    CMD
00716 34ED 86 11 C2    LDA    A    #$11      FSUB
00717 34EF BD 33A3      JSR    CMD
00718 34F2 DE 58        LDX    DEL
00719 34F4 6F 00        CLR    X
00720 34F6 48          ASL    A
00721 34F7 2B 02        BMI    C3
00722 34F9 6C 00        INC    X
00723 34FB 08 C3        INX
00724 34FC DF 58        STX    DEL
00725 34FE BD 33C1      JSR    INCHAN
00726 3501 96 59        LDA    A    DEL+1
00727 3503 84 7F        AND    A    #$7F
00728 3505 81 00        CMP    A    #$00
00729 3507 26 C7        BNE    C1
00730                   *
00731                   *
00732 3509 DE 46 COMP2  LDX    DELPTR  DELETION OF ADJACENT CHANNELS
00733 350B E6 01        LDA    B    1,X
00734 350D 17 C4        TBA
00735 350E E6 02        LDA    B    2,X
00736 3510 4D          TST    A
00737 3511 26 04        BNE    C5
00738 3513 6F 00        CLR    X
00739 3515 6F 02        CLR    2,X
00740 3517 08 C5        INX
00741 3518 DF 58        STX    DEL
00742 351A 96 59        LDA    A    DEL+1
00743 351C 84 7F        AND    A    #$7F
00744 351E 81 7E        CMP    A    #$7E
00745 3520 26 EB        BNE    C4

```

DISP

Motorola M68SAM Cross-Assembler

Page 16

```

00746 3522 39          RTS
00747                *
00748                *
00749 3523 8D 50    DISP  BSR    SWEEP    CRT DISPLAY ROUTINE
00750 3525 2B FC          BMI    DISP
00751 3527 8D 4C    DBNC  BSR    SWEEP    READS KEYBOARD, DEBOUNCES KEYS
00752 3529 2A FC          BPL    DBNC    AND INTERPRETS KEYS
00753 352B 8D 48          BSR    SWEEP
00754 352D 2A F8          BPL    DBNC
00755 352F B6 8008 KEY  LDA  A  KEYBD
00756 3532 84 1F          AND  A  #$1F
00757 3534 81 18    STRNG1 CMP  A  #$18    ONE - DISPLAY CO SPECTRUM
00758 3536 26 07          BNE    STRNG2
00759 3538 CE B000          LDX    #DCO
00760 353B DF A4          STX    DPTR
00761 353D 20 E4          BRA    DISP
00762 353F 81 19    STRNG2 CMP  A  #$19    TWO - DISPLAY QUADRATURE SPECTRUM
00763 3541 26 07          BNE    STRNG3
00764 3543 CE B100          LDX    #DQUAD
00765 3546 DF A4          STX    DPTR
00766 3548 20 D9          BRA    DISP
00767 354A 81 1A    STRNG3 CMP  A  #$1A    THREE - DISPLAY AUTO1
00768 354C 26 07          BNE    STRNG4
00769 354E CE B200          LDX    #DAUTO1
00770 3551 DF A4          STX    DPTR
00771 3553 20 CE          BRA    DISP
00772 3555 81 1B    STRNG4 CMP  A  #$1B    FOUR - DISPLAY AUTO2
00773 3557 26 07          BNE    PTEST
00774 3559 CE B300          LDX    #DAUTO2
00775 355C DF A4          STX    DPTR
00776 355E 20 C3          BRA    DISP
00777 3560 81 17    PTEST CMP  A  #$17    BLANK - STOP AND GO TO MONITOR
00778 3562 26 BF          BNE    DISP
00779 3564 86 18          LDA  A  #$18
00780 3566 B7 8020          STA  A  FCNTRL    STOP FFT PROCESSOR
00781 3569 CE 30D4          LDX    #START
00782 356C FF A048          STX    $A048    SET RESTART POINTER
00783 356F 8E A07F          LDS    #$A07F    SET STACK POINTER
00784 3572 7E E11C          JMP    $E11C    GO TO MONITOR
00785                *
00786                *
00787 3575 DE A4    SWEEP  LDX    DPTR    SUBROUTINE TO GENERATE
00788 3577 86 07          LDA  A  #7      X AND Y AXES FOR CRT
00789 3579 97 A6          STA  A  RAMPH
00790 357B 5F          RMPH  CLR  B
00791 357C A6 00    YDATA LDA  A  X
00792 357E B7 D204          STA  A  DAC3    DAC3 - Y AXIS SPECTRUM
00793 3581 A6 01          LDA  A  1,X
00794 3583 B7 D205          STA  A  DAC3+1
00795 3586 08          INX

```

DISP

Motorola M68SAM Cross-Assembler

Page 17

```

00796 3587 08          INX
00797 3588 96 A6      LDA A  RAMPH
00798 358A B7 D202    STA A  DAC2      DAC2 - X AXIS RAMP
00799 358D C0 04      RMPL  SUB B  #4
00800 358F F7 D203    STA B  DAC2+1
00801 3592 17          TBA
00802 3593 84 1F      AND A  #$1F
00803 3595 26 F6      BNE      RMPL
00804 3597 5D          TST B
00805 3598 26 E2      BNE      YDATA
00806 359A 7A 00A6    DEC      RAMPH
00807 359D 96 A6      LDA A  RAMPH
00808 359F 81 F7      CMP A  #$F7
00809 35A1 26 D8      BNE      RMPH
00810 35A3 86 07      LDA A  #7
00811 35A5 B7 D202    STA A  DAC2
00812 35A8 86 FF      LDA A  #$FF
00813 35AA B7 D203    STA A  DAC2+1
00814 35AD B7 D204    STA A  DAC3
00815 35B0 B7 D205    STA A  DAC3+1
00816                *
00817 35B3 B6 8008 PRESS LDA A  KEYBD      CHECK KEYBOARD
00818 35B6 B6 8009      LDA A  KEYBD+1
00819 35B9 39          RTS
00820                *
00821 35BA 5F          DVAND CLR B          SUBROUTINE TO COMBINE
00822 35BB CE 3F00      LDX      #DVCTR1    CO AND QUAD DELETION VECTORS
00823 35BE A6 00      DVAND1 LDA A  X
00824 35C0 A4 80          AND A  $80,X
00825 35C2 27 01      BEQ      DVAND2
00826 35C4 5C          INC B
00827 35C5 A7 00      DVAND2 STA A  X
00828 35C7 08          INX
00829 35C8 8C 3F80      CPX      #DVCTR1+$80
00830 35CB 26 F1      BNE      DVAND1
00831 35CD 39          RTS
00832                *
00833 35CE CE 006D MNOUT LDX      #MEAN1    SUBROUTINE TO OUTPUT CO AND QUAD
00834 35D1 BD 3340      JSR      DISCON    MEANS TO CHART RECORDER
00835 35D4 CE D206      LDX      #DAC4
00836 35D7 BD 35E3      JSR      DACOUT
00837 35DA CE 0076      LDX      #MEAN2
00838 35DD BD 3340      JSR      DISCON
00839 35E0 CE D208      LDX      #DAC5
00840 35E3 B6 5000 DACOUT LDA A  TOS      DAC OUTPUT SUBROUTINE
00841 35E6 43          COM A
00842 35E7 A7 00          STA A  X
00843 35E9 B6 5000      LDA A  TOS
00844 35EC 43          COM A
00845 35ED A7 01          STA A  1,X

```

DISP

Motorola M68SAM Cross-Assembler

Page 18

```

00846 35EF 39          RTS
00847                *
00848 35F0 96 A7      NOUT    LDA A   OLDN      SUBROUTINE TO OUTPUT NO. OF
00849 35F2 80 40          SUB A   #$40      CHANNELS NOT DELETED TO RECORDER
00850 35F4 5F          CLR B
00851 35F5 47          ASR A
00852 35F6 56          ROR B
00853 35F7 47          ASR A
00854 35F8 56          ROR B
00855 35F9 47          ASR A
00856 35FA 56          ROR B
00857 35FB 43          COM A
00858 35FC 53          COM B
00859 35FD B7 D20A     STA A   DAC6
00860 3600 F7 D20B     STA B   DAC6+1
00861 3603 39          RTS
00862                *
00863 3604 CE 0068      CLPOUT LDX     #CLIPS  SUBROUTINE TO OUTPUT LOG OF
00864 3607 8D 38          BSR     LR4TOS  NO. OF CLIPS TO RECORDER
00865 3609 86 34          LDA A   #$34    CHSD
00866 360B BD 33A3       JSR     CMD
00867 360E 86 1C          LDA A   #$1C    FLTD
00868 3610 BD 33A3       JSR     CMD
00869 3613 86 08          LDA A   #8      LOG
00870 3615 BD 33A3       JSR     CMD
00871 3618 CE 3639       LDX     #KMUL
00872 361B BD 331C       JSR     LDTOS
00873 361E 86 12          LDA A   #$12    FMUL
00874 3620 BD 33A3       JSR     CMD
00875 3623 CE 363D       LDX     #KSUB
00876 3626 BD 331C       JSR     LDTOS
00877 3629 86 11          LDA A   #$11    FSUB
00878 362B BD 33A3       JSR     CMD
00879 362E 86 1F          LDA A   #$1F    FIXS
00880 3630 BD 33A3       JSR     CMD
00881 3633 CE D20C       LDX     #DAC7
00882 3636 7E 35E3       JMP     DACOUT
00883                *
00884 3639 00          KMUL    FCB     0,0,$80,$0A
          363A 00
          363B 80
          363C 0A
00885 363D 00          KSUB    FCB     0,0,$80,$0C
          363E 00
          363F 80
          3640 0C
00886                *
00887 3641 A6 03      LR4TOS  LDA A   3,X      SUBROUTINE TO LOAD TOS FROM
00888 3643 B7 5000     STA A   TOS      LOCATIONS INDICATED BY X
00889 3646 A6 02      LDA A   2,X      IN REVERSE ORDER

```

DISP

Motorola M68SAM Cross-Assembler

Page 19

```

00890 3648 B7 5000          STA A  TOS
00891 364B A6 01  LR2TOS LDA A  1,X
00892 364D B7 5000          STA A  TOS
00893 3650 A6 00  LR1TOS LDA A  X
00894 3652 B7 5000          STA A  TOS
00895 3655 39              RTS
00896                      *
00897 3656 BD 3331 FRQOUT JSR      CL4TOS  SUBROUTINE TO OUTPUT L.O.
00898 3659 D6 65              LDA B  FREQ  FREQUENCY TO RECORDER
00899 365B C4 3F              AND B  #$3F
00900 365D 8D 26              BSR      UNPCK
00901 365F D6 66              LDA B  FREQ+1
00902 3661 8D 22              BSR      UNPCK
00903 3663 D6 67              LDA B  FREQ+2
00904 3665 8D 26              BSR      DIGITH
00905 3667 CE 3681          LDX      #FRQSUB
00906 366A 8D DF              BSR      LR2TOS
00907 366C 86 6D              LDA A  #$6D      SSUB
00908 366E BD 33A3          JSR      CMD
00909 3671 CE 3683          LDX      #FRQMUL
00910 3674 8D D5              BSR      LR2TOS
00911 3676 86 6E              LDA A  #$6E      SMUL
00912 3678 BD 33A3          JSR      CMD
00913 367B CE D20E          LDX      #DAC8
00914 367E 7E 35E3          JMP      DACOUT
00915                      *
00916 3681 0000          FRQSUB FDB      $0000
00917 3683 0001          FRQMUL FDB      $0001
00918                      *
00919 3685 37              UNPCK  PSH B              SUBROUTINE TO CONVERT PACKED
00920 3686 8D 05              BSR      DIGITH  BCD NUMBER TO BINARY
00921 3688 33              PUL B
00922 3689 C4 0F              AND B  #$0F
00923 368B 20 04              BRA      DIGITL
00924                      *
00925                      *
00926 368D 54              DIGITH LSR B
00927 368E 54              LSR B
00928 368F 54              LSR B
00929 3690 54              LSR B
00930 3691 86 0A          DIGITL LDA A  #$0A
00931 3693 B7 5000          STA A  TOS
00932 3696 BD 333B          JSR      CL1TOS
00933 3699 86 6E              LDA A  #$6E      SMUL
00934 369B BD 33A3          JSR      CMD
00935 369E F7 5000          STA B  TOS
00936 36A1 BD 333B          JSR      CL1TOS
00937 36A4 86 6C              LDA A  #$6C      SADD
00938 36A6 7E 33A3          JMP      CMD
00939                      *

```

DISP

Motorola M68SAM Cross-Assembler

Page 20

```

00940 36A9 DE 92  IRACIA LDX  CASPTR  ROUTINE FOR TAPE RECORDER OUTPUT
00941 36AB 96 92          LDA  A  CASPTR
00942 36AD 26 0F          BNE     SPECT  CHECK IF HEADER OR SPECTRA
00943 36AF 8C 006C        CPX    #HEAD+17
00944 36B2 26 1B          BNE     WRITE
00945 36B4 86 1C          LDA  A  #$1C  ENABLE 1 HZ INTERRUPTS
00946 36B6 B7 8043        STA  A  HZ+1  WHEN HEADER COMPLETED
00947 36B9 CE B800        LDX    #CO
00948 36BC DF 92          STX    CASPTR  SET POINTER TO CO SPECTRUM
00949                                *
00950 36BE 8C C000 SPECT  CPX    #$C000  CHECK IF ALL SPECTRA COMPLETED
00951 36C1 27 19          BEQ     CSOUT
00952 36C3 8C C001        CPX    #$C001
00953 36C6 27 1F          BEQ     CASSTP
00954 36C8 96 93          LDA  A  CASPTR+1  CHECK IF ADDRESS IS EVEN OR ODD
00955 36CA 44          LSR  A
00956 36CB 25 02          BCS     WRITE  IF EVEN, INC. X TWICE TO SKIP
00957 36CD 08          INX          LAST TWO BYTES OF SPECTRAL COMPONENT
00958 36CE 08          INX
00959                                *
00960 36CF E6 00  WRITE  LDA  B  X  OUTPUT BYTE INDICATED BY X
00961 36D1 F7 8011        STA  B  ACIATR
00962 36D4 DB 91          ADD  B  CKSM
00963 36D6 D7 91          STA  B  CKSM
00964 36D8 08          INX
00965 36D9 DF 92          STX    CASPTR
00966 36DB 3B          RTI
00967                                *
00968 36DC D6 91  CSOUT  LDA  B  CKSM  OUTPUT CHECKSUM
00969 36DE C0 DD          SUB  B  #$DD
00970 36E0 F7 8011        STA  B  ACIATR
00971 36E3 08          INX
00972 36E4 DF 92          STX    CASPTR
00973 36E6 3B          RTI
00974                                *
00975 36E7 C6 1D  CASSTP  LDA  B  #$1D  DISABLE TAPE INTERRUPTS
00976 36E9 F7 8010        STA  B  ACIACR  AND TURN TAPE OFF
00977 36EC C6 34          LDA  B  #$34
00978 36EE F7 8007        STA  B  RDRCTL
00979 36F1 3B          RTI
00980                                *
00981 36F2 B6 8042  IRQHZ  LDA  A  HZ  1 HZ CLOCK ROUTINE
00982 36F5 96 61          LDA  A  TIME+2  COUNTS SECONDS, MINUTES, AND HOURS
00983 36F7 8B 01          ADD  A  #1  FOR TIME OF DAY
00984 36F9 19          DAA
00985 36FA 97 61          STA  A  TIME+2
00986 36FC 81 60          CMP  A  #$60
00987 36FE 25 1F          BCS     IRQHZ1
00988 3700 7F 0061        CLR    TIME+2
00989 3703 96 60          LDA  A  TIME+1

```

DISP

Motorola M68SAM Cross-Assembler

Page 21

```

00990 3705 8B 01      ADD A  #1
00991 3707 19        DAA
00992 3708 97 60     STA A  TIME+1
00993 370A 81 60     CMP A  #$60
00994 370C 25 11     BCS    IRQHZ1
00995 370E 7F 0060   CLR    TIME+1
00996 3711 96 5F     LDA A  TIME
00997 3713 8B 01     ADD A  #1
00998 3715 19        DAA
00999 3716 97 5F     STA A  TIME
01000 3718 81 24     CMP A  #$24
01001 371A 25 03     BCS    IRQHZ1
01002 371C 7F 005F   CLR    TIME
01003 371F 3B        IRQHZ1 RTI
01004                *
01005 3720 05        K10E8  FCB    5,$F5,$E1,O
        3721 F5
        3722 E1
        3723 00
01006 3724 00        K10E6  FCB    0,$F,$42,$40
        3725 0F
        3726 42
        3727 40
01007 3728 00        K10E4  FCB    0,O,$27,$10
        3729 00
        372A 27
        372B 10
01008 372C 00        K10E2  FCB    0,O,O,$64
        372D 00
        372E 00
        372F 64
01009                *
01010 3730 BD 3641  BYTE4  JSR    LR4TOS  SUBROUTINE TO PRINT NO. OF CLIPS
01011 3733 86 34      LDA A  #$34      CHSD
01012 3735 BD 33A3     JSR    CMD       CONVERTS COMPLEMENT OF 4 BYTE
01013 3738 CE 3720     LDX    #K10E8   INTEGER TO DECIMAL FOR PRINTING
01014 373B 86 37      BYTE41 LDA A  #$37  PTOD
01015 373D BD 33A3     JSR    CMD
01016 3740 BD 3641     JSR    LR4TOS
01017 3743 86 2F      LDA A  #$2F      DDIV
01018 3745 BD 33A3     JSR    CMD
01019 3748 86 37      LDA A  #$37      PTOD
01020 374A BD 33A3     JSR    CMD
01021 374D 8D 16      BSR    STKLST
01022                *
01023 374F BD 3641     JSR    LR4TOS
01024 3752 86 2E      LDA A  #$2E      DMUL
01025 3754 BD 33A3     JSR    CMD
01026 3757 86 2D      LDA A  #$2D      DSUB
01027 3759 BD 33A3     JSR    CMD

```

DISP

Motorola M68SAM Cross-Assembler

Page 22

```

01028 375C 08          INX
01029 375D 08          INX
01030 375E 08          INX
01031 375F 08          INX
01032 3760 8C 3730     CPX      #K10E2+4
01033 3763 26 D6       BNE      BYTE41
01034 3765 F6 5000 STKLST LDA B   TOS
01035 3768 F6 5000     LDA B   TOS
01036 376B F6 5000     LDA B   TOS
01037 376E F6 5000     LDA B   TOS
01038 3771 20 56       BRA      INT2
01039
01040 3773 86 0D       PRINT LDA A   #$0D      SUBROUTINE TO PRINT TIME,
01041 3775 BD 37FO     JSR      OUTCH      L.O. FREQUENCY, NO. OF CLIPS,
01042 3778 86 0A       LDA A   #$0A      AND NO. OF CHANNELS NOT DELETED
01043 377A BD 37FO     JSR      OUTCH
01044 377D 96 5F       LDA A   TIME
01045 377F BD 37DC     JSR      OUT2H
01046 3782 86 3A       LDA A   #$3A      :
01047 3784 BD 37FO     JSR      OUTCH
01048 3787 96 60       LDA A   TIME+1
01049 3789 BD 37DC     JSR      OUT2H
01050 378C 86 3A       LDA A   #$3A      :
01051 378E BD 37FO     JSR      OUTCH
01052 3791 96 61       LDA A   TIME+2
01053 3793 BD 37DC     JSR      OUT2H
01054 3796 86 20       LDA A   #$20      SP
01055 3798 BD 37FO     JSR      OUTCH
01056
01057 379B 96 65       LDA A   FREQ
01058 379D BD 37DC     JSR      OUT2H
01059 37A0 96 66       LDA A   FREQ+1
01060 37A2 BD 37DC     JSR      OUT2H
01061 37A5 96 67       LDA A   FREQ+2
01062 37A7 BD 37E2     JSR      OUTHL
01063 37AA 86 20       LDA A   #$20      SP
01064 37AC BD 37FO     JSR      OUTCH
01065 37AF CE 0068     LDX      #CLIPS
01066 37B2 BD 3730     JSR      BYTE4
01067 37B5 86 20       LDA A   #$20      SP
01068 37B7 BD 37FO     JSR      OUTCH
01069 37BA D6 A7       LDA B   OLDN
01070
01071 37BC 4F          INTOUT CLR A
01072 37BD 4C          INT1  INC A      SUBROUTINE FOR 1 BYTE BINARY
01073 37BE C0 64       SUB B   #$64      TO DECIMAL CONVERSION AND PRINTING
01074 37C0 24 FB       BCC      INT1
01075 37C2 CB 64       ADD B   #$64
01076 37C4 8B 2F       ADD A   #$2F
01077 37C6 BD 37FO     JSR      OUTCH

```

DISP

Motorola M68SAM Cross-Assembler

Page 23

```

01078 37C9 4F      INT2  CLR A
01079 37CA 4C      INT3  INC A
01080 37CB C0 0A      SUB B  #$0A
01081 37CD 24 FB      BCC  INT3
01082 37CF CB 0A      ADD B  #$0A
01083 37D1 8B 2F      ADD A  #$2F
01084 37D3 BD 37FO     JSR  OUTCH
01085 37D6 17      TBA
01086 37D7 8B 30      ADD A  #$30
01087 37D9 7E 37FO     JMP  OUTCH
01088                *
01089 37DC 36      OUT2H PSH A      OUTPUT HEX BYTE AS 2 ASCII
01090 37DD 8D 03      BSR  OUTHL  CHARACTERS
01091 37DF 32      PUL A
01092 37E0 20 04      BRA  OUTHR
01093 37E2 44      OUTHL LSR A
01094 37E3 44      LSR A
01095 37E4 44      LSR A
01096 37E5 44      LSR A
01097 37E6 84 0F      OUTHR AND A  #$0F
01098 37E8 8B 30      ADD A  #$30
01099 37EA 81 39      CMP A  #$39
01100 37EC 23 02      BLS  OUTCH
01101 37EE 8B 07      ADD A  #7
01102                *
01103 37F0 37      OUTCH PSH B      OUTPUT ONE ASCII CHARACTER
01104 37F1 FF AOOF     STX  XTMP
01105 37F4 CE 8004     LDX  #TTYPIA
01106 37F7 C6 0A      IOUT  LDA B  #$0A
01107 37F9 6A 00      DEC  X
01108 37FB 8D 19      BSR  DE
01109 37FD 8D 13      IOUT1 BSR  DEL1
01110 37FF A7 00      STA A  X
01111 3801 0D      SEC
01112 3802 46      ROR A
01113 3803 5A      DEC B
01114 3804 26 F7      BNE  IOUT1
01115 3806 E6 02      IOUT2 LDA B  2,X
01116 3808 58      ASL B
01117 3809 2A 02      BPL  IOS
01118 380B 8D 05      BSR  DEL1
01119 380D FE AOOF IOS  LDX  XTMP
01120 3810 33      PUL B
01121 3811 39      RTS
01122                *
01123 3812 6D 02      DEL1 TST  2,X
01124 3814 2A FC      BPL  DEL1
01125 3816 6C 02      DE    INC  2,X
01126 3818 6A 02      DEC  2,X
01127 381A 39      RTS

```

DISP

Motorola M68SAM Cross-Assembler

Page 24

```

01128      *
01129 381B 96 AC      CHFREQ LDA A   NFREQ+2
01130 381D 97 67      STA A   FREQ+2
01131 381F 9B B5      ADD A   FINC+2
01132 3821 19      DAA
01133 3822 97 AC      STA A   NFREQ+2
01134 3824 96 AB      LDA A   NFREQ+1
01135 3826 97 66      STA A   FREQ+1
01136 3828 99 B4      ADC A   FINC+1
01137 382A 19      DAA
01138 382B 97 AB      STA A   NFREQ+1
01139 382D 96 AA      LDA A   NFREQ
01140 382F 97 65      STA A   FREQ
01141 3831 99 B3      ADC A   FINC
01142 3833 19      DAA
01143 3834 97 AA      STA A   NFREQ
01144      *
01145 3836 91 AD      CMP A   FMAX
01146 3838 26 OE      BNE     SYNTH
01147 383A DE AB      LDX     NFREQ+1
01148 383C 9C AE      CPX     FMAX+1
01149 383E 26 08      BNE     SYNTH
01150      *
01151 3840 DE B1      INFREQ LDX     FMIN+1
01152 3842 DF AB      STX     NFREQ+1
01153 3844 96 B0      LDA A   FMIN
01154 3846 97 AA      STA A   NFREQ
01155      *
01156 3848 DE AB      SYNTH  LDX     NFREQ+1
01157 384A FF 4001      STX     LATCH+1
01158 384D 96 AA      LDA A   NFREQ
01159 384F B7 4000      STA A   LATCH
01160 3852 8A 80      ORA A   #$80
01161 3854 B7 4000      STA A   LATCH
01162 3857 84 7F      AND A   #$7F
01163 3859 B7 4000      STA A   LATCH
01164 385C 39      RTS
01165      *
01166      END

```

Appendix 4 - Robust Estimation Program

The following is a listing of the FORTRAN program used for robust maximum-likelihood estimation on the recorded spectra.


```

1      C      PROGRAM READS RAW SPECTRA FROM UNIT 7,
2      C      WRITES RESULTS ON UNIT 6.
3      C      PERFORMS 3 SIGMA ROBUST ESTIMATION' ON AUTO SPECTRA.
4      C      ESTIMATES VARIANCE OF CROSS SPECTRA FROM FIRST DECILES
5      C      OF AUTO SPECTRA.
6      C      FINDS ROBUST LOCATION ESTIMATE FOR CROSS SPECTRA
7      C      USING PROCEDURE COMBINING REJECTION, HUBER ESTIMATION
8      C      AND BIWEIGHT ESTIMATION.
9      C      RECORDS ESTIMATES PLUS NUMBERS OF OUTLIERS FOUND AND TOTAL
10     C      ABSOLUTE POWER DELETED.
11     C
12     C      VARIABLES USED:
13     C      AMEAN(4) - MEANS
14     C      CLIPS - COMPLEMENT OF NUMBER OF CLIPS RECORDED DURING SPECTRUM
15     C      CLP - NUMBER OF CLIPS
16     C      ERR - INDICATOR FOR RECORDING ERROR
17     C      FILE - FILE NUMBER FOR SPECTRUM
18     C      FREQ - SECOND LOCAL OSCILLATOR FREQUENCY
19     C      ICRIT(4) - CRITERIA SATISFIED DURING ESTIMATIONS ITERATIONS
20     C      IER - ERROR INDICATOR FOR SUBROUTINE BEIUGR
21     C      IOPT(5) - CONTROL CODES FOR SUBROUTINE BEIUGR
22     C      IPERM(108,2) - VECTORS FOR PERMUTATIONS OF CROSS SPECTRA
23     C                        DURING ORDERING
24     C      NDEL(2) - NUMBER OF DELETION ITERATIONS
25     C      NOUT(2) - NUMBER OF OUTLIERS
26     C      PSI(600,2) - PSI FUNCTIONS FOR ROBUST MAXIMUM LIKELIHOOD ESTIMATION
27     C                        1 - BIWEIGHT  2 - HUBER
28     C      R(512) - ARRAY FOR FORMAT CONVERSION OF SPECTRA
29     C      S(108) - TEMPORARY STORAGE FOR ORDERED AUTO SPECTRA
30     C      SDEV(4) - STANDARD DEVIATIONS
31     C      SPECT(126,4) - RAW SPECTRA 1-IN PHASE, 2-QUADRATURE, 3,4-AUTO
32     C      SPORD(108,2 ) - ORDERED CROSS SPECTRA 1-IN PHASE, 2-QUADRATURE
33     C      SQ(108,2) - SQUARES OF AUTO SPECTRAL COMPONENTS
34     C      STAT(5) - MEAN,MAX,MIN,MEDIAN,VARIANCE
35     C      STRES(6,4) - ARRAY OF STATISTICS OF SPECTRA
36     C      SUM(2) - SUMS FOR STANDARD DEVIATION CALCULATIONS
37     C      THETA(2) - ROBUST LOCATION ESTIMATES
38     C      TOLD(2) - PREVIOUS LOCATION ESTIMATES
39     C      X(600) - INCREMENTAL X VALUES FOR PSI FUNCTION GENERATION
40     C      TIME - TIME WHEN SPECTRUM WAS RECORDED
41     C      DER(600,2) - DERIVATIVES OF PSI FUNCTIONS
42     C      IDV(108) - VECTOR INDICATING DELETED POINTS
43     C      REAL AMEAN(4),SDEV(4),X(600),TOLD(2),SUM(2)
44     C      INTEGER IPERM(108,2),ICRIT(4),NOUT(2),NDEL(2)
45     C      INTEGER CLP,IOPT(5)/1,0,0,1,1/,IER
46     C      REAL S(108),STAT(5),STRES(6,4),SQ(108,2)
47     C      INTEGER ERR,FILE,TIME,INT,FREQ,CLIPS
48     C      REAL SPECT(126,4),R(512)
49     C      EQUIVALENCE (ERR,R(1)),(FILE,R(2)),(TIME,R(3)),(INT,R(4))
50     C      EQUIVALENCE (FREQ,R(5)),(CLIPS,R(6)),(SPECT(1,1),R(7))
51     C      REAL PSI(600,2),DER(600,2),THETA(2),SPORD(108,2)
52     C      INTEGER IDV(108)
53     C      COMMON PSI,DER,THETA,SPORD,IDV
54     C
55     C      GENERATE HUBER AND BIWEIGHT INFLUENCE CURVES
56     C      AND THEIR DERIVATIVES
57     C
58     C      H=0.1000E-01
59     C      DO 5 I=1,600
60     5      X(I)=(I-1)*H

```



```

61      DO 7 I=1,500
62      7      PSI(I,1)=X(I)*(1.0-(X(I)/5.）**2)**2
63      DO 8 I=501,600
64      8      PSI(I,1)=0.0
65      DO 9 I=1,150
66      9      PSI(I,2)=X(I)
67      DO 10 I=151,600
68      10     PSI(I,2)=1.5
69      CALL DERIV(PSI(1,1),DER(1,1))
70      CALL DERIV(PSI(1,2),DER(1,2))
71      C
72      C      READ A RECORD
73      C
74      20     READ(7,30,END=99)(R(I),I=1,512)
75      30     FORMAT(32A4)
76      IF(ERR.NE.0)GO TO 20
77      CLP=-CLIPS-1
78      WRITE(6,40)FILE,TIME,INT,FREQ,CLP
79      40     FORMAT('O',Z2,2X,Z6,2X,Z6,2X,Z6,2X,I10)
80      C
81      C      FIND MEAN,STD DEV,MEDIAN,FIRST DECILE,
82      C      MAX AND MIN FOR AUTO SPECTRA
83      C
84      DO 80 I=3,4
85      DO 50 J=1,108
86      50     S(J)=SPECT(J+9,I)
87      CALL VSRTA(S,108)
88      C      IMSL LIBRARY SUBROUTINE FOR ORDERING ACCORDING TO SIZE
89      CALL BEIUGR(S,108,IOPT,STAT,IER)
90      C      IMSL LIBRARY SUBROUTINE FOR FINDING STATISTICS
91      STRES(1,I)=STAT(1)
92      STRES(2,I)=SQRT(STAT(5))
93      STRES(3,I)=STAT(4)
94      STRES(4,I)=S(11)
95      STRES(5,I)=S(108)
96      STRES(6,I)=S(1)
97      WRITE(6,70)(STRES(J,I),J=1,6)
98      70     FORMAT(' ',6(E10.4,2X))
99      80     CONTINUE
100     C
101     C      CHANNEL DELETIONS FOR AUTO SPECTRA
102     C
103     DO 170 I=1,2
104     K=I+2
105     DO 90 J=1,108
106     90     SQ(J,I)=SPECT(J+9,K)**2
107     C
108     C      INITIALIZE MEAN AND STD DEV
109     C
110     AMEAN(K)=STRES(3,K)
111     SDEV(K)=STRES(2,K)
112     ITER=0
113     NLAST=108
114     C
115     C      DELETE CHANNELS
116     C
117     100     DMAX=3.*SDEV(K)
118     ITER=ITER+1
119     DO 110 J=1,108
120     IDV(J)=1

```



```

121      110      IF (ABS(SPECT(J+9,K)-AMEAN(K)).GT.DMAX)IDV(J)=0
122      C
123      C      DELETE ADJACENT CHANNELS
124      C
125              NOW=IDV(2)
126              IF (IDV(1).EQ.O)IDV(2)=O
127              DO 130 J=2,107
128              NEXT=IDV(J+1)
129              IF (NOW.NE.O)GO TO 120
130              IDV(J-1)=O
131              IDV(J+1)=O
132      120      NOW=NEXT
133      130      CONTINUE
134              IF (NOW.EQ.O)IDV(107)=O
135      C
136      C      FIND MEAN,STD DEV,AND NO. OF CHANNELS AFTER DELETIONS
137      C
138              NCHAN=O
139              SUMM=O.
140              SUMS=O.
141              DO 140 J=1,108
142              IF (IDV(J).EQ.O)GO TO 140
143              SUMM=SUMM+SPECT(J+9,K)
144              SUMS=SUMS+SQ(J,I)
145              NCHAN=NCHAN+1
146      140      CONTINUE
147              AMEAN(K)=SUMM/NCHAN
148              SDEV(K)=SQRT((SUMS-(SUMM**2)/NCHAN)/NCHAN)
149              IF (NCHAN.EQ.NLAST)GO TO 150
150              IF (ITER.GT.20)GO TO 150
151              NLAST=NCHAN
152              GO TO 100
153      C
154      C      WRITE RESULTS
155      C
156      150      WRITE(6,160)AMEAN(K),SDEV(K),NCHAN,ITER
157      160      FORMAT(' ',E10.4,2X,E10.4,2X,I3,2X,I2)
158      170      CONTINUE
159      C
160      C      FIND MEAN, STD DEV, MEDIAN,MAX AND MIN FOR CROSS SPECTRA
161      C
162              DO 210 I=1,2
163              DO 200 J=1,108
164              SPORD(J,I)=SPECT(J+9,I)
165              IPERM(J,I)=J
166      200      CONTINUE
167              CALL VSRTR(SPORD(1,I),108,IPERM(1,I))
168              CALL BEIUGR(SPORD(1,I),108,IOPT,STAT,IER)
169              STRES(1,I)=STAT(1)
170              STRES(2,I)=SQRT(STAT(5))
171              STRES(3,I)=STAT(4)
172              STRES(4,I)=O.O
173              STRES(5,I)=SPORD(108,I)
174              STRES(6,I)=SPORD(1,I)
175              WRITE(6,70)(STRES(J,I),J=1,6)
176      210      CONTINUE
177      C
178      C      ESTIMATE SIGX AND NORMALIZE SPECTRA
179      C
180              SIGX=(1.+1.3/SQRT(FLOAT(INT)))*

```



```

181      .SQRT(STRES(4,3)*STRES(4,4)/(2.*INT))
182      DO 230 I=1,2
183      DO 220 J=1,108
184      220 SPORD(J,I)=SPORD(J,I)/SIGX
185      230 THETA(I)=STRES(3,I)/SIGX
186      C
187      C      INITIALIZE DELETION VECTOR
188      C
189      DO 240 J=1,108
190      240 IDV(J)=1
191      ITDEL=0
192      NMAX=0
193      NDEL(1)=0
194      NDEL(2)=0
195      C
196      C      FIND NUMBER OF REMAINING CHANNELS AND STD DEV
197      C
198      250 NCHAN=0
199      SUM(1)=0.0
200      SUM(2)=0.0
201      DO 260 J=1,108
202      IF(IDV(J).EQ.0)GO TO 260
203      NCHAN=NCHAN+1
204      SUM(1)=SUM(1)+(SPORD(J,1)-THETA(1))**2
205      SUM(2)=SUM(2)+(SPORD(J,2)-THETA(2))**2
206      260 CONTINUE
207      IF(NCHAN.GT.0)GO TO 270
208      SDEV(1)=0.0
209      SDEV(2)=0.0
210      GO TO 275
211      270 SDEV(1)=SQRT(SUM(1)/NCHAN)
212      SDEV(2)=SQRT(SUM(2)/NCHAN)
213      275 DO 280 J=1,4
214      280 ICRIT(J)=0
215      C
216      C      CHECK CRITERIA FOR END OF DELETIONS
217      C
218      IF(SDEV(1).LE.1.25)ICRIT(1)=1
219      IF(SDEV(2).LE.1.25)ICRIT(2)=1
220      IF(NDEL(1).LT.NMAX)ICRIT(3)=1
221      IF(NDEL(2).LT.NMAX)ICRIT(4)=1
222      IF((ICRIT(1)+ICRIT(2)).EQ.2)GO TO 400
223      IF((ICRIT(3)+ICRIT(4)).EQ.2)GO TO 400
224      ITDEL=ITDEL+1
225      NMAX=NMAX+5
226      ITER=0
227      C
228      C      REINITIALIZE DELETION VECTOR
229      C
230      285 DO 290 J=1,108
231      290 IDV(J)=1
232      C
233      C      START DELETIONS WITH SPECTRUM HAVING LARGEST STD DEV
234      C
235      I=2
236      IF(SDEV(2).GT.SDEV(1))I=1
237      295 I=MOD(I,2)+1
238      C
239      C      FIND MAXIMUM OUTLIER
240      C

```



```

241      NDEL(I)=0
242      300      DO 310 J=1,108
243              K=J
244              IF(IDV(K).NE.O)GO TO 320
245              310      CONTINUE
246                  GO TO 370
247              320      SMIN=THETA(I)-SPORD(K,I)
248                  DO 330 J=1,108
249                      L=109-J
250                      IF(IDV(L).NE.O)GO TO 340
251                      330      CONTINUE
252                          GO TO 370
253              340      SMAX=SPORD(L,I)-THETA(I)
254                  IF(SMAX.GE.SMIN)GO TO 350
255                  SMAX=SMIN
256                  L=K
257      C
258      C      CHECK IF MAX OUTLIER EXCEEDS DELETION CRITERION
259      C
260      350      IF(SMAX.LT.6.O)GO TO 370
261          NDEL(I)=NDEL(I)+1
262      C
263      C      DELETE OUTLIER PLUS ADJACENT CHANNELS
264      C
265          IDV(L)=O
266          IORIG=IPERM(L,I)
267          NADJ=1
268          IF(SMAX.GE.10.)NADJ=2
269          DO 360 J=1,108
270              IF(IABS(IPERM(J,I)-IORIG).LE.NADJ)IDV(J)=O
271      360      CONTINUE
272      C
273      C      DELETE MORE IF MAXIMUM ALLOWED NOT REACHED
274      C
275          IF(NDEL(I).LT.NMAX)GO TO 300
276      370      ITER=ITER+1
277      C
278      C      CHECK IF BOTH SPECTRA DONE
279      C
280          IF(MOD(ITER,2).EQ.1)GO TO 295
281          TOLD(1)=THETA(1)
282          TOLD(2)=THETA(2)
283      C
284      C      FIND HUBER ESTIMATES
285      C
286          CALL MEST(2)
287      C
288      C      CHECK IF MAX NUMBER OF ITERATIONS ALLOWED EXCEEDED
289      C
290          IF(ITER.GE.6)GO TO 250
291      C
292      C      CHECK IF ESTIMATES HAVE CONVERGED
293      C
294          IF(ABS(THETA(1)-TOLD(1)).GT.O.1)GO TO 285
295          IF(ABS(THETA(2)-TOLD(2)).GT.O.1)GO TO 285
296          GO TO 250
297      C
298      C      WHEN DELETIONS COMPLETED, WRITE RESULTS
299      C
300      400      AMEAN(1)=THETA(1)*SIGX

```



```

301      AMEAN(2)=THETA(2)*SIGX
302      SDEV(1)=SDEV(1)*SIGX
303      SDEV(2)=SDEV(2)*SIGX
304      WRITE(6,410)ITDEL,NCHAN,(ICRIT(I),I=1,4),SIGX,
305      .(AMEAN(I),SDEV(I),I=1,2)
306      410  FORMAT(' ',I2,1X,I3,1X,4I1,5(2X,E10.4))
307      C
308      C      FIND BIWEIGHT ESTIMATES
309      C
310      CALL MEST(1)
311      C
312      C      FIND NO. OF OUTLIERS AND TOTAL ABSOLUTE POWER DELETED
313      C
314      DO 440 I=1,2
315      NOUT(I)=0
316      SMIN=THETA(I)-5.0
317      SMAX=THETA(I)+5.0
318      SUM(I)=0.0
319      DO 430 J=1,108
320      IF(IDV(J).EQ.0)GO TO 420
321      IF(SPORD(J,I).LE.SMIN)GO TO 420
322      IF(SPORD(J,I).LT.SMAX)GO TO 430
323      420  NOUT(I)=NOUT(I)+1
324      SUM(I)=SUM(I)+ABS(SPORD(J,I)-THETA(I))
325      430  CONTINUE
326      440  CONTINUE
327      SUM(1)=SUM(1)*SIGX
328      SUM(2)=SUM(2)*SIGX
329      AMEAN(1)=THETA(1)*SIGX
330      AMEAN(2)=THETA(2)*SIGX
331      WRITE(6,450)(AMEAN(I),NOUT(I),SUM(I),I=1,2)
332      450  FORMAT(' ',2(E10.4,2X,I3,2X,E10.4,2X))
333      GO TO 20
334      99  CONTINUE
335      RETURN
336      END
337      C
338      C      SUBROUTINE TO PERFORM ROBUST MAXIMUM LIKELIHOOD ESTIMATION
339      SUBROUTINE MEST(NPSI)
340      REAL PSI(600,2),DER(600,2),THETA(2),SPORD(108,2)
341      INTEGER IDV(108)
342      COMMON PSI,DER,THETA,SPORD,IDV
343      DO 30 I=1,2
344      ITER=0
345      T=THETA(I)
346      5  SUMM=0.0
347      SUMD=0.0
348      DO 10 J=1,108
349      IF(IDV(J).EQ.0)GO TO 10
350      U=(SPORD(J,I)-T)*100.
351      INDEX=IFIX(ABS(U)+0.5)+1
352      IF(INDEX.GT.600)INDEX=600
353      SUMM=SUMM+SIGN(PSI(INDEX,NPSI),U)
354      SUMD=SUMD+DER(INDEX,NPSI)
355      10  CONTINUE
356      IF(SUMD.LT.1.0)SUMD=1.0
357      DELTA=SUMM/AMAX1(SUMD,5.0)
358      T=T+DELTA
359      ITER=ITER+1
360      IF(ITER.GT.10)GO TO 20

```



```

361      IF(ABS(DELTA).GT.0.01)GO TO 5
362      20  THETA(I)=T
363      30  CONTINUE
364      RETURN
365      END
366      C
367      C  SUBROUTINE TO FIND DERIVATIVE OF PSI FUNCTION
368      SUBROUTINE DERIV(PSI,DER)
369      REAL PSI(600),DER(600)
370      H=0.1000E-01
371      DER(1)=(PSI(2)-PSI(1))/H
372      DER(600)=(PSI(600)-PSI(599))/H
373      DO 10 I=2,599
374      10  DER(I)=(PSI(I+1)-PSI(I-1))/(2.*H)
375      RETURN
376      END
END OF FILE

```


Appendix 5 - FFT Processor Schematics

The schematics and IC lists are organized in accordance with the associated circuit boards. The circuit boards and their designating letters are the Window Board (W), the Butterfly Processor (F), the Power Computation Board (P), and the Accumulation Board (A).

IC Numbers for Window Board

U200	7428
U201	74LS30
U202	74LS30
U203	7404
U204	74LS157

U205	74LS157
U206	74LS365
U207	74LS365
U208	25LS22
U209	25LS14

U210	25LS15
U211	74LS02
U212	74S04
U213	74S00
U214	74LS138

U215	74LS293
U216	CD4002
U217	74LS03
U218	74S00
U219	74S74

U220	74S112
U221	74LS14
U222	74C164
U223	CD4030
U224	CD4027

U225	MC6810
U226	CD4030
U227	CD4030
U228	74C161
U229	74C161

U230	CD4013
U231	CD4015

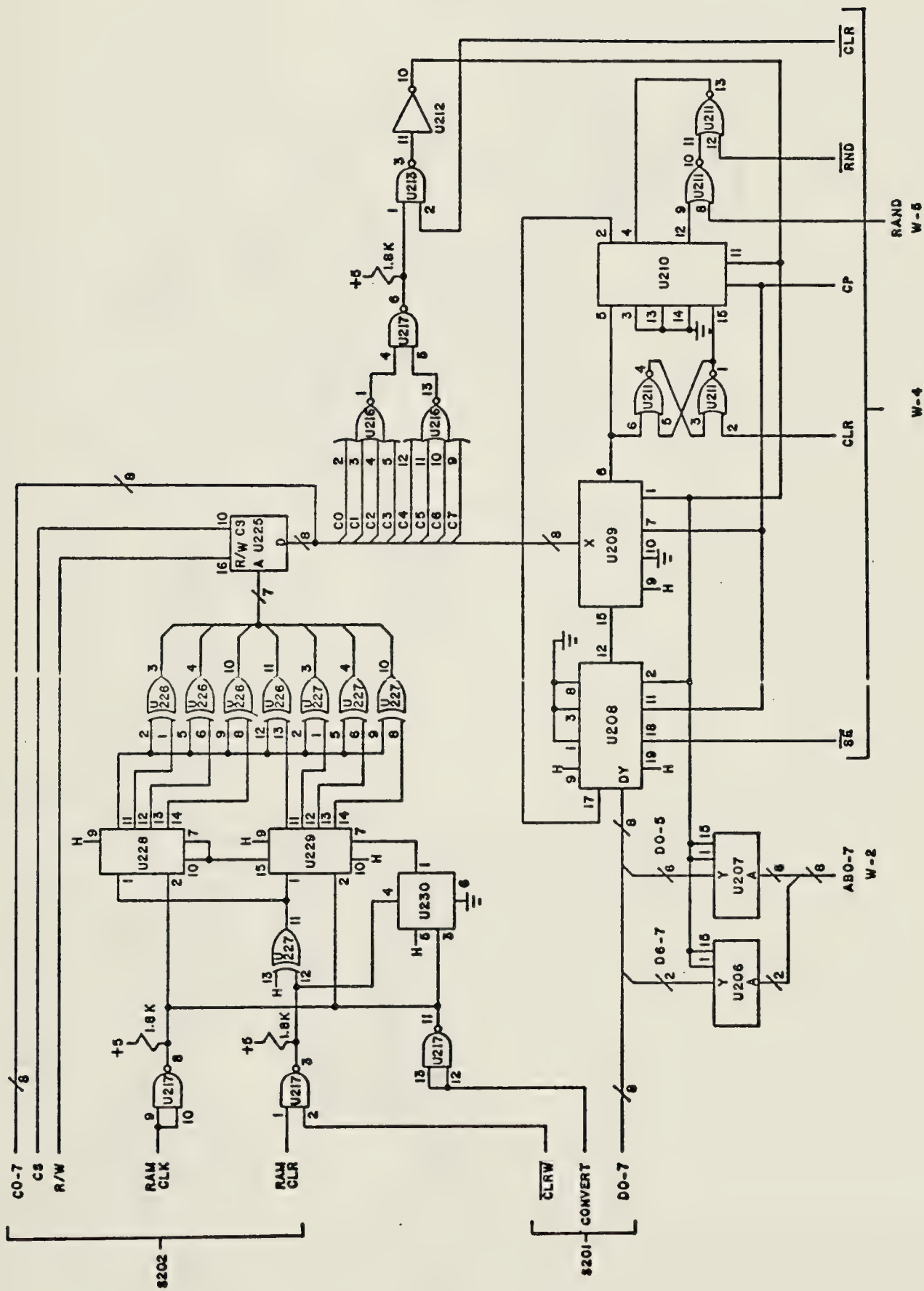


Figure A5.2. Schematic W-3
Window Multiplier and Coefficient Memory

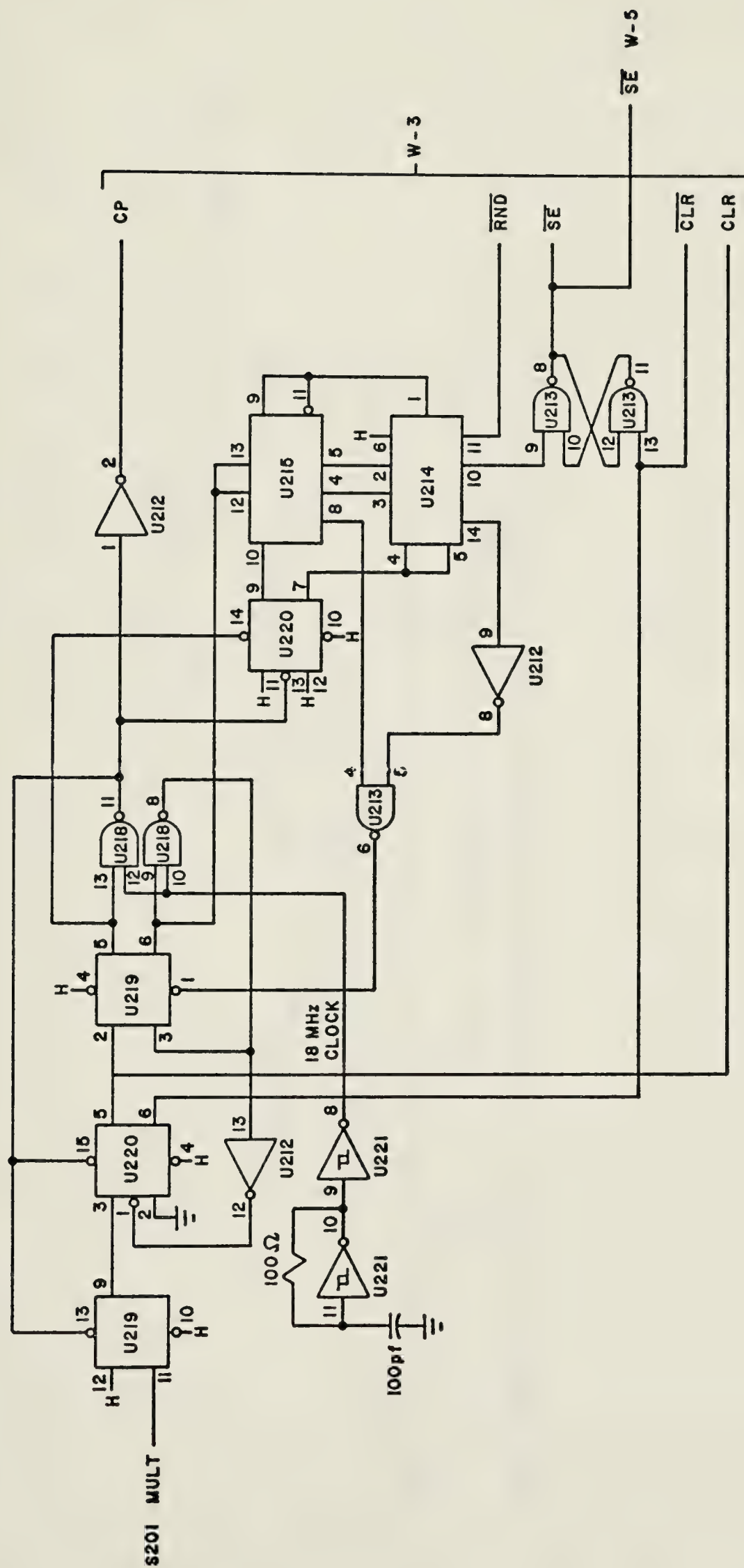


Figure A5.3. Schematic W-4 Window Control and Clocking

IC Numbers for Butterfly Processor Board

U1	D3604	U41	74151	U76	74LS04
U2	D3604	U42	74LS02	U77	74LS00
U3	74LS161	U43	74LS365	U78	74LS00
U4	74LS161	U44	74LS125	U79	74LS125
U5	25LS14	U45	91L01	U80	74LS125
U6	25LS14	U46	91L01	U81	74LS10
U7	25LS15	U47	91L01	U82	74LS10
U8	25LS14	U48	91L01	U83	74LS10
U9	25LS14	U49	74LS157	U84	L4LS10
U10	74LS00	U50	74LS157	U85	74LS04
U11	74S74	U51	74LS126	U86	74LS125
U12	74S74	U52	74LS125	U87	74LS125
U13	74S112	U53	74LS126	U88	74157
U14	74LS20	U54	74LS86	U89	74191
U15	25LS22	U55	74LS161	U90	74LS74
U16	25LS22	U56	74LS161	U91	74LS74
U17	25LS15	U57	91L01	U92	74LS01
U18	25LS15	U58	91L01	U93	74LS221
U19	25LS22	U59	91L01		
U20	25LS22	U60	91L01		
U21	74S00	U61	74LS157		
U22	74S00	U62	74LS157		
U23	74S00	U63	74LS126		
U24	74LS293	U64	74LS125		
U25	74LS14	U65	74LS126		
U26	74LS112	U66	74LS86		
U27	74LS112	U67	25LS22		
U28	74LS14	U68	74LS09		
U29	74LS10	U69	74LS157		
U30	74LS10	U70	CD4050		
U31	74LS123	U71	74125		
U32	74LS123	U71A	74175		
U33	74LS365	U72	74125		
U34	74LS10	U72A	74175		
U35	7428	U73	7474		
U36	7428	U73A	7474		
U37	74LS157	U74	74LS86		
U38	74LS01	U74A	74LS86		
U39	74LS123	U75	74LS00		
U40	74LS161	U75A	74LS00		

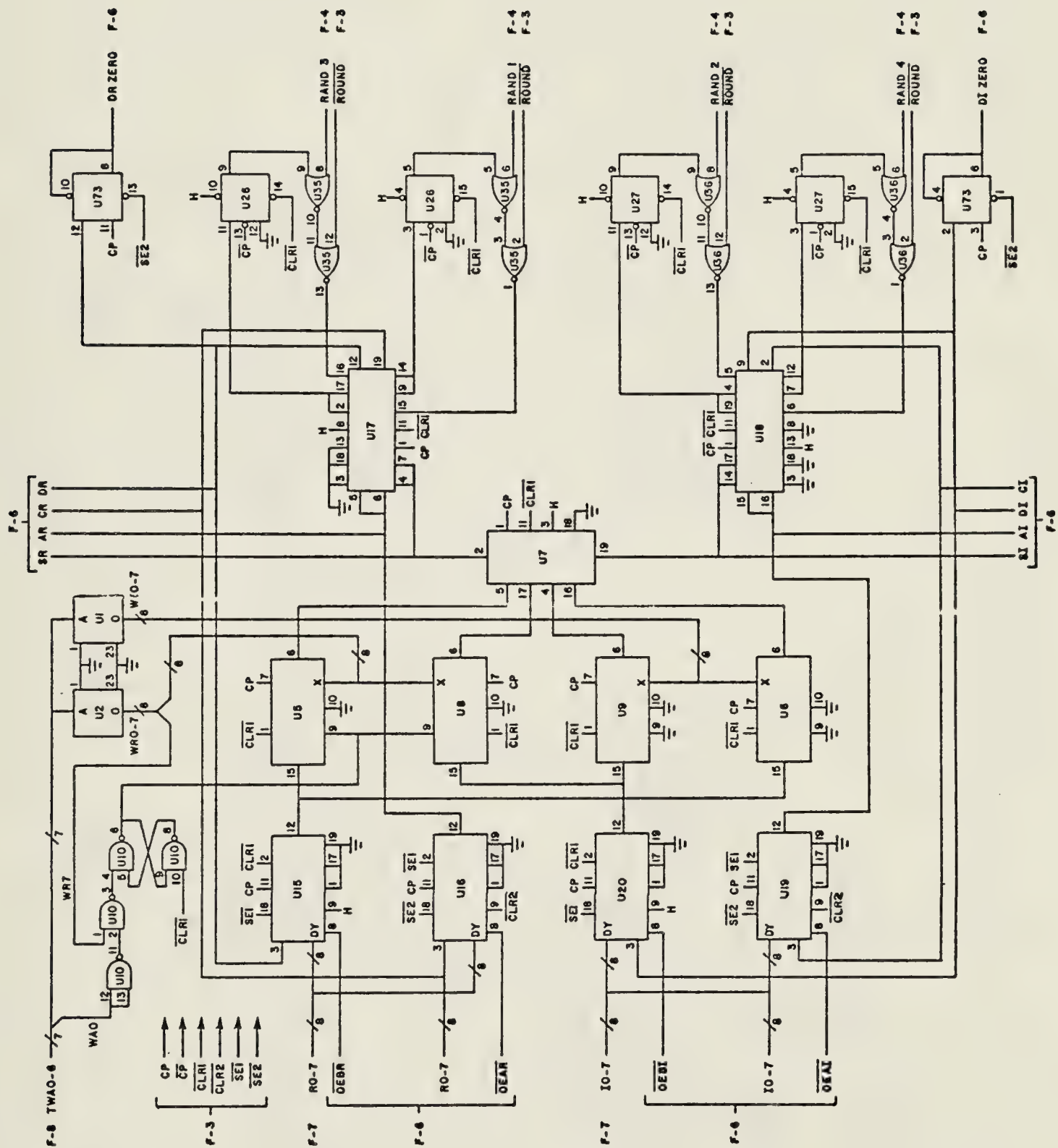


Figure A5.5. Schematic F-2
Butterfly Processor

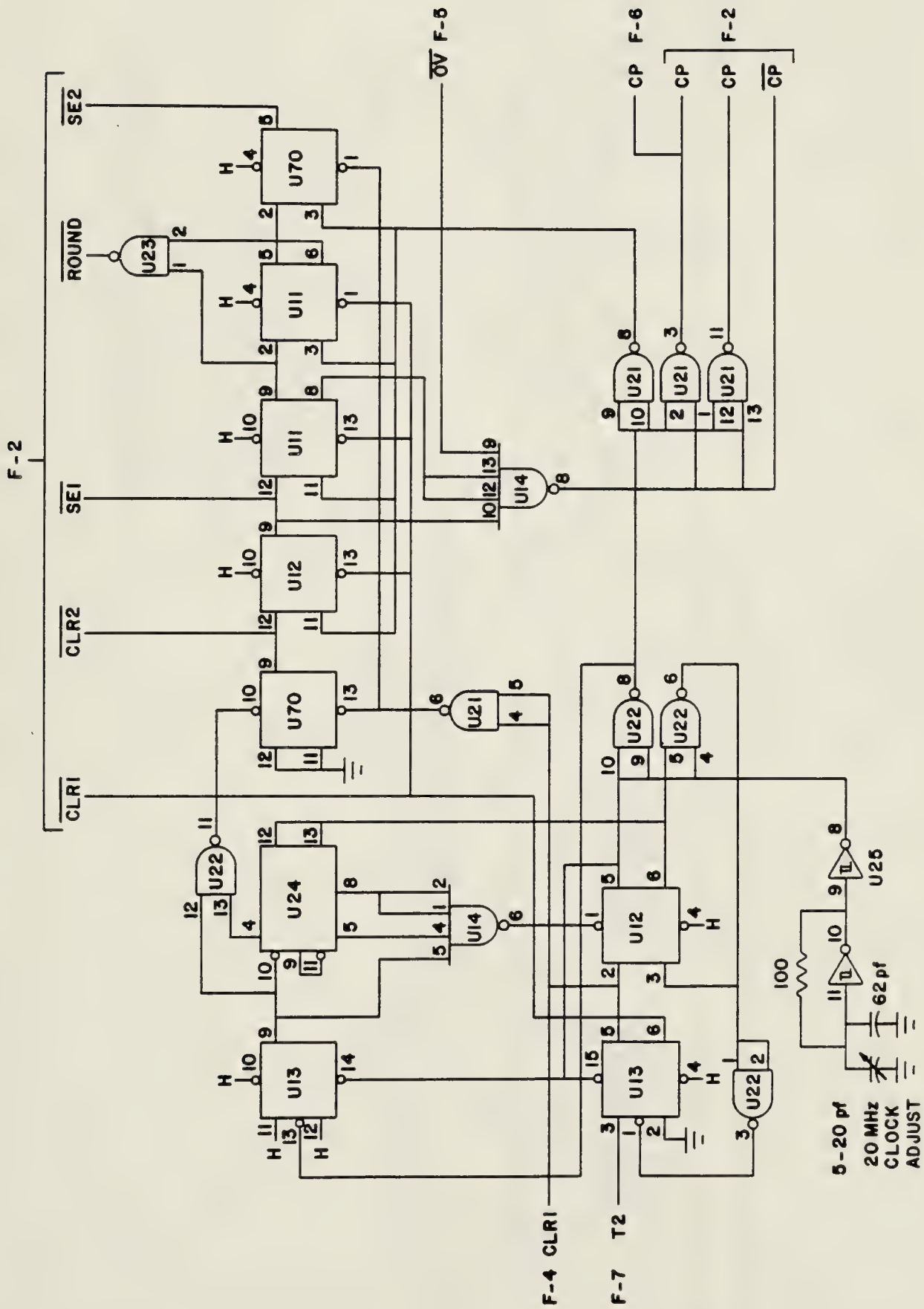


Figure A5.6. Schematic F-3
FFT Control and Clocking

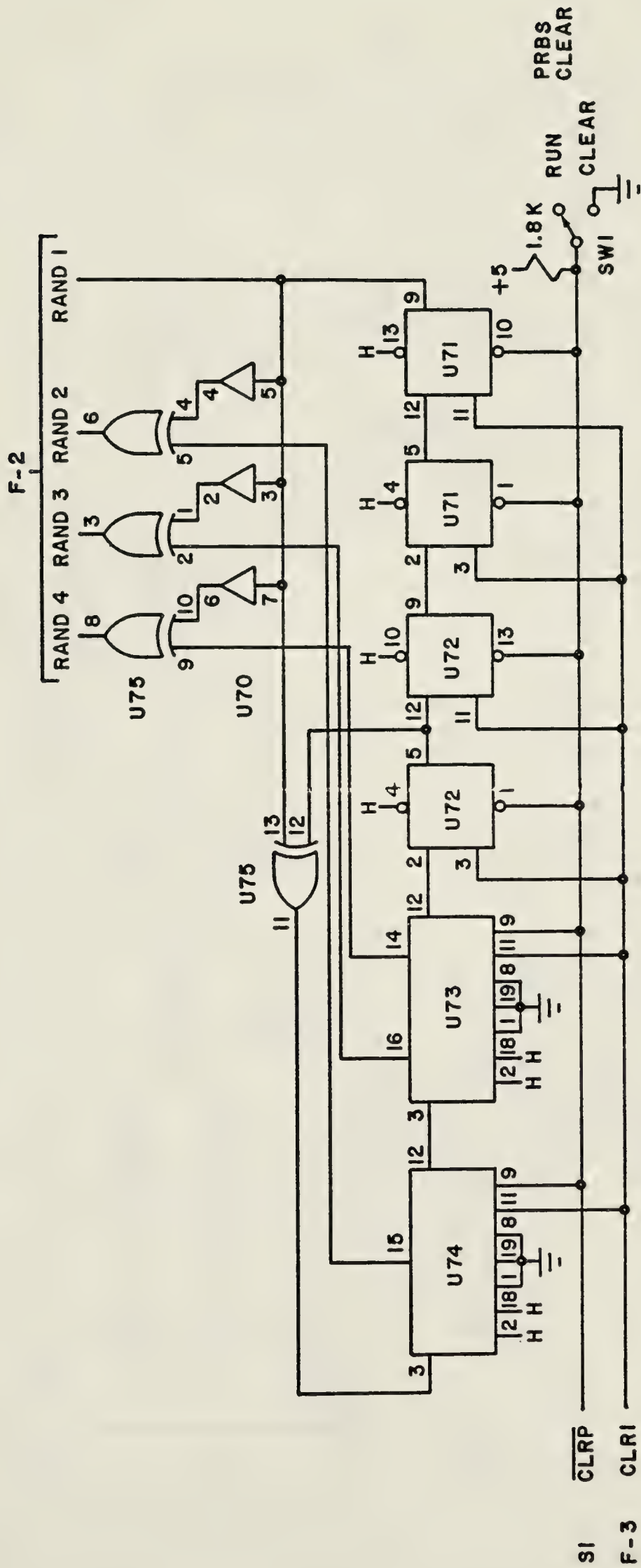


Figure A5.7. Schematic F-4
FFT Pseudorandom Sequence Generator

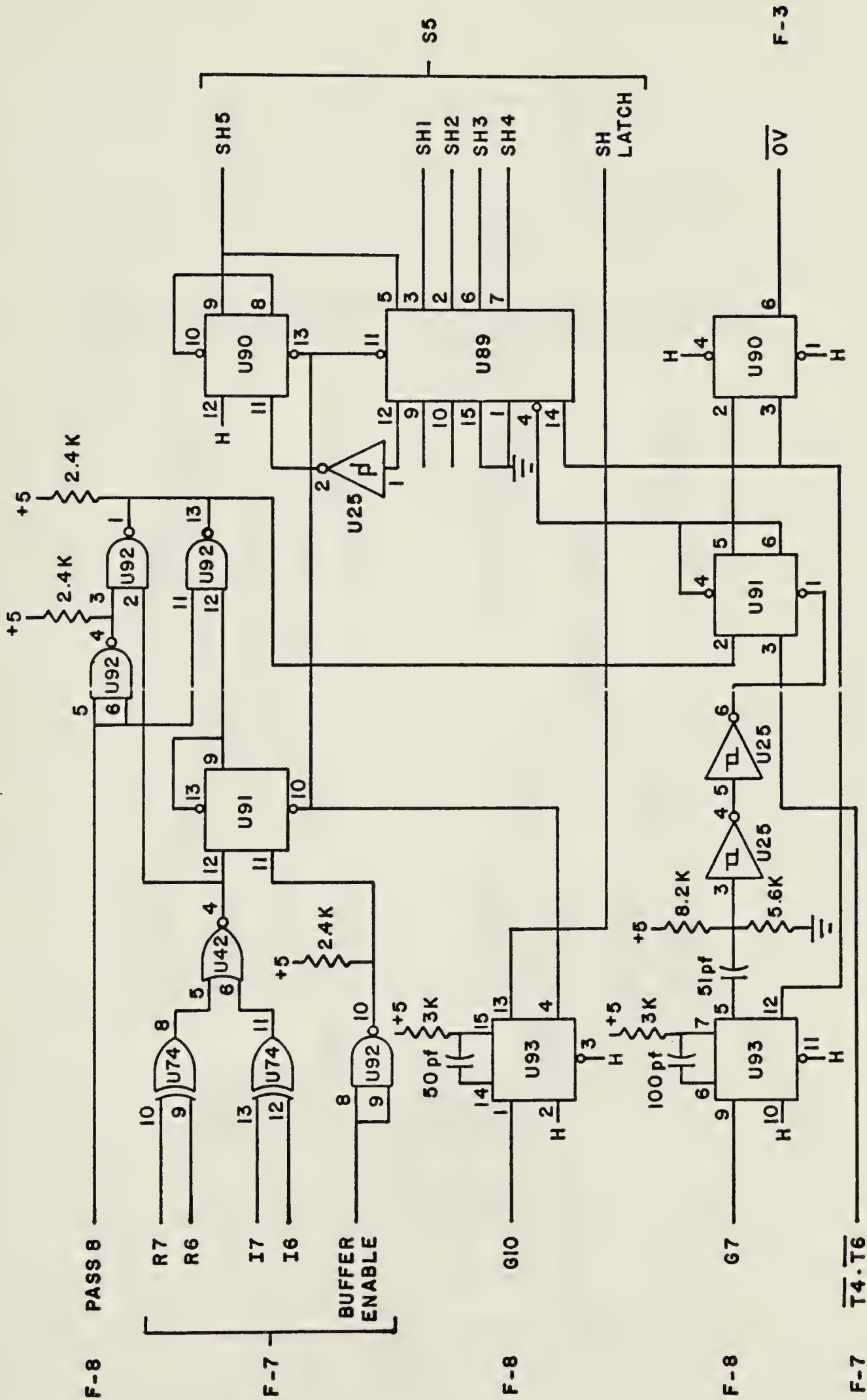


Figure A5.8. Schematic F-5
Overflow Anticipation and Scaling Counter

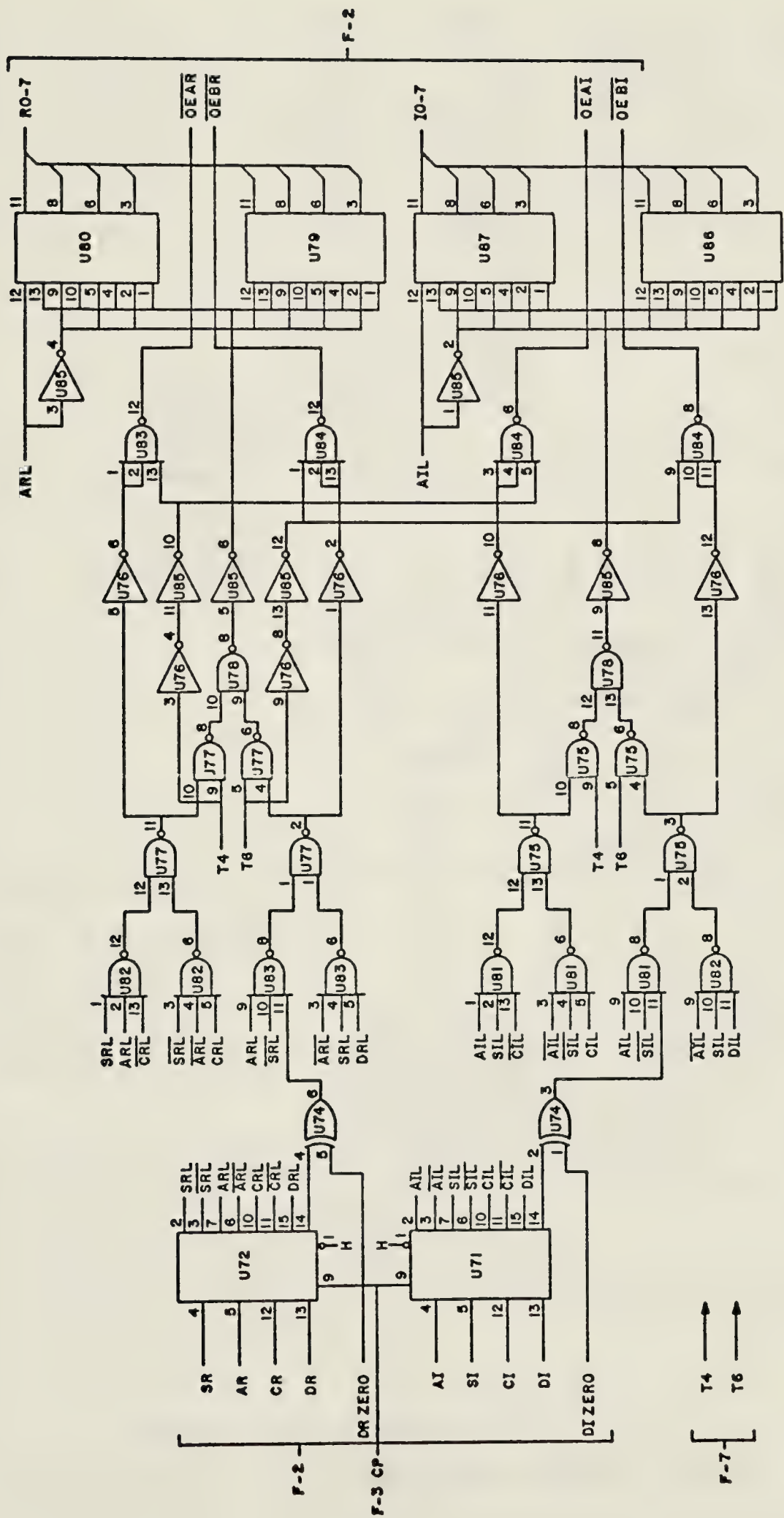


Figure A5.9. Schematic F-6
Overflow Correction

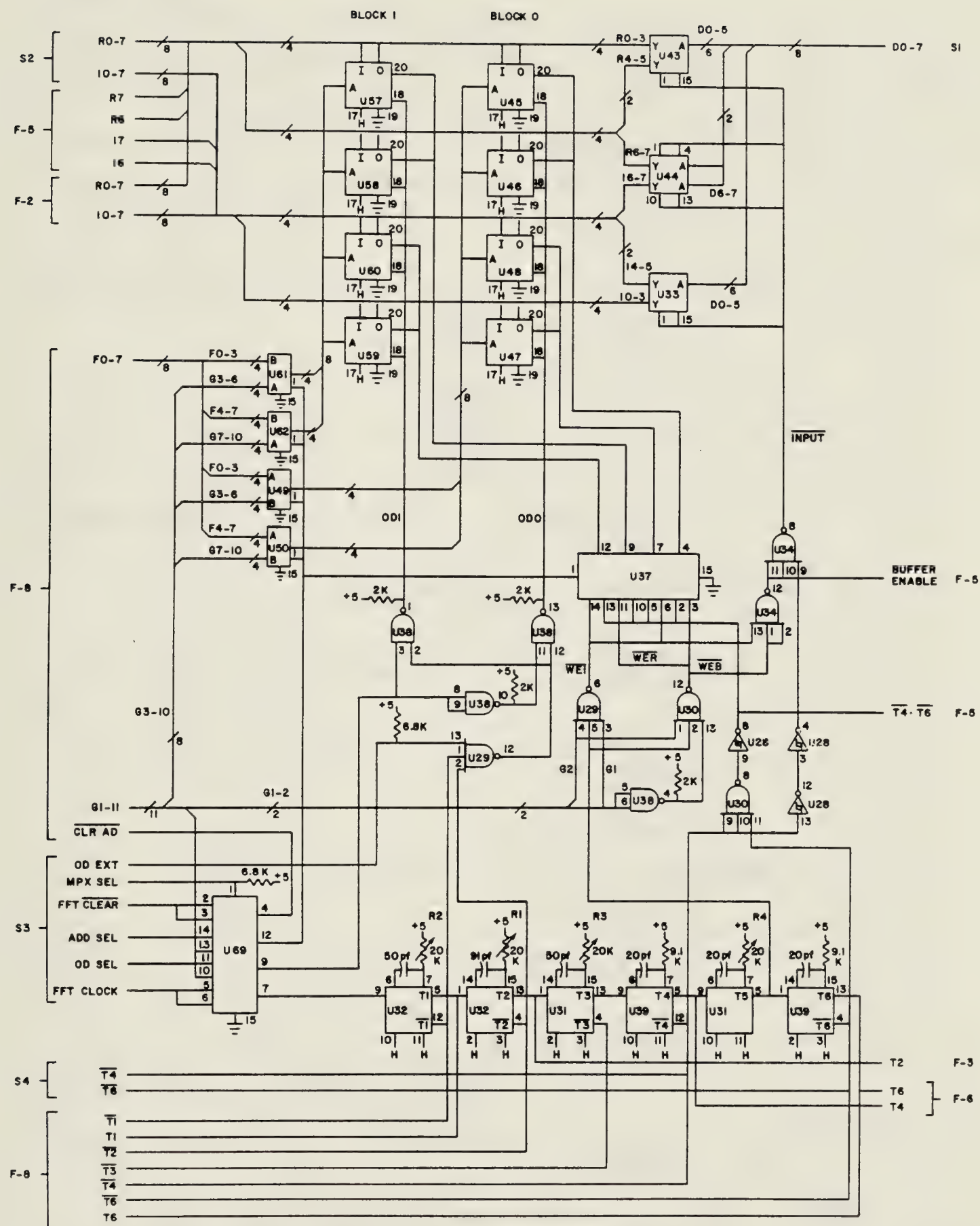


Figure A5.10. Schematic F-7

Input Buffer and FFT Timing

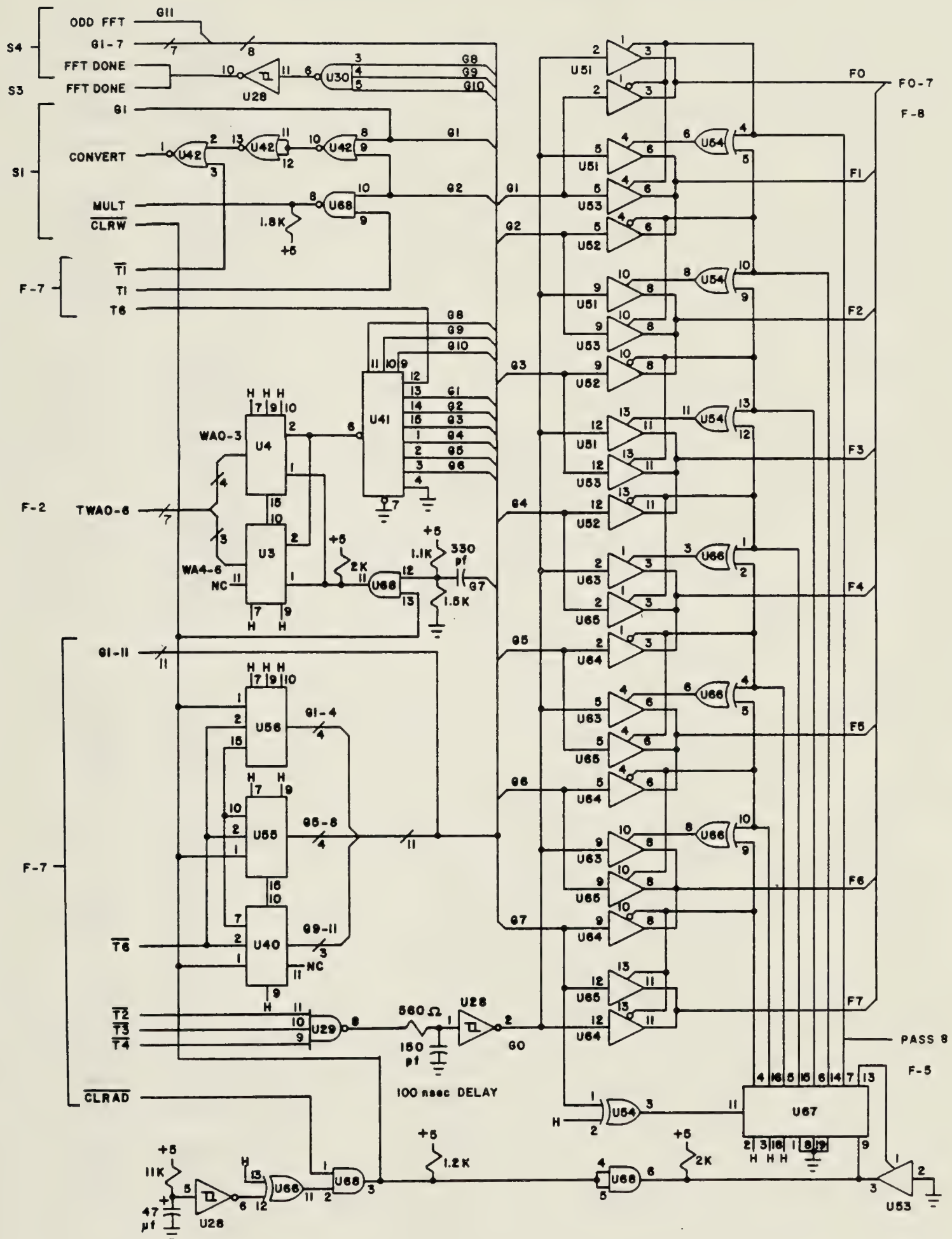


Figure A5.11. Schematic F-8
FFT Address Generation

IC Numbers for Power Computation Board

U100	25LS22
U101	25LS22
U102	25LS22
U103	74LS20
U104	TDC1008J

U105	74LS174
U106	74LS174
U107	74LS08
U108	7474
U109	74LS74

U110	74LS00
U111	CD4016
U112	CD4016
U113	74LS00
U114	74S188

U115	74S188
U116	74163
U117	74LS04
U145	91L01
U146	91L01

U147	91L01
U148	91L01
U149	74LS83
U150	74LS83
U151	74LS86

U152	74LS86
U153	7402
U155	91L01
U156	91L01
U157	91L01

U158	91L01
U159	74LS157
U160	74LS157
U161	74LS161
U162	74LS161

U163	74LS10
U164	7474

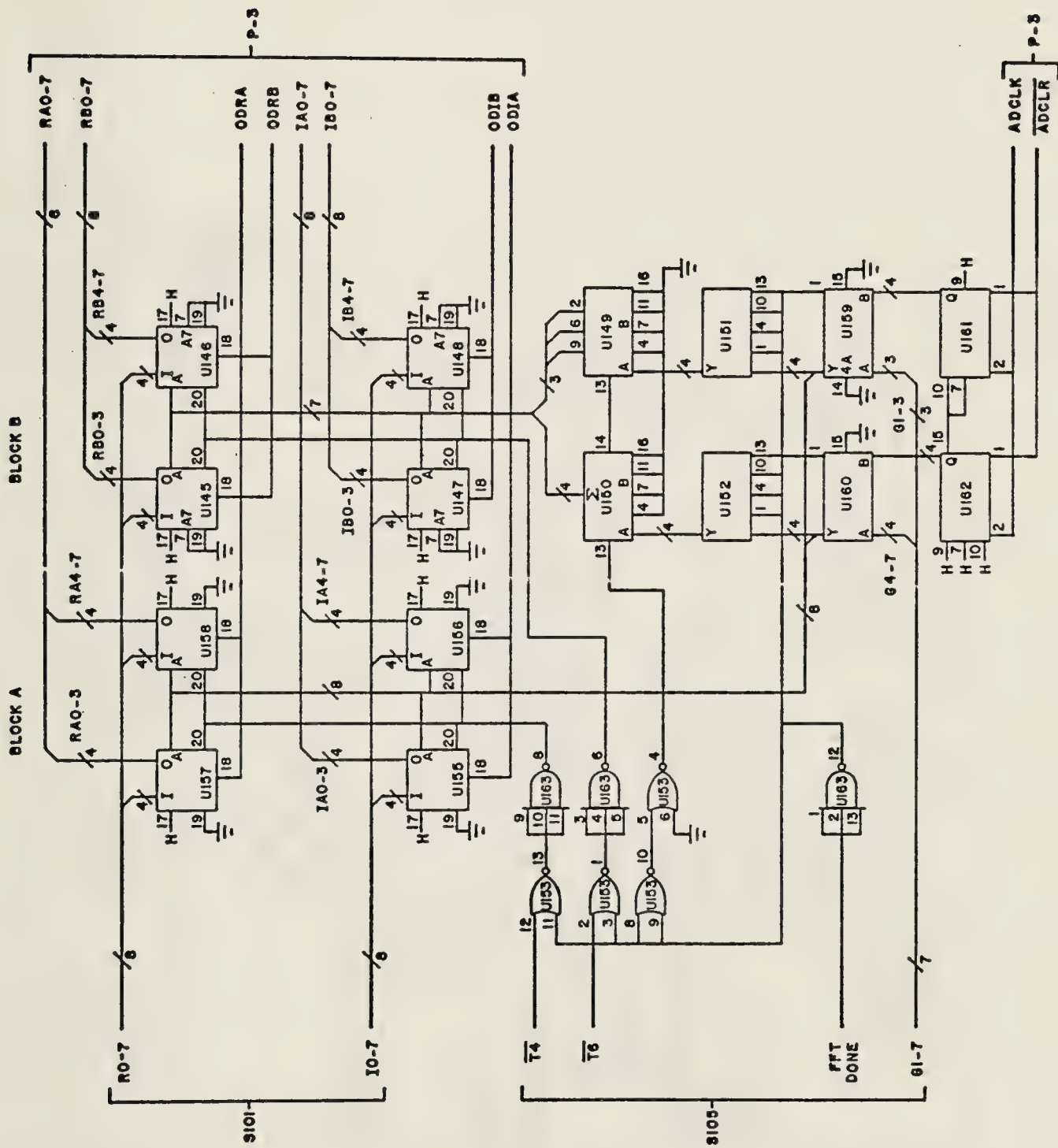


Figure A5.12. Schematic P-2
Output Buffer and Address Generation

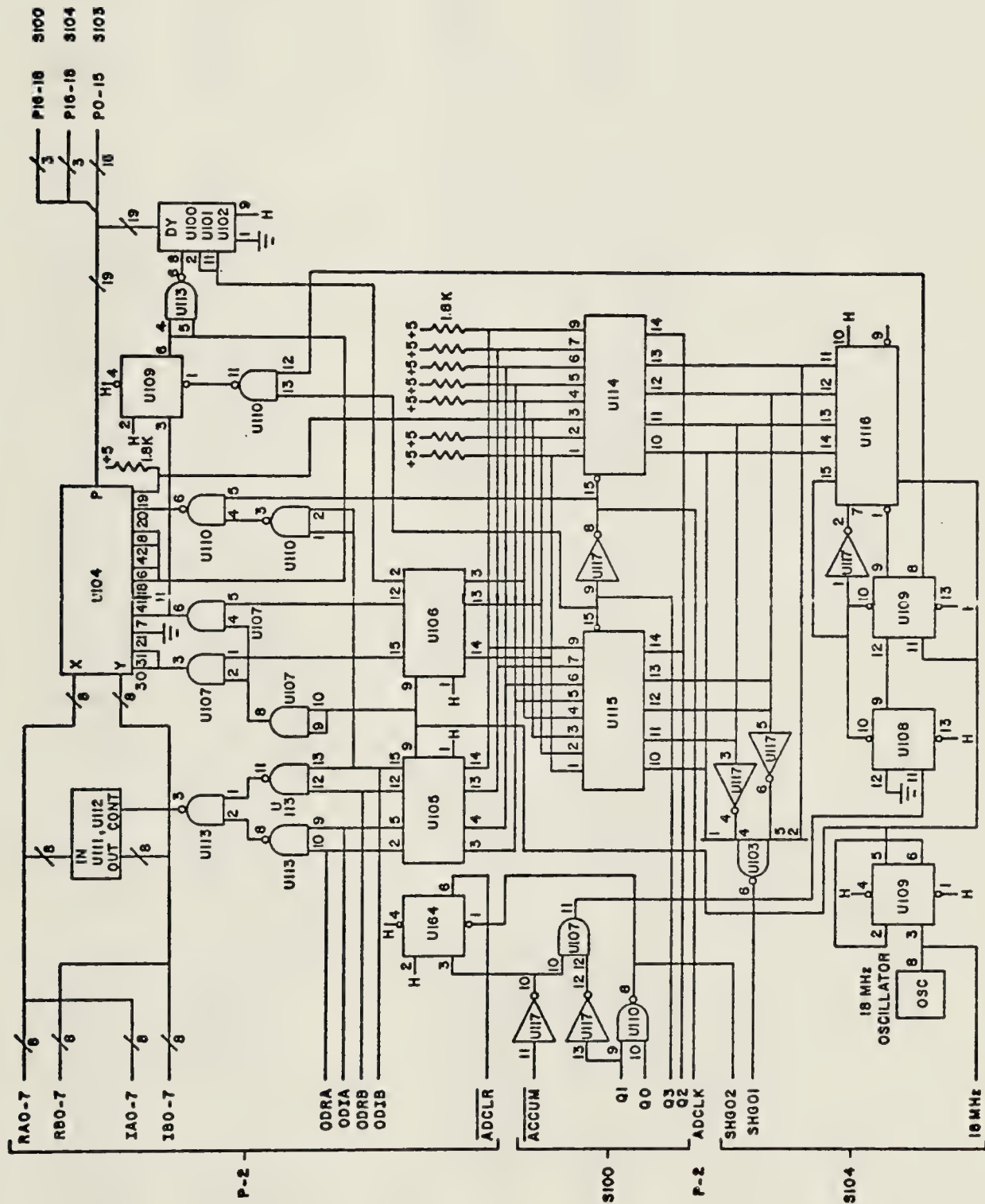


Figure A5.13. Schematic P-3
Power Computation and Control

IC Numbers for Accumulation Board

U400	74LS174	U450	74174
U401	74174	U451	74365
U402	74174	U452	CCD450A
U403	74163	U453	74174
U404	74163	U454	74365
U405	74163	U455	74365
U406	74LS14	U456	74365
U407	7476	U457	74365
U408	7476	U458	7400
U409	74163	U459	7404
U410	7474	U460	74LS181
U411	7410	U461	74LS181
U412	74LS324	U462	74LS181
U413	7474	U463	74LS181
U414	7476	U464	74LS181
U415	74LS01	U465	74LS181
U416	7400	U468	7474
U417	7402	U469	74LS01
U418	7474	U470	74198
U419	7474	U471	74198
U420	MC1488	U472	74182
U421	74LS157	U473	74198
U422	74157	U474	74198
U427	74LS365	U475	74198
U428	74LS365	U476	74198
U429	74LS365	U477	74182
U430	74LS174	U480	74LS174
U431	7400	U481	74LS161
U438	75365	U482	74S10
U439	74LS123	U483	74S04
U440	74LS123	U484	74S00
U441	74365	U485	74LS00
U442	74365	U486	74S174
U443	74365	U487	74LS00
U444	74174	U488	7404
U445	74365	U489	7404
U446	CCD450A		
U447	74174		
U448	74365		
U449	CCD450A		

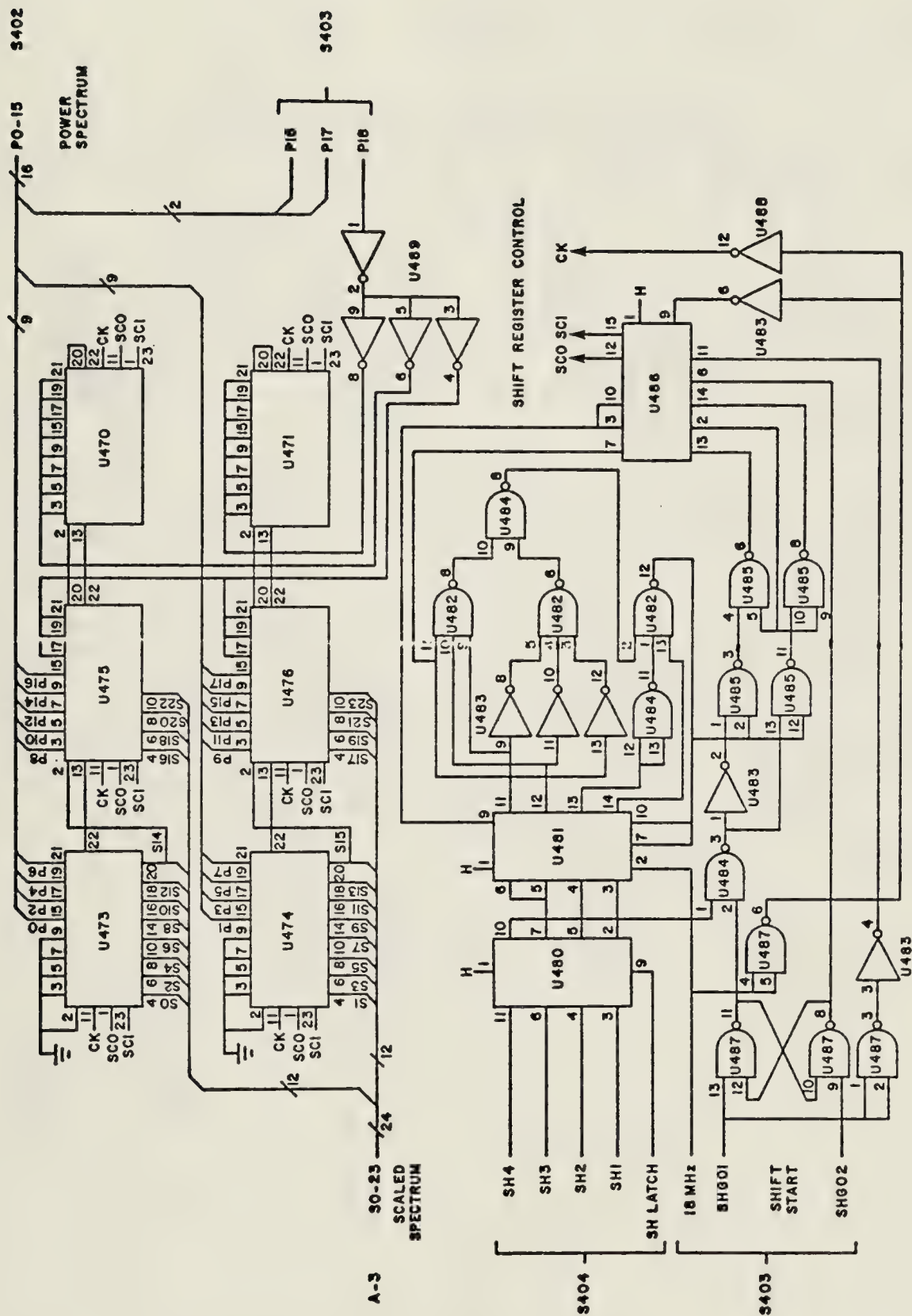


Figure A5.14. Schematic A-2
Scaling Registers and Control

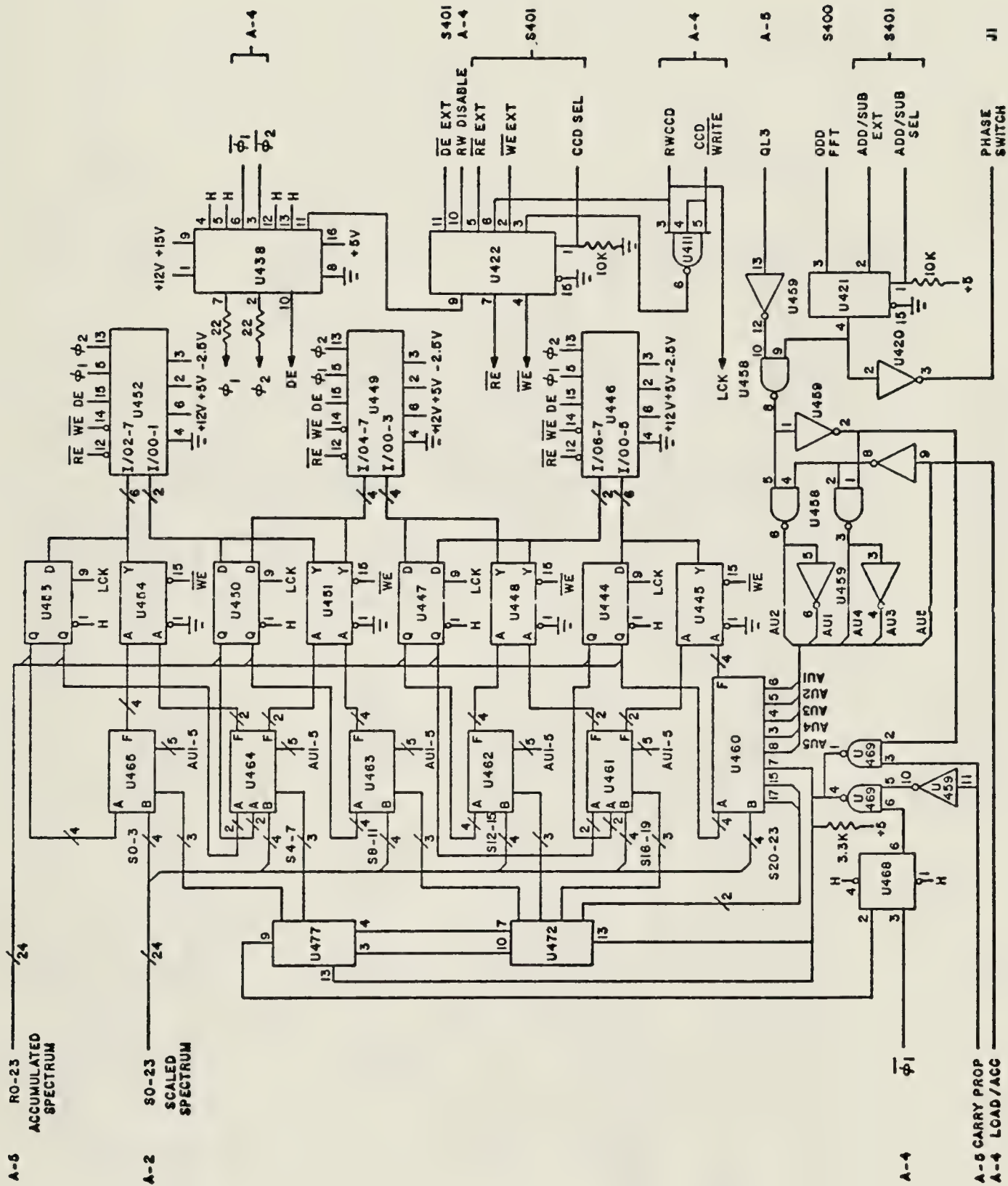


Figure A5.15. Schematic A-3

Accumulation and CCD Memory

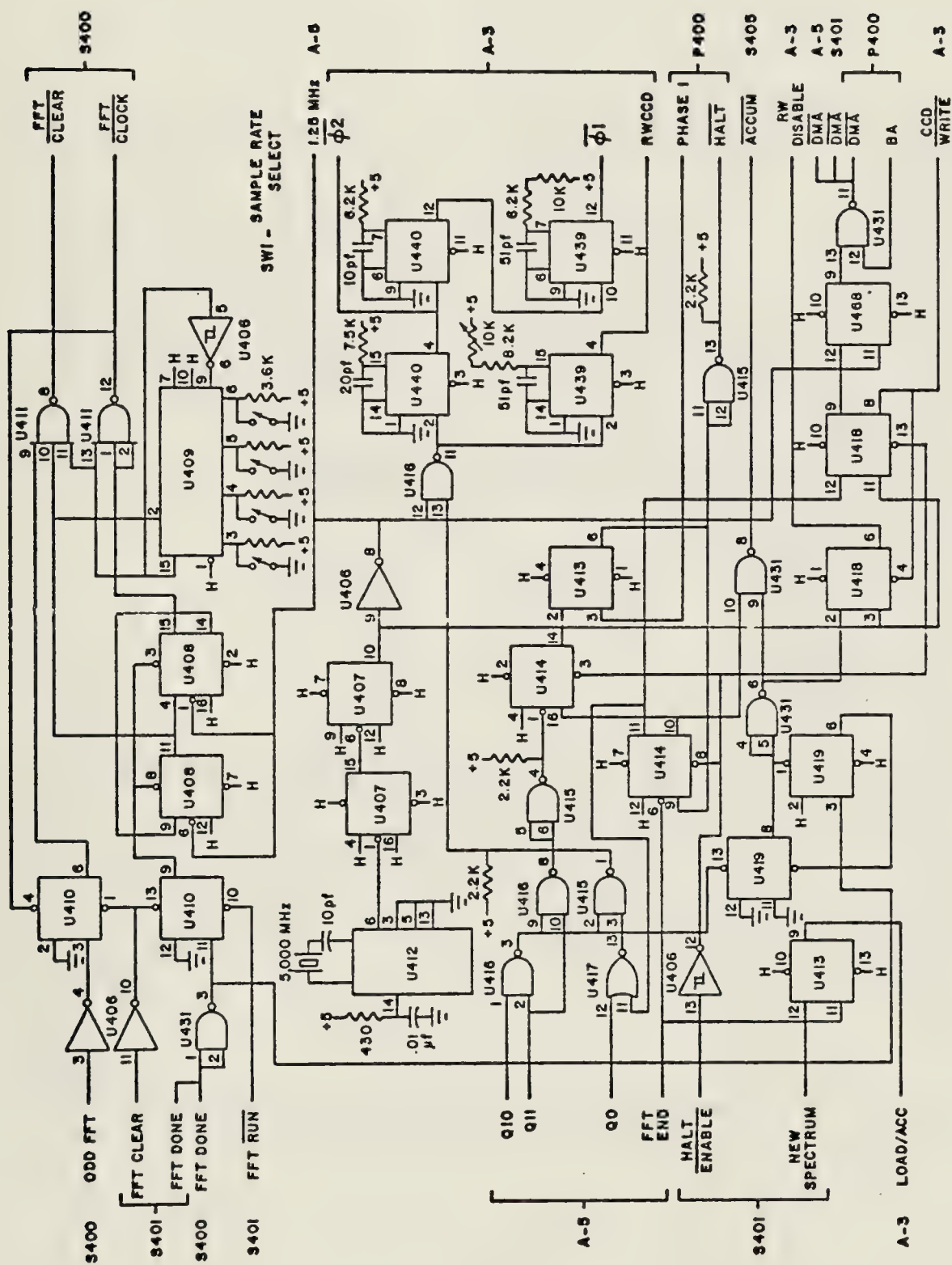


Figure A5.16. Schematic A-4
Master Clock and DMA Control

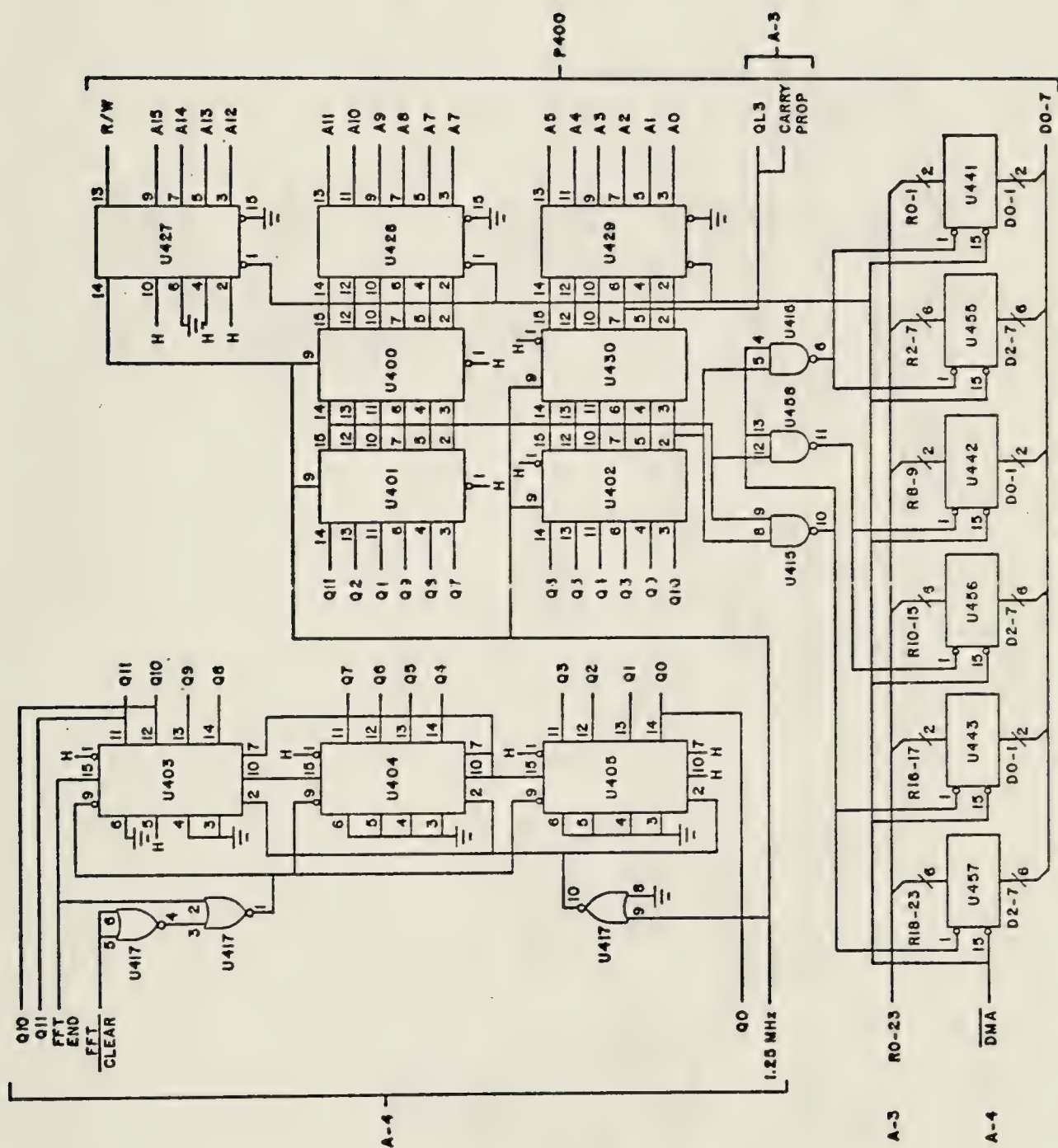


Figure A5.17. Schematic A-5
DMA Buffers and Address Generation

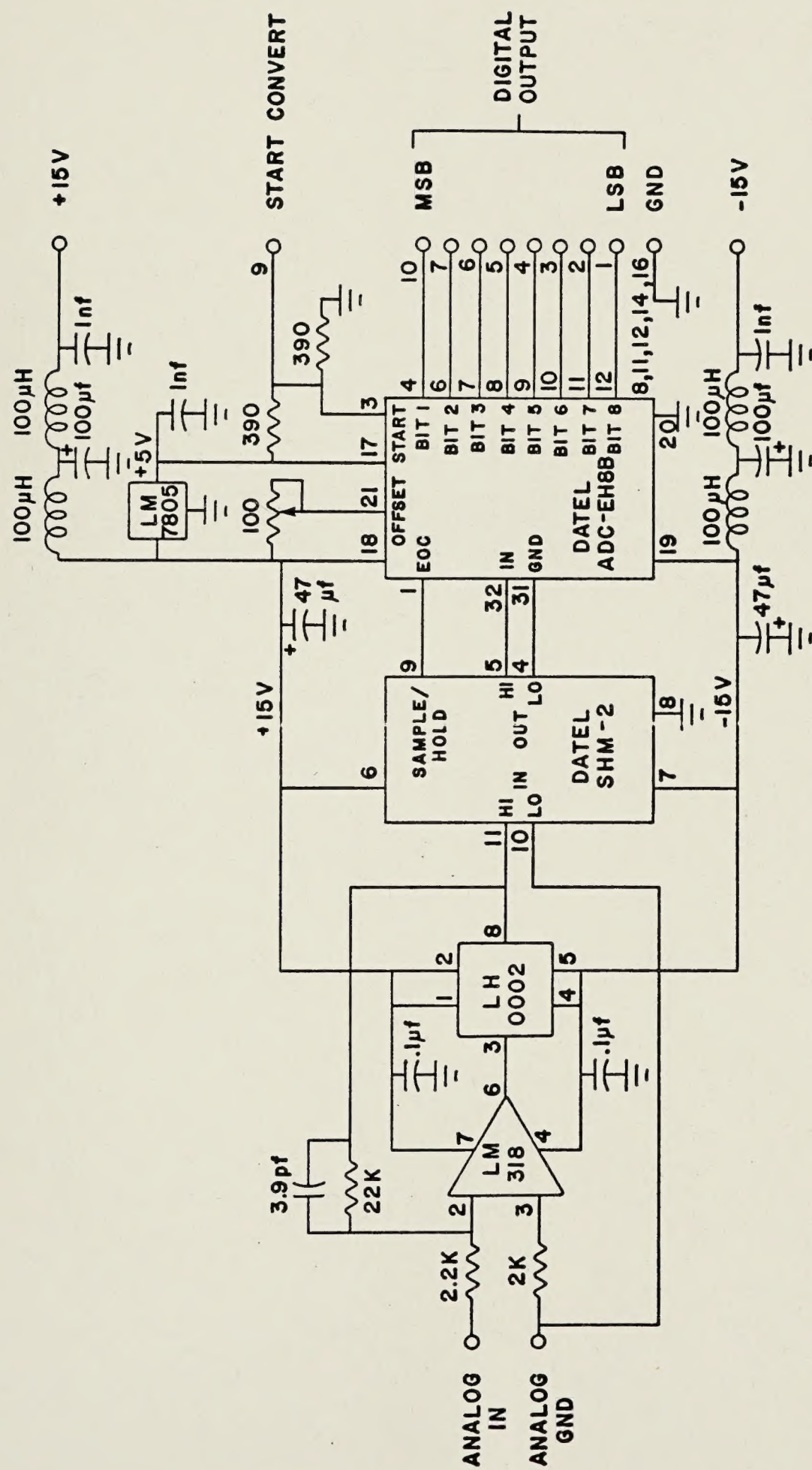


Figure A5.18. Analog-to-Digital Conversion

B30308